DYNAMIC MODELLING AND REPAIR OF CRACKS FOR FATIGUE LIFE ENHANCEMENT USING PIEZOELECTRIC ACTUATOR

Thesis submitted by

SOURAV PATTANAYAK

Doctor of Philosophy

(Engineering)

DEPARTMENT OF MECHANICAL ENGINEERING

FACULTY COUNCIL OF ENGINEERING & TECHNOLOGY

JADAVPUR UNIVERSITY

KOLKATA, INDIA

2025

JADAVPUR UNIVERSITY

KOLKATA-700032, INDIA

INDEX NO.-195/19/E

1. **Title of the thesis:**

   Dynamic Modelling and Repair of Cracks for Fatigue Life Enhancement Using Piezoelectric Actuator

2. **Name, Designation & Institution of the Supervisors:**

   Prof. Prasanta Sahoo
   Professor, Department of Mechanical Engineering
   Jadavpur University, Kolkata-700032

   Prof. Goutam Pohit
   Professor, Department of Mechanical Engineering
   Jadavpur University, Kolkata-700032

3. **List of Publications:**

   Referred Journal

   I. **Pattanayak, S.**, Roy, S., Sahoo, P. and Pohit, G. (2025). Strengthening of an Edge-Cracked Plate Under Bending Using Piezoelectric Actuators. Applied Research, 1-10. https://doi.org/10.1002/appl.70013. **(Indexing: ESCI)**

   II. **Pattanayak, S.**, Roy, G. and Pohit, G. (2024). A novel approach to enhance the structural integrity of a bottom-edge cracked I-beam with piezoelectric actuators. Mechanics of Advanced Materials and Structures, 1–20. https://doi.org/10.1080/15376494.2024.2423062. (**Indexing: SCIE)**

   III. **Pattanayak, S.**, Roy, G. and Pohit, G. (2024). Piezoelectric Actuator/Patch-Based Hybrid Repair and Fatigue Life expansion of a Double-Edged Damaged Plate: an analytical approach and numerical validation. Arabian Journal for Science and Engineering, 49(8), 11479–11499. https://doi.org/10.1007/s13369-023-08703-x. (**Indexing: SCIE)**

   IV. **Pattanayak, S.** and Pohit, G. (2023). Reduction in Mode-I SIF of an edge cracked C-Shaped specimen using piezoelectric actuator. E3S Web of Conferences, 430, 01293. https://doi.org/10.1051/e3sconf/202343001293. (**Indexing: Scopus)**

V. **Pattanayak, S.**, Roy, S., Sahoo, P. and Pohit, G. (2025). Active Repair of Cracks Emanating from Elliptical Holes Using Piezoelectric Actuators: A Study on Stress Intensity Factor Reduction and Fatigue Life Extension. **(To be communicated).**

Book Chapter

I. **Pattanayak, S.** And Pohit, G. (2025). Study on Fatigue Crack Propagation Reduction and Extended Service Life in an Arc-Shaped Cracked Specimen Using Piezoelectric Patch. In: Sahoo, P., Barman, T.K. (eds) Advances in Materials, Manufacturing and Design. INCOM 2024. Lecture Notes in Mechanical Engineering. Springer, Singapore. https://doi.org/10.1007/978-981-97-6667-3_22. **(Indexing: Scopus)**

4. **List of Patents:** Nil

5. **List of Presentations in National/International/Conferences/Workshops:**

I. **Pattanayak, S.**, Roy, S., Sahoo, P. and Pohit, G. (2024). "Strengthening of an Edge-Cracked Plate Under Bending Using Piezoelectric Actuators" presented at the 2nd International Conference on Emerging Aspects Of Manufacturing, Thermal And Design Engineering (MATHED-2024), NIT Hamirpur, Hamirpur, Himachal Pradesh, India, December 2024 **(Paper ID-90)**.

II. **Pattanayak, S.** and Pohit, G. (2024). "An Approach to Reduce Crack Propagation in An Arc-Shaped Cracked Specimen Via Piezoelectric Patch" presented at the 2nd International Conference on Mechanical Engineering (INCOM 2024), Jadavpur University, Kolkata, West Bengal, India, January 2024 **(Paper ID-INCOM24-0213)**.

III. **Pattanayak, S.** and Pohit, G. (2023). "Reduction in Mode-I SIF of an Edge Cracked C-Shaped Specimen Using Piezoelectric Actuator," presented at the 14th International Conference on Materials Processing and Characterization (ICMPC 2023), GRIET Hyderabad, Hyderabad, Telangana, India, March 2023 **(Paper ID-1861)**.

"Statement of Originality"

I, **Sourav Pattanayak**, registered on **28.06.2019**, do hereby declare that this thesis entitled "***DYNAMIC MODELLING AND REPAIR OF CRACKS FOR FATIGUE LIFE ENHANCEMENT USING PIEZOELECTRIC ACTUATOR***" contains a literature survey and original research work done by the undersigned candidate as part of Doctoral studies.

All information in this thesis has been obtained and presented in accordance with existing academic rules and ethical conduct. I declare that, as required by these rules and conduct, I have fully cited and referred all materials and results that are not original to this work.

I also declare that I have checked this thesis as per the "Policy on Anti-Plagiarism, Jadavpur University, 2019", and the level of similarity, as checked by iThenticate software, is **2** %.

Signature of Candidate: Sourav Pattanayak

(Sourav Pattanayak) 06/05/2025

Date:

Certified by Supervisors:

(Signature with date, seal)

1. Prasanta Sahoo 06/05/2025

(Prof. Prasanta Sahoo)

Professor
Dept. of Mechanical Engineering
Jadavpur University, Kolkata-32

2. Goutam Pohit 6/5/25

(Prof. Goutam Pohit)

Professor
Dept. of Mechanical Engineering
Jadavpur University, Kolkata-32

This page is intentionally left blank

CERTIFICATE FROM THE SUPERVISORS

*This is to certify that the thesis entitled "**DYNAMIC MODELLING AND REPAIR OF CRACKS FOR FATIGUE LIFE ENHANCEMENT USING PIEZOELECTRIC ACTUATOR**" submitted by Shri **Sourav Pattanayak**, who got his name registered on 28.06.2019 for the award of Ph. D. (Engineering) degree of Jadavpur University is absolutely based upon his own work under the supervision of* **Prof. Prasanta Sahoo** and **Prof. Goutam Pohit** *and that neither his thesis nor any part of the thesis has been submitted for any degree/diploma or any other academic award anywhere before.*

1. Prasanta Sahoo

(Prof. Prasanta Sahoo) 06/05/2025

Signature of the Supervisor and date with Office Seal

Professor
Dept. of Mechanical Engineering
Jadavpur University, Kolkata-32

2. Goutam Pohit 6/5/25

(Prof. Goutam Pohit)

Signature of the Supervisor and date with Office Seal

Professor
Dept. of Mechanical Engineering
Jadavpur University, Kolkata-32

This page is intentionally left blank

Acknowledgment

At this juncture, I find myself at the conclusion of my PhD research after more than five years of continuous effort at Jadavpur University. I take this opportunity to express my sincere gratitude to all those who have supported and encouraged me throughout this journey. Without their guidance, encouragement, and unwavering support, this achievement would not have been possible.

First and foremost, I would like to express my deepest gratitude to my esteemed supervisor, Prof. Goutam Pohit, Department of Mechanical Engineering, Jadavpur University, for his invaluable support, insightful suggestions, and continuous encouragement from the very beginning of this PhD research. His methodical guidance and mentorship have been instrumental in shaping this thesis. I am equally indebted to my respected supervisor, Prof. Prasanta Sahoo, Department of Mechanical Engineering, Jadavpur University, for his consistent guidance and encouragement throughout the course of this work. Their combined support has had a profound impact on my academic development and the successful completion of my research.

I am grateful to Jadavpur University for granting me the opportunity to pursue my PhD in the Department of Mechanical Engineering. I also extend my sincere thanks to the Head of the Department, faculty members, and staff for their cooperation and support during my research period.

I would like to specially thank Dr. Goutam Roy, a former PhD scholar of my supervisor and a dear friend, for his generous help and valuable guidance during the initial stages of my research. This work would not have taken shape without his constant support.

I am thankful to my colleagues at the Department of Mechanical Engineering, Haldia Institute of Technology, for their encouragement and support. I would particularly like to thank Dr. Supriyo Roy and Dr. Abhishek Samanta for their insightful suggestions and constant motivation from the very beginning of this journey. I also wish to express my gratitude to the Head of the Department and the Principal of Haldia Institute of Technology for their kind support and encouragement throughout the duration of my PhD.

My heartfelt thanks go to all my friends who have stood by me and supported me through the ups and downs of this journey. I am profoundly grateful to my family, especially my mother

and my beloved wife, whose unwavering belief in me, boundless love, and endless encouragement have been my greatest strength.

Lastly, I express my sincere thanks to all the teachers who have guided me over the years and instilled in me the values, knowledge, and passion that have carried me through this endeavor.

Sourav Pattanayak

Dedicated

To My Father

Late Snehadri Pattanayak

This page is intentionally left blank

Abstract

Cracks in engineering structures pose a significant threat to their integrity, leading to the propagation of the cracks and potentially catastrophic failure. These cracks, often originating from stress concentrations or material defects, weaken the structure, reduce its load-bearing capacity, and accelerate fatigue failure. Consequently, effective crack repair and structural health monitoring are crucial for ensuring the safety and longevity of critical components.

Previous research has primarily focused on static crack repair using piezoelectric materials, demonstrating their ability to reduce stress intensity factors (SIF) under static loading. However, a comprehensive analysis of fatigue life enhancement, incorporating both the active and passive effects of piezoelectric patches, remains largely unexplored. Specifically, the passive stiffening effect of the patch and the combined "hybrid" repair effect have not been analytically modeled and validated against finite element (FE) solutions. Additionally, these repair techniques are not yet utilized for complex structures like cracked I-beams, cracks emanating from the elliptical hole, arc-shaped cracked specimens, cracked plates under bending, etc.

This thesis aims to develop and validate analytical models for passive, active, and hybrid crack repair using piezoelectric materials to enhance fatigue life under cyclic loading. The primary objectives are to develop analytical models that accurately predict the SIF and fatigue crack growth rate (FCGR) in cracked plates and beams repaired with piezoelectric patches under various loading conditions. Additionally, this thesis aims to investigate the individual and combined effects of passive stiffening and active actuation on crack behavior and to conduct a parametric study to determine the optimal thickness and voltage application to the piezoelectric actuators for maximum crack mitigation and fatigue life extension. At last, the developed analytical model is validated against finite element (FE) simulations using ABAQUS.

The methodology employed in this thesis is based on linear elastic fracture mechanics (LEFM) principles. The SIF is calculated using established solutions for cracked structures, and the weight function method (WFM) and crack surface widening energy release rate are used to determine the SIF induced by piezoelectric actuation. The passive effect of the piezoelectric patch is determined using Rose's equations. The superposition principle combines the effects of mechanical loading and piezoelectric actuation. Fatigue crack growth is predicted using the standard crack growth model, considering various stress and voltage ratios.

The analytical models developed in this thesis were rigorously validated against FE solutions obtained using ABAQUS software. This validation process involved comparing the calculated SIF and fatigue life predictions with the FE results under various loading conditions and repair configurations. The consistency between the analytical and FE results confirms the accuracy and reliability of the proposed models.

The main findings of the thesis demonstrate that piezoelectric patches, particularly in hybrid repair configurations, significantly reduce SIF and extend fatigue life. Hybrid repair, combining passive stiffening and active actuation, consistently outperformed individual passive or active repair methods. Active repair using strategically placed piezoelectric actuators mitigates crack propagation in various structural geometries, including plates with elliptical holes, arc-shaped specimens, and I-beams. The parametric studies revealed that thin actuators are optimal for low mechanical loads, while thick actuators perform better under higher loads as they are prone to mechanical failure. Furthermore, applying external voltages to piezoelectric actuators induces controlled deformations, significantly reducing FCGR and enhancing structural integrity. This research provides a robust context for designing and implementing effective piezoelectric-based crack repair strategies, contributing to developing safer and more durable engineering structures.

K_I	SIF of the cracked specimen without repair
K_P	SIF after passive repair
K_P^*	Modified SIF of passive repair after considering bending effect
K_{Piezo}	SIF due to the actuation of the piezoelectric patch
K_A	SIF after active repair
K_H	SIF after hybrid repair
K_I^{Me}	SIF due to mechanical loading for an I-beam
K_I^{MP}	SIF due to bending moment produced by the piezoelectric actuation for an I-beam
K_I^{FP}	SIF due to axial load produced by the piezoelectric actuation for an I-beam
K_I^{Piezo}	Total SIF due to the piezoelectric actuation for an I-beam
K_I^{Total}	Total SIF after repair for an I-beam for an I-beam
K_{max}	Maximum SIF corresponds to maximum stress
K_{min}	Minimum SIF corresponds to minimum stress
ΔK	SIF range ($K_{max} - K_{min}$)
ΔK_{th}	Threshold SIF range $\left(MPa\sqrt{mm}\right)$
K_r	Reference stress intensity factor
K_{IC}	Fracture toughness
a	Crack length
a_c	Critical crack length
a_o	Initial crack length
c	Length of the crack emanating from elliptical hole
$F\left(\frac{a}{W}\right)$	Non-dimensional geometry correction factor (GCF) for double edge cracked plate
$F_1\left(\frac{a}{W}\right)$ and $F_2\left(\frac{a}{W}, \frac{X}{W}, \frac{W}{R}\right)$	Non-dimensional geometry correction factor (GCF) for arc-shaped specimen
$F\left(\frac{a}{h}\right)$	Non-dimensional geometry correction factor (GCF) for edge cracked plate under bending
W	Half-width/width of the specimen
A	Cross-sectional area of specimen (m^2)
t	Thickness of the specimen
E	Young's modulus of the specimen
A_R	Cross cross-sectional area of the patch

E_P	Young's modulus of the patch
t_P	Thickness of the patch
W_P and L_P	Half-width/width/length of the patch
H_P and h_P	Height of the patch
T	Width of the distributed electrode
d_{31}	Piezoelectric strain coefficient (m/V)
G_A	Shear modulus of the adhesive material
t_A	Adhesive thickness
a_1	Semi-major axis of elliptical hole
b_1	Semi-minor axis of elliptical hole
t_w	Thickness of the web portion of the I-beam.
t_f	Thickness of the flange of the I-beam
h_w	Height of the flange of the I-beam
W_f	Width of the flange of the I-beam
Y_{nc}	Change in the location of the neutral axis for the cracked and un-cracked sections
h	Height of the plate
L	Length of the plate under bending
S	Stiffness ratio
$\bar{c}$	Physical parameters related to passive repair
k	spring constant
y_{max}	The distance of the extreme fibers of the cracked plate from the neutral axis
C_m	Coefficient depends on the structure's geometry for a plate containing elliptical hole
I_{Plate}	Moment of inertia of the plate
I_{Patch}	Moment of inertia of the patch
I	Moment of inertia of the I-beam
n	Ratio of modulus of elasticity
$h(x,c)$ and $h(x,y,a)$	Weight function
$u_r(x,c)$	Crack opening displacements
$\frac{da}{dN}, \frac{dc}{dN}$	Fatigue crack growth rate (FCGR)
C, m, p and q	Constant related to fatigue crack growth model
M_c	Bending moment at the cracked section of the I-beam

M_e	Bending moment due to the mechanical load on the I-beam
M_a and M_P	Bending moment produced due to the piezoelectric actuation
M	Bending moment produced in a plate under bending
F_P	Force developed in a structure due to the actuation by bonded piezoelectric actuators
N	Axial force applied to the I-beam.
P	Point load on the cracked plate under three point bending scenario
V	Applied voltage
V_{max}	Maximum applied voltage
V_{min}	Minimum applied voltage
ΔV	Difference in voltage $(V_{max} - V_{min})$
υ	Poisson's ratio of the specimen
β	Shear stress transfer length
$\sigma_{Piezo}(x)$	Stress produced by the piezoelectric patch
σ_p	Bending stress produced by piezoelectric actuation
$(\sigma_{Piezo})_{max}$	Maximum stress produced by the piezoelectric patch under V_{max}
$(\sigma_{Piezo})_{min}$	Minimum stress produced by the piezoelectric patch under V_{min}
$\Delta\sigma_{Piezo}$	Range of stress produced by the piezoelectric patch $[(\sigma_{Piezo})_{max} - (\sigma_{Piezo})_{min}]$
σ_{max}	Maximum applied stress
σ_{min}	Minimum applied stress
$\Delta\sigma$	Stress range $(\sigma_{max} - \sigma_{min})$
σ_0	Uniaxial tensile load
σ	Stress developed in a plate under bending
σ_P	Reduced stress at the crack plane after fixing the patch
σ_R	Stress developed in the patch
σ_y	Stress distribution along the loading direction in the presence of elliptical hole
σ_0	Tensile stress
ρ	Radius of curvature or the radius of the auxiliary circle at a point on the ellipse
Λ	Piezoelectric strain
ψ	Non-dimensional parameter related to stress developed by piezoelectric patch
α	A constant related to piezoelectric stress
ζ and ξ	Parameters related to the geometry of the I-beam

$\lambda_1, \lambda_2, \eta_1$ and η_2	Parameters related to the beam geometry and crack length

Subscripts

c	Cracked-section of the I-beam
uc	Uncracked-section of the I-beam
s	Specimen
p	Piezoelectric patch

Abbreviations

AR	Aspect ratio of the elliptical hole
BCF	Bending Correction Factor
FCGR	Fatigue Crack Growth Rate
GCF	Geometry Correction Factor
LEFM	Linear Elastic Fracture Mechanics
SIF	Stress Intensity Factor
WFM	Weight Function Method

Contents

This page is intentionally left blank

List of Figures

This page is intentionally left blank

List of Tables

This page is intentionally left blank

Chapter 1

INTRODUCTION

1.1 Background and Motivation

Structural integrity is a critical concern across various engineering disciplines, as components and structures are subjected to cyclic loading, environmental effects, and operational stresses that can lead to crack initiation and propagation. Cracks are harmful to the performance and longevity of structural components, leading to catastrophic failures if not addressed efficiently. The presence of cracks significantly reduces the load-bearing capacity of structures, accelerates material degradation, and, in many cases, results in unexpected breakdowns. Understanding the behavior of materials under these conditions is essential for designing reliable and safe structures that can withstand these challenges. Engineers must carefully analyze and predict how different materials will respond to these factors in order to prevent catastrophic failures. By effectively repairing cracks in structures, engineers can prolong the lifespan of the materials and prevent further deterioration. Therefore, the development of efficient crack repair techniques is imperative to ensure the safety, reliability, and service life of engineering structures.

Cracks in structural components can originate from several sources, including manufacturing defects, material imperfections, thermal stresses, fatigue loading, and accidental impacts. Once a crack forms, it propagates under cyclic loading, leading to progressive material failure. The severity of a crack depends on several factors, including its size, shape, location, and orientation relative to the applied load. Cracks tend to grow due to stress concentration at their tips, accelerating structural degradation. The stress intensity factor (SIF) governs crack growth behavior, and if it exceeds the critical fracture toughness of the material, rapid fracture can occur. Structural failures due to fatigue cracks have been widely recognized in aerospace, automotive, civil, and marine engineering applications. Aircraft fuselage components, bridges, offshore platforms, and railway tracks are particularly susceptible to fatigue-related failures. Cracks can cause catastrophic consequences without appropriate mitigation strategies, leading to human casualties, financial losses, and environmental hazards. Thus, developing robust crack repair methods is essential to enhance the fatigue life of structures and prevent failures.

Mitigating the effects of cracks is crucial to extending the service life of structural components and ensuring operational safety. Several strategies have been developed to address crack formation and propagation, including routine inspections, damage detection techniques, and active and passive repair methods. Crack repair methods aim to arrest crack growth, reduce stress concentration at the crack tip, or enhance the structural integrity of the damaged component. Traditional repair techniques, such as composite patching, stop-hole drilling, welding etc. have been extensively used, but they have inherent limitations that demand exploring more advanced and efficient repair methods.

The need for durable structures across various engineering fields has significantly influenced the evolution of crack repair techniques. Initially, manual methods like riveting and mechanical fastening were prevalent for aircraft and ship repairs in the early 20^{th} century. The mid-20^{th} century saw the rise of welding, which provided a more substantial solution for repairing metallic components. By the late 20^{th} century, composite patch repair techniques gained attention, especially in aerospace applications where weight reduction and fatigue resistance were critical. Composite patching is a prominent method for repairing cracked metallic and composite structures, introducing adhesive bonding technology allowed for the practical application of composite patches, marking a pivotal advancement in repair methodologies, utilizing bonded composite patches to redistribute stresses and mitigate stress intensity factors at crack tips. These patches are favored in aerospace and marine applications due to their high strength-to-weight ratios and excellent fatigue resistance. However, their effectiveness is influenced by adhesive properties, patch thickness, bonding processes, and environmental factors such as moisture absorption and temperature fluctuations, which can compromise long-term performance. In contrast, welding is a traditional repair technique that restores structural integrity by fusing cracked regions through heat application, followed by post-weld treatments to alleviate residual stresses. Despite extensive use across various industries, welding presents challenges, including potential alterations to material microstructure, the introduction of residual stresses, and the creation of heat-affected zones that may lead to new cracks under cyclic loading. Furthermore, welding is not universally applicable, particularly for high-strength alloys and fatigue-sensitive components. Concurrently, stop-hole techniques became popular for their cost-effectiveness in halting crack propagation in infrastructure maintenance. The stop-hole method offers a straightforward and cost-effective approach to halt crack propagation by drilling a hole at the crack tip and redistributing stress concentrations. While this technique is easy to implement, it serves only as

a temporary fix, as cracks can re-initiate from the drilled hole edges, and it does not enhance the structural strength of the component, limiting its use in critical applications. Shape memory alloys (SMAs) were introduced in the early 21st century as a self-healing mechanism that can return to its original shape upon heating, making them a promising solution for crack repair and enhancing crack mitigation strategies. SMAs can apply compressive forces to crack surfaces when integrated into cracked structures, reducing stress intensity and preventing propagation. Despite their self-healing capabilities and adaptability, the application of SMAs is constrained by high costs, complex manufacturing, and the necessity for precise temperature control to activate their properties. Recently, piezoelectric actuators have emerged, providing real-time stress control and adaptive repair capabilities. Integrating innovative materials, real-time monitoring systems, and automated technologies have transformed crack repair methodologies, advancing the way for more efficient and sustainable engineering solutions.

Piezoelectric materials, which can convert electrical energy into mechanical strain, have emerged as a promising solution for active crack repair over conventional methods. Unlike passive repair methods, piezoelectric actuators offer real-time control over stress distribution in cracked structures. Piezoelectric actuators induce strain in the material by applying an external voltage, counteracting the stress concentration at the crack tip, and effectively reducing the stress intensity factor (SIF). This approach enables adaptive crack repair, providing a dynamic and efficient solution to mitigate crack-related failures. Furthermore, integration with structural health monitoring (SHM) enables real-time crack growth detection and mitigation, with the actuators adapting to changing load conditions via voltage adjustments to prevent further propagation. Piezoelectric actuators' lightweight and non-intrusive nature minimizes structural design modifications, contrasting with welding or composite patching methods, which may alter material properties or increase weight. Consequently, these actuators' continuous stress distribution adjustment significantly enhances structural integrity, particularly in applications with repeated loading cycles, such as aerospace and automotive structures. Finally, their minimal energy requirements and potential for integration with renewable energy sources, like vibration energy harvesting, contribute to energy efficiency and sustainability in long-term applications.

This thesis is motivated by the critical need for effective crack repair techniques to ensure the safety and longevity of engineering structures subjected to cyclic loading and environmental effects. Traditional crack repair methods have limitations, prompting the exploration of more advanced solutions. This thesis investigates the potential of piezoelectric actuators for active

crack repair, aiming to leverage their ability to dynamically control stress distribution and enhance fatigue resistance in cracked structures. This approach seeks to overcome the limitations of passive repair methods and provide a more efficient and sustainable solution for structural health management.

1.2 Literature Review

Traditional repair methods like welding and bolting face stress concentration and durability limitations. Modern research explores innovative solutions, such as shape memory alloys and piezoelectric actuators, which enhance structural performance. Piezoelectric actuators enable real-time stress mitigation and load redistribution, which have been proven effective through various studies. An extensive literature review in connection to the related area of work in the present thesis is explained in the current section. This literature review explores the role of fracture mechanics associated with the repair technique as the repair capability is assessed through the reduction of the stress intensity factor (SIF), followed by the discussion of the current state of research concerning different aspects of repairing structural components with a specific focus on the application of piezoelectric actuators.

1.2.1 Significance of Fracture Mechanics in Repair Technique Evaluation

The evaluation of structural repair techniques for cracked components is fundamentally based on fracture mechanics and fatigue crack propagation principles. Cracks significantly reduce the load-bearing capacity of the structure and increase the risk of failure, particularly under cyclic loading conditions. Fracture mechanics offers a comprehensive analytical framework for understanding crack initiation and propagation, allowing for the quantification of the forces driving these processes. Fatigue crack propagation occurs over time due to repeated stress cycles and is crucial for measuring long-term structural integrity. When a crack forms, it creates a stress concentration at its tip, leading to potential propagation if the stress intensity factor (SIF, K_I) exceeds the fracture toughness (K_{IC}) of the material. This critical limit is a key material property that predicts failure conditions [Dowling et al. (2021)]. The analysis of crack behavior typically employs Linear Elastic Fracture Mechanics (LEFM) and Elastic-Plastic Fracture Mechanics (EPFM). LEFM is suitable for scenarios where the tiny plastic zone at the crack tip allows linear elastic analysis. Conversely, EPFM is necessary for cases involving significant plastic deformation, often seen in ductile materials or under high loads. The J-integral in EPFM quantifies the energy available for crack growth, while the energy release rate (G) defines the energy available for crack extension per unit area. Crack propagation becomes

likely when G exceeds its critical limit (G_C), which can lead to catastrophic failure [Anderson (2017), Broek (1982)]. Non-destructive testing (NDT) methods, such as ultrasonic and radiographic testing, are essential for evaluating the integrity of repaired structures and monitoring crack growth. These techniques enable early defect detection, facilitating proactive maintenance. By integrating fracture mechanics with NDT, decision-making is enhanced, repair strategies are optimized, and overall structural reliability is improved [Ahmad and Bond (2018)].

The Stress Intensity Factor (SIF) is a critical parameter in fracture mechanics that characterizes the stress state near a crack tip and is essential for predicting crack growth and fatigue life [Anderson (2017)]. Accurate SIF calculations inform whether a crack will propagate or remain stable under applied loads. Various methods have been developed for SIF determination, including analytical, numerical, experimental, and hybrid techniques like the weight function method and the superposition principle, each with distinct strengths and limitations based on crack configuration, material properties, and loading conditions. Analytical solutions provide exact SIF expressions for simple geometries, typically derived from linear elastic fracture mechanics (LEFM). The most prevalent analytical approach stems from Irwin's (1957) stress field equations, utilizing conformal mapping, Westergaard functions, or complex variable techniques [Tada et al. (2000)]. Solutions exist for standard cases, such as edge-cracked plates and center-cracked panels, but these methods are limited to idealized geometries and loading conditions. Although analytical methods yield quick results, their application is confined to scenarios with well-defined boundary conditions. Numerical methods, particularly Finite Element Analysis (FEA), are extensively used for complex geometries and loading conditions. FEA computes stress fields near crack tips using mesh refinement strategies, including quarter-point and singularity elements [Raju and Newman (1979)]. Techniques like the J-integral, displacement correlation method, and virtual crack closure technique (VCCT) are commonly employed for SIF extraction [Anderson (2017)]. The accuracy of FEA depends on mesh density and element type, with adaptive meshing strategies enhancing precision. The Boundary Element Method (BEM) is another effective numerical approach, particularly for infinite domains, requiring discretization only on boundaries [Aliabadi (2003)]. Despite being computationally intensive, numerical methods offer high accuracy and flexibility for real-world applications. Hybrid approaches combining FEA and BEM have been explored to leverage the strengths of both techniques. The weight function method provides rapid SIF estimation across various loading conditions without extensive computational resources, although its

applicability relies on precomputed weight functions [Shivakumar and Raju (1992)]. The superposition principle simplifies complex loading scenarios by decomposing them into simpler cases with known SIF solutions, which is beneficial for mixed-mode fracture analysis [Rice (1968)]. SIF calculation methods have evolved from classical analytical techniques to advanced numerical and experimental methodologies. The method choice hinges on the geometry's complexity, loading conditions, and required accuracy. While analytical and weight function methods are efficient for simpler cases, numerical and experimental techniques offer greater flexibility for real-world applications, with ongoing developments in hybrid methods enhancing SIF determination in engineering practice. This literature review focuses on applying Digital Image Correlation (DIC) in experimental studies to determine Stress Intensity Factors (SIF) in various materials, highlighting the limited use of PZT for reducing SIF and enhancing damage performance. DIC has been recognized for accurately capturing 2D and 3D strain fields, making it suitable for SIF calculations [Tavares et al. (2014)]. Hamam et al. (2007) utilized DIC to assess SIF variations in a steel specimen during fatigue cycles, employing a decomposition of displacement fields onto elastic fields. Mogadpalli and Parameswaran (2008) extended this approach to orthotropic composite materials, analyzing edge-cracked unidirectional fiber composites under tensile loads. They recorded displacement fields using DIC to determine SIF. Richter-Trummer et al. (2010) introduced a methodology for in situ SIF determination in damaged structures, combining DIC with an overdetermined algorithm to enhance measurement accuracy and address rigid body motion challenges. Further applications of DIC include studies on crack propagation in materials such as pure titanium [Mathieu et al. (2012)], where SIF was assessed alongside T-stress and plastic zone size. Tasdemir (2013) employed a single edge-notch bend test on polycarbonate to simultaneously measure mode I SIF, capturing force, displacement, and near-crack images. Tavares et al. (2014) integrated experimental and numerical methods to evaluate SIF for modes I and II based on Linear Elastic Fracture Mechanics (LEFM). Roux-Langlois et al. (2015) simulated fatigue crack growth using Williams' series, validating experimental data through DIC and X-FEM methods, while Harilal et al. (2015) focused on SIF determination in Al 2014-T6 alloy specimens using DIC to analyze strain fields around cracks. Gonzáles et al. (2017) explored SIF and pseudo-SIFs in fatigue cracks, considering factors like crack tip plasticity. Manthiramoorthy and Krishnaveni (2017) applied DIC to determine mode I SIF in compact tension specimens of polycarbonate. Mokhtarishirazabad et al. (2018) presented a structural health monitoring approach using DIC on aluminum alloy 2024-T3 specimens under cyclic loading, aiming to measure SIF continuously. Lastly, Dai et al. (2020) combined DIC with acoustic emission methods to analyze

SIF, crack tip positions, and fracture process zones in concrete specimens subjected to three-point bending. Overall, the reviewed studies demonstrate the versatility and effectiveness of DIC in SIF determination across various materials and loading conditions while also indicating a gap in applying PZT to enhance damage performance [Yoneyama et al. (2006)].

The progression of fatigue cracks, which is a process that is both progressive and time-dependent, has a significant impact on the durability and longevity of components that have been repaired. Even when the material is subjected to stress levels lower than its yield strength, cyclic loading can cause cracks that gradually propagate throughout the material [Dowling et al. (2021), Suresh (1998)]. Paris' Law, a relationship based on empirical data, establishes a correlation between the fatigue crack growth rate (da/dN) and the stress intensity factor (ΔK) range. This relationship is a powerful predictive tool for estimating the remaining fatigue life of structures that have been repaired [Paris and Erdogan (1963)]. There is a direct correlation between the efficacy of a repair technique and its capacity to effectively reduce the value of ΔK, significantly slowing down the propagation of cracks. Factors influencing fatigue crack growth include the stress ratio (SR), intrinsic material properties, loading frequency, and environmental conditions. Understanding fracture mechanics and fatigue crack propagation is imperative for developing advanced repair methodologies. Each repair technique reduces the stress intensity factor at the crack tip, preventing further crack propagation. Fracture mechanics principles allow engineers to quantify these effects and select the most effective repair strategy. By analyzing SIF analysis, energy release rate assessments, and fatigue crack growth predictions, engineers can create optimized repair strategies to ensure that repaired components maintain structural integrity under operational loads.

1.2.2 Review of Conventional and Advanced Repair Techniques

Various crack repair techniques have been developed to ensure the longevity and reliability of engineering structures. These techniques can be broadly categorized into conventional (passive) and advanced (active) methods. This section comprehensively reviews both approaches, highlighting their advantages, limitations, and recent advancements. Welding is one of the most commonly used repair techniques for cracked metallic structures [Al-Karawi et al. (2020), Rodríguez-Sánchez et al. (2011)]. The primary advantage of welding is the complete fusion of the material, restoring the mechanical integrity of the component. However, it needs careful execution to avoid residual stresses and microstructural changes that accelerate fatigue damage [Guo and Li (2024)]. Post-weld heat treatments are often necessary to ensure longevity [Gurney (1979)]. Mechanical fastening is widely used in aerospace and automotive

industries to repair structural cracks [Chan and Vedhagiri (2001), Kradinov et al. (2002)]. This method involves attaching reinforcements using bolts or rivets, such as doubler plates or straps. The fasteners redistribute the load, reducing the crack tip's stress intensity. However, bolted repairs often lead to a stress concentration around the fastener holes, which can initiate secondary cracks. Additionally, this method increases the structure's weight and may affect its aerodynamic properties in aircraft applications. Stop drilling is a temporary crack mitigation technique where a hole is drilled at the crack tip to reduce stress concentration and slow down crack propagation [Ayatollahi et al. (2014)]. This method is often used with other repair techniques, such as bonding or bolted reinforcements. However, extensive drilling and machining may be required for bolting, resulting in additional material removal and structural weakness [Li et al. (2021)]. Adhesive bonding involves using high-strength epoxy resins or polymer-based adhesives to bond composite or metallic patches over cracks, commonly applied in aircraft structural repair. This technique distributes stresses over a larger area, reducing stress intensity factors (SIF) and enhancing fatigue resistance [Chan and Vedhagiri (2001), Colombi and Fava (2015), Davis and Bond (1999), Mohammadi et al. (2021), Park et al. (1992), Tsamasphyros et al. (2001), Yu and Wu (2017, 2018)]. Composite patch repair with carbon-fiber-reinforced polymer (CFRP) has effectively reduced crack propagation and increased structural integrity [Hasegawa et al. (2015), Li et al. (2021), Liu et al. (2022), Mohammadi et al. (2021)]. Studies indicate that double-sided repairs provide significantly better fatigue resistance and SIF reduction than single-sided repairs [Ouinas et al. (2007)]. Finite element analyses have demonstrated that repairing a structure on both sides can halve the SIF compared to single-sided repairs, improving load distribution and slowing crack growth ([Errouane et al. (2014), Wang et al. (2018)]. Experimental assessments of single- and double-sided repairs in aircraft structures further confirm that two-sided reinforcement maintains structural integrity by limiting out-of-plane bending and crack propagation [Duong et al. (2006), Duong and Wang (2004), Li et al. (2020)]. Hybrid composite patches have proven effective in repairing cracked components, especially in aluminum and steel structures [Valadi et al. (2020). Additionally, stop-hole techniques—where symmetrical holes are drilled along a crack's path—help reduce stress concentration and crack growth rates [Ayatollahi et al. (2014)]. Studies have demonstrated that combining FRP reinforcement with stop-hole techniques enhances fatigue life, particularly in steel structures under cyclic loading [Liu et al. (2009)]. Prestressing CFRP patches in repairs has improved fatigue by minimizing residual stresses and crack growth rates [Ghafoori et al. (2012)]. Finite element modeling indicates that prestressed CFRP-wrapped steel pipes with through-wall cracks reduce SIF significantly, strengthening structural integrity

[Kong et al. (2023)]. Adhesive-bonded repairs significantly extend fatigue life by redistributing stress and delaying crack propagation. In particular, CFRP and glass-fiber-reinforced polymer (GFRP) patches have been shown to enhance fatigue performance by reducing stress intensity at crack tips [Chen et al. (2018), Ghafoori et al. (2012), Hafiz and Wahab (2015), Huang et al. (2022)]. However, environmental factors such as moisture and high temperatures can degrade the bond quality, necessitating careful adhesive selection and environmental protection [Kondratiev et al. (2021), Tan et al., (2021)]

The rise of active repair techniques such as shape memory alloy (SMA) and Piezoelectric materials has been facilitated by advancements in material science [Wang and Wu (2012)]. SMAs, such as Ni-Ti alloys, have gathered attention for their ability to induce compressive stresses around crack tips, thereby reducing crack propagation forces. Shape memory alloys (SMAs) can be used to apply compressive stresses at crack tips, retarding crack growth by changing their shape upon heating and reducing the SIF. Combining prestressed CFRP and shape memory alloys (SMA) further enhances crack-arresting effects [Deng et al. (2023)]. However, their temperature-dependent effectiveness may limit their applicability in certain conditions, and techniques require precise control and may not be suitable for large-scale structures. Piezoelectric actuators present a dynamic solution for active crack repair [Aabid et al. (2022, 2023)]. When subjected to an electric field, these actuators generate localized compressive stresses that reduce SIF at crack tips. Recent studies have shown that applying appropriate voltage levels to bonded piezoelectric patches can significantly extend the fatigue life of cracked components. Furthermore, piezoelectric materials can be integrated with structural health monitoring systems for real-time damage detection and repair. However, crack repair techniques are evolving, with conventional and advanced methods playing crucial roles in maintaining structural integrity. Crack repair techniques have evolved from conventional passive to advanced active control strategies. While traditional approaches such as welding and adhesive bonding remain widely used, innovative materials like SMAs and piezoelectric actuators pave the way for next-generation repair solutions. Additionally, hybrid repair approaches combining multiple techniques could offer enhanced durability and efficiency in structural repair and fatigue life extension.

1.2.3 Fundamentals and Application of Piezoelectric Materials

Piezoelectric materials exhibit a unique electromechanical coupling phenomenon, enabling the direct conversion between mechanical stress and electrical potential. This fundamental property, governed by the piezoelectric effect, has facilitated extensive application

across multiple domains, including structural health monitoring, adaptive control, energy harvesting, and active vibration suppression. The continual advancement in material engineering, computational modeling, and fabrication techniques has further expanded the capabilities of piezoelectric materials, making them integral to developing intelligent structures, biomedical devices, and energy-autonomous systems.

The operational principle of piezoelectric materials is based on their ability to generate an electric charge in response to applied mechanical stress (direct piezoelectric effect) and to undergo mechanical deformation upon exposure to an electric field (inverse piezoelectric effect). This bidirectional coupling is exploited in various sensing and actuation applications. Among commercially available piezoelectric materials, Lead Zirconate Titanate (PZT) remains the most widely utilized due to its high piezoelectric coefficient, dielectric permittivity, and electromechanical coupling efficiency [Arnau and Soares (2008), Badr and Ali (2011), Nogas-Ćwikiel (2011)]. Unlike polymer-based materials such as PVDF, which offer flexibility but limited actuation strength, PZT provides high actuation capacity across a wide frequency range. Although alternatives like LT, SPN [Bafandeh et al. (2015)], PMN [Nijmeijer et al. (1997)], and LMN [Taeyong Lee and Lakes (2001)] have specific advantages, PZT's superior performance, reliability, cost-effectiveness, and ease of integration with both metallic and composite substrates make it the optimal choice. The constitutive equations governing piezoelectricity establish the relationship between mechanical stress, strain, electric field, and polarization, forming the foundation for the mathematical modeling of piezoelectric-based systems [Hall (2001)]. The modeling of piezoelectric behavior involves coupled electromechanical equations governed by constitutive relationships, where the electric displacement and strain depend on applied electric fields and stresses, respectively [Liu (2008)]. These equations allow for precise predictions of material behavior under complex loading conditions, facilitating the optimization of piezoelectric devices for specific applications. Several models, such as the Rayleigh-Ritz approximation and finite element-based electromechanical coupling models, have been proposed to predict piezoelectric behavior in real-world applications [Duan et al. (2010)]. However, piezoelectric properties are temperature and frequency-dependent, affecting performance in high-temperature applications or dynamic loading conditions [Alaimo et al. (2011)]. Furthermore, frequency-dependent performance variations impact their suitability for ultrasonics, vibration control, and guided wave applications [Park et al. (2003)].

Piezoelectric sensors play a crucial role in SHM by detecting structural damage and assessing integrity. Piezoelectric sensors leverage the direct piezoelectric effect to transduce

mechanical deformations into electrical signals, making them highly effective for structural health monitoring (SHM) [Duan et al. (2010)]. These sensors are widely employed to detect variations in stress distribution, crack propagation, and delamination in composite materials. Inoue et al. (2015) examined the performance of PZT bimorph structures in enhancing sensitivity, demonstrating that an increase in layer thickness significantly improves voltage output. Similarly, Wang (2010) analyzed piezoelectric sensor configurations in simply supported beams, underscoring their applicability in real-time strain monitoring. These findings highlight the efficacy of piezoelectric sensors in ensuring the structural integrity of critical components, particularly in aerospace and civil infrastructure applications. Additionally, advanced distributed sensor networks, wireless sensor technology, and data fusion techniques have enabled real-time damage detection and prognosis, allowing for predictive maintenance strategies that enhance safety and operational efficiency. Impedance-based SHM relies on the electromechanical impedance (EMI) technique, where changes in impedance spectra indicate structural degradation [Park et al. (2003)]. Roy et al. (2021a, 2021b) developed an analytical model and finite element analysis to monitor damage in short and slender beams and presented non-destructive methods to identify cracks in structural components using a piezoelectric sensor.

Piezoelectric materials have been extensively investigated for energy harvesting, wherein ambient mechanical vibrations are converted into usable electrical energy. This approach is advantageous for powering autonomous sensing systems and wireless communication devices. Integrating PZT-based harvesters into microelectromechanical systems (MEMS) has facilitated the miniaturization of self-sustaining sensor networks [Aabid et al. (2021), Elahi (2021)]. Additionally, advances in composite piezoelectric materials with enhanced flexibility and superior electromechanical coefficients have significantly improved the efficiency of energy harvesting mechanisms. Recent studies have also explored hybrid configurations incorporating multiple energy conversion modalities to optimize energy capture and storage capabilities. Emerging research is focused on enhancing the durability and efficiency of piezoelectric energy harvesters through advanced materials, such as graphene-based piezoelectric composites and flexible polymer-based harvesters, which exhibit high mechanical compliance while maintaining energy conversion efficiency. Furthermore, integrating energy harvesting modules with low-power electronics has enabled the development of self-powered sensor networks for aerospace, biomedical, and environmental applications.

Piezoelectric actuators are integral to active structural control strategies, offering precise and rapid response to externally applied voltages. These actuators are extensively employed for shape morphing, vibration reduction, and fatigue crack mitigation. The theoretical framework for piezoelectric control is based in the electromechanical constitutive relations, which define the interaction between mechanical displacement and applied electric potential [Chee et al. (1998)]. Active damping techniques involve the integration of piezoelectric actuators with feedback control systems to mitigate resonant vibrations and noise [Duan et al. 2010). Moreover, piezoelectric actuators have been widely adopted in aerospace and automotive applications for enhancing structural resilience and optimizing performance under dynamic loading conditions [Abuzaid et al. (2015b)]. Recent advancements in adaptive control algorithms and machine learning techniques have enabled real-time optimization of piezoelectric actuator performance, further improving their efficacy in mitigating structural vibrations [Lin et al. (2013)]. Piezoelectric materials, especially PZT-based ones, are crucial in sensing, actuation, energy harvesting, and active control applications due to their high sensitivity, low power consumption, and real-time monitoring capabilities.

1.2.4 Piezoelectric Actuators based Active Repair/Control Techniques

Piezoelectric actuators are extensively used for active control applications, including vibration suppression, shape adaptation, and crack mitigation. The literature on PZT-based active repair/control techniques primarily focuses on three key approaches: analytical methods, numerical simulations, and experimental validation. By strategically integrating PZT actuators within damaged structures, previous researchers have demonstrated significant improvements in structural integrity, load-bearing capacity, and overall durability. The combination of analytical, numerical, and experimental approaches has enabled a comprehensive understanding of the interaction between electromechanical forces and fracture mechanics, thereby advancing repair strategies.

Several analytical models have been developed to assess the impact of PZT actuators on the stress intensity factor (SIF) of cracked structures. Theoretically, theoretical frameworks have used fracture mechanics models to include the electromechanical interaction that PZT patches cause. Much work has been done using weight function techniques and J-integral formulations to determine how much the stress intensity factor (SIF) goes down when PZT actuators are used [Kumar (2018)]. Crawley and De Luis (1987) made static and dynamic models to see how voltage affects controlling the behavior of structures with piezoelectric patches for smart systems. They also conducted a scaling analysis to compare the efficiency of

different piezoelectric materials in transmitting strain to the substructure. A study by Alaimo et al. (2009) used a multidomain approach to create a two-dimensional boundary integral formulation that could model cracks and combine piezoelectric patches with structures. Their analysis considers perfect and imperfect adhesive interfaces, employing a "spring model" for traction-displacement relationships. The study was expanded to examine how things change over time by combining piezoelectric and elastic coupling and measuring dynamic stress intensity factors using the dual reciprocity method. The focus was on how changes in dynamic conditions affect how well piezoelectric crack repair works [Alaimo et al. (2011)]. Liu (2007) explored using multi-layered piezoelectric patches for repairing cracked structures using two-dimensional finite element analyses. Results show that lower repair voltages are more efficient and safer, while factors like crack contact conditions and friction have minimal impact. The optimal design choices involve increasing layers, extending patch length, and minimizing thickness. Based on this, they introduced two repair criteria: slope continuity and fracture mechanics [Liu (2008a)]. It is emphasized how important it is to look at crack tip fields and contact conditions in order to figure out the repair voltage accurately. It is also confirmed that using higher voltages might hurt the results of the repair. An investigation was conducted regarding applying piezoelectric actuators to mitigate stress concentration around a hole [Shah et al. (1994)]. The SCF value around a hole in a cylinder can be considerably diminished through the strategic placement of actuators [Allahyari and Golabi (2020)]. Roy et al. (2023) conducted a study to find out how bad a crack was using sensing tools and developed a way to restore dynamic responsiveness using steady-state vibration analysis and piezoelectric material. Wang et al. (2013c) looked into the shear effect of a crack at the interface between a piezoelectric actuator and an elastic substrate. They formulated a way to understand the stresses and energy release rates at the crack interface in a piezoelectric composite adhesive, and they discussed about how electrical loading, geometry, and material mismatch affect this. Fesharaki et al. (2015, 2016, 2017, 2020) aimed to find the best placement of piezoelectric patches to reduce stress concentration in plates under tension. They used particle swarm optimization to analyze patch area, voltage, and stiffness ratios. Results showed that optimal patch locations depend on stiffness and thickness ratios. The study also identified different actuator placement models based on stiffness ratios, demonstrating their effectiveness in stress reduction across different plate types.

Wang and Quek (2004) looked into how piezoelectric patches could be used to fix delaminated beams while they were being loaded statically. They focused on reducing shear

stress singularities at the tips of the delamination by looking at fracture mechanics. They conducted fracture mechanics analysis to determine the necessary voltages for effective repair. They also extended their work to investigate piezoelectric layers for repairing delaminated beams under compressive forces, eliminating stress discontinuities that can lead to fracture. The right voltage setting for the piezoelectric layers and testing of the buckling load of delaminated beams in different situations have been suggested [Wang et al. (2005)]. Another study suggested a design for discrete electrodes on the patches, calculating the necessary voltages and examining how these voltages affect the size and location of the delamination Wu and Wang (2010a). Another work by Duan et al. (2008) presented a methodology for using piezoelectric patches to repair delaminated beams under static loading, addressing singularity caused by shear stresses. They conducted parametric studies to demonstrate the effectiveness of the repair methodology and proposed an index for assessing repair effectiveness. Shindo et al. (2013) looked into how piezoelectric actuators could control delamination in woven fabric composites when loaded in Mode I. They specifically considered a double cantilever beam (DCB) specimen made of woven glass fiber reinforced polymer (GFRP). This study included finite element analysis to compare predictions with experimental results and investigate how actuator placement affects the effectiveness of the repair. Later, this study discussed how woven glass fiber-reinforced polymer composites delaminated when loaded with piezoelectric actuators in Mode I at cryogenic temperatures. It showed that piezoelectric control is a good way to handle delamination at liquid nitrogen temperatures [Shindo et al. (2013). Rabinovitch (2007) investigated how piezoelectric materials could control edge stresses and stop debonding failure in reinforced concrete beams that were strengthened with composite materials. A mathematical model was also created to test how well piezoelectric actuators work at creating counteracting stresses, which solves problems in civil engineering applications. Narayanan and Balamurugan (2003) presented a model for laminated structures with integrated piezoelectric sensors and actuators, accounting for temperature effects and electromechanical coupling. The study looked at different ways to control active vibration and found that the linear quadratic regulator (LQR) method works best, especially for lowering peak voltages in piezo actuator layers. While Wu and Wang (2010b) conducted a closed-loop feedback control repair method for delaminated beam structures, they used piezoelectric patches to create local shear forces and reduce stress singularities in cases of different delamination sizes and alignments. Alaimo et al. (2016) suggested a one-dimensional method for layered smart beams that uses Hermite shape functions and state space representation for first-order shear deformation beam theory and electro-elastic couplings to improve the simulation of passive and active vibration-damping systems. Wang

(2002) derived an equation that describes the piezoelectric effect in columns and used the direct difference method to solve an eigenvalue problem. This showed that the column structure's ability to bend can be greatly increased by carefully placing the piezoelectric layers and applying the right voltages. Wang and Chase (2003) looked into how piezoelectric materials could be used to improve the buckling strength of composite structures that had fatigue cracks. It suggested an analytical model to determine how crack features affect buckling and showed that small piezoelectric patches can effectively compensate for structural integrity loss. Wang and Quek (2005) looked into the buckling strength of column structures that were cracked and suggested using piezoelectric materials to make the structures stronger so that they could handle less buckling. It used a model to investigate how boundary constraints and sensor placement affect the voltage sent to piezoelectric patches and looked at a crack that caused rotation to stop. Maleki and Mohammadi (2017) analyzed how stable cracked functionally graded material columns are when they are affected by piezoelectric patches. They modeled the crack as a rotational massless spring. This study revealed that the crack reduces load capacity based on location and depth, while strategically placed piezoelectric patches can mitigate these effects and enhance the column's buckling performance under applied voltage. Khiem et al. (2023) conducted a modal analysis of a cracked Timoshenko beam combined with a piezoelectric layer. They examined how the beam's vibrational characteristics affected the crack parameters and material properties. The study proposed a novel indicator for crack detection through modal sensor charge, demonstrating its potential advantages over traditional methods. Wang et al. (2002) presented a method for repairing a cracked beam under external load using a piezoelectric material to induce a local moment that aids in closing the crack for effective repair. The study demonstrated how the required actuation voltage varies with factors such as the distance from the applied force to the crack, the crack's position along the beam, and the thickness ratio of the piezoelectric patch to the beam. Using the perturbation method, Ashtari (2016) devised an analytical answer for how a cracked beam fixed with a piezoelectric patch would bend. A model for calculating the patches' dimensions revealed that the beam's thickness, length, applied load, and crack characteristics all have an impact. Wu and Wang (2011) proposed a method for effectively repairing a notched cantilever beam under dynamic loading using piezoelectric patches. A sensor patch keeps track of the stress concentration, and an actuator patch applies an actuation voltage. Wang (2010) showed a model that used active control methods to stabilize the first two buckling modes of simply supported and cantilevered beams. The piezoelectric actuators and optimal feedback control increased the beams' buckling loads. The results show that the designed linear quadratic regulator (LQR) controller stabilizes

the beams well, and segmented actuators placed in the best way for buckling control work best. Ariaei et al. (2010) devised a way to use piezoelectric patches to fix broken beams when they are under a moving mass. Their method focused on changing the broken beam's first natural frequency to match that of a healthy beam. The research showed that applying an outside voltage to the piezoelectric patch effectively lowers crack singularity, increases beam deflection, and produces results that are very similar to those of a beam that isn't cracked. Cheng et al. (2007) created a new type of composite pipe joint system with piezoelectric layers that made the joint stronger by spreading out stress better under different loads. A detailed investigation of the system's behavior under torsion loading, utilizing theoretical modeling and numerical examples, was carried out by Cheng and Li (2008) to assess the impact of the piezoelectric layers on adhesive layer stresses.

Cheng and Taheri (2005) developed an adhesive joint system using electromechanical piezoelectric patches to control bending moments and reduce stress concentration in the adhesive layer. Their further study [Cheng et al. (2006)] assessed joint strength enhancement through electric field adjustments and piezoelectric sensors/actuators. Khalili et al. (2010) created an adhesively bonded single lap joint to reduce peel and shear stress concentrations by surface bonding piezoelectric patches. They developed an analytical model to assess stress distribution, evaluate the influence of electric fields, and analyze the effects of patch characteristics on joint performance. A study by Jin et al. (2010) investigated how partially deboned adhesive layers affected the electromechanical behavior of piezoelectric actuators when subjected to high-frequency loads. They proposed a model that simulates shear deformation, explaining its effects on the actuators' dynamic response and stress transfer mechanisms. Jin and Wang (2011) investigated an analytical study to comprehend how the mechanical and geometrical properties of the adhesive layer affect the electromechanical behavior of a piezoceramic actuator, focusing on interfacial debonding and its influence on the layered structure's response. Abuzaid et al. (2020) examined how piezoelectric actuators could change stress concentration factors (SCFs) in aluminum plates with half-circle notches. Their findings demonstrated that SCFs decrease linearly with active piezoelectric actuators, enhancing structural load-carrying capacity. Also, another study showed an analytical model for the mode-I stress intensity factor in cracked plates with bonded piezoelectric actuators. It showed that these actuators could reduce the severity of the crack when they were used in the extension mode [Abuzaid et al. (2017a)]. A new geometrical weight function method was formed to figure out the Mode-I stress intensity factor (SIF) for using piezoelectric actuators to

actively fix a plate that has a crack along one edge [Abuzaid et al. (2018b)]. The same approach derived the mode-I SIF for active repairs in center-cracked plates [Abuzaid et al. (2018a)]. Kumar et al. (2020b) explored piezoelectric materials for repairing cracks in structures subjected to thermo-mechanical loading, demonstrating that double patches are more effective than single ones. In addition, optimal voltage and patch placement were evaluated for enhanced crack repair efficacy.

The finite element method is widely used in engineering, particularly for structural analysis and repair techniques. This portion of the literature review investigates the application of the finite element (FE) method in active repair techniques employing piezoelectric (PZT) patches. Recent advancements in commercial software, particularly ABAQUS, ANSYS, and COMSOL Multiphysics, offer coupled electro-mechanical simulations to model and simulate piezoelectric-actuated crack repair mechanisms. One of the numerical modeling methods is coupled field analysis, which looks at how stress is distributed by combining the electromechanical properties of piezoelectric materials with the structural analysis framework. The second part of the Fracture Mechanics Approach uses Virtual Crack Closure Techniques (VCCT) and contour integral methods to figure out the stress intensity factor (SIF) values for different loading conditions. Early research in fracture mechanics, like that by Chan et al. (1970) and Rybicki and Kanninen (1977), laid the groundwork for using finite element methods to find stress intensity factors (SIF) at crack tips. This foundation has since been built upon and expanded in numerous subsequent studies. Subsequent studies explored dynamic load repairs on cracked structures through electromechanical admittance approaches, employing 3D FEM modeling [Providakis (2007)]. The results demonstrated improved load-bearing capacity and crack closure in the structures. Caimmi and Pavan (2013) made a further contribution by using FE models and linear elastic fracture mechanics (LEFM) to study single-fiber composite fractures and check SIF across crack fronts. Their study found that the fiber-matrix interface properties greatly influenced the fracture behavior. Recent research has focused on integrating PZT patches for structural repair. Platz et al. (2011) found the best places to put patches to lower the cyclic stress intensity near crack tips. Abuzaid et al. (2015a, 2015b) looked at how changes in adhesive shear modulus affect nodal stress distributions. In their subsequent work, [Abuzaid et al. (2017b)] utilized ANSYS's SOLID226 element to model PZT patches, revealing the significance of adhesive properties on repair performance under mode I crack propagation. More research into PZT patch configurations, like that by Kumar et al. (2020a), showed that different repair methods work well on orthotropic composite plates. Studies have shown that

PZT actuators can enhance surface integrity and delay crack initiation under extreme loads [Zaccardi et al. (2022)]. Additionally, the combination of patch configurations and PZT actuators has proven to be highly effective in improving the structural integrity of orthotropic composite plates. Duan et al. (2008) used ABAQUS to look at delaminated beams under static loads and moment equilibrium methods to test PZT-based active repairs. Duan et al. (2008) looked into how PZT patches could create local shear forces on delaminated sections and used FE methods to prove the design worked. The results demonstrated significant improvements in the structural integrity of the delaminated beams. The virtual crack closure technique (VCCT) has further been implemented to model delamination in composite materials with PZT patches [Orifici and Krueger (2012)], while Shindo et al. (2013a) investigated PZT actuator control over delamination in CFRP laminates under mode I loading, including experiments at cryogenic temperatures [Shindo et al. (2013b)]. Their work calculated strain energy release rates (SERR) based on stress and displacement metrics at crack fronts. Computational models incorporating PZT actuator properties, stress distributions, and dynamic loading conditions have been widely developed by Zhu and Liu (2021). The extended finite element method (XFEM) has been instrumental in simulating crack growth in repaired structures, revealing that optimal voltage application significantly decreases SIF [Kumar et al. (2021)]. Numerical simulations on a cracked cantilever beam reveal that the adhesive layer significantly influences repair performance, requiring higher voltages for imperfect bonds [Alaimo et al. (2009)]. These studies collectively highlighted the importance of patch dimensions and voltage variations in optimal repair outcomes, emphasizing the versatility and effectiveness of the FE method in conjunction with PZT patches for structural repair.

Numerous experimental methodologies have been conducted regarding recent advancements in applying piezoelectric materials, specifically PZT (lead zirconate titanate) patches, for monitoring and repairing structural damage. Recent studies have proposed various methodologies to optimize the measurement of stress intensity factors (SIF) in cracked plates utilizing strain gauges and piezoelectric actuators (PZT). Sarangi et al. (2010b, 2010a) introduced a finite element (FE) technique to determine the optimal locations for strain gauges on aluminum plates, focusing on elastic strain evaluation. Younis and Kang (2011) emphasized the importance of selecting appropriate strain gauges for specific applications, enhancing measurement accuracy through dimensionless curves and a refined hole-drilling method. Platz et al. (2011) explored the effects of PZT-controlled reinforcement near crack tips, demonstrating that mechanical compression can mitigate crack propagation. Wu and Wang (2011) investigated

the impact of bonded PZT actuators on notched cantilever beams under dynamic loads through experiments. Sarangi et al. (2013) further confirmed the significance of optimal strain gauge placement for accurately determining mode I SIF using a single strain gauge training technique. Abuzaid et al. (2018b) conducted experiments on edge-cracked plates repaired with bonded PZT actuators, utilizing strain gauges to measure SIF during mode I crack propagation. Fesharaki et al. (2020) employed a particle swarm optimization (PSO) algorithm to identify optimal PZT actuator patterns in thin plates, demonstrating reduced stress concentrations through experimental and numerical validation. Huynh et al. (2019) developed a PZT-based structural monitoring system for damage detection, integrating experimental and numerical approaches to define the sensing area of PZT materials. Another investigation focused on determining SIFs in cracked plates with bonded PZT actuators subjected to thermo-mechanical loading, revealing significant reductions in SIFs with varying actuator voltages [Kumar et al. (2020b)]. The sensors identified the stress field at the crack tip, and an appropriate voltage was applied to the actuator patch to minimize the severity of the crack. Overall, the literature highlighted a rigorous effort to improve SIF measurement techniques and crack repair methodologies through the innovative application of strain gauges and PZT actuators.

1.3 Research Gap and Objectives of the Thesis

From the literature survey, it is evident that composite and piezoelectric-based static repairs have been effective in reducing crack severity. Moreover, there is a lack of research on how piezoelectric patches improve fatigue life, especially with their passive stiffening effect. Previous studies have focused mainly on static loading conditions and simpler geometries, neglecting the complex interactions between passive and active repair mechanisms under cyclic loading. Exploration in applying active repair techniques to complex geometries such as I-beams, plates with elliptical holes, and arc-shaped specimens is lacking. Furthermore, detailed analysis and validation of fatigue repair techniques using piezoelectric patches with finite element (FE) solutions are required. The lack of research highlights the need for further investigation into the effectiveness of active repair techniques in complex geometries under cyclic loading. Detailed FE analysis and validation are essential to better understand the potential benefits of piezoelectric patches in improving fatigue life. Ultimately, this research will pave the way for developing more reliable and durable structures in the future.

In response to the identified research gap, this thesis undertakes to develop and validate analytical models designed explicitly for piezoelectric-based crack repair. The methodology

begins by establishing the initial state of the cracked structure, where the SIF of unrepaired structure is computed to assess the impact of piezoelectric-based crack repair. After the initial calculation, the passive repair method is applied, with Rose's equations used to determine the corrected SIF by incorporating a bending correction factor. Subsequently, the piezoelectric effect is quantified using the weight function method (WFM) and the surface widening energy release rate, providing a detailed understanding of the stress induced by the piezoelectric material. The superposition principle in LEFM is used to integrate mechanical and piezoelectric contributions, yielding the total post-repair SIF. Under cyclic loading, establishing the SIF range remains essential for understanding the structural response to varying loads. It is determined by assessing the maximum and minimum loads experienced by the structure, offering a comprehensive evaluation of the SIF range for various crack lengths. Ultimately, this determined SIF range forms the basis for computing the fatigue crack growth rate (FCGR). This rate is then utilized to estimate the structure's fatigue life, based on the fatigue crack growth rate (FCGR). This estimation considers the crack's growth progression until it reaches the critical length defined by the material's fracture toughness.

The novelty of this thesis lies in developing the first unified analytical–numerical framework that integrates both passive stiffening and active actuation of piezoelectric patches for fatigue life enhancement under cyclic loading of a double-edged cracked plate. Unlike existing studies limited to static repair and simple geometries, this work extends active repair methodologies to complex structural forms such as bottom-edged cracked I-beam, a crack emanating from the elliptical hole of a plate, an arc-shaped specimen with an edge crack, and an edge-cracked plate under bending. This thesis introduces geometry-specific analytical models coupled with FE validation to accurately quantify SIF reduction and fatigue life improvement.

The main objective of this thesis is to develop and validate analytical models for piezoelectric-based crack repair, focusing on enhancing fatigue life and structural integrity. The following objectives are aimed at the present thesis:

1. To develop and validate an analytical model for hybrid repair (passive and active) of double-edged cracked plates, demonstrating the combined effectiveness of piezoelectric patch stiffness and actuation in reducing the stress intensity factor (SIF) and extending fatigue life under cyclic loading. A parametric study is to be conducted to optimize geometric dimensions and voltage ratios and the performance of hybrid repair with individual passive and active repair methods.

2. To formulate and validate an analytical model for repairing bottom-edge cracked I-beams using piezoelectric patches, accounting for the shifted neutral surface induced by the crack. Evaluation of the SIF and fracture loads under static loading is to be carried out. A parametric study is to be conducted to optimize patch thickness, and the fatigue crack growth rate (FCGR) and fatigue life under varying repair voltages are to be assessed relative to unrepaired conditions.
3. To develop a closed-form analytical solution for the SIF of cracks emanating from elliptical holes in tensile plates repaired with strategically placed piezoelectric actuators. The solution is to be validated through numerical simulations. The effects of elliptical hole geometry, crack propagation characteristics, and actuator configurations on the SIF are to be analyzed, and fatigue crack growth and fatigue life are evaluated for various geometries.
4. To apply Linear Elastic Fracture Mechanics (LEFM) principles to analyze and mitigate fatigue crack growth rates (FCGR) in arc-shaped edge-cracked specimens using piezoelectric patches. The mode-I SIF under actuation is to be determined via the Weight Function Method (WFM). An analytical model for cyclic tensile loading is to be developed, and the influence of repair voltage on the SIF range and FCGR is to be systematically evaluated.
5. To develop and validate an analytical model for repairing edge-cracked plates subjected to bending loads through strategically placed piezoelectric actuators. The SIF is to be computed using Tada's formula combined with the superposition principle. The effectiveness of counteracting bending moments in reducing SIF is to be demonstrated, with model validation performed through ABAQUS simulations.

1.4 Description of the thesis

The application of piezoelectric actuators for active crack repair and fatigue life extension of various structural configurations is investigated in the present thesis. Through analytical investigation and numerical validation, this thesis explores the effectiveness of piezoelectric actuators in reducing the Stress Intensity Factor (SIF), thereby enhancing structural integrity.

Chapter 2 proposes a hybrid repair approach for repairing a double-edged cracked plate using piezoelectric actuators. The problem formulation involves deriving SIF expressions for the cracked plate under different repair conditions—passive, active, and hybrid. The weight function method is utilized to determine SIF under actuation. A methodology is developed to estimate fatigue crack growth rate (FCGR) and fatigue life parameters. Finite Element Analysis

(FEA) is performed in ABAQUS CAE, and the FE results are validated against analogous experimental and numerical data. The discussion on how different parameters, such as voltage ratio, patch thickness, and externally applied voltage, influence the improvement of fatigue life is also reported.

Chapter 3 focuses on the structural integrity enhancement of a bottom-edge cracked I-beam using piezoelectric actuators. The SIF for unrepaired and actively repaired I-beams is derived from the crack surface widening energy release rate, followed by an estimated fracture load and fatigue life. The Finite Element (FE) model of the cracked I-beam with a bonded piezoelectric patch is developed, and mesh sensitivity analysis is conducted for accuracy. Various validation studies are performed to compare the analytical, numerical, and experimental results. The effects of piezoelectric actuator thickness on fracture load and fatigue life are analyzed to assess the viability of active repair in significant structural components. Furthermore, this study extends to repairing cracks emanating from an elliptical hole, a critical scenario in aerospace and mechanical structures.

Chapter 4 uses the weight function to determine the SIF for piezoelectric actuation, followed by the calculation of total SIF using the superposition principle. The estimation of FCGR and fatigue life is carried out to quantify the repair effectiveness. The Finite Element (FE) model incorporates a piezoelectric patch integrated with the cracked specimen, and the results are validated against the present findings. A parametric analysis investigates the influence of repair voltage, patch thickness, crack length, semi-major axis length, and aspect ratio on SIF reduction and fatigue life enhancement.

In the next problem, the repair capability is investigated for an edge-cracked arc-shaped specimen using piezoelectric actuators in Chapter 5. The SIF for cracked and repaired specimens is derived, followed by an estimation of FCGR and fatigue life. The study analyzes the effects of crack length, piezoelectric actuator thickness, and actuator size on the repair effectiveness. The findings provide insights into the viability of using piezoelectric-based repair strategies for curved structural components subjected to cyclic loading.

In Chapter 6, the strengthening of an edge-cracked plate under bending using piezoelectric actuators is addressed. The SIF of the cracked specimen is formulated, and the effectiveness of piezoelectric patch-based repair is evaluated through analytical and numerical methods. Numerical analysis is carried out in ABAQUS to simulate both the cracked and repaired conditions, followed by a validation study. The influence of crack length on the reduction of SIF is discussed in this chapter, and an assessment of the improvement in mechanical performance due to active repair is concluded.

Chapter 2

HYBRID REPAIR OF DOUBLE-EDGED CRACKED PLATE USING PIEZOELECTRIC ACTUATOR

2.1 Introduction

Any damage to a structural component results in its inability to function. Most failures occur due to ongoing fatigue stress, damaging the structure. Moreover, a damaged structure may exhibit increased vibration, a significant decrease in overall loading capacity, and potential complete failure. Damage restoration, such as composite patch repair, piezoelectric actuation, and stop-hole techniques, offers a cost-effective approach to prolonging the lifespan of damaged components. Repairing cracked components involves utilizing various methods, including applying composite patches, leveraging the actuation effect of piezoelectric materials, employing the stop-hole technique, and combining stop-hole and FRP patches to address different loading conditions. Chapter 1 discusses the relevant literature on composite and metallic patches, shape memory alloys (SMAs), and stop-hole techniques for effectively repairing structural failures in the 1.2.2 section. Even though composite patch repair has been widely investigated and proved to be very effective, the severity of the crack cannot be adjusted as the loading scenario changes. As a result, piezoelectric materials have gained popularity due to the ability to control repairs with externally applied voltage as needed. The use of piezoelectric actuators for structural health monitoring and repairing of the cracked component is discussed in Chapter 1 under the 1.2.3 section. Subsequently, the role of piezoelectric actuators in reducing mode-I SIF is discussed in Chapter 1 under Section 1.2.4. The piezoelectric patches efficiently decrease the Stress Intensity Factor (SIF) when activated appropriately. Leveraging the weight function method (WFM) facilitates the formation of a precise analytical model to assess the Stress Intensity Factor (SIF) induced by the piezoelectric actuator stress within the framework of Linear Elastic Fracture Mechanics (LEFM).

The double-edged cracked plate is a crucial geometry among different structural configurations due to its occurrence in critical load-bearing components. Understanding crack propagation and its mitigation in such plates is essential for ensuring long-term structural integrity and safety. Previous research has primarily focused on passive repair using

composite patches for double-edged cracked plates [Wang et al. (2018)], demonstrating significant improvements in structural integrity. However, these methods cannot actively control the crack's severity as loading conditions change. To address this limitation, piezoelectric actuators offer an innovative solution by introducing mechanisms for active repair. However, only a few investigations have revealed the combined effect of piezoelectric materials and other repair techniques. To attain additional benefits from piezoelectric materials, the stiffness effect of the patch can be combined with the active effect when the patch is placed on the cracked surface to reduce the severity of the crack. No analytical model has been developed that combines the passive and active effects (voltage effect) of piezoelectric materials. So, the present research work focuses on proposing a model based on this novel approach and subsequently investigating the influence of passive and active repairs (hybrid repair) on cracked specimens under fatigue loading. One of the advantages of this hybrid repair method is the ability to make a wide range of potential repairs by simply applying one patch on the cracked surface. The passive effect is enough to decrease the Stress Intensity Factor (SIF) and prolong the fatigue life for small crack lengths under low loading conditions. In a critical environment, this can be accomplished by supplying external voltage as required. The cracked plate is modeled using linear elastic fracture mechanics (LEFM). Rose's equation and the Bending Correction Factor (BCF) are used to model the passive repair method. The weight function method (WFM) is being considered for modeling active repair. Paris Law [Paris and Erdogan (1963)] is used to determine the fatigue crack growth rate (FCGR) and the service life of a structure. The developed analytical model for passive and active repair, i.e., hybrid repair, is verified with the FE solutions using ABAQUS. This research is significant as it offers a versatile and effective repair methodology for double-edged cracked plates, improving structural integrity, extending fatigue life, and providing adaptability to varying loading conditions. Integrating passive and active repair mechanisms in the proposed hybrid approach offers a comprehensive solution for fatigue life under various loading conditions, ensuring structural durability and adaptability to different stress levels.

2.2 Problem Formulation

This investigation utilized a double-edge cracked infinite plate under cyclic tensile load for evaluation, as shown in Figure 2.1. To mitigate the influence of the crack, a piezoelectric actuator/patch is placed on the crack surfaces/the high-stress region to utilize the passive and active effects as well. The actuator utilizes an external electric field to induce

compression stress near the cracked front. Due to stress redistribution, it tends to mitigate crack singular stresses, resulting in a reduction in SIF. Because of the linearity of the materials, the superposition concept is used. As long as loading remains uniform, the SIF for linear elastic materials is additive. Thus, the superposition approach permits SIF solutions for complicated configurations to be developed from basic examples with well-established solutions. The width of the crack is taken to be the same as that of the cracked plate. The following sections describe the methodology followed for the analytical model and subsequent analysis.

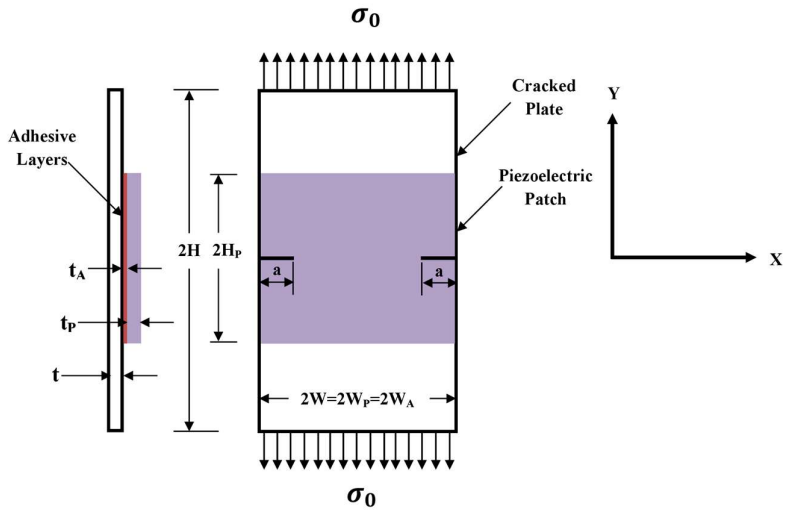

Figure 2.1: Cracked plate repaired with piezoelectric actuator/patch

2.2.1 SIF Calculation for the Cracked Plate

In order to determine SIF, Tada's theoretical approach [Tada et al. (2000)] was employed. The expression of the Mode-I SIF is given by Eq. (2.1) based on linear elastic fracture mechanics (LEFM) of a cracked rectangular plate of infinite size where mode-I is considered the only operative opening mode.

$$K_I = \sigma_0\sqrt{\pi a} \tag{2.1}$$

where σ_0 is the uniaxial tensile stress applied on the cross-section of the plate at an infinite distance (Figure 2.1) with crack length 'a'. When the geometry of the cracked body affects the crack length, considering the non-dimensional geometry correction factor (GCF), $F\left(\frac{a}{W}\right)$, the mode-I SIF may be redefined as Tada et al. (2000),

$$K_I = \sigma_0\sqrt{\pi a}\,.F\left(\frac{a}{W}\right) \tag{2.2}$$

where 'W' is the half-width of the cracked plate and the expression for F $\left(\frac{a}{W}\right)$ is given by,

$$F\left(\frac{a}{W}\right) = \frac{1.122 - 0.561\left(\frac{a}{W}\right) - 0.205\left(\frac{a}{W}\right)^2 + 0.47\left(\frac{a}{W}\right)^3 - 0.19\left(\frac{a}{W}\right)^4}{\sqrt{1-\frac{a}{W}}} \tag{2.3}$$

2.2.2 SIF Reduction via Passive Repair

In the case of passive repair, a cracked structure with a piezoelectric actuator/patch attached to the plate is considered. However, no actuation voltage is applied. Based on the superposition concept, stress distribution between the plate and piezoelectric patch, as shown in Figure 2.2, can be given by,

$$\sigma_0 A = \sigma_P A + \sigma_R A_R \tag{2.4}$$

where σ_P is the reduced effective stress along the potential crack route [Rose and Wang (2002), Wang et al. (2018)] after fixing the piezoelectric patch under uniform uniaxial stress σ_0, σ_R is the stress developed in the patch, A and A_R are the cross-sectional area of the plate and patch, respectively.

Figure 2.2: Stress distribution between the plate and piezoelectric patch

The reduced SIF is given by Eq. (2.5)

$$K_P = \sigma_P\sqrt{\pi a} \tag{2.5}$$

The 1-D theory of bonded joints [Rose (1988)] is utilized to reduce the stress the plate shares and is expressed by Eq. (2.6),

$$\sigma_P = \frac{\sigma_0}{1+S} \tag{2.6}$$

where S is the stiffness ratio between the patch and the cracked plate and is given by

$$S = \frac{E_P \cdot W_P \cdot t_P}{E \cdot W \cdot t} \tag{2.7}$$

where E, W, and t and E_P, W_P, and t_P are Young's modulus, half-width, and thickness of the cracked plate and the piezoelectric patch, respectively.

Shear stress distribution will occur in the y-direction as the patch covers the crack length. [Rice (1972)] described the upper bond SIF for an infinite cracked plate with a physical parameter $\bar{c}$, and the expression is as follows:

$$K_P = \sigma_P \sqrt{\pi \bar{c}} \tag{2.8}$$

where,

$$\bar{c} = \frac{1}{\pi k} \tag{2.9}$$

Where k represents the spring constant and is given by Eq. (2.10)

$$k = \frac{\beta S}{(1+S)(1-\upsilon^2)} \tag{2.10}$$

Where υ represents the Poisson's ratio of the cracked rectangular plate and β represents the shear stress transfer length in a characteristic adhesively bonded joint and is given by Eq. (2.11),

$$\beta = \sqrt{\frac{G_A}{t_A}\left(\frac{1}{E_P t_P} + \frac{1}{Et}\right)} \tag{2.11}$$

Where G_A and $t_A$are the shear modulus and adhesive thickness respectively. From Eq. (2.9) and (2.10), $\bar{c}$ can be written as,

$$\bar{c} = \frac{(1+S)}{S} \cdot \frac{(1-\upsilon^2)}{\pi \beta} \tag{2.12}$$

Because Eq. (2.8) is determined for an infinite crack length, the resultant SIF is for the top bond to the infinite cracked Plate. These estimations are restrained due to the patch's reinforcing effect. As a result, the calculated findings are the lowest SIF bound for an infinite cracked plate reinforced by a single-sided patch [Zheng (2007)]. For an arbitrary crack length, the following equation has been developed to compute the SIF for an infinite cracked plate using a single-sided patch [Rose (1988), Zheng (2007)].

$$K_P = \sigma_P \cdot \sqrt{\frac{\pi a \bar{c}}{a + \bar{c}}} \tag{2.13}$$

When the crack becomes extremely short, the results obtained from Eq. (2.13) are close to the results that were obtained from Eq. (2.1). When the crack's length is relatively long, the calculated results of Eq. (2.13) provide the same findings as Eq. (2.8). This research demonstrates that Eq. (2.13) falls inside the upper and lower bounds as described by Wang et al. (2018).

The equation has been modified considering the geometry of the cracked plate as proposed by Tada et al. (2000).

$$K_P = \sigma_P . \sqrt{\frac{\pi ac}{a+c}} \cdot F\left(\frac{a}{W}\right) \tag{2.14}$$

The previously mentioned mathematical approaches for studying cracked, adhesively bonded structures are for extensional loading, and it is assumed that both the cracked and patch layers have no bending stiffness. The existence of a crack in one layer of a bonded structure causes out-of-plane bending due to the loss of symmetry resulting from the crack. Out-of-plane bending enhances the stress intensity components. Bending's influence (increase in stress intensity parameters) in a structure develops as the crack length rises. This increase in stress intensity parameters will impact the propagation of fracture rates and must be considered in the study. The stress singularities in front of the crack tips eliminate the force transmitted at the cracking plane due to a crack in a single cracked layer. When such a cracked layer is part of an adhesively bonded structure, the same force release at the crack plane is taken in part by the cracked layer in the form of stress singularities, as with a single cracked layer, and the balance of the force is transmitted to the right next patch layer via the adhesive. The force in each plate near the plane of the cracking will differ from that at the ends due to the force transferred to the patch layer. At the crack's plane, the net internal unequal force between the two layers equals the force transferred from the crack to the patch layer. The bending can be attributed to this inconsistent force. Considering this bending effect, a Bending Correction Factor (BCF) is introduced by Ratwani (1979), and a modified SIF can be expressed by Eq. (2.15).

$$K_P^* = (1 + BCF) \cdot K_P \tag{2.15}$$

The bending correction factor (BCF) is given by Ratwani (1979),

$$BCF = a \cdot y_{max} \cdot \left(1 - \frac{K_P}{K_I}\right) \cdot \frac{t \cdot (t + t_P)}{I} \tag{2.16}$$

Where y_{max} is the distance of the extreme fibres of the cracked plate from the neutral axis given by Eq. (2.17),

$$y_{max} = t + Z \tag{2.17}$$

where,

$$Z = S \cdot \frac{(t + t_P + 2t_A)}{2(1+S)} \tag{2.18}$$

'I' is the moment of inertia of the repaired plate given by Eq. (2.19).

$$I = I_{Plate} + n.I_{Patch} \tag{2.19}$$

I_{Plate} and I_{Patch} are the moment of inertia of the plate and patch, respectively, and n is the ratio of modulus of elasticity.

Where,

$$n = \frac{E_P}{E} \tag{2.20}$$

$$I_{Plate} = W \cdot \frac{t^3}{12} + W_P \cdot t \cdot Z^2 \tag{2.21}$$

$$I_{Patch} = W_P \cdot \frac{t_P^3}{12} + W_P \cdot t_P \cdot \frac{\left[\frac{t_P}{2} + t_A + \left(\frac{t}{2} - Z\right)\right]^2}{4} \tag{2.22}$$

Combining the Eqs. (2.16) to (2.22), the parameter BCF can be found and the modified SIF after passive repair can be expressed as:

$$K_P^* = (1 + BCF) \cdot \frac{\sigma_0}{1 + S} \cdot \sqrt{\frac{\pi a \bar{c}}{a + \bar{c}}} \cdot F\left(\frac{a}{W}\right) \tag{2.23}$$

2.2.3 SIF Reduction via Active and Hybrid Repair

2.2.3.1 Active Repair

The SIF is calculated using the concept of the superposition principle of LEFM, where two cases are taken into account and combined. The cases are described as follows: the cracked plate is subjected to mechanical loading only, and the plate is only under actuation (no mechanical loading). The SIF after active repair can be written as,

$$K_A = K_I + K_{Piezo} \tag{2.24}$$

where SIF under actuation effect, K_{Piezo} is evaluated by weight function method (WFM) as proposed by Bueckner (1970) and K_I is computed in the section 2.2.1. The weight function is evaluated using the y-direction displacement obtained by the Westergaard stress function [Anderson (2017)]. Now the solution of K_{Piezo} may thus be obtained from the following statement for a cracked body using weight function $h(x, y, a)$ and piezoelectric stress $\sigma_{Piezo}(x)$ [Abuzaid et al. (2018b)].

$$K_{Piezo} = \int_0^a \{h(x, y, a) \cdot \sigma_{Piezo}(x)\} dx \tag{2.25}$$

For any boundary condition, K_{Piezo} can be computed once WFM is known for a particular geometry. The weight function of a system with a cracked linear elastic body under a symmetrical load needs knowledge of the reference SIF from Eq. (2.1) as well as the specific geometry's mode-I stress system. The reference SIF under the action of σ_{Piezo} can be written as

$$K_r = \sigma_{Piezo}\sqrt{\pi a} \tag{2.26}$$

The weight function for a 2D cracked structure under mode-I opening load is as follows:

$$h(x, y, a) = \frac{\acute{E}}{2K_r}\frac{du_y}{da} \tag{2.27}$$

where $\acute{E} = E$ for plane stress and $\acute{E} = E/(1-\nu^2)$ for plane strain conditions. u_y is the plate's displacement in the y direction. The in-plane crack opening displacement for mode-I opening as per the Westergaard stress function [Anderson (2017)] is given as,

$$u_y = \pm\frac{2\sigma_{Piezo}}{\acute{E}}\sqrt{x(a-x)} \tag{2.28}$$

As the plate is double-edge cracked with crack length a, differentiating u_y with respect to a,

$$\frac{du_y}{da} = \pm\frac{\sigma_{Piezo}}{\acute{E}}\sqrt{\frac{x}{a-x}} \tag{2.29}$$

Now substituting Eqs. (2.26) and (2.29) in Eq. (2.27) and the weight function can be found as,

$$h(x, y, a) = \frac{1}{\sqrt{4\pi a}}\sqrt{\frac{x}{a-x}} \tag{2.30}$$

Piezoelectric actuators are bonded on the cracked plate completely where σ_{Piezo} is the stress produced by the piezoelectric actuators, which has an equal perpendicular distribution to the crack surface. d_{31} is the only effective mode which is piezoelectric strain coefficient. Under the application of the external voltage V, the shear force produced by the piezoelectric actuators is given by [Crawley and de Luis (1987)],

$$F_{Piezo} = \frac{EtT}{\psi + \alpha}\cdot\Lambda \tag{2.31}$$

Where T is the distributed electrode width. ψ is a non-dimensional parameter given by Eq. (2.32). α is a constant that depends on the type of loading and for extensional loading its value is $\alpha = 2$ [Crawley and de Luis (1987)].

$$\psi = \frac{EWt}{E_P W_P t_P} \tag{2.32}$$

Λ is the piezoelectric strain given by,

$$\Lambda = \frac{d_{31}}{t_P} \cdot V \tag{2.33}$$

σ_{Piezo} can be computed from the Eqs. (2.31) - (2.33) and is expressed as follows,

$$\sigma_{Piezo} = \frac{EtT}{A(\psi + \alpha)} \cdot \frac{d_{31}}{t_P} V \tag{2.34}$$

Where A is the effective cross-sectional area of the plate.

As the solution obtained by Eq. (2.25) is based on the application of LEFM, the effect of the geometry of any infinite plate is to be taken into account using the dimensionless geometry correction factor proposed by Tada et al. (2000) and Eq. (2.25) may be modified as,

$$K_{Piezo} = \left[\int_0^a \{h(x, y, a) \cdot \sigma_{Piezo}\} \cdot dx \right] \cdot F\left(\frac{a}{W}\right) \tag{2.35}$$

Now, using Eq. (2.2) and Eq. (2.35), K_A can be expressed as,

$$K_A = \left[\sigma_0 \sqrt{\pi a} + \int_0^a h(x, y, a) \cdot \sigma_{Piezo} \cdot dx \right] \cdot F\left(\frac{a}{W}\right) \tag{2.36}$$

2.2.3.2 Hybrid Repair

The expression of SIF as represented by Eq. (2.36), holds suitable for active repair only, i.e., the passive reinforcement effect is not considered. Since this research is not only concerned with active repair but also focuses on its passive effect, an innovative repair method is established that encompasses the idea of merging both repair methods and is termed a 'hybrid' repair. The superposition principle is used again by considering the cases: the plate is attached with a non-activated patch under mechanical loading (no voltage), and the plate is only under actuation (no mechanical loading). The SIF after hybrid repair can be written as $K_H = K_P^* + K_{Piezo}$ where K_P^* is calculated in section 2.2.2, while K_{Piezo} is in the previous discussion. The final expression of SIF can be expressed as,

$$K_H = \left[(1 + BCF) \cdot \frac{\sigma_0}{1 + S} \cdot \sqrt{\frac{\pi a \bar{c}}{a + \bar{c}}} + \int_0^a h(x, y, a) \cdot \sigma_{Piezo} \cdot dx \right] \cdot F\left(\frac{a}{W}\right) \tag{2.37}$$

2.2.4 Methodology for Fatigue Crack Growth Rate (FCGR) and Fatigue Life Estimation

In this section, fatigue crack growth rate (FCGR) and service life of a cracked structure are estimated under cyclic tension. For this purpose, the Paris crack growth model for mode-I is adopted and is expressed as [Paris and Erdogan (1963)],

$$\frac{da}{dN} = C \cdot (\Delta K)^m \tag{2.38}$$

The above expression gives the FCGR (mm/cycle). C and m are the material constants for a particular value of stress ratio (R).

The difference in SIF for maximum and minimum loading is necessary for this study and may be calculated using the previous sections' derivations. The change in SIF ($\Delta K = K_{max} - K_{min}$) is influenced by the change in stress quantity only ($\Delta\sigma = \sigma_{max} - \sigma_{min}$) in all cases under consideration, such as without repair, passive repair, active repair, and hybrid repair. To find out the fatigue life as well as the fatigue crack growth rate for all the above scenarios, Eq. (2.38) is integrated from initial crack length a_o to final crack length a_f. During numerical integration, a small incremental crack extension Δa_i is recorded for an incremental number of cycles ΔN_i and can be written as $a_{i+1} = a_i + \Delta a_i$ and $N_{i+1} = N_i + \Delta N_i$ respectively. Under cyclic tensile load, there is an increase in crack length and it reaches the value of critical crack length a_c $(a_f \rightarrow a_c)$ after any number of loading cycles. To find the fatigue life of a damaged structure, the above-mentioned numerical integration is to be carried out between a_o and a_c. The fracture toughness of the plate material is given by $K_{IC} = \sigma_0\sqrt{\pi a_c} \cdot F\left(\frac{a_c}{W}\right)$. The critical length depends on the applied stress and configuration of the cracked structure.

2.2.4.1 Without repair

From Eq. (2.2), the SIF range can be written as,

$$\Delta K_I = \Delta\sigma \cdot \sqrt{\pi a} \cdot F\left(\frac{a}{W}\right) \tag{2.39}$$

Putting this value in Eq. (2.38) we have,

$$\begin{cases} \dfrac{da}{dN} = C \cdot \left[\Delta\sigma \cdot \sqrt{\pi a}\,.F\left(\dfrac{a}{W}\right)\right]^m \\ dN = \dfrac{da}{C \cdot \left[\Delta\sigma \cdot \sqrt{\pi a}\,.F\left(\dfrac{a}{W}\right)\right]^m} \end{cases} \tag{2.40}$$

In order to calculate the propagated crack length after the N loading cycle, numerical integration of Eq. (2.40) is performed.

$$N_f = \int_0^{N_f} dN = \int_{a_o}^{a_{f=}a_c} \frac{da}{C \cdot \left[\Delta\sigma \cdot \sqrt{\pi a}\,.F\left(\dfrac{a}{W}\right)\right]^m} \tag{2.41}$$

2.2.4.2 Passive Repair

From Eq. (2.23), SIF range can be written as

$$\Delta K_P^* = (1 + BCF) \cdot \frac{\Delta\sigma}{1+S} \cdot \sqrt{\frac{\pi ac}{a+c}} \cdot F\left(\frac{a}{W}\right) \tag{2.42}$$

Putting this value in Eq. (2.38) we have,

$$\begin{cases} \dfrac{da}{dN} = C \cdot \left[(1 + BCF) \cdot \dfrac{\Delta\sigma}{1+S} \cdot \sqrt{\dfrac{\pi ac}{a+c}} \cdot F\left(\dfrac{a}{W}\right)\right]^m \\ dN = \dfrac{da}{C \cdot \left[(1 + BCF) \cdot \dfrac{\Delta\sigma}{1+S} \cdot \sqrt{\dfrac{\pi ac}{a+c}} \cdot F\left(\dfrac{a}{W}\right)\right]^m} \end{cases} \tag{2.43}$$

In the same way, we can calculate the fatigue life after passive repair and given below,

$$N_f = \int_0^{N_f} dN = \int_{a_o}^{a_{f=}a_c} \frac{da}{C \cdot \left[(1 + BCF) \cdot \dfrac{\Delta\sigma}{1+S} \cdot \sqrt{\dfrac{\pi a\bar{c}}{a+\bar{c}}} \cdot F\left(\dfrac{a}{W}\right)\right]^m} \tag{2.44}$$

2.2.4.3 Active Repair

From Eq. (2.36), SIF range for only active repair can be written as,

$$\Delta K_A = \left\{\Delta\sigma\sqrt{\pi a} + \int_0^a h(x, y, a) \cdot \Delta\sigma_{Piezo} \cdot dx\right\} \cdot F\left(\frac{a}{W}\right) \tag{2.45}$$

where,

$$\begin{cases} \Delta\sigma_{Piezo} = \dfrac{EtT}{A(\psi+\alpha)} \cdot \dfrac{d_{31}}{t_P} \cdot \Delta V \\ \Delta V = V_{max} - V_{min} \end{cases} \tag{2.46}$$

Putting this value in Eq. (2.38) we have,

$$\begin{cases} \dfrac{da}{dN} = C \cdot \left[\left\{ \Delta\sigma\sqrt{\pi a} + \displaystyle\int_0^a h(x,y,a) \cdot \Delta\sigma_{Piezo} \cdot dx \right\} \cdot F\left(\dfrac{a}{W}\right) \right]^m \\ dN = \dfrac{da}{C \cdot \left[\left\{ \Delta\sigma\sqrt{\pi a} + \int_0^a h(x,y,a) \cdot \Delta\sigma_{Piezo} \cdot dx \right\} \cdot F\left(\dfrac{a}{W}\right) \right]^m} \end{cases} \tag{2.47}$$

and the fatigue life is given by,

$$N_f = \int_0^{N_f} dN = \int_{a_o}^{a_{f=a_c}} \frac{da}{C \cdot \left[\left\{ \Delta\sigma\sqrt{\pi a} + \int_0^a h(x,y,a) \cdot \Delta\sigma_{Piezo} \cdot dx \right\} \cdot F\left(\dfrac{a}{W}\right) \right]^m} \tag{2.48}$$

2.2.4.4 Hybrid Repair

From Eq. (2.37), SIF range can be written as

$$\Delta K_H = \left\{ (1+BCF) \cdot \frac{\Delta\sigma}{1+S} \cdot \sqrt{\frac{\pi a \bar{c}}{a+\bar{c}}} + \int_0^a h(x,y,a) \cdot \Delta\sigma_{Piezo} \cdot dx \right\} \cdot F\left(\frac{a}{W}\right) \tag{2.49}$$

Putting this value in Eq. (2.38) we have,

$$\begin{cases} \dfrac{da}{dN} = C \cdot \left[\left\{ (1+BCF) \cdot \dfrac{\Delta\sigma}{1+S} \cdot \sqrt{\dfrac{\pi a \bar{c}}{a+\bar{c}}} + \displaystyle\int_0^a h(x,y,a) \cdot \Delta\sigma_{Piezo} \cdot dx \right\} \cdot F\left(\dfrac{a}{W}\right) \right]^m \\ dN = \dfrac{da}{C \cdot \left[\left\{ (1+BCF) \cdot \dfrac{\Delta\sigma}{1+S} \cdot \sqrt{\dfrac{\pi a \bar{c}}{a+\bar{c}}} + \int_0^a h(x,y,a) \cdot \Delta\sigma_{Piezo} \cdot dx \right\} \cdot F\left(\dfrac{a}{W}\right) \right]^m} \end{cases} \tag{2.50}$$

and the fatigue life is given by,

$$\begin{aligned} N_f &= \int_0^{N_f} dN \\ &= \int_{a_o}^{a_{f=a_c}} \frac{da}{C \cdot \left[\left\{ (1+BCF) \cdot \dfrac{\Delta\sigma}{1+S} \cdot \sqrt{\dfrac{\pi a \bar{c}}{a+\bar{c}}} + \int_0^a h(x,y,a) \cdot \Delta\sigma_{Piezo} \cdot dx \right\} \cdot F\left(\dfrac{a}{W}\right) \right]^m} \end{aligned} \tag{2.51}$$

2.3 Finite Element Analysis (FEA) Using ABAQUS

In order to validate the results obtained from the numerical analysis, an FE model is developed by modelling a structure with a piezoelectric patch. At first, three deformable bodies are created and 2 planar shells are created to model the Plate, piezoelectric patch, adhesive layer, and cracks with the dimensions, material properties, and damage parameters as given in Table 2.1-2.5. The plate model is partitioned into two geometries to incorporate the crack on both sides of the plate. The piezoelectric patch model is defined with a local material orientation by creating a datum where axis 3 is kept along the depth of the patch model. It is to be noted that ABAQUS takes direction 3 as the polarization direction. The piezoelectric patch and cracked plates are attached by using tie interaction under the interaction module. The model is simulated under a static step where the cyclic load is applied by creating a tabular amplitude and selecting the created amplitude as the variation of the magnitude of load with time. The external voltage on the piezoelectric patch is applied by creating two electrical boundary conditions on the two opposite faces of the patch. The voltage of the face attached to the adhesive is kept zero and the other face is given a finite value. Subsequently, for validation purposes, three more deformable bodies are created under the part module to model the cracked plate and two piezoelectric patches with the dimensions as considered in the published literature by Abuzaid et al. (2018b). For the analysis, material properties as mentioned by Abuzaid et al. (2018b) are assigned to the plate model and piezoelectric patch models. Thenceforth as required a seam crack at the middle of one side of the plate is considered.

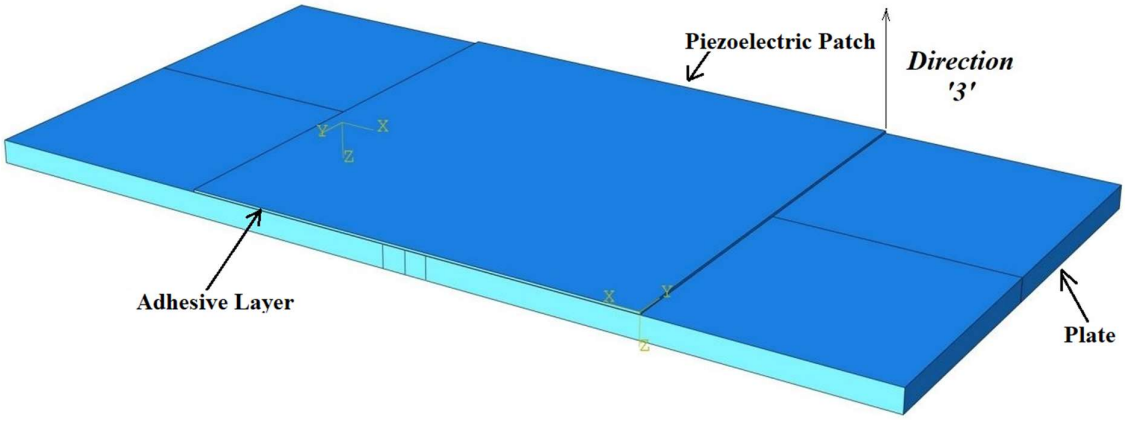

Figure 2.3: Model of the cracked plate with an assembled piezoelectric patch on the ABAQUS platform

The propagation of a crack is considered to be in quasi-static condition, i.e., the crack grows very slowly such that at every instant, the problem can be regarded as static and can be performed by the extended finite element method (XFEM). Without re-meshing the model, XFEM enables the investigation of fracture growth along solution-dependent paths. The maximum principal stress value is specified to initiate the crack propagation in the material definition. XFEM analysis is performed under the static step. Figure 2.3 depicts the 3D model with the tied piezoelectric patch with an adhesive layer and the location of the crack. Figure 2.4 shows the selected crack domain and the planar element that is required to specify the XFEM crack.

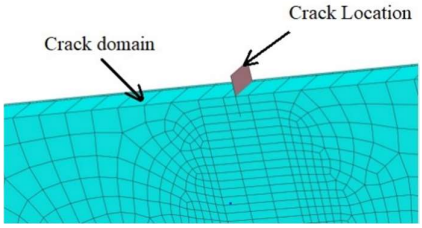

Figure 2.4: Depiction of the crack domain, crack location, and meshing condition for XFEM analysis

2.4 Validation Study

2.4.1 Validation of the Present FE Model

In order to validate the efficacy of the present analytical approach and finite element analysis, results obtained by both methods are compared with the experimental and numerical results published by Abuzaid et al. (2018b). The material properties, geometric properties, loading conditions, and boundary conditions are considered identical to those of Abuzaid et al. (2018b). Two piezoelectric patches are bonded by an adhesive layer, as shown in Figure 2.5.

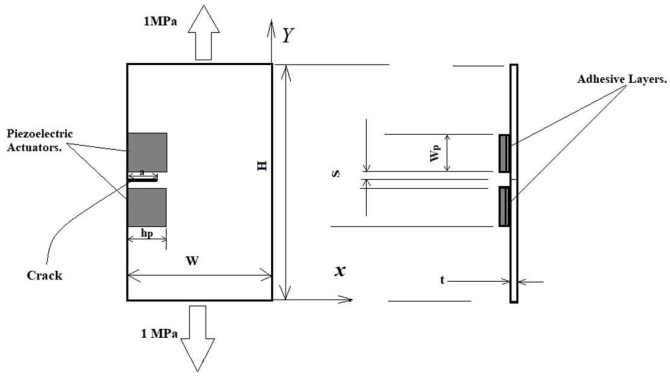

Figure 2.5: Schematic illustration of the considered cracked plate with bonded piezoelectric patch as used in the experimental work of Abuzaid et al. (2018b)

Figure 2.6(a) and (b) depict the finite element model of the plate discretized by hexahedral elements and its deformed shape, respectively. Figure 2.7 presents the comparison of the present theoretical and FE analysis with the experimental results published by Abuzaid et al. (2018b). The results of the present analysis match pretty well with that of the published literature.

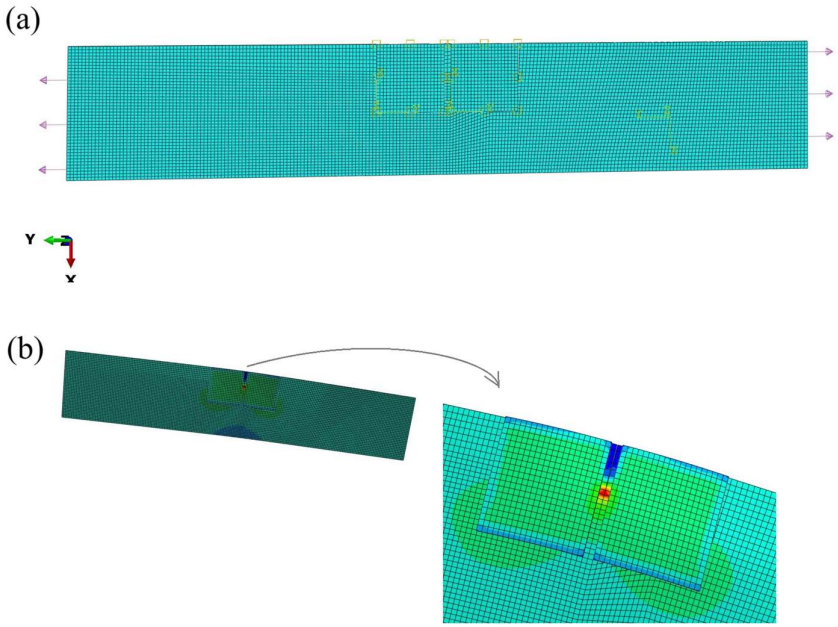

Figure 2.6: FE model of the cracked plate with attached piezo actuators considered for validation (a) before simulation (b) after simulation

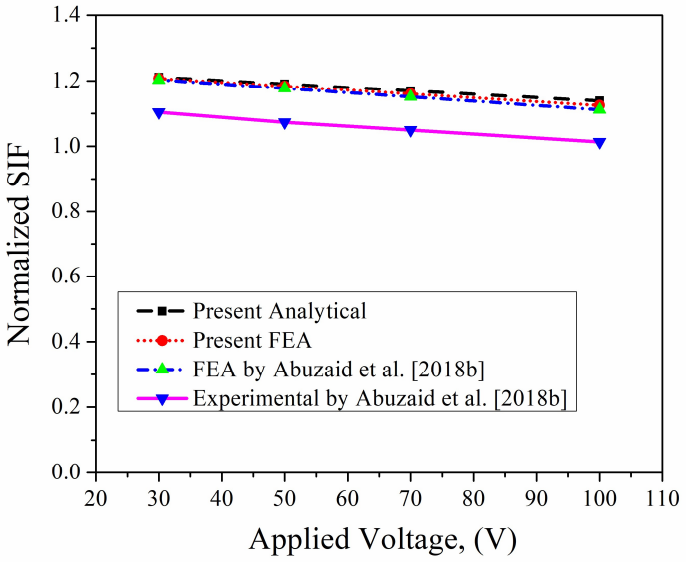

Figure 2.7: Comparison of the present results with the published experimental and numerical results in Abuzaid et al. (2018b)

2.4.2 Validation of Proposed Analytical Model Using ABAQUS

The present analytical approach aims to intend that a piezoelectric patch can slow down the fatigue crack growth rate. In addition to the analytical approach, a Finite element analysis (FEA) with the help of ABAQUS Standard CAE is performed to match the results. XFEM (Extended Finite Element) cracks are incorporated into the plate, and the model is simulated using a static step to facilitate crack propagation under cyclic loading. The model is discretized by hexahedral elements with 0.00015 m approximate global size. The sweep meshing technique with the medial axis algorithm is considered for discretization. The cyclic load is applied in the static step by creating a tabular amplitude, which varies the load with time as required. Where the maximum and minimum stress values are 330 MPa and 33 MPa, respectively. The adhesive layer is sandwiched between the plate and the piezoelectric patch, as mentioned by Kumar et al. (2023). The mating faces of the adhesive layer to the piezoelectric patch and the adhesive layer to the plates are assembled by using tie interaction from the interaction module. An electrical boundary condition of zero voltage is applied on the face of the piezoelectric patch, which is attached to the adhesive layer.

For the analysis, the parameters related to the geometry of the plate, piezoelectric patch (PZT-5H), and adhesive are given in Table 2.1. The material properties are mentioned in Table 2.2-2.4, respectively. The fatigue properties of the plate Al 2024-T3 are given in Table 2.5.

Table 2.1: Parameters about the geometry of the repaired configurations as shown in Figure 2.1

Dimensions	**Al 2024-T3 (mm)**	**PZT-5H (mm)**	**Resin Epoxy (mm)**
Height	H=200	H_P=100	H_A=100
Width	W=100	W_P=100	W_A=100
Thickness	t=1.6	t_P=0.5, 0.75 and 1	t_A=0.05, 0.075 and 1

Table 2.2: Mechanical properties of Al 2024-T3 plate material

Elastic Modulus (E) (GPa)	**Poisson's ratio (v)**	**Tensile yield strength (MPa)**	**Ultimate tensile strength (MPa)**	**Density Kg/m^3**
74	0.33	345	483	2780

Table 2.3: Properties of piezoelectric material PZT-5H

Piezoelectric coefficient (10^{-12} C/N)	**Flexibility coefficient (10^{-12} m²/N)**	**Dielectric constant**	**Density Kg/m³**
$d_{31} = -274$ $d_{33} = 593$ $d_{15} = 741$	$s_{11} = 16.5, s_{12} = -4.78, s_{14} = -8.45,$ $s_{33} = 20.7, s_{44} = 43.5, s_{66} = 2(s_{11} - s_{12})$	$k_{11} = 3130$ $k_{31} = 3400$	7600

Table 2.4: Material properties of resin epoxy

Elastic Modulus (E_A) (GPa)	**Poisson's ratio ν_A**	**Tensile yield strength (T_A) (MPa)**	**Shera Modulus (G_A) (GPa)**	**Density (Kg/m³)**
2.8	0.35	30	1.05	1210

Table 2.5: Fracture properties of Al 2024-T3 and Paris law material constants at stress ratio R=0.1 [Ayatollahi et al. (2014)]

$\Delta K_{th}\ (MPa\sqrt{m})$	$K_{IC}\ (MPa\sqrt{m})$	**C**	**m**
3.61	33.16	7.172×10^{-8}	3.0089

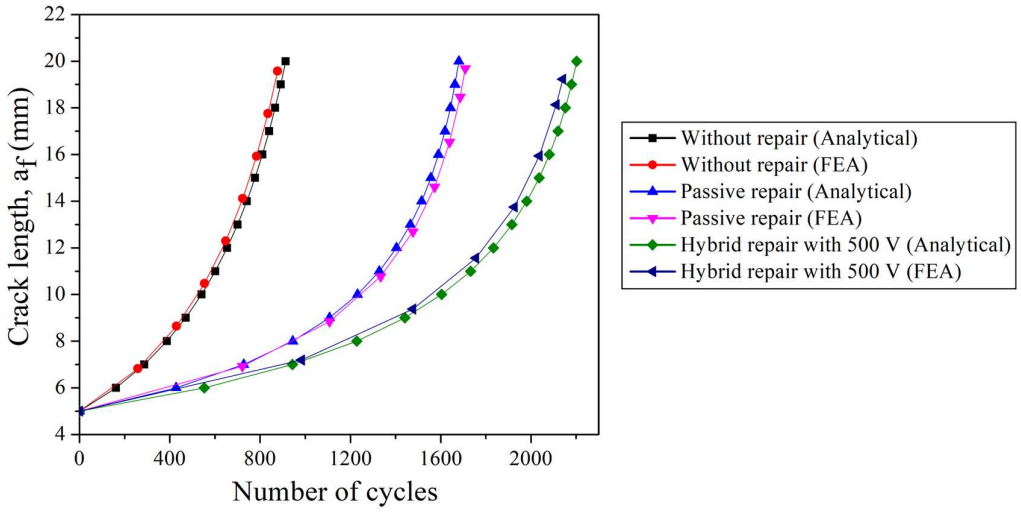

Figure 2.8: Comparison of present analytical results with the results obtained by FEA in ABAQUS

It should be mentioned that 500V is provided to the piezoelectric patch to slow down the crack propagation rate. Thereafter, the results are compared for authentication, and the same are shown in Figure 2.8. The graphical comparison between the results obtained by FEA and the analytical method shows a good match. The deformed FE models of the cracked plate with propagated crack before and after attaching the piezoelectric patch are displayed in Figure 2.9. The simulated finite element models at the three conditions without repair (without patch), passive repair (patch without voltage actuation), and active repair (with actuated patch) are depicted in Figure 2.9(a), (b), and (c).

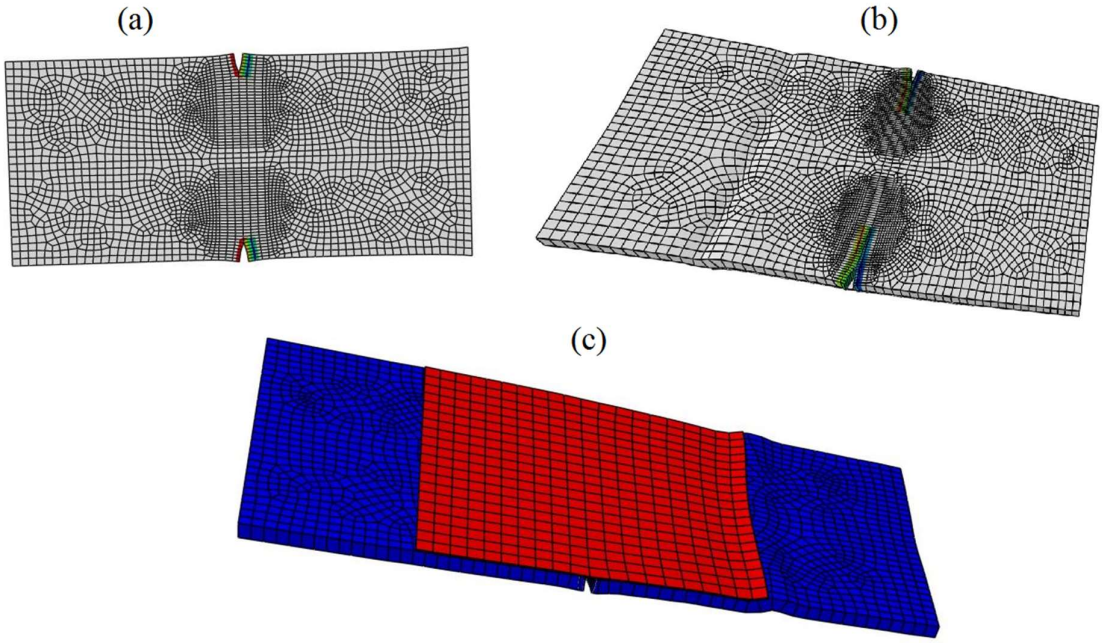

Figure 2.9: Deformed FE model of the cracked plate with propagated crack (a) before attaching the piezoelectric patch (b) after attaching the piezoelectric patch (c) after attaching the piezoelectric patch and applying a voltage of 500 V

2.5 Results and Discussion

Once the output of the numerical simulation is matched with the FE analysis, further investigation is carried out to determine the fatigue life and FCGR under cyclic loading without repair, passive repair, active repair, and hybrid repair of the cracked plate using the analytical method proposed in this work.

2.5.1 Fatigue Life of the Cracked Plate

The cracked plate without repair (plate without patch) is subjected to a cyclic load between 8 KN and 0.8 KN, which results in $\sigma_{max} = 50$ MPa, $\sigma_{min} = 5$ MPa, and the Stress

Ratio (SR) of 0.1. The same stress ratio is maintained for all the subsequent analyses. Crack length is propagated under fatigue loading and reaches the critical crack length of a_c, when $(\mathrm{K_I})_{\text{Without repair}} = \mathrm{K_{IC}}$. The corresponding number of cycles $\mathrm{N_f}$ provides the fatigue life, which is calculated using Eq. (2.41). Figure 2.10(a) represents the increase in crack length without a repaired plate concerning the number of loading cycles (N) and Figure 2.10(b) shows the change in FCGR (da/dN) against SIF range (ΔK).

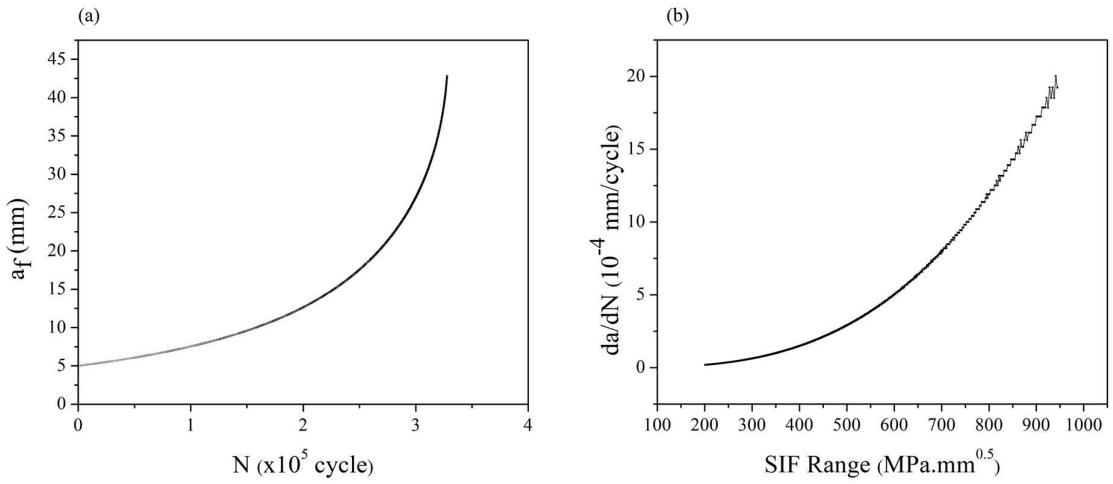

Figure 2.10: The results of the without repaired plate (a) Final crack length vs. number of loading cycles (b) Fatigue crack growth rate vs. SIF range

2.5.2 Fatigue Life Enhancement via Passive Repair

The bonded piezoelectric patch is attached to the plate. However, no voltage is applied to the patch. SIF is reduced significantly due to its passive effect, i.e., due to the stiffness of the patch material. The fatigue life is calculated for passive repair using Eq. (2.44). This repair method is affected by the piezoelectric patch thickness, $t_{P,}$ and adhesive thickness, t_A. To study the effect of thicknesses and to choose the best possible thicknesses of the patch and adhesive, an investigation is carried out for different patch thicknesses, $t_P = 0.5, 0.75, and\ 1\ mm$, and different adhesive thicknesses $t_A = 0.05, 0.075\ and\ 0.1\ mm$

Figure 2.11 demonstrates the propagation of crack length concerning the number of loading cycles for different patches and adhesive thicknesses. From Eq. (2.42), it is clear that da/dN provides a fixed value for a particular value of ΔK for all parameters related to different repair configurations. However, ΔK attains a specific value after a different number of loading cycles for various configurations. Thus, for proper comparison of FCGR concerning the SIF range, choosing an optimum number of loading cycles is essential. In the

concerned case, the change in FCGR (da/dN) with respect to SIF range (ΔK) within 3×10^5 cycles are shown in Figure 2.12 for different adhesive thicknesses. The crack growth rate can be delayed by maintaining a higher patch thickness. The crack growth rate without a repair plate is also included in the figure.

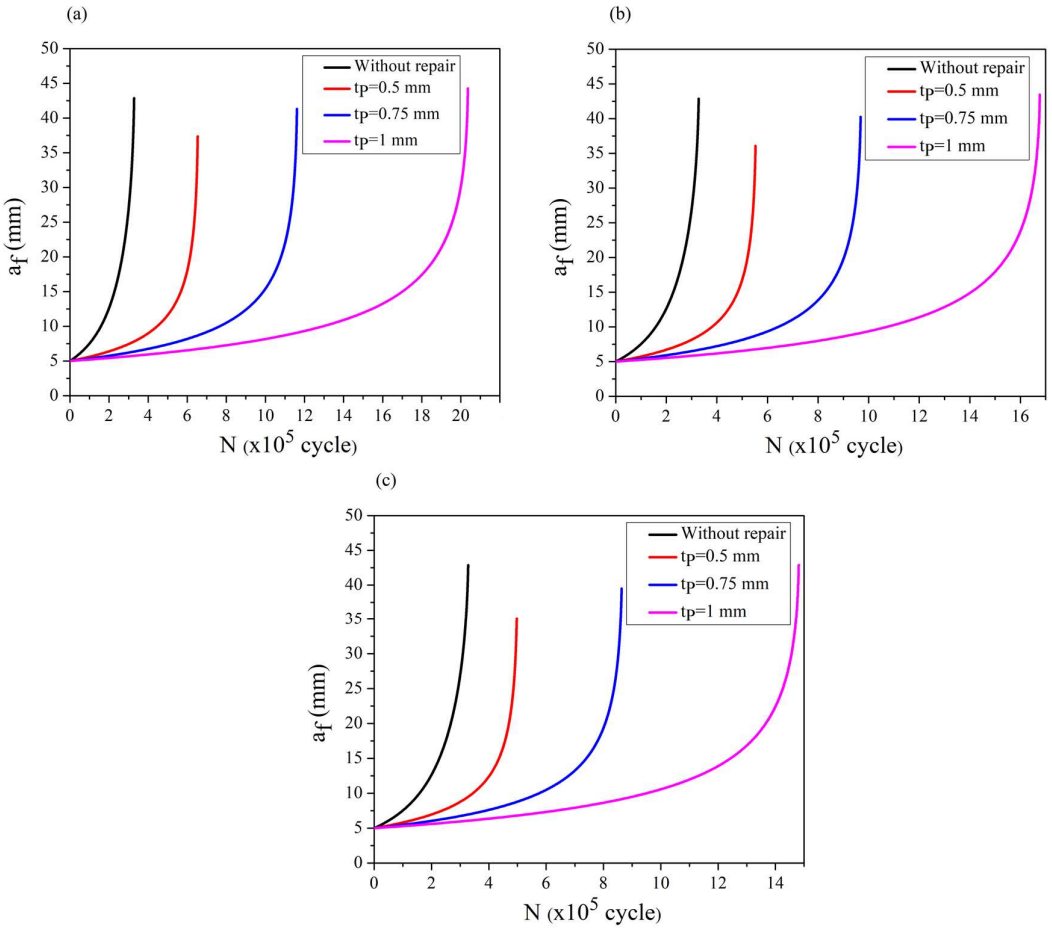

Figure 2.11: Change in crack length with loading cycles for passive repair configurations (a) t_A=0.05mm (b) t_A=0.075mm (c) t_A=0.1mm

Figure 2.13 demonstrates the variation of fatigue life (N_f) for different patches and adhesive thicknesses. As can be seen, passive repair enhances the fatigue life by 99.31%, 254%, and 520% for patch thicknesses 0.5 mm, 0.75 mm, and 1 mm, respectively, compared to without repair condition when the adhesive thickness is kept at 0.05 mm. For different adhesive thicknesses (0.075 mm and 0.1 mm), it is found that fatigue life can be enhanced by 68.56%, 195.25%, 411% and 51.73%, 163.23%, 351.95% as compared to without repair condition. The fatigue life is also increased by 77.6% and 211.5% for patch thickness 0.75 mm and 1 mm, respectively, compared to the fatigue life obtained when patch thickness is 0.5

mm. This is found as better stress distribution occurs for higher patch thickness, which results in lower crack tip stress and lower SIF and, hence, an increase in fatigue life. A higher patch thickness is more efficient for the passive repair of any cracked structure.

However, fatigue life decreases with the increase in adhesive thickness for a particular patch thickness. Fatigue life is reduced by 15.4% and 23.8% for the adhesive thickness of 0.075 mm and 0.1 mm, respectively, compared to the fatigue life obtained for the adhesive thickness of 0.05 mm when patch thickness is kept at 0.5 mm. This may be a consequence of inadequate load transfer to the patch, resulting in reduced load sharing. For low adhesive thickness, the crack growth rate is found to be minimal, as described in Figure 2.12. So, for better repair performance, thickness adhesive is to be chosen.

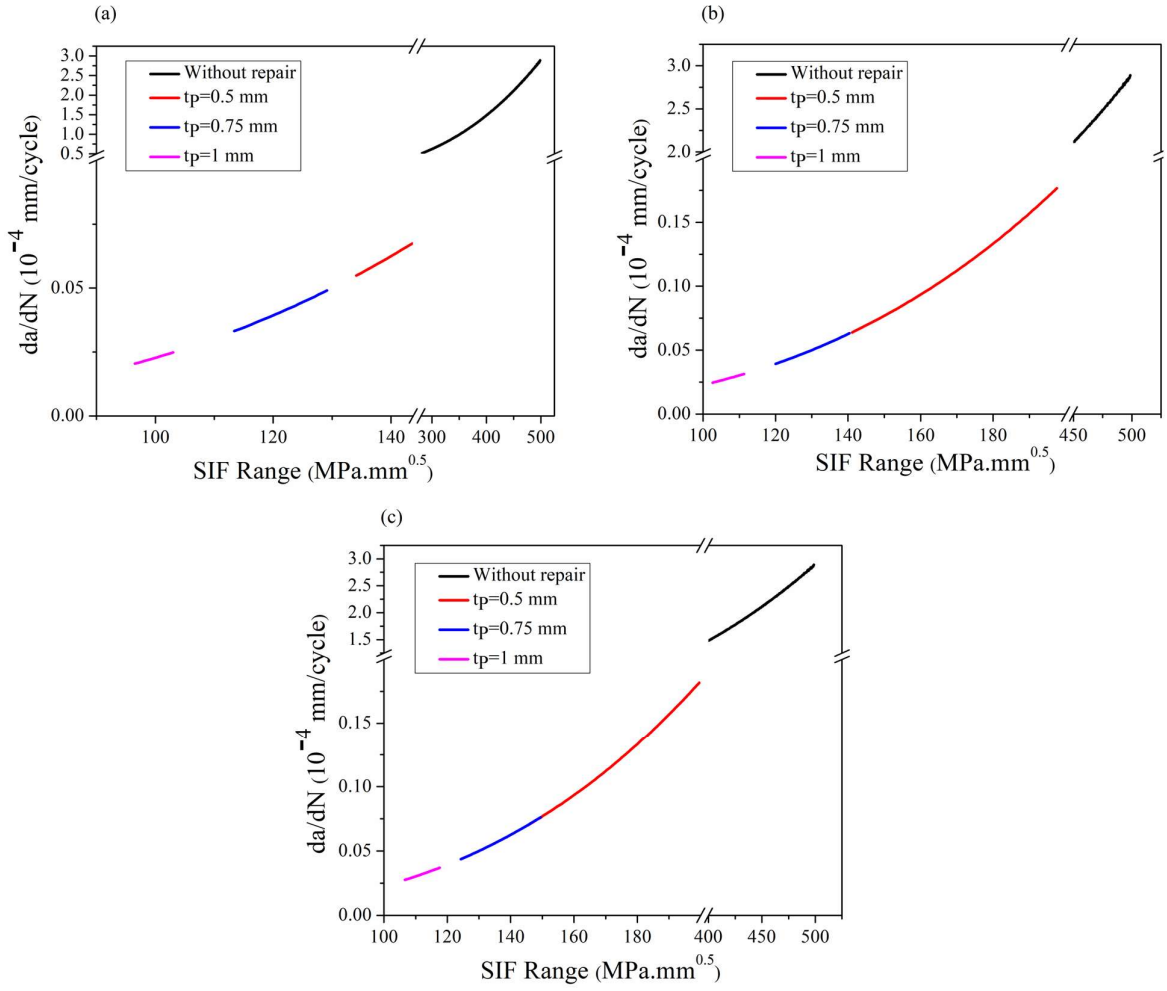

Figure 2.12: Fatigue crack growth rate vs SIF Range for passive repair configuration (a) $t_A = 0.05mm$ (b) $t_A = 0.075mm$ (c) $t_A = 0.1mm$

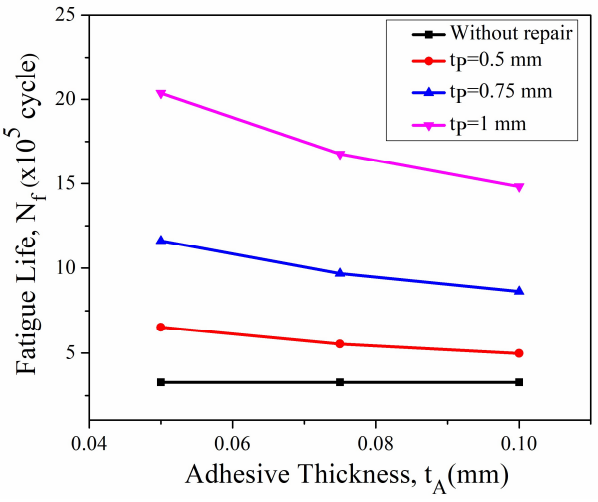

Figure 2.13: Fatigue life vs. adhesive thickness for various patch thicknesses for a passive repair illustration

2.5.3 Fatigue Life Enhancement via Active Repair

This section discusses the repair performance of only actuation by the piezoelectric patch, neglecting the passive effect. This discussion is made to have the appropriate voltage ratio (VR), thickness, and externally applied voltage of the patch. For this analysis, the thickness of the adhesive is kept low, say 0.05 mm, as higher adhesive thickness leads to a decrease in the load transfer to the cracked plate and, hence, low repair performance.

2.5.3.1 Effect of Voltage Ratio (VR)

Since the repair method is carried out under fatigue loading, choosing the proper voltage ratio is essential. ($VR = V_{min}/V_{max}$) applied to the patch for better performance. The fatigue crack growth rate depends on the SIF range (ΔK) and the fatigue life additionally depends on K_{max} as fatigue life is calculated when K_{max} becomes equal to the K_{IC}. So, minimizing SIF range (ΔK) and maximizing the number of cycles required to reach the fracture toughness ($K_{max} = K_{IC}$) is the significant attention of this analysis. Voltage ratio (VR) is taken as 0, 0.2, 0.4, 0.6, 0.8, and 1.0 with $V_{max} = 500\ V$.

The change in crack length against the loading cycle is shown in Figure 2.14(a) for various voltage ratios. Because the maximum voltage is fixed in this case, the maximum SIFs are the same for all voltage ratios, and thus the critical crack length is identical. It is observed that the number of loading cycles required to reach the critical crack length ($a_c = 43.77\ mm$) drops with a rising voltage ratio. Figure 2.14(b) illustrates the change in the rate of fatigue development of cracks about the SIF range (ΔK) within 10^5 cycles, and it indicates that

the voltage ratio has a significant influence on crack growth rate and that the zero-voltage ratio ($VR = 0\ or\ V_{min} = 0$) offers the most delayed crack growth.

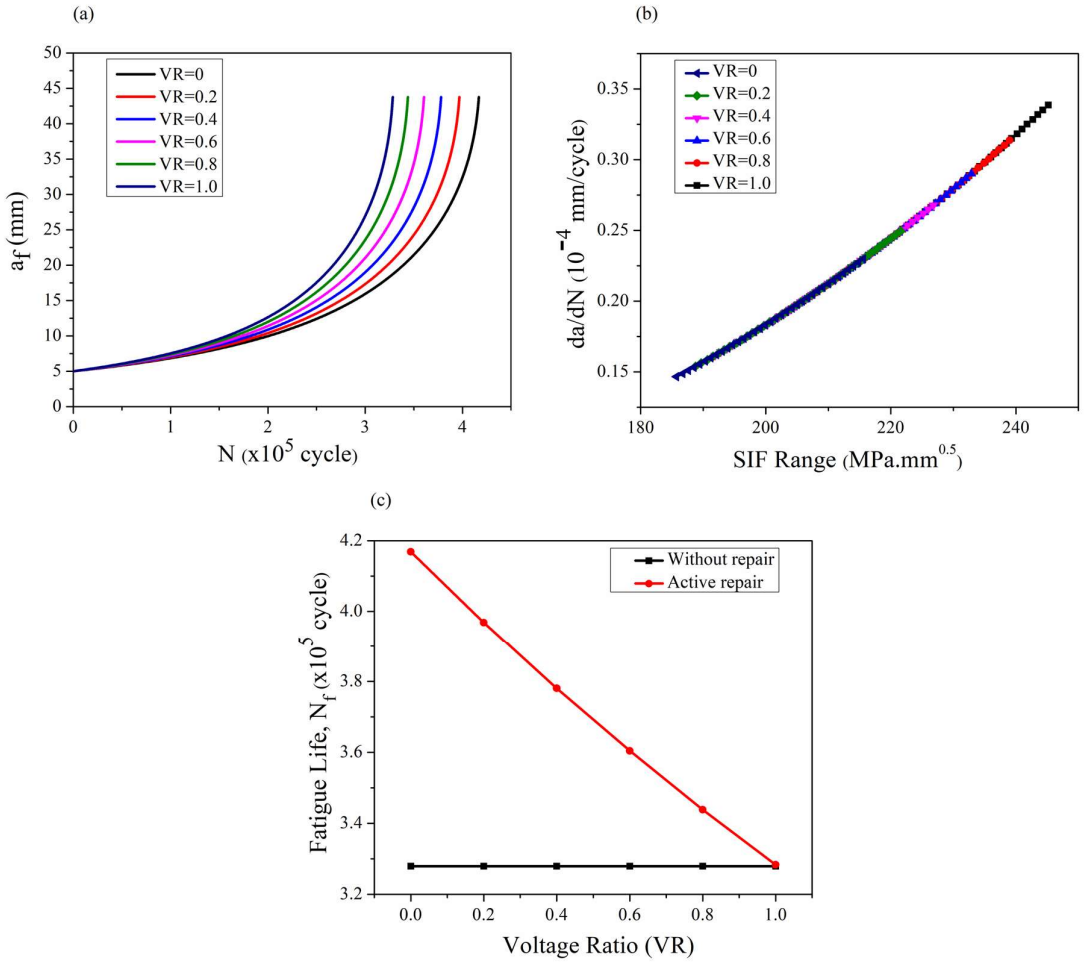

Figure 2.14: The results of active repair for various voltage ratios keeping V_{max}=500 V (a) Crack length vs loading cycle (b) Fatigue crack growth rate vs SIF range (c) Fatigue life

It is observed that the maximum fatigue life is obtained when VR = 0, and it decreases as VR increases while V_{max} is kept constant at 500 V. The fatigue life is improved by 27.12%, 21%, 15.28%, 9.92%, 4.85%, and 0.12% corresponding to VR = 0, 0.2, 0.4, 0.6, 0.8, and 1, respectively, as compared to without repair cases as seen in Figure 2.14(c). For active repair,

$$\Delta K = \left\{\Delta\sigma\sqrt{\pi a} + \left[\int_0^a h(x,y,a)\cdot\{E\cdot t\cdot T\cdot d_{31}\cdot \Delta V/A\cdot t_P\cdot(\psi+\alpha)\}\cdot dx\right]\right\}\cdot F\left(\frac{a}{W}\right) \quad (2.52)$$

The second term of Eq. (2.52) provides the change in SIF under voltage application, which is a negative quantity. The second term vanishes when VR=1.0 a $\Delta V = 0$. In order to minimize ΔK, ΔV must be maintained at a higher value which results in low FCGR. To

maximize the fatigue life, K_{max} is to be lowered by applying a higher V_{max}. So, for the best repair performance, V_{min} should be equal to zero i.e., VR = 0 to maintain maximum ΔV for a fixed value of V_{max}. Furthermore, the findings show that even at constant voltage, where there is no change in ΔK, a slight increase in fatigue life is obtained. This is because the application of continuous voltage lowers K_{max}, i.e., $\left(K_{A,max}\right)_{at\ 500\ V} < \left(K_{I,max}\right)_{without\ repair}$ and more cycles are required to reach K_{IC}.

2.5.3.2 Effect of Piezoelectric Patch Thickness

The thickness of piezoelectric actuators plays an essential role in repair performance. It was reported in previous research [Abuzaid et al. (2018a)] that thin actuators with high voltage provide the best result. This happens because the compressive force produced at the crack surface by the piezoelectric patch is inversely proportional to the thickness of the patch. For this reason, a 500 V maximum voltage (V_{max}) is taken to study the effect of piezoelectric patch thickness for $t_P = 0.5, 0.75, and\ 1\ mm$. The change in final crack length concerning the number of loading cycles is shown in Figure 2.15(a). The fatigue life is decreased by 3.53% for the case when the piezoelectric patch is increased from 0.5 mm to 0.75 mm, 6.05% for the case when the piezoelectric patch is increased from 0.5 mm to 1 mm, and 2.61% when it is changed from 0.75 mm to 1 mm as shown in Figure 2.15(b).

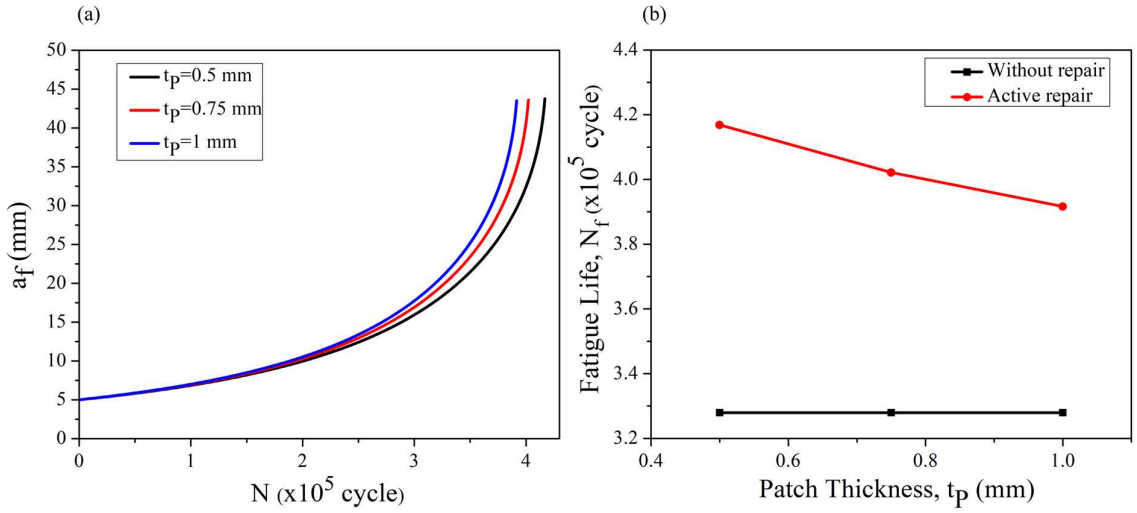

Figure 2.15: The results of active repair for different patch thicknesses (a) Crack length vs. loading cycle (b) Fatigue life

2.5.3.3 Effect of Maximum Applied Voltage

For the investigation of the effect of the maximum applied voltage applied to the patch on performance, an investigation has been carried out by varying the maximum voltage (V_{max}) from 500 V to 1000 V. Given that, the permissible limit of the electric field is considered as 2 kV/mm; consequently, the maximum applied voltage for the lowest thickness among all considered thicknesses (e.g., 0.5 mm) becomes 1000 V. The piezoelectric patch thickness is kept at 0.5 mm. Crack length is calculated against several loading cycles for the plate only under actuation (active repair) as represented in Figure 2.16(a). The variation of FCGR (da/dN) concerning the SIF range (ΔK) within 10^5 cycles are plotted in Figure 2.16(b) and lower crack growth is observed for the higher applied voltage. This is due to the higher reduction of stress at the crack tip hence lowering the SIF.

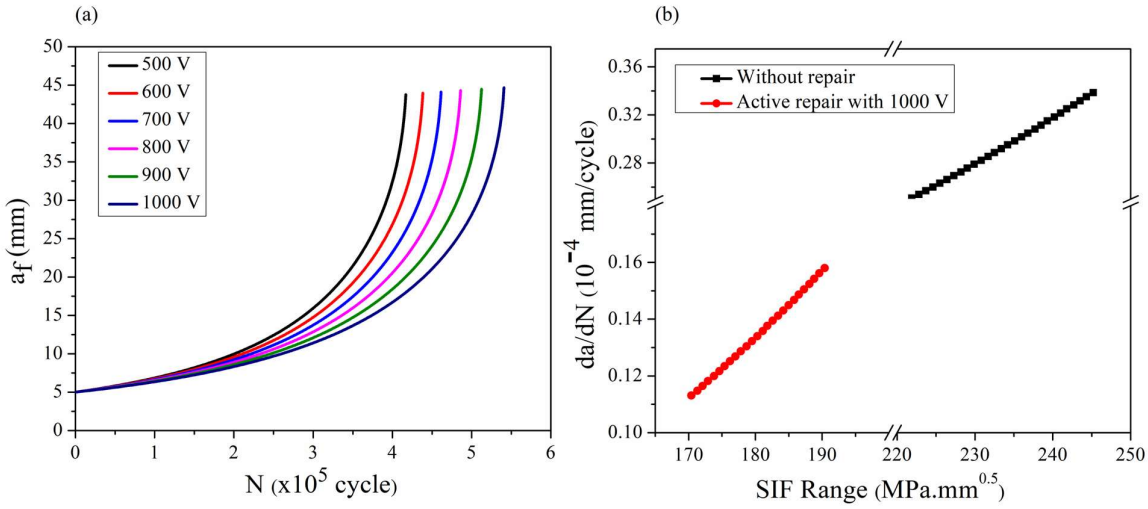

Figure 2.16: The results of active repair for various applied external maximum voltages (a) Crack length vs loading cycle (b) Fatigue crack growth rate vs SIF range

According to Figure 2.17(a), the fatigue life extends as the applied external voltage rises. The findings indicate that the fatigue life can be enhanced by 27.12%, 33.68%, 40.7%, 48.22%, 56.27%, and 64.92% for the voltages 500 V, 600 V, 700 V, 800 V, 900 V, and 1000 V respectively concerning without repair condition as shown in Figure 2.17(b). The percentage increase in fatigue life when applied external voltages are increased from 500 V is summarized in Figure 2.17(b). It is found that the fatigue life is improved by 5.16%, 10.6%, 16.5%, 22.9%, and 29.73% when the applied voltage is increased by an amount of 100 V, 200 V, 300 V, 400 V, and 500 V respectively from the applied voltage of 500 V. It has been observed that for each 100 V rise, fatigue life could have increased by around 5-7% for this

repair configuration as shown in Figure 2.17(c). The plate structure, crack geometry, and applied mechanical load determine the voltage requirement, and a suitable range of external voltage is chosen accordingly.

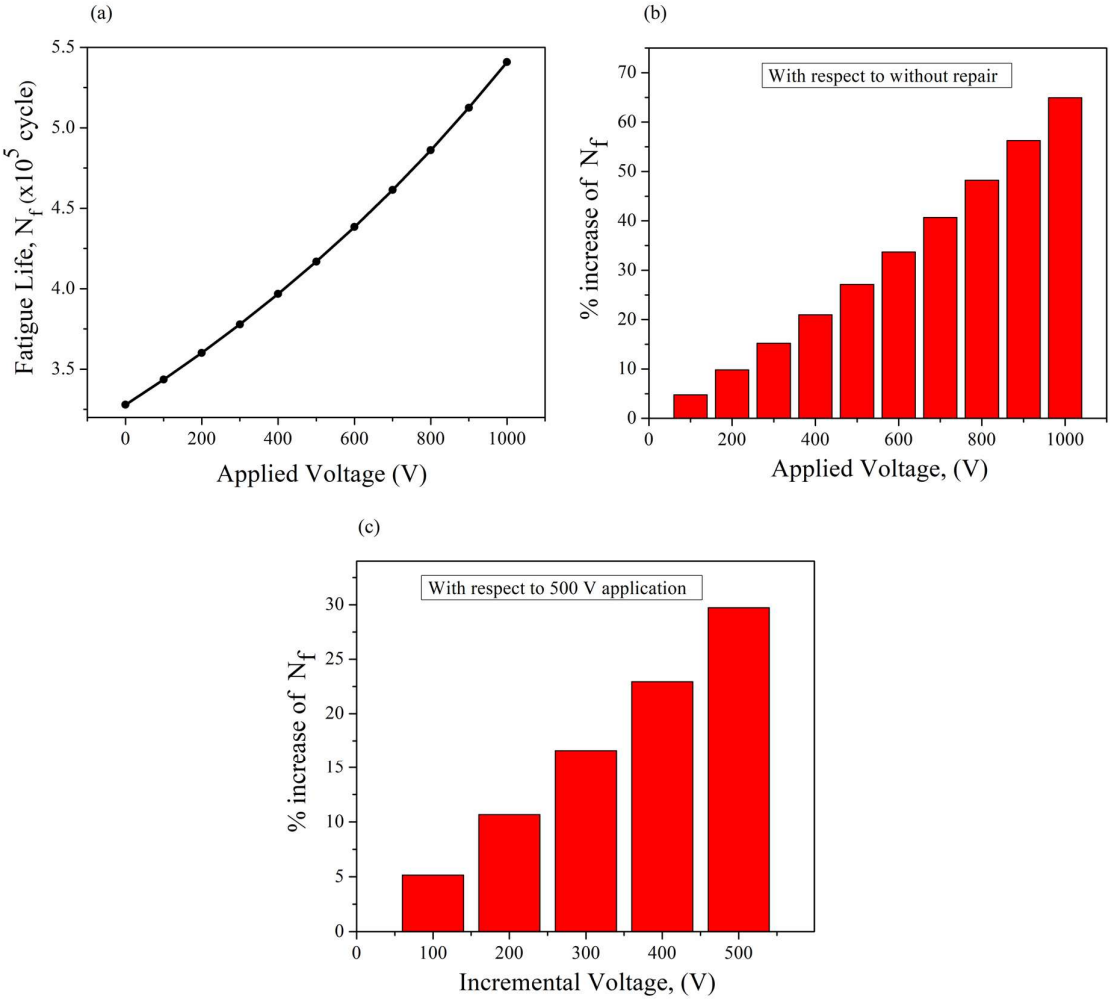

Figure 2.17: (a) Fatigue life for different external applied voltage (b) Increase in fatigue life for different external applied voltage compared to without repair (c) Increase in fatigue life for incremental applied voltages concerning 500 V application

2.5.4 Fatigue Life Enhancement via Hybrid Repair

It is clear from the results of the previous sections that an increase in patch thickness (t_P) results in a longer fatigue life for passive repair. It has been shown in 2.5.3.2 that increasing t_P will reduce the fatigue life in the case of only active repair given that the piezoelectric patch produces less strain at higher t_P. Results from the hybrid repair methodology, which combines passive and active repair, are reported in this section. An

optimal value of t_P must be maintained to achieve the best performance. Additionally, it has been found that zero voltage ratio (VR) offers the best repair and, subsequently, a longer fatigue life.

The crack length corresponding to the loading cycle is calculated with $t_P = 0.5$ mm and zero voltage ratio as represented in Figure 2.18(a) for various applied voltages in connection with a without repair case. The number of loading cycles required to reach the critical crack length increases as the externally applied voltages increase. Under 100V, 500V, and 1000V applications, hybrid repair enhances fatigue life by 111.95%, 174.88%, and 294.92%, respectively, compared to without repair conditions. The change in crack growth rate against the SIF range within 3×10^5 cycles are also determined and plotted in Figure 2.18(b) for the cases such as without repair, and hybrid repair with 500 V and 1000 V. It can be highlighted that the rise in voltage significantly slows the crack growth rate and thus improves fatigue life.

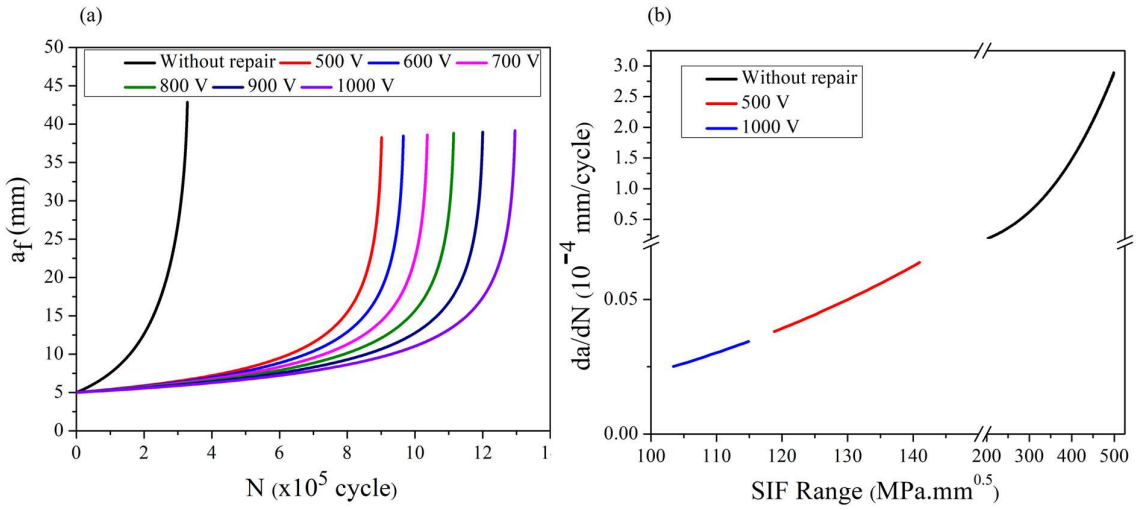

Figure 2.18: The results of hybrid repair for various applied voltages (a) Crack length vs. loading cycle (b) Fatigue crack growth rate vs. SIF range

Figure 2.19 represents the variation of the fatigue life concerning the patch thickness for different applied external voltages. It has been found that better fatigue life is obtained for the higher t_P and external voltage. Even though the results show that higher thickness leads to better fatigue life, choosing an optimum lower thickness is preferable. If a higher thickness is selected, the passive effect remains unaffected even if the mechanical load increases while actuation is reduced due to its high thickness. If a lower thickness is chosen, the passive effect

is slightly reduced. Still, the actuation effect can be enhanced by raising the externally applied voltages, as it provides better actuation for thin patches.

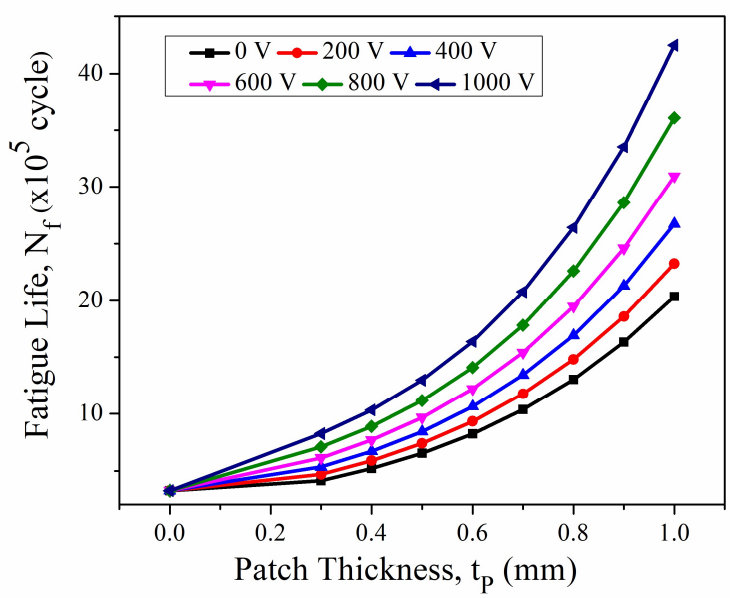

Figure 2.19: Fatigue life vs. patch thickness for various applied voltages in a hybrid repair case

In this repair method, the influence of the external voltage is an important consideration. Following the mechanical loading and desired service life, the proper voltage range is chosen. Figure 2.20 depicts the fatigue life relative to the different applied external voltage for all repair methods while maintaining $t_P = 0.5$ mm and VR=0 to show a more detailed illustration. Since the fatigue life of passive repair and without repair conditions is independent of voltage, a constant fatigue life has been found for these cases, as can be seen in Figure 2.20. The results of hybrid repair are identical to those of passive repair if no voltage is applied to the patch, simulating the situation where the plate is not given any actuation. A significant improvement in fatigue life is observed with a rise in voltage as the actuation delivered to the plate encounters the action while the passive effect remains unchanged.

Additionally, an illustration demonstrates how well active, passive, and hybrid repairs perform compared to those without repair. The percentage increase in fatigue life for different repair cases compared to without repair for various external voltages is reported in Figure 2.21(a). Hybrid repair provides maximum fatigue life enhancement as compared to other repair methods. It is observed that hybrid, passive, and active repairs exhibit 174.88%, 99.31%, and 27.12% improvement in fatigue life, respectively, as compared to without repair conditions under the application of 500 V. Passive repair is found to have a constant increase

in fatigue life than without repair, and this finding holds across all voltages because passive repair has no actuation effect.

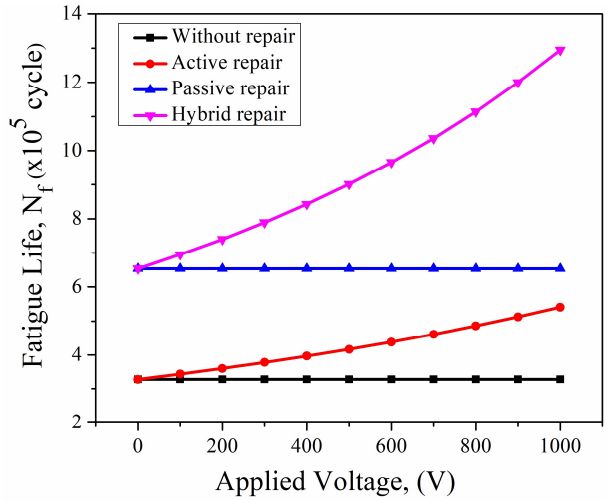

Figure 2.20: The variation in fatigue life about the applied external voltage for all repair techniques

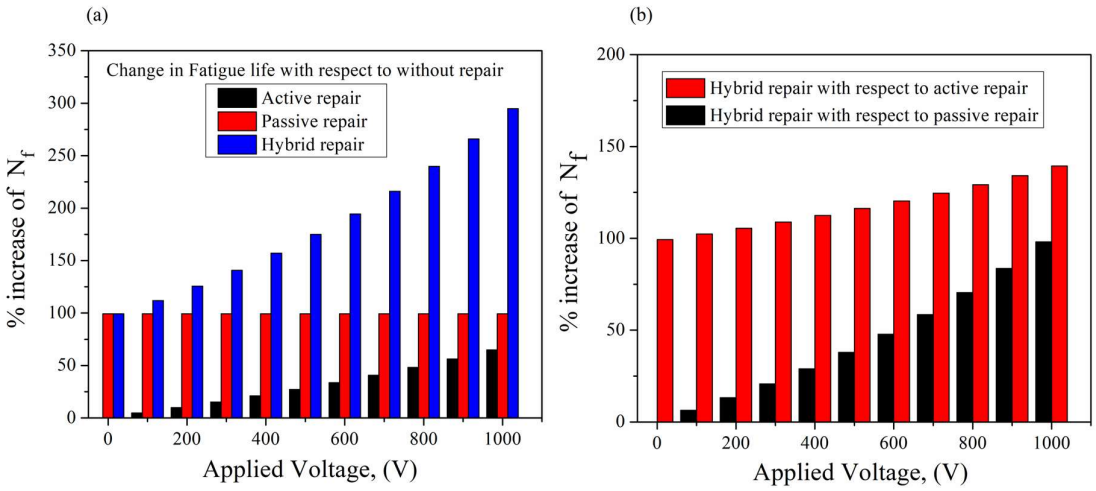

Figure 2.21: The percentage increase in fatigue life for different applied external voltages (a) hybrid, active, and passive repair over without repair (b) hybrid repair over active and passive repair

Since it is evident that hybrid repair provides the best performance, another illustration has been made to demonstrate how well a hybrid repair can deliver longer service life when compared to passive and active repair, as depicted in Figure 2.21(b). In contrast to passive repair, hybrid repair shows 6.34%, 37.92%, and 98.14% enhanced fatigue life under 100 V, 500 V, and 1000 V applications. Furthermore, hybrid repair shows 102.32%, 116.23%, and

139.46% improved fatigue life compared to active repair under 100 V, 500 V, and 1000 V applications.

When the applied voltage is increased from 0 to 100, the fatigue life is increased by 6.34%. When 500 V and 1000 V are applied, the fatigue life is increased by 29.69% and 86.32%, respectively, concerning 100 V applications. Fatigue life rises by 43.67% when the voltage is increased from 500 V to 1000 V. Every 100 V increase leads to a 6% to 8% rise in fatigue life. This change is slightly higher at higher voltages, possibly due to the dominance of the actuation effect over the passive effect.

2.6 Summary

This chapter uses the reverse piezoelectric effect to develop an analytical model for repairing a double-edge cracked infinite plate. The hybrid repair is carried out by considering the actuation effect and the passive effect of the patch due to its strong bond with the cracked plate. The combined effect of the patch sharing the external load and the compressive stress caused by the actuation of the piezoelectric patch under external voltage results in a significant stress reduction at the crack tip. This investigation is conducted under cyclic tensile load with R=0.1 and various voltage ratios. Afterward, a validation study is carried out to examine the accuracy of the proposed analytical model using ABAQUS FE solutions and published experimental results.

Discussions on Outcomes, which can be made from the results, are listed below:

- The investigation demonstrates that different repair techniques, such as active, passive, and hybrid repair, improve the fatigue life of the cracked structure in contrast to those without repair. The hybrid repair case exhibits the best performance.
- The passive effect can extend the service life. The thickness of the patch and adhesive also has an impact on the repair. The best results are obtained by combining a lower thickness with a larger surface area. Adhesive selection has significance as bond strength largely depends on the adhesive's properties.
- Active repair is very suitable because it provides a wide range of repairs by applying different voltages and placing a single patch on the cracked plate. It can be carried out using constant voltage as well as cyclic voltages. The best fatigue life is obtained with a zero-voltage ratio instead of a continuous voltage applied throughout the loading cycle. The higher thickness of the patch reduces the fatigue life.

- The piezoelectric patch performs best when combined with its active and passive effects. The passive impact becomes more significant at low applied voltage, but higher voltage results in a higher actuation effect and, thus, longer fatigue life. The best suitable thickness is reported because very high thickness at constant voltage provides less performance.

This page is intentionally left blank

Chapter 3

STRUCTURAL INTEGRITY ENHANCEMENT OF A BOTTOM-EDGE CRACKED I-BEAM USING PIEZOELECTRIC ACTUATORS

3.1 Introduction

Beams are fundamental structural elements widely employed across diverse engineering applications, from bridges and buildings to aircraft and machinery. These essential components are designed to withstand various loads, ensuring the stability and safety of the structures they support. While beams can possess various cross-sectional shapes, including rectangular, C-shaped, and T-shaped, the I-beam stands out due to its exceptional efficiency in resisting bending loads. This efficiency arise from its optimized distribution of material, maximizing strength while minimizing weight. However, beams are susceptible to fatigue and damage over time, particularly under cyclic loading like any structural element. The initiation of cracks, whether due to material flaws or operational stresses, poses a significant threat to structural integrity. Unaddressed cracks can propagate rapidly, leading to catastrophic failures, highlighting the critical importance of early detection and effective repair strategies.

A comprehensive review of existing literature reveals various repair techniques, including prestressed patches, shape memory alloys (SMAs), and composite patches. While these passive methods have demonstrated effectiveness, their performance can be compromised by variations in the loading environment. This limitation has encouraged interest in active repair techniques, particularly those utilizing piezoelectric actuators. Despite numerous studies on piezoelectric repair, a notable gap exists in applying these actuators to enhance the fatigue life of cracked structural members, especially I-beams. Although studies have explored repairing rectangular beams with piezoelectric actuators and I-beams with prestressed composite patches, an analytical approach specifically tailored to address bottom-edge cracks in I-beams remains unexplored. This research gap presents a unique method to develop an innovative repair strategy that utilizes the versatility of piezoelectric materials to significantly improve the structural integrity and lifespan of I-beams.

This chapter addresses the critical issue of crack propagation in I-beams by developing a novel analytical model for a bottom-edge cracked I-beam repaired with a strategically placed piezoelectric patch. The main objective is to deliver an opposing moment to counteract the moment induced by external loading, considering the shift in the neutral surface due to the crack. This analysis integrates fundamental principles of fracture mechanics and piezoelectricity to derive mathematical expressions for the stress intensity factor (SIF) and fracture loads. This study validates the proposed analytical model through finite element (FE) simulations using ABAQUS under various configurations. Furthermore, this study assesses static repair performance by evaluating the SIF and fracture loads for various crack lengths and repair voltages. A parametric study determines the optimal patch thickness for maximum repair effectiveness. Finally, the fatigue crack growth rate (FCGR) and fatigue life are evaluated under different repair voltages, comparing the results with those of an unrepaired I-beam.

3.2 Problem Formulation

The chapter focuses on developing SIF solutions for a configuration of cracked I-beam repaired with piezoelectric actuators. This section proposes SIF solutions for a cracked I-beam strengthened using piezoelectric materials. The geometry of the repaired I-beam is shown in Figure 3.1, indicating that the piezoelectric actuator is attached to the top flange of the beam while the crack present on the I-beam is on the bottom side. A four-point bending specimen is utilized to conduct this study where loads are applied at L/4 distance from the ends, and the piezoelectric patch is fixed at the mid-position of the beam on a span of length L/2. The width of the patch is the same as the width of the top flange of the I-beam. The initial crack length is greater than the thickness of the bottom flange. The voltage is so applied to the patch that a tensile force is created at the upper fiber of the top flange of the beam, resulting in the transfer of axial force and a moment at the geometric center of the cracked section. Hence, an opposite moment is developed as that of the applied moment, which minimizes the stress at the crack tip. The formulation of the SIF solutions for different loading combinations acted simultaneously involves a rigorous analytical approach [Ghafoori and Motavalli (2011)] using the concept of crack surface widening energy release rate [Xie et al. (2004)]. The interaction between the I-beam and the piezoelectric reinforcement determines the force exerted on the upper fiber of the top flange of the beam [Crawley and de Luis (1987)]. The neutral axis is shifted due to the presence of the crack, and the SIF under actuation is calculated accordingly. The superposition principle is then utilized to calculate the overall SIF of the I-beam

strengthened with piezoelectric actuators. The fracture load is investigated in a static repair scenario under constant voltage application, whereas in cyclic loading, repetitive voltage is applied to the patch with a zero-phase difference from the mechanical loading.

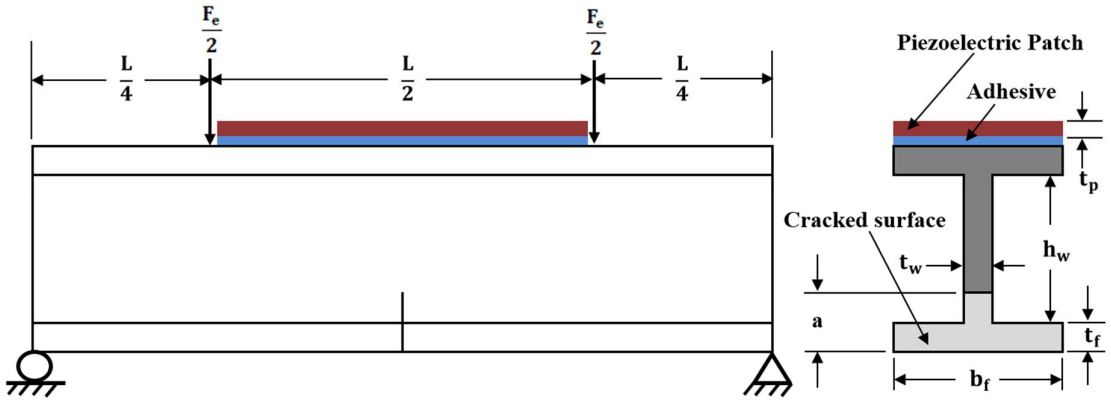

Figure 3.1: Geometry of the bottom edge-cracked I-beam repaired with the integration of the piezoelectric patch

3.2.1 SIF of Cracked I-Beams

Analytical solutions of SIF are introduced for a cracked I-beam by Ghafoori and Motavalli (2011). The established analytical solutions utilize the crack surface widening energy release rate to calculate the SIF. The experimental results and FE simulations using ABAQUS are used to verify the proposed model. The schematic view of the cracked half-length I-beam is shown in Figure 3.2. The SIF of the cracked I-beam considering plane-stress condition is given by Ghafoori and Motavalli (2011),

$$K_I = \left[\left\{-\frac{N^2}{A} - \frac{(M_c - Y_{nc}\cdot N)^2}{I} + N^2(\lambda_1+\lambda_2) + M_c^2(\eta_1+\eta_2)\right\}\frac{\pi}{t_w}\right]^{\frac{1}{2}} \tag{3.1}$$

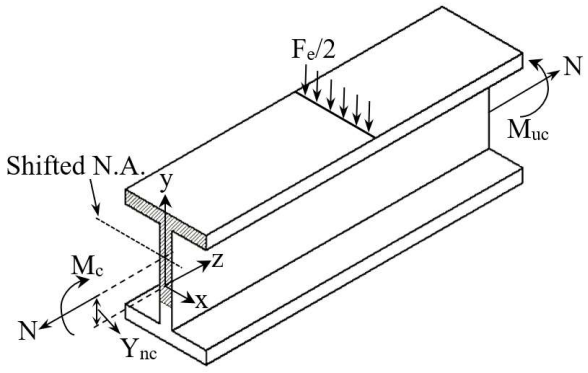

Figure 3.2: Schematic diagram of half-length cracked I-beam

where Y_{nc} is the change in the location of the neutral axis for the cracked and un-cracked sections, M_c is the bending moment at the cracked section, and 'N' is the axial force. 'A' and 'I' are the uncracked section's area, and the moment of inertia, respectively, and t_w is the thickness of the web portion of the beam. Subscript 'c' stands for cracked cross-section and 'uc' for un-cracked cross-section. λ_1, λ_2, η_1 and η_2 are parameters related to the beam geometry and crack length [Ghafoori and Motavalli (2011)]. The details of these parameters are given in Appendix A.

This study examines the cracked beam subjected to a total load of F_e as shown in Figure 3.1, resulting in a net-bending moment $M_e = F_e \cdot L/8$ at the cracked section. Axial force (N) is considered to be zero. Thus, the SIF of the cracked I-beam only under the bending moment M_e is expressed as,

$$K_I^{M_e} = M_e \left[\left\{ -\frac{1}{I} + (\eta_1 + \eta_2) \right\} \frac{\pi}{t_w} \right]^{\frac{1}{2}} \tag{3.2}$$

3.2.2 SIF Reduction via Piezoelectric Actuators

The schematic diagram for a cracked I-beam strengthened by a piezoelectric actuator is shown in Figure 3.1. The top fiber of the I-beam experiences compressive stress under external load. The piezoelectric actuator is placed at the top of the I-beam to counteract this bending moment. The piezoelectric strain coefficient d_{31} is considered the only effective mode, indicating that the patch is polarized in the y-direction (3-direction of the patch) and extensional strain occurs along the length of the beam (1-direction of the patch). For the present study, the force exerted by the patch is assumed only on the top fiber of the top flange of the I-beam, and under the application of the external voltage V, this force is given by Crawley and de Luis (1987),

$$F_P = \frac{E t_f T}{\psi + \alpha} \Lambda \tag{3.3}$$

where T is the distributed electrode width. ψ is a non-dimensional parameter given by Eq. (*3.4*). α is a constant that depends on the type of loading, and for bending, its value is $\alpha = 6$ Crawley and de Luis (1987).

$$\psi = \frac{E W_f t_f}{E_P W_P t_P} \tag{3.4}$$

Λ is the piezoelectric strain given by,

$$\Lambda = \frac{d_{31}}{t_P} V \tag{3.5}$$

Where $E, W_f, \text{and } t_f$ are Young's modulus, the width of the flange, and the thickness of the flange for the beam, respectively and $E_P, W_P, \text{and } t_P$ are Young's modulus, width, and thickness of the patch, respectively.

This force exerted at the top layer of the cracked I-beam is being transferred as the combined effect of a compressive force F_P and a moment M_P at the neutral surface of the uncracked section of the beam. The overall SIF contribution by the actuation of the piezoelectric material is calculated using the superposition principle.

The SIF under the pure bending moment M_P is given by,

$$K_I^{M_P} = M_P \left[\left\{ -\frac{1}{I} + (\eta_1 + \eta_2) \right\} \frac{\pi}{t_w} \right]^{\frac{1}{2}} \tag{3.6}$$

where M_P is defined as,

$$M_P = F_P \left(t_f + \frac{h}{2} \right) \tag{3.7}$$

The SIF under the loading of pure axial force F_P is given by,

$$K_I^{F_P} = F_P \left[\left\{ -\frac{1}{A} + (\lambda_1 + \lambda_2) + Y_{nc}^2 (\eta_1 + \eta_2) \right\} \frac{\pi}{t_w} \right]^{\frac{1}{2}} \tag{3.8}$$

The final expression of the SIF due to the actuation effect of the piezoelectric material is obtained by adding the SIF due to M_P and the axial force F_P using the superposition principle and written as,

$$K_I^{Piezo} = K_I^{M_P} + K_I^{F_P} \tag{3.9}$$

The total SIF is obtained by adding the individual SIF contribution by the piezoelectric actuator and the external loading and given by,

$$K_I^{Total} = K_I^{M_e} + K_I^{Piezo} \tag{3.10}$$

It is to be noted that when the term K_I^{Piezo} is calculated alone, it gives a negative value as the compressive stress is developed at the crack tip, which tends to close the crack. But when

combined with the SIF due to the external loading, this term K_I^{Piezo} is being deducted from the K_I^{Me} and a reduced K_I^{Total} is obtained.

The Eq.(*3.10*) can be rewritten as,

$$K_I^{Total} = \left\{M_e + F_P\left(t_f + \frac{h}{2}\right)\right\}\left[\left\{-\frac{1}{I} + (\eta_1 + \eta_2)\right\}\frac{\pi}{t_w}\right]^{\frac{1}{2}} + F_P\left[\left\{-\frac{1}{A} + (\lambda_1 + \lambda_2) + Y_{nc}^2(\eta_1 + \eta_2)\right\}\frac{\pi}{t_w}\right]^{\frac{1}{2}} \quad (3.11)$$

The total SIF K_I^{Total} in a beam is influenced by crack length 'a', external bending moment M_e, and tensile force F_P produced at the top flange of the I-beam. In the actuated mode of the piezoelectric patch, the total SIF $\left(K_I^{Total}\right)$ initially remains negative $\left(K_I^{Piezo} > K_I^{Me}\right)$ until the external bending moment surpasses a specific threshold value $\left(K_I^{Me} \geq K_I^{Piezo}\right)$. This situation arises from the compressive axial force and negative bending moment imposed by the piezoelectric patch on the cracked section of the beam. The behavior of the crack shows different modes with increasing external load under constant actuation by the piezoelectric patch, as discussed by [Ghafoori et al. (2012)]. Initially, compressive stress at the crack tip maintains a passive crack mode. Negative SIFs imply compressive stress fields but hold no physical significance. The crack gradually opens as the external bending moment exceeds a threshold value $M_{e,th}$ at which $K_I^{Me,th} = K_I^{Piezo}$, resulting in $K_I^{Total} = 0$. When compressive stress vanishes around the crack tip, the crack becomes fully active and transitions to a tensile stress field $\left(K_I^{Me} > K_I^{Piezo}\right)$ occurs. Failure modes include fracture failure of the beam and piezoelectric patch if stresses exceed materials' permissible limits. In this analysis, external loading is chosen above the threshold value $M_{e,th}$ for the occurrence of active crack mode $\left(K_I^{Me} \geq K_I^{Piezo}\right)$, so that $K_I^{Total} > 0$.

3.2.3 Methodology for Fracture Load Estimation

The maximum load-carrying capacity of cracked I-beams depends on the crack size, its location, and the properties of the beam material. When a beam is cracked, its structural integrity is compromised, and it will have a lower load-carrying capacity than an intact beam beyond a certain amount of load, resulting in catastrophic failure for a given crack geometry. As far as the fracture load of an I-beam is concerned, fracture mechanics criteria are commonly used to evaluate the impact of cracks on maximum load-carrying capacity. Based

on linear-elastic fracture mechanics (LEFM), the maximum load-carrying capacity of the cracked I-beam is determined when the SIF reaches the fracture toughness of the material.

3.2.3.1 Fracture Load Estimation Without Repair

To calculate the fracture load (F_{fl}^{wr}), the SIF $\left(K_I^{M_e}\right)$ for the cracked beam as obtained by Eq. (*3.2*) is made equal to the fracture toughness (K_{IC}) and is given by,

$$K_I^{M_e} = K_{IC} = \frac{F_{fl}^{wr} \cdot L}{8}\left[\left\{-\frac{1}{I} + (\eta_1 + \eta_2)\right\}\frac{\pi}{t_w}\right]^{\frac{1}{2}}$$
$$F_{fl}^{wr} = \frac{8 \cdot K_{IC}}{L\left[\left\{-\frac{1}{I} + (\eta_1 + \eta_2)\right\}\frac{\pi}{t_w}\right]^{\frac{1}{2}}} \tag{3.12}$$

3.2.3.2 Fracture Load Estimation with Active Repair

To calculate the fracture load (F_{fl}^{ar}), the SIF for the cracked beam after repair, as obtained by Eq. (*3.11*), is made equal to the fracture toughness (K_{IC}) and is given by,

$$K_I^{Total} = K_{IC} = \left\{\frac{F_{cr}^{ar} \cdot L}{8} + F_P \cdot \left(t_f + \frac{h}{2}\right)\right\}\left[\left\{-\frac{1}{I} + (\eta_1 + \eta_2)\right\} \cdot \frac{\pi}{t_w}\right]^{\frac{1}{2}} + F_P$$
$$\cdot \left[\left\{-\frac{1}{A} + (\lambda_1 + \lambda_2) + Y_n^2 \cdot (\eta_1 + \eta_2)\right\} \cdot \frac{\pi}{t_w}\right]^{\frac{1}{2}} \tag{3.13}$$
$$F_{cr}^{ar} = \frac{8}{L}\left[\frac{K_{IC} - F_P\left[\left\{-\frac{1}{A} + (\lambda_1 + \lambda_2) + Y_n^2(\eta_1 + \eta_2)\right\} \cdot \frac{\pi}{t_w}\right]^{\frac{1}{2}}}{\left[\left\{-\frac{1}{I} + (\eta_1 + \eta_2)\right\}\frac{\pi}{t_w}\right]^{\frac{1}{2}}} - F_P\left(t_f + \frac{h}{2}\right)\right]$$

3.2.4 Methodology for FCGR and Fatigue Life Estimation

In this section, an attempt is made to estimate the fatigue crack growth (FCG) and service life of a cracked structure subjected to cyclic tension. For this purpose, the most common expression of the FCG model developed at NASA and first published by Forman, and Mettu (1990), describes all three regions of the well-known crack growth curve [Anderson (2017)].

$$\frac{da}{dN} = C \cdot (\Delta K)^m \cdot \frac{\left(1 - \frac{\Delta K_{th}}{\Delta K}\right)^p}{\left(1 - \frac{K_{max}}{K_{Ic}}\right)^q} \tag{3.14}$$

The expression mentioned above describes the FCGR (in millimeters per cycle). C, m, p, and q are experimentally determined material constants. Determining the SIF range ($\Delta K = K_{max} - K_{min}$) between maximum and minimum loading is of the utmost importance for this study. This SIF range can be determined by derivation from previous sections. The difference in SIF (ΔK) is influenced by the range in load magnitude ($\Delta F_e = F_{e,max} - F_{e,min}$) and the change in applied repair voltage ($\Delta V = V_{max} - V_{min}$) across all analyzed cases. The crack growth concerning the number of loading cycles is determined by taking the incremental crack propagation (Δa_i) against incremental loading cycles (ΔN_i), where $\Delta a_i = a_{i+1} - a_i$ and $\Delta N_i = N_{i+1} - N_i$. In every iteration, Δa_i is calculated for a specific ΔN_i. Then, crack length (a_f), SIF range (ΔK), and maximum SIF (K_{max}) are updated. This iteration is repeated until either the maximum SIF (K_{max}) reaches the value of the fracture toughness (K_{IC}) or the crack length (a_f) reaches the critical crack length a_c. The fatigue life for all the situations can be directly obtained by integrating Eq. (14) from the initial crack length a_o to the final crack length, a_f ($a_f = a_c$). The critical crack length (a_c) depends upon the applied load, the structural configuration of the cracked beam, and the repair parameters. It is determined from the fracture toughness (K_{IC}) of the beam material and is given by,

$K_{IC} = \left(K_I^{M_e}\right)_{at\ a_c}$ for without repair condition

$K_{IC} = \left(K_I^{Total}\right)_{at\ a_c}$ for active repair condition

3.2.4.1 Fatigue Life Without Repair

From Eq. (3.2), the SIF range can be written as,

$$\Delta K_I^{M_e} = \Delta M_e \left[\left\{-\frac{1}{I} + (\eta_1 + \eta_2)\right\}\frac{\pi}{t_w(1-\nu^2)}\right]^{\frac{1}{2}} \tag{3.15}$$

Putting this value in Eq. (3.14), we have,

$$\frac{da}{dN} = C \cdot \left[\Delta M_e \left[\left\{-\frac{1}{I} + (\eta_1 + \eta_2)\right\}\frac{\pi}{t_w(1-\nu^2)}\right]^{\frac{1}{2}}\right]^m \cdot \frac{\left(1 - \frac{\Delta K_{th}}{\Delta M_e\left[\left\{-\frac{1}{I}+(\eta_1+\eta_2)\right\}\frac{\pi}{t_w(1-\nu^2)}\right]^{\frac{1}{2}}}\right)^p}{\left(1-\frac{K_{max}}{K_{Ic}}\right)^q} \tag{3.16}$$

and,

$$dN = \frac{da}{C\cdot\left[\Delta M_e\left[\left\{-\frac{1}{I}+(\eta_1+\eta_2)\right\}\frac{\pi}{t_w(1-\nu^2)}\right]^{\frac{1}{2}}\right]^m \cdot \frac{\left(1-\frac{\Delta K_{th}}{\Delta M_e\left[\left\{-\frac{1}{I}+(\eta_1+\eta_2)\right\}\frac{\pi}{t_w(1-\nu^2)}\right]^{\frac{1}{2}}}\right)^p}{\left(1-\frac{K_{max}}{K_{Ic}}\right)^q}}$$

Fatigue life without repair condition is obtained from the numerical integration of Eq. (3.16),

$$N_f = \int_0^{N_f} dN = \int_{a_o}^{a_{f=}a_c} \frac{da}{C\cdot\left[\Delta M_e\left[\left\{-\frac{1}{I}+(\eta_1+\eta_2)\right\}\frac{\pi}{t_w(1-\nu^2)}\right]^{\frac{1}{2}}\right]^m \cdot \frac{\left(1-\frac{\Delta K_{th}}{\Delta M_e\left[\left\{-\frac{1}{I}+(\eta_1+\eta_2)\right\}\frac{\pi}{t_w(1-\nu^2)}\right]^{\frac{1}{2}}}\right)^p}{\left(1-\frac{K_{max}}{K_{Ic}}\right)^q}} \tag{3.17}$$

3.2.4.2 Fatigue Life Enhancement via Active Repair

From Eq. (3.11), the SIF range can be written as,

$$\begin{aligned}\Delta K_I^{Total} = &\left\{\Delta M_e + \Delta F_P\left(t_f+\frac{h}{2}\right)\right\}\left[\left\{-\frac{1}{I}+(\eta_1+\eta_2)\right\}\frac{\pi}{t_w(1-\nu^2)}\right]^{\frac{1}{2}} \\ &+ \Delta F_P\left[\left\{-\frac{1}{A}+(\lambda_1+\lambda_2)+Y_n^2(\eta_1+\eta_2)\right\}\frac{\pi}{t_w(1-\nu^2)}\right]^{\frac{1}{2}}\end{aligned} \tag{3.18}$$

Putting this value in Eq. (3.14), one obtains,

$$\frac{da}{dN} = C\cdot\left[\left\{\Delta M_e + \Delta F_P\left(t_f+\frac{h}{2}\right)\right\}\left[\left\{-\frac{1}{I}+(\eta_1+\eta_2)\right\}\frac{\pi}{t_w}\right]^{\frac{1}{2}} + \Delta F_P\left[\left\{-\frac{1}{A}+(\lambda_1+\lambda_2)+Y_n^2(\eta_1+\eta_2)\right\}\frac{\pi}{t_w}\right]^{\frac{1}{2}}\right]^m \frac{\left(1-\frac{\Delta K_{th}}{\left\{\Delta M_e+\Delta F_P\left(t_f+\frac{h}{2}\right)\right\}\left[\left\{-\frac{1}{I}+(\eta_1+\eta_2)\right\}\frac{\pi}{t_w}\right]^{\frac{1}{2}}+\Delta F_P\left[\left\{-\frac{1}{A}+(\lambda_1+\lambda_2)+Y_n^2(\eta_1+\eta_2)\right\}\frac{\pi}{t_w}\right]^{\frac{1}{2}}}\right)^p}{\left(1-\frac{K_{max}}{K_{Ic}}\right)^q} \tag{3.19}$$

and,

$$dN = \frac{da}{C\cdot\left[\left\{\Delta M_e+\Delta F_P\left(t_f+\frac{h}{2}\right)\right\}\left[\left\{-\frac{1}{I}+(\eta_1+\eta_2)\right\}\frac{\pi}{t_w}\right]^{\frac{1}{2}}+\Delta F_P\left[\left\{-\frac{1}{A}+(\lambda_1+\lambda_2)+Y_n^2(\eta_1+\eta_2)\right\}\frac{\pi}{t_w}\right]^{\frac{1}{2}}\right]^m \cdot \frac{\left(1-\frac{\Delta K_{th}}{\left\{\Delta M_e+\Delta F_P\left(t_f+\frac{h}{2}\right)\right\}\left[\left\{-\frac{1}{I}+(\eta_1+\eta_2)\right\}\frac{\pi}{t_w}\right]^{\frac{1}{2}}+\Delta F_P\left[\left\{-\frac{1}{A}+(\lambda_1+\lambda_2)+Y_n^2(\eta_1+\eta_2)\right\}\frac{\pi}{t_w}\right]^{\frac{1}{2}}}\right)^p}{\left(1-\frac{K_{max}}{K_{Ic}}\right)^q}$$

and,

Fatigue life after repair is obtained from the numerical integration of Eq. (3.19),

$$N_f = \int_0^{N_f} dN = \int_{a_o}^{a_{f=}a_c} \frac{da}{C\cdot\left[\left\{\Delta M_e+\Delta F_P\left(t_f+\frac{h}{2}\right)\right\}\left[\left\{-\frac{1}{I}+(\eta_1+\eta_2)\right\}\frac{\pi}{t_w}\right]^{\frac{1}{2}}+\Delta F_P\left[\left\{-\frac{1}{A}+(\lambda_1+\lambda_2)+Y_n^2(\eta_1+\eta_2)\right\}\frac{\pi}{t_w}\right]^{\frac{1}{2}}\right]^m} \cdot \frac{\left(1-\frac{\Delta K_{th}}{\left\{\Delta M_e+\Delta F_P\left(t_f+\frac{h}{2}\right)\right\}\left[\left\{-\frac{1}{I}+(\eta_1+\eta_2)\right\}\frac{\pi}{t_w}\right]^{\frac{1}{2}}+\Delta F_P\left[\left\{-\frac{1}{A}+(\lambda_1+\lambda_2)+Y_n^2(\eta_1+\eta_2)\right\}\frac{\pi}{t_w}\right]^{\frac{1}{2}}}\right)^p}{\left(1-\frac{K_{max}}{K_{Ic}}\right)^q} \tag{3.20}$$

3.3 Finite Element (FE) Modelling using ABAQUS and Validation

In this section, Finite element models have been developed using the commercial FE software package ABAQUS to evaluate the SIF and fracture load. However, the present study aims to reduce the SIF at the crack root by applying external voltage on the attached piezoelectric patch at the top of the I-beam under the four-point loading situation. Therefore, the numerical model mainly comprises an I-beam, piezoelectric patch, and adhesive layer. Firstly, two cracked I-beams are modeled: one with a seam crack to determine the SIF and another with an XFEM crack. The results obtained from the present FE simulation are validated with the available experimental results [Ghafoori and Motavalli (2011)] under static load to check the accuracy of the FE model. Secondly, another model with the integrated piezoelectric patch is developed, and results obtained from the analytical model are compared with the results of the FE simulation.

3.3.1 Modeling of the cracked I-beam

To perform the analysis, an I-section is created using the sketch section of the part module of ABAQUS CAE, and then the section is extruded for the required length. The beam model is partitioned to apply the loading at the L/4 distance from both ends. After that, the beam is partitioned again by creating a cell to incorporate a crack by assigning a seam crack from the interaction module, as shown in Figure 3.3a. The dimensions of the partitions are adjusted to account for the various crack lengths. The beam is further partitioned to discretize the model smoothly by hexahedral elements Figure 3.3b. A static step is created, and the required boundary conditions are applied at the ends by controlling displacements to simulate the cracked I-beam.

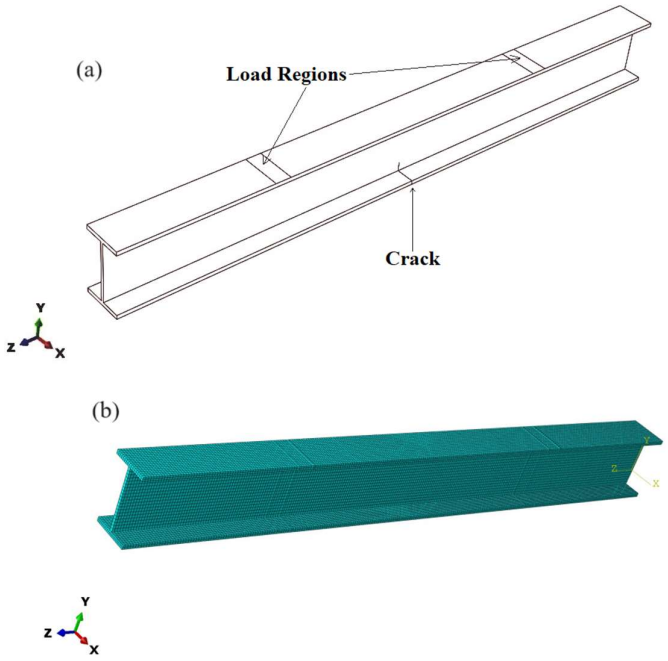

Figure 3.3: (a) Wireframe model of the beam describing the partitions for crack and load (b) the discretized beam model

3.3.2 Modeling of the cracked I-beam repaired with bonded piezoelectric patch

Two rectangular sections are created and extruded to form the piezoelectric patch and the adhesive layer. Using the assembly module, the instances are created and the patch is attached between the two load regions (length of L/2). The piezoelectric patch to the adhesive layer and the adhesive layer to the beam's top surface are bonded by tie interaction under the interaction module. The seam crack is assigned to the created cell partitions at the mid-span using the interaction module. The assembled model with seam crack is shown in Figure 3.4. The Piezoelectric patch instance is separately assigned with a datum where the 'Z' or '3' axis is taken along the thickness (Figure 3.4) since the polarization direction is 'Z' or '3'. The assembled model is meshed by a hexahedral element, and the piezoelectricity is defined to the respective part by applying the piezoelectric element type under the mesh module. The two ends of the beam are fixed by creating an 'Encastre' boundary condition (B.C.) in which all the degrees of freedom ceased under the initial step. Subsequently, another electrical boundary condition is applied on the face of the piezoelectric patch, which is in contact with the adhesive layer to keep the voltage zero on that face. The loads are given by creating two load lines. A static general step is created to apply the loading.

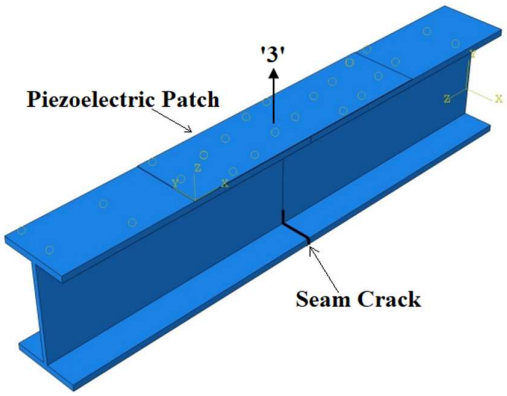

Figure 3.4: 3D Model of an I-Sectional beam with a crack at the bottom and an attached piezoelectric patch on the top face

3.3.3 Modeling of Propagating Crack

The propagation of cracks is modeled in ABAQUS with the aid of the Extended Finite Element Method (XFEM), which allows precise modeling of cracks by enriching standard finite elements with additional degrees of freedom to capture crack propagation with minimal remeshing [Belytschko and Black (1999)]. A 3D rectangular planar shell part was created with a length equal to the crack length and width, the same as that of the beam, to make the XFEM crack. The planar object is fitted at the mid-span of the beam. The fracture criteria are defined in the material property of the beam under the property module. The 3D rectangular planar shell is defined as a crack under the interaction module while creating the XFEM crack, and the beam is defined as the crack domain, as shown in Figure 3.5.

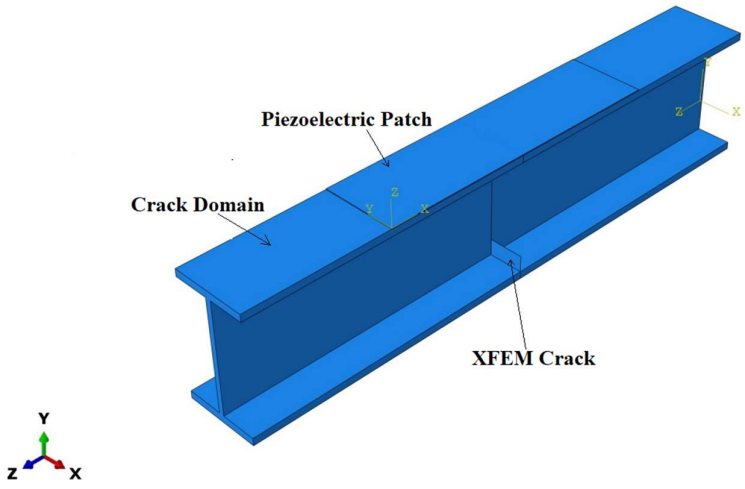

Figure 3.5: A model representing the XFEM crack and its domain of an I-beam of length 500 mm with a 20 mm crack length with a bonded piezoelectric patch

3.3.4 Mesh Sensitivity Analysis

Mesh sensitivity analysis is essential to ensure the accuracy of finite element (FE) models, especially when validating results against analytical or experimental data. For this study, the goal was to determine the appropriate mesh size for accurately capturing the stress intensity factor (SIF). The analytical SIF for the crack length of 20 mm is 945 MPa.mm$^{0.5}$ when subjected to a 10 kN load. Mesh sizes ranging from coarse (0.05 m) to fine (0.005 m) were considered here. The FE model was analyzed with varying mesh sizes, ranging from coarse to fine. Table 3.1 compares mesh size, SIF, and the relative error to the analytical SIF. Results show that with mesh sizes smaller than 0.008 m, the SIF stabilizes. As a result, there is no significant improvement while increasing computational time, indicating convergence. A mesh size of 0.008 m was chosen as the optimal balance between accuracy and computational efficiency. Therefore, 0.008 m is the best choice for FE modeling to accurately validate the SIF against the analytical result.

Table 3.1: Mesh convergence study

Global approximate element Size (m)	Analytical SIF (MPa.mm$^{0.5}$)	Numerical SIF (MPa.mm$^{0.5}$)	Error (%)
0.05	945.52	816.95	13.60
0.03		845.21	10.61
0.015		872.80	7.69
0.01		908.43	3.92
0.008		930.83	1.55
0.007		932.24	1.40
0.006		932.72	1.35
0.005		933.19	1.30

3.3.5 Validation of FE Model for a Cracked I-Beam Without Repair

To validate the present FE model of the cracked I-beam, results obtained from the present FE analysis are compared with the experimental results obtained by Ghafoori and Motavalli (2011). The considered experimental investigation was conducted for a fatigue loading of 1 kN to 10 kN with an initial crack length of 12.2 mm on a steel I-beam. The geometric properties are t_f = 6.2 mm, b_f = 65 mm, h =107.4 mm, t_w=4.4 mm, and L=1000 mm. In the present FE analysis, the total load of 10 kN is divided into two halves and is applied in

the trim strips created by face partitioning at the 250 mm distance from both ends. After applying the load, the stress distribution is obtained and represented in Figure 3.6 for the crack length of 20 mm. The SIF range (ΔK) is taken from the literature, and the numerical SIF is recorded from the FE analysis for maximum and minimum loading for different crack lengths as depicted in Table 3.2, showing a good agreement with the present FE modeling.

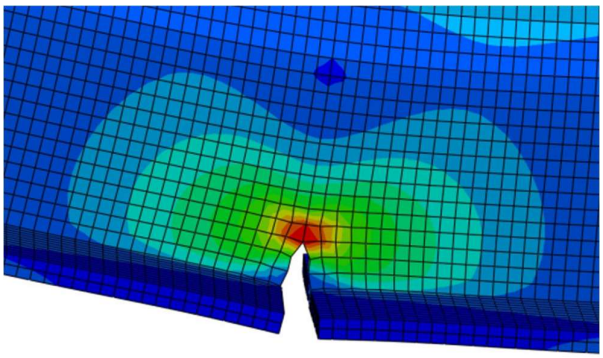

Figure 3.6: Stress distribution at the root of 20 mm crack under 10 kN load

Table 3.2: Comparison of the SIF range (ΔK) of the present FE model with the experimental study [Ghafoori and Motavalli (2011)]

Case	**Crack Length (mm)**	**SIF range (ΔK) $(\mathbf{MPa\sqrt{mm}})$**	
		Present FE	**Experimental** [Ghafoori and Motavalli (2011)]
Cracked steel I-beam	15	802.19	809.19
	20	842.61	851.61
	25	900.53	912.53

Another analysis is conducted to determine the fracture load and demonstrate the accuracy of a propagating crack. A statically loaded cracked steel I-beam is modeled on the ABAQUS platform with a crack length of 74 mm to validate this scenario [Ghafoori and Motavalli (2011)]. In this present XFEM analysis, the magnitude of the load is estimated at which the crack starts propagating. The estimated load, i.e., critical load for the mentioned crack depth, is 16.2 kN for the present FE analysis, which is pretty close to that of 15.9 kN for the experimental study [Ghafoori and Motavalli (2011)].

Furthermore, the crack begins propagating when SIF reaches the fracture toughness of the material, and the corresponding load is the fracture load. In this stage, the crack will propagate even under constant loading, resulting in catastrophic component failure. Figure 3.7 represents the deformed configuration where the crack propagation has just started. As the applied loading continues to increase, the beam approaches complete failure, as shown in Figure 3.8. It is worth noting that the two deformed views are provided in Figure 3.8 to clearly illustrate the occurrence of the final failure of the beam, which could well correlate and give insights into the actual failure of a beam in practice. The first deformed view of Figure 3.8 indicates that the propagating crack reached the top flange, whereas the second shows the I-beam's complete failure.

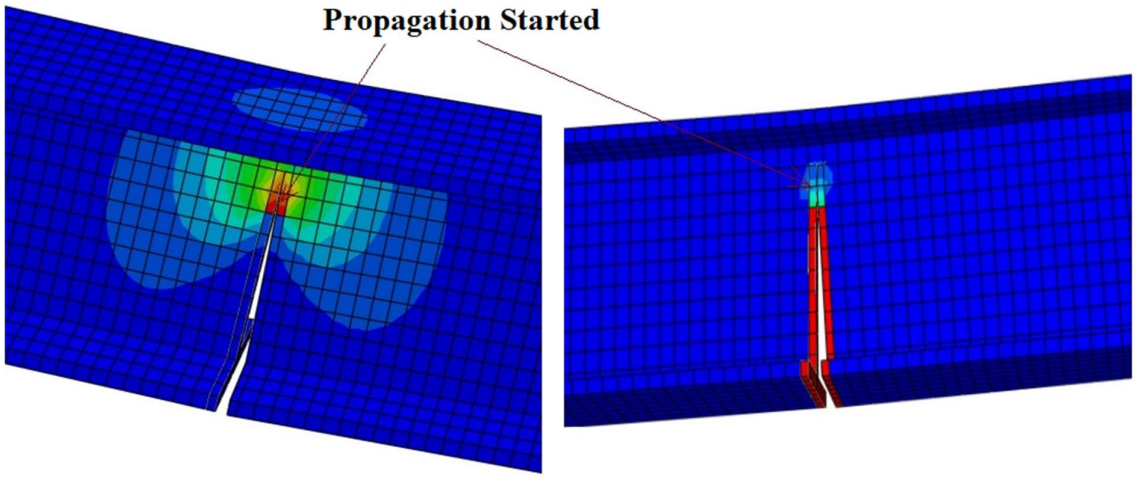

Figure 3.7: A deformed view of the cracked beam focusing on the crack root shows the crack propagation initiation

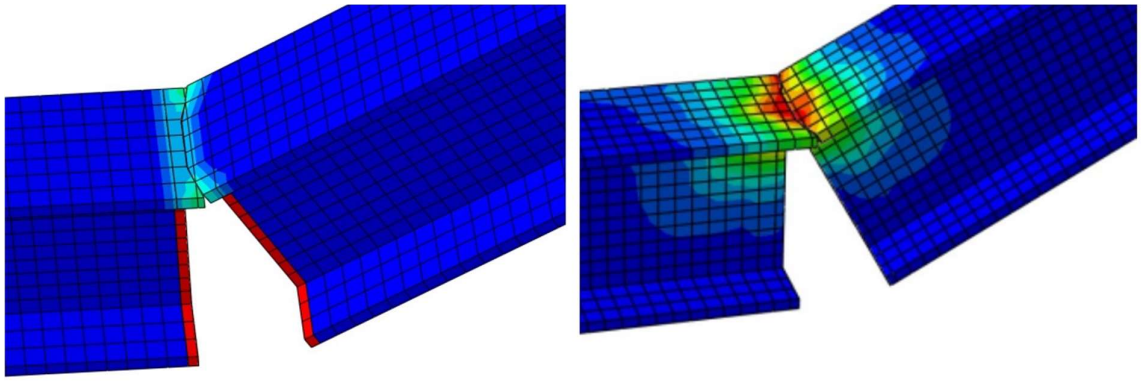

Figure 3.8: A deformed view of the cracked beam focusing on the crack root showing the final fracture

3.3.6 Validation of Analytical Model for Active Repair

In the previous section, the FE model was well-verified for cracked steel I-beam for static loading and under-crack propagation scenarios. The analytical model developed in this article for the bottom edge-cracked I-beam with the integration of the piezoelectric patch (Figure 3.1) is now verified with the FE analysis. The I-beam is made of Al 6061-T6, whereas PZT-5H is utilized for actuation, and resin epoxy is used to fix the piezoelectric patch to the beam. The dimensions of the I-beam and piezoelectric patch are taken as mentioned in Table 3.3 for both FE and analytical analysis. The material properties of the I-beam are mentioned in Table 3.4.

Table 3.3: Parameters of the geometry

Dimensions	**Al 6061-T6 (mm)**	**PZT-5H (mm)**
Height	h_{max}=76.2	h_p=0.5
Width	b_f=63.5	b_p=63.5
Thickness	t_w=3.81, t_f=3.81	0.5
Length	500	250

Table 3.4: Mechanical properties and crack growth parameters of Al 6061-T6 material [Fossati et al. (2021)]

Parameter	**Value**
Elastic Modulus (E_s)(GPa)	68.9
Poisson's ratio (ν)	0.33
Tensile yield strength (MPa)	276
Ultimate tensile strength (MPa)	310
Density (Kg/m^3)	2700
$\Delta K_{th}\left(MPa\sqrt{mm}\right)$ at SR=0.1	45.52
$K_{IC}\left(MPa\sqrt{mm}\right)$	938.2
C	5.079e-10
m	2.3
p	0.5
q	0.5

3.3.6.1 Validation of Active Repair by Static Voltage

A 500 mm long cracked I-beam is modeled using the ABAQUS platform with various crack lengths. A four-point bending scheme is used, applying a load of 1 kN magnitude (a total load of 2 kN) along partitioned sections to develop a constant bending moment. A piezoelectric actuator is mounted to the top flange between the load regions to generate an opposite local bending moment when voltage is applied. The simulation is conducted without actuating the piezoelectric patch, then attempting to repair the crack by actuating the patch externally under 500 V. The numerical SIF is recorded for various crack lengths for both cases. The analytical results obtained from Eqs. (3.2) and (3.11) are compared with the numerical results of ABAQUS and represented in Table 3.5, revealing a good agreement with the numerical one. Figure 3.9(a) and (b) illustrate the deformed configurations of the I-beam before and after voltage is applied. The axial normal stress component of the beam is measured at the nearest node to the crack root. A considerable stress reduction is found at the root after applying the voltage, indicating enhanced structural integrity of the beam.

Table 3.5: Comparison of analytical SIF with the FE solutions for Al 6061-T6 I-beam repaired with PZT-5H

Repair Voltage (V)	Crack Length (mm)	SIF $\left(\mathbf{MPa}\sqrt{\mathbf{mm}}\right)$	
		Analytical	FE
0	10	163.04	169.04
	15	185.36	192.36
	20	209.68	217.68
500	10	195.4	210.4
	15	222.5	232.5
	20	252.2	259.2

3.3.6.2 Validation of Analytical Model for Fracture Load

Another FE analysis is performed to validate the use of piezoelectric actuation to arrest the propagating crack, leading to an increase in fracture load. A beam with a 20-mm crack length is simulated to measure the fracture load under piezoelectric actuation. The crack propagates when the total load is 7.39 kN without applying voltage to the piezoelectric patch. When a 200 V external voltage field is applied to the top face of the attached piezoelectric patch, the crack propagation is arrested. Figure 3.10a shows the propagation of the XFEM crack before applying the external voltage to the patch. In contrast, Figure 3.10b shows that

the crack propagation gets arrested after applying the suitable voltage to the piezoelectric patch. The study suggests that crack propagation can be stopped by applying a considerable amount of external voltage to the piezoelectric patch due to the maximum SIF reducing to some extent and becoming less than the fracture toughness, potentially preventing crack propagation. The fracture load is computed analytically using the formula provided by Eqs. (3.12) and (3.13). The analytical and FE findings of the fracture load are illustrated in Table 3.6 for the cases without and with 100-500 V actuation for a 20 mm crack length.

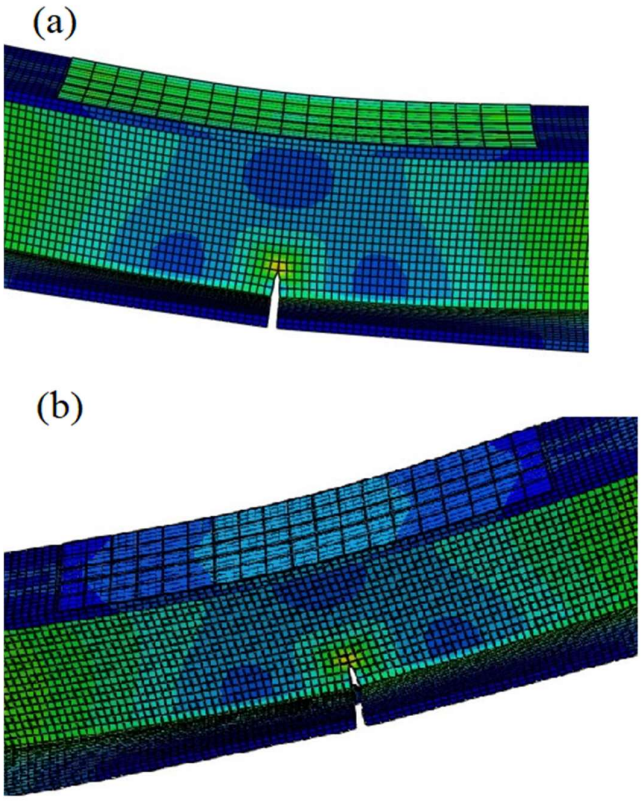

Figure 3.9: FE deformed cracked I-beam (crack length=20 mm) with piezoelectric patch (a) before applying voltage (b) after applying 500 V

Table 3.6: Comparison of analytical fracture load (F_{fl}) with the FE solutions for Al 6061-T6 cracked I-beam

Fracture Load, F_{fl} (kN)						
Repair Voltage (V)	0	100	200	300	400	500
Present Analytical	7.44	7.51	7.58	7.64	7.71	7.78
FE analysis	7.39	7.46	7.52	7.59	7.66	7.72

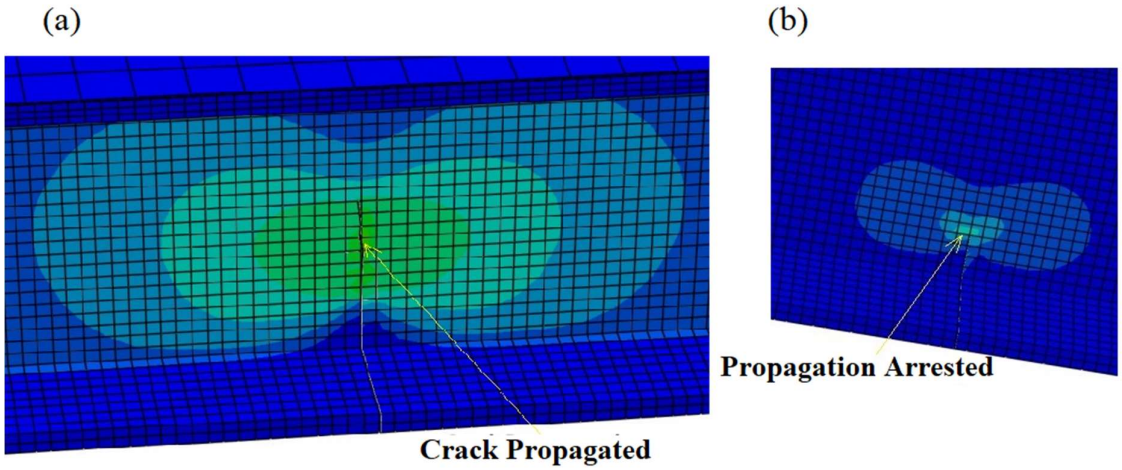

Figure 3.10: (a) Propagated XFEM Crack under applied load before piezoelectric actuation (b) Propagation of crack is arrested by applying an external voltage of 200 V on the patch

3.3.6.3 Validation of Analytical Model for Fatigue Crack Growth (FCG)

FE approaches for crack growth simulation often involve tedious manual modeling to modify crack depths. Therefore, fatigue crack growth (FCG) is calculated instead of fatigue life, and the FCG obtained from the FE simulation is used to validate the analytical modeling. FE analysis is done by remodeling with different crack lengths starting from 5 mm to 20 mm with an increment of 1 mm. SIF values of considered crack lengths are obtained from numerical simulations at maximum and minimum loading. The fatigue crack growth (FCG) calculation is done based on well-established LEFM for cracked members, and the modeling of fatigue crack propagation is performed with SIF ranges (ΔK) obtained from the numerical simulation [Chen et al. (2018), Huang et al. (2022)]. The number of loading cycles for different crack lengths can be determined from the expression given by Eq. (3.21),

$$\Delta N = \frac{\Delta a}{C \cdot (\Delta K)^m \cdot \frac{\left(1 - \frac{\Delta K_{th}}{\Delta K}\right)^p}{\left(1 - \frac{K_{max}}{K_{Ic}}\right)^q}} \tag{3.21}$$

The loading is provided in a range of 0.2 kN to 2 kN. The voltage corresponding to minimum loading is kept at 0 V, and 500 V is applied for the maximum loading for a particular loading cycle. The analytical and numerical fatigue crack growth curves are presented in Figure 3.11, showing good agreement.

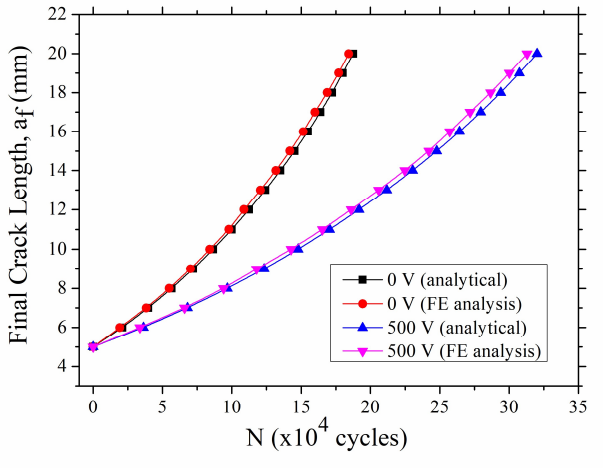

Figure 3.11: Comparison of numerical and analytical fatigue crack growth (FCG) against the number of loading cycles

3.4 Results and Discussion

Once the findings of the analytical approach are validated with FE analysis for all defined configurations, a study is conducted to determine the SIF and fracture load. In contrast, using the analytical method proposed in this work, the SIF range, FCGR, and fatigue life are calculated under cyclic tensile loading without repair and with repair under various repair voltages.

3.4.1 Comparison of Repaired and Without Repaired I-Beams

The SIFs are estimated under static loading using Eqs. (3.2) and (3.11) without and with repair configurations, respectively, under a constant load of 1 kN at each load point (total 2 kN). The repair voltages applied during this investigation were 100, 200, 300, 400, and 500 V, and the crack length ranges from 5mm to 50mm. The thickness of the patch employed in this comparison study is 0.5 mm. Figure 3.12a depicts the variation of SIF about crack length at various repair voltages. It shows a significant reduction in SIF compared to the configuration without repair after applying voltages. The amount of SIF reduction is higher as the repair voltage increases due to the piezoelectric material providing a counter-moment similar to the applied moment at the crack plane, reducing stress at the crack tip. Higher repair voltages show the most significant reduction as the actuation effect increases with the increase of repair voltages. The results are taken until the SIF reaches the material's fracture toughness. The enlarged view of the illustration near the fracture toughness for various repair voltages is shown separately, as represented in Figure 3.12b. It has been found that the critical crack

length increases for the higher repair voltages and given by 56.2 mm for without repair configuration, whereas 56.8 mm, 57.4 mm, 58 mm, 58.6 mm, and 59.2 mm for 100, 200, 300, 400, and 500 V respectively. Figure 3.13 depicts the reduction percentage in SIF after repair compared to the condition without repair for various repair voltages and crack lengths of 10 mm, 20 mm, 30 mm, 40 mm, and 50 mm. This illustration shows that the highest reduction is achieved for larger cracks under a fixed repair voltage. For example, 16.61 % and 17.97 % reductions are achieved for crack lengths 5 mm and 50 mm, respectively, under 500 V repair voltage. This is found as the patch is attached to the top flange of the beam while the crack is on the bottom side, and due to this, the shock of actuation produced by the patch is less for short crack.

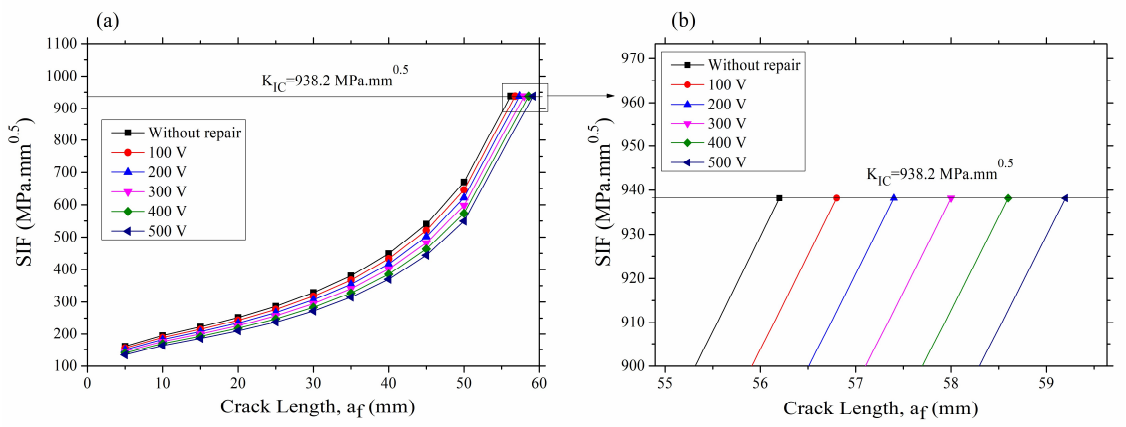

Figure 3.12: SIF vs. Crack length for various repair voltages

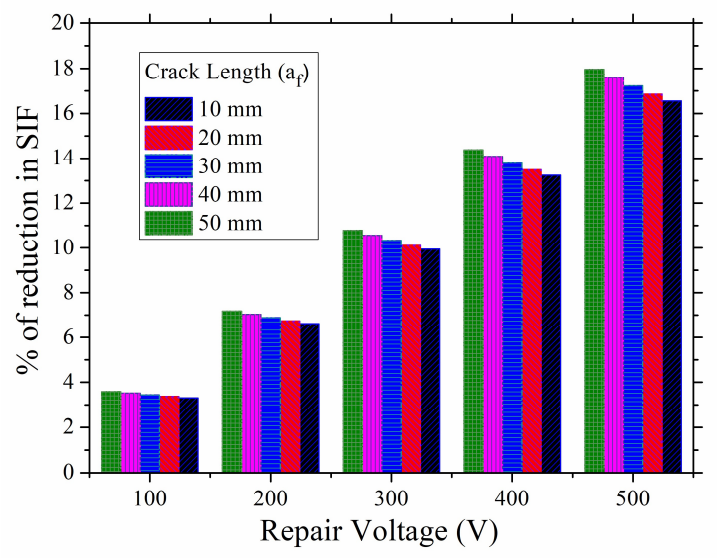

Figure 3.13: Effect of repair voltages on the percentage of reduction in SIF concerning without repair conditions for various crack length

3.4.2 Influence of Piezoelectric Patch Thickness

Choosing the proper thickness of the piezoelectric patch is very important, as the actuation mainly produced depends on the stiffness ratio and the piezoelectric strain [Zhou et al. (2024)]. In the previous discussions, the thickness was taken as 0.5 mm for the conciseness of the validation study. However, to understand the role of patch thickness on repair performance, a study has been conducted for different thicknesses ranging from 0.1 mm to 1 mm. Every piezoelectric material has a specific maximum limit of applied electric field above which it does not function properly [Cheng et al. (2000), Royston and Houston (1998), Udayakumar et al. (1995)]. The maximum voltage that can be used for a piezoelectric material depends on the thickness of the material, as the electric field is represented by kilovolts per unit thickness. Typically, the maximum electric field that can be applied to a piezoelectric material is 1-2 kV per millimeter. Therefore, to discuss the influence of the thickness of the piezoelectric material, this comparison study is carried out at voltages lower than the maximum voltage that the material of the lowest thickness can take within the range of thickness under consideration. In this case, the thicknesses are taken from 0.1 mm to 1 mm. Since the maximum electric field does not exceed 2 kV per millimeter, 200 volts at 0.1 mm is the highest possible limit. Figure 3.14 represents the SIF concerning patch thickness for different applied voltages. This study is done for two different crack lengths, 25mm and 50 mm. From this parametric illustration, it is clear that a higher reduction in SIF is found for the lower thickness of the patch under the above-mentioned conditions. The SIFs presented here are the same for all thicknesses under 0 V application, as the patch has no actuation effect. Since the thickness of the patch is very small compared to the cross-sectional dimension of the I-beam, the passive effect is not considered here.

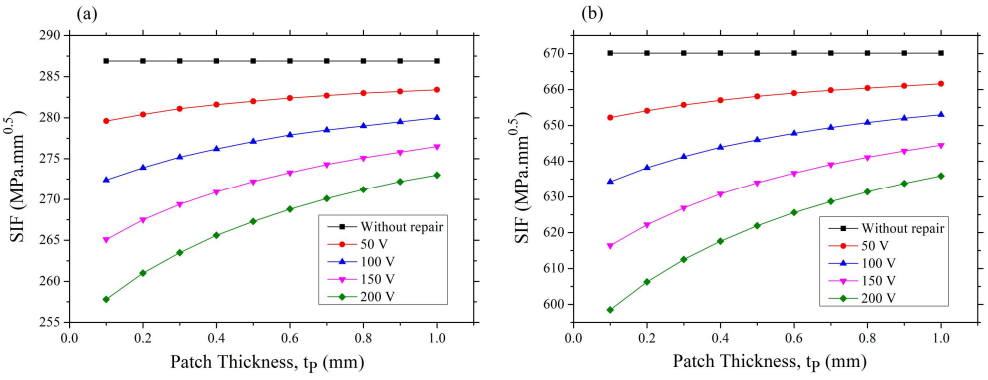

Figure 3.14: Variation of SIF for different thicknesses of the piezoelectric patch under various repair voltages (Electric field < 2kV/mm) (a) 25 mm (b) 50 mm

The prior discussion indicates that a thin patch can yield favorable outcomes when minimal actuation is necessary, specifically under conditions of relatively low mechanical load and constraints on the maximum absolute voltage. Nevertheless, it is more so when the external mechanical load is significantly less. Repair using thin piezoelectric material becomes less efficient as the mechanical load increases after a patch is fixed permanently to the beam. Therefore, an analysis has been performed to represent the maximum repair capabilities for various patch thicknesses at the fixed electric field. The amount of applied voltage for a particular thickness is calculated from the maximum allowable electric field, which has been taken as 2 kV/mm for this study. For this instance, the maximum permissible repair voltage for 0.1 mm is 200 V, whereas, for 1 mm, it is 2000 V. Figure 3.15a shows the SIF after repair for different thicknesses ranging from 0.1 mm to 1 mm and the voltage applied for each thickness so that, in all cases, the electric field remains fixed at 2 kV/mm. Figure 3.15b illustrates the percentage of reduction in SIF under the maximum permissible electric field of 2 kV/mm, demonstrating that a patch with 1 mm thickness shows maximum reduced SIF for all the crack lengths.

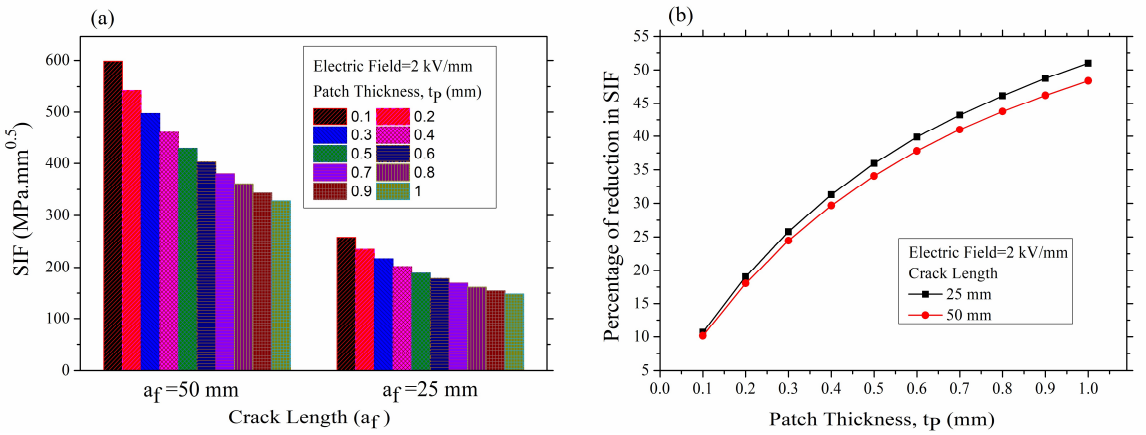

Figure 3.15: (a) SIFs for various patch thicknesses (b) the percentage of reduction in SIF for various patch thicknesses (Electric field =2 kV/mm)

Table 3.7 summarizes the advantages and limitations of thin and thick patches, along with the justification for choosing optimum patch thickness From the above illustrations, it can be seen that reduction in SIF is more significant for lower thickness when a lower range of repair voltage is chosen. Nevertheless, the lower thickness of the patch leads to mechanical failure [Anton et al. (2012), Wang et al. (2019)]. However, if the external mechanical load increases for a given configuration, a patch of low thickness becomes less effective. Furthermore, the maximum repair capacity is lower for lower patch thicknesses. Considering

these scenarios, the 0.5 mm thickness is chosen as it strikes a balance between reducing SIF and maintaining mechanical stability under different load conditions while also allowing sufficient voltage application without risking failure. It ensures sufficient repair performance under moderate voltage while avoiding the failure risks of a thinner patch and the high voltage requirements of a thicker patch.

Table 3.7: Comparison of Patch Thickness: Performance, Limitations, and Suitability

Patch Thickness	Advantages	Limitations/Justifications
0.1 mm	• Provides higher SIF reduction at low voltage (200 V). • Performs well under light mechanical loads. • Ideal for minimal actuation across bonded surfaces.	• Limited repair capacity under high loads. • Less effective as mechanical load increases. • Prone to mechanical failure under higher load conditions
1 mm	• Offers higher repair capacity. • Achieves maximum SIF reduction under heavy loads. • Designed for improved mechanical stability under significant loads.	• Less efficient under low voltage. • Requires higher voltage for maximum actuation (2000 V). • Comparatively higher voltage is required for minimal actuation.
0.5 mm (Chosen)	• Balances repair capacity and mechanical reliability. • Requires moderate voltage (1000 V). • Effective under both low and moderate load conditions. • Suitable for varying load conditions.	• Though it does not provide the greatest reduction in SIF compared to a 1 mm patch, it eliminates the mechanical failure risks associated with 0.1 mm, making it an excellent choice.

3.4.3 Fracture Load Evaluation

The fracture load of any cracked I-beam is highly influenced by the length of the crack and the repair voltage, as can be found in Eqs. (3.12) and (3.13). Figure 3.16 depicts the variation in fracture load concerning repair voltage for various crack lengths. It is to be noted

that the application of zero voltage denotes the fracture load without repair conditions. As the crack length increases, the fracture load gradually decreases for all the repair configurations due to increased stress at the crack tip with the crack length. Figure 3.17 shows the percentage increase in fracture load for various repair voltages corresponding to conditions at different crack lengths. From this illustration, it is found that, for a given repair voltage, a shorter crack length results in a lower percentage increase in fracture load than a longer crack. This illustration clearly shows that a smaller voltage is required to improve the structural integrity of the beam when a short crack is present whenever needed to enhance the same percentage of fracture load as compared to a longer crack. Due to the large crack, the shifting of the neutral axis is more significant, i.e., Y_n is higher, resulting in higher $K_I^{F_P}$, as mentioned in Eq. (3.8). Therefore, $K_I^{F_P}$ will have more contributions in K_I^{Piezo} even at fixed repair voltages, as found in Eq. (3.9). This is why increasing the fracture load by a higher percentage with a lower voltage at a larger crack is possible.

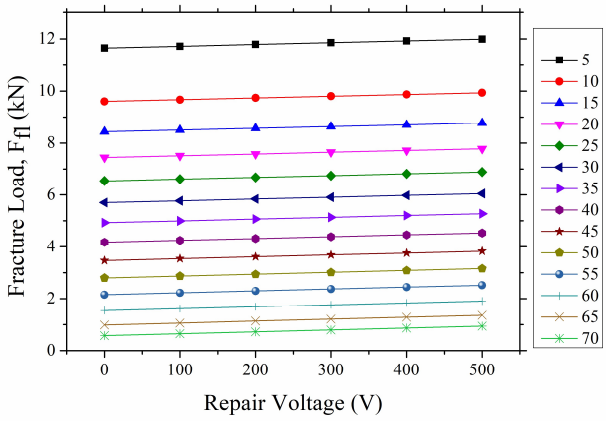

Figure 3.16: Variation of fracture load under different repair voltages for various crack lengths

Furthermore, to understand the effect of repair voltage on fracture load for different crack lengths, a study has been conducted where fracture load for various repair voltages is plotted against the crack length ranging from 25 mm to 30 mm, as represented in Figure 3.18. A suitable fracture load of 6.3 kN is chosen for this illustration. It has been observed that the beam can withstand this load when the crack length is 26.4 mm. After repairing with piezoelectric material, the same amount of load can be survived by the cracked beam when the crack lengths are 26.8, 27.2, 27.6, 28, and 28.4 mm under the repair voltages 100, 200, 300, 400, and 500 V, respectively. This example illustrates that by applying voltage, the effective crack length of the 28.4 mm crack beam can be reduced to 26.4 mm.

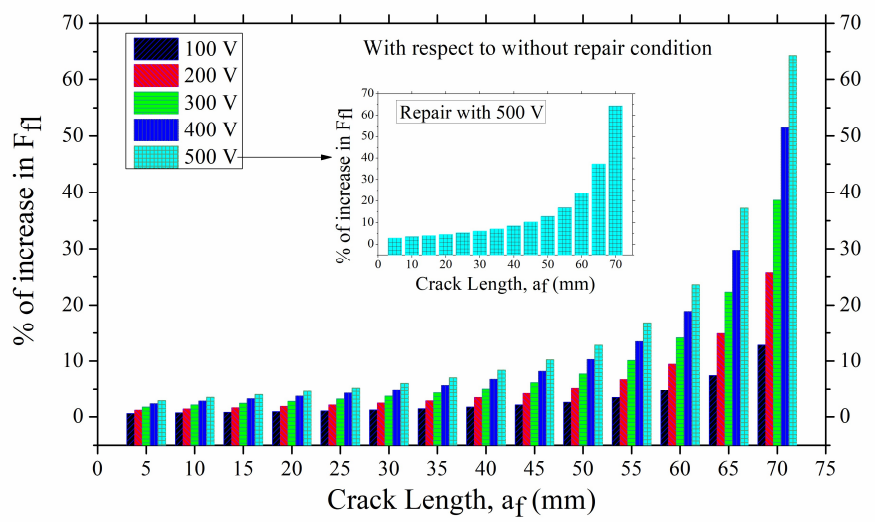

Figure 3.17: Percentage of increase in fracture load for various crack lengths and repair voltages

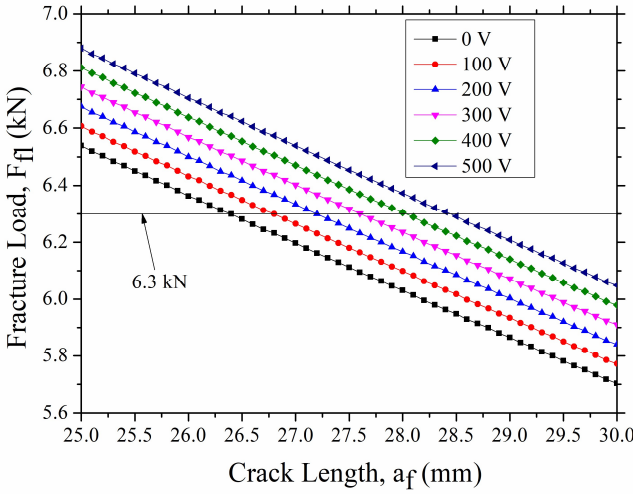

Figure 3.18: Variation of fracture load for a crack length ranging between 25 mm to 30 mm under different repair voltage

3.4.4 Fatigue Crack Growth (FCG) and Fatigue Life Analysis

The fatigue loading on the cracked beam causes the propagation of the crack length, which is a function of external loading, beam geometry, and material properties. This analysis is carried out for fixed loading and beam geometry, but the only variable is the repair voltage. The cyclic loading range is chosen from 2 kN to 0.2 kN, and the results presented in this section are based on various repair voltages. The SIF range is calculated from Eqs. (3.15) and (3.18) between the upper and lower limits of the fatigue loading for different crack lengths,

and the variation of SIF range for different crack lengths is represented in Figure 3.19 various repair voltages. The SIF range is calculated until the maximum SIF reaches the material's fracture toughness. The results clearly show that the SIF range is increasing with the increase in crack length. It is also clear that the SIF range is reduced for a given crack length with a higher repair voltage. The enlarged representation of Figure 3.19 shows that when the crack propagates to 40 mm, the SIF range is reduced by 3.91%, 7.82%, 11.73%, 15.65%, and 19.56% as compared to without repair condition under the repair voltage of 100 V, 200 V, 300 V, 400 V, and 500 V, respectively. Before repair, when the value of the SIF range goes to 500 MPa.mm$^{0.5}$, the length of the propagated crack is found to be 45.7 mm. Now, after repairing it with a repair voltage of 500 V, the length of the propagated crack is 50.72 mm when the SIF range reaches the same previous value.

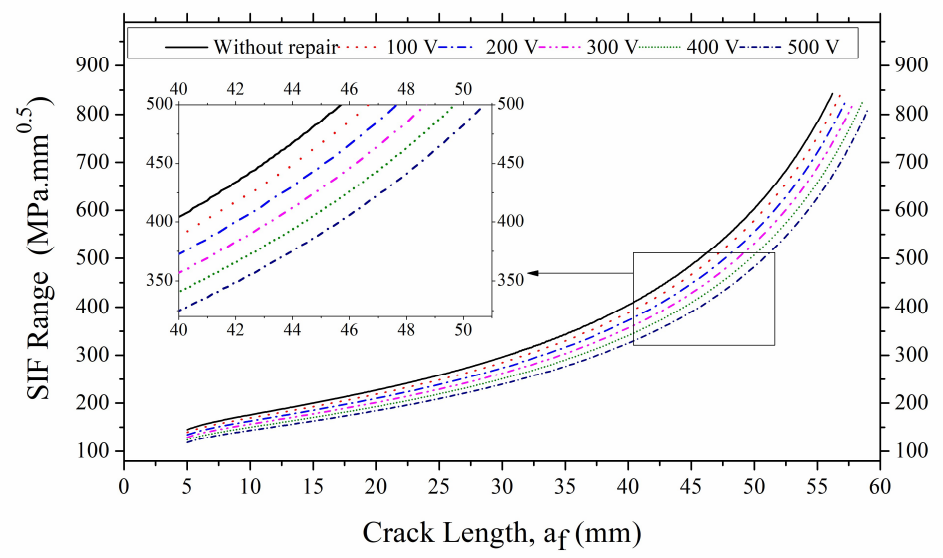

Figure 3.19: SIF Range vs. Crack length for various repair voltages

It is to be noted that the term ΔF_P of Eq. (3.18) depend on the change in applied voltage ΔV. These terms vanish when a constant voltage is applied throughout the loading cycles. Therefore, the SIF range remains unchanged before and after repair. As reported in Chapter 2, the zero voltage ratio (VR) provides the best repair performance. In order to minimize ΔK, ΔV must be maintained at a higher value. The maximum SIF (K_{max}) would be lowered by applying a higher maximum voltage (V_{max}) to maximize the fatigue life. Therefore, V_{min} is equal to zero for the best repair performance i.e., VR = 0, to maintain maximum ΔV for a fixed value of V_{max}. The fatigue crack growth (FCG) concerning several loading cycles is computed until the critical crack length (a_c) is reached for the corresponding repair configuration. Figure 3.20 represents different repair voltage configurations without

and with different repair voltages. The findings demonstrated that the repair with a 500 V shows the most delayed growth of the crack compared to the one without a repair case. The reduction in the SIF range due to the actuation by the piezoelectric patch leads to delayed crack growth, as the SIF range drives crack growth. For example, it takes 272693 cycles to reach 50 mm crack length, whereas it is 469523 cycles when repaired with a 500 V, as represented in Figure 3.20.

The SIF range (ΔK) after different loading cycles is greatly influenced after repairing with various voltages, as described in Figure 3.21. A drastic rise in the SIF range is found after a different number of loading cycles for different repair voltages. This exceptional increase is observed after 250000 cycles for without repair case, whereas it is after 450000 cycles through repair with 500 voltage, as shown in Figure 3.21.

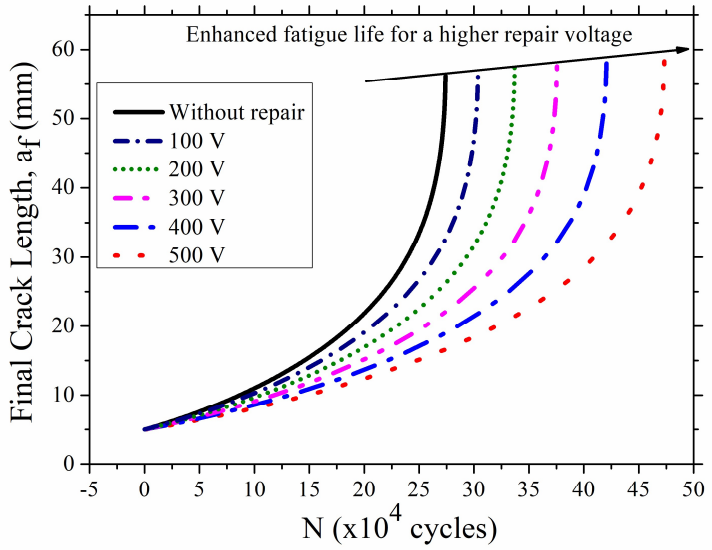

Figure 3.20: Crack length vs. number of loading cycles for various repair voltage

However, a sharp increase in crack growth is observed for each repair voltage after a specific loading cycle, as seen in Figure 3.20 Figure 3.21. For each repair voltage, after a few cycles of this rapid growth, the crack length reaches the critical crack length, and the corresponding number of loading cycles determines its fatigue life. To further illustrate the fatigue life enhancement after repair, Figure 3.22 shows an increase in fatigue life under various repaired voltages compared to without repair conditions, against zero repair voltage. Figure 3.22 also depicts the percentage improvement in fatigue life under different repair voltages. A 10.78%, 22.94%, 37.01%, 53.43%, and 72.7% enhanced fatigue life is achieved under the repair voltages of 100 V, 200 V, 300 V, 400 V, and 500 V, respectively. As the illustration shows, the repaired beam's fatigue life is higher and has occurred for two reasons.

Firstly, the actuation offered by the piezoelectric patch reduces the SIF range (ΔK) by lowering the maximum SIF (K_{max}). At the same time, the minimum SIF (K_{min}) remains the same due to zero V application at the minimum external mechanical loading. This slows the crack propagation, requiring more loading cycles to reach the material's fracture toughness. Secondly, as the maximum SIF goes down, it takes more loading cycles to reach the critical crack length, after which the material will have uncontrolled crack growth, resulting in complete failure.

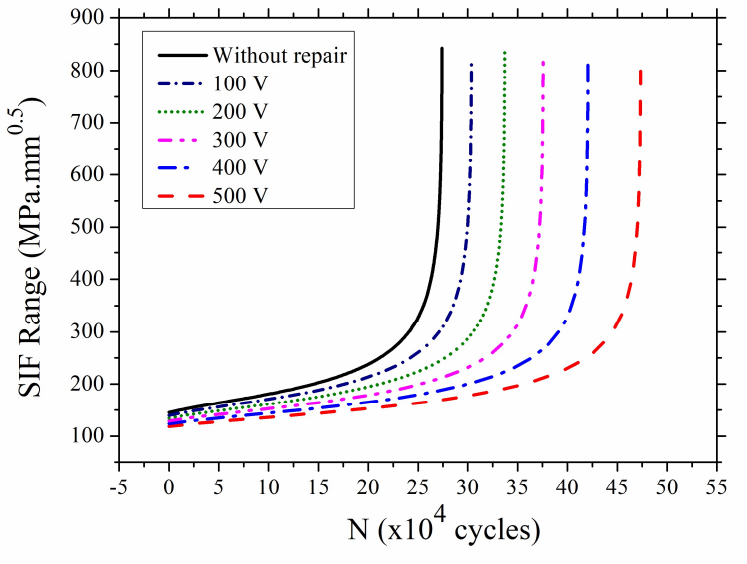

Figure 3.21: SIF Range vs Number of loading cycles (N)

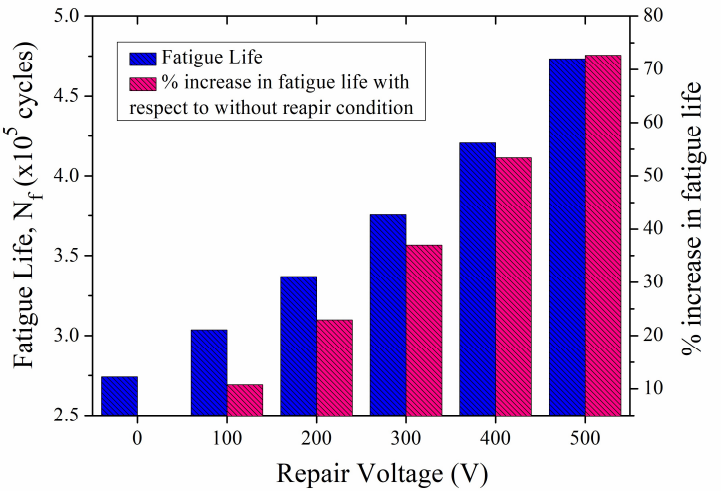

Figure 3.22: Fatigue life and the increase in fatigue life concerning without repair conditions

Figure 3.23 demonstrates the log-log plot of FCGR concerning the SIF range (ΔK) for different repair voltages. The plot is obtained similarly to the standard FCGR model for all the repair configurations [Anderson (2017)]. In this analysis, the loading is chosen so that the SIF

range remains higher than the threshold limit of the material ($\Delta K > \Delta K_{th}$) at the beginning of the cycle, resulting in obtaining the plot in regions II and III only. However, it is observed in Figure 3.23 that the straight line segment indicates Region II, where stable crack growth is observed. It is also worth noting that exponential growth describes Region III, where crack growth is very rapid due to high ΔK values. Since the crack growth is very fast in Region III, the value of maximum SIF (Kmax) reaches the fracture toughness of the material (K_{IC}) rapidly, resulting in the complete failure of the beam.

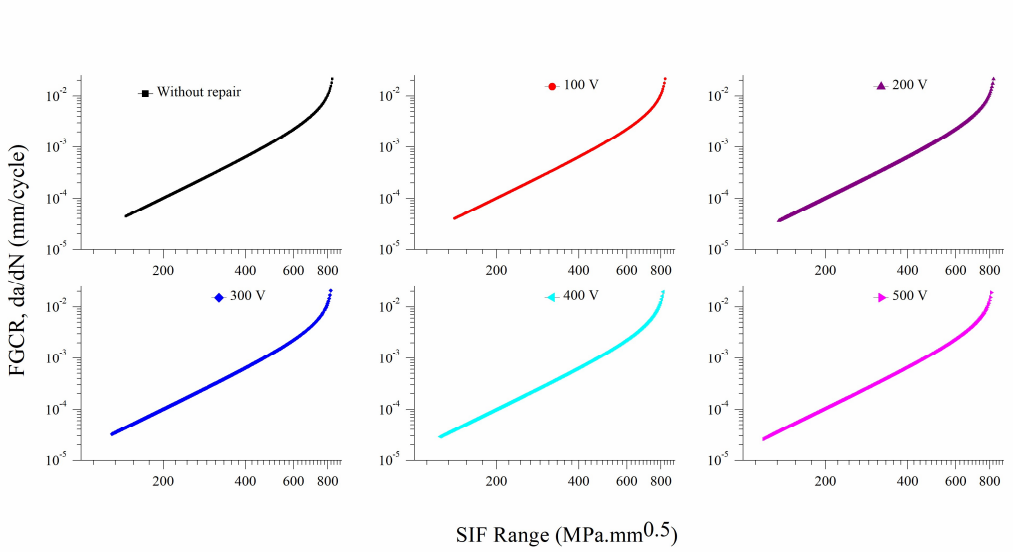

Figure 3.23: FCGR vs. SIF Range for various repair voltages

The FCGR concerning the propagated crack length for without and with repair cases is represented in Figure 3.24. It is clear from the observations that the FCGR drops significantly after the repair, and 500 V shows a more significant reduction. This is due to the reduced SIF range, which stimulates the propagation. In the beginning, the change in the FCGR concerning the crack length is minimal. It starts to grow effectively between 35 mm and 40 crack length, as shown in Figure 3.24. Again, between 45 mm and 55 mm, it is observed to increase very sharply as the value of the SIF range also increases rapidly in this region. After repairing with the piezoelectric patch at a certain crack length, a significant reduction of FCGR is observed compared to the case without repair. After repairing with 500 V, the lowest FCGR is observed. For example, when the FCGR reaches 0.004 mm/cycle, the crack lengths advanced are 52.8 mm, 53.5 mm, 54.2 mm, 55 mm, 55.7 mm, and 56.5 mm corresponds to without repair, 100 V, 200 V, 300 V, 400 V, and 500 V, respectively, as shown in Figure 3.24.

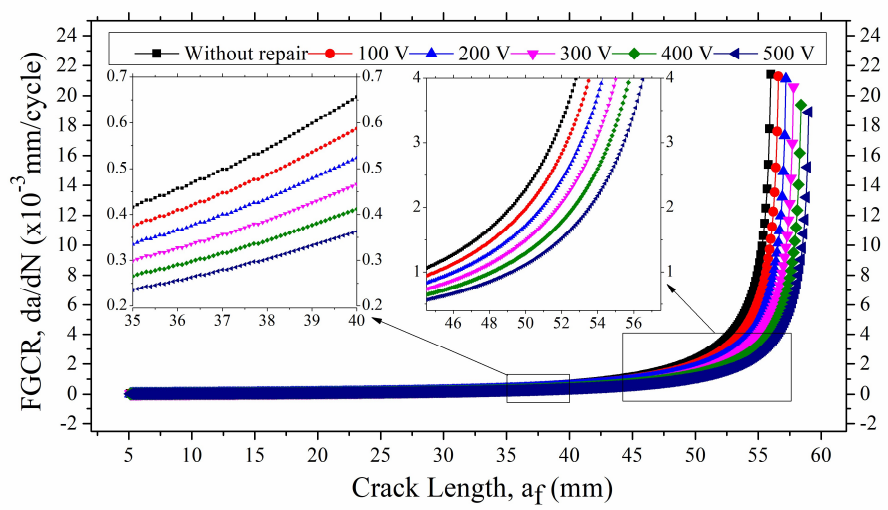

Figure 3.24: FCGR vs. final crack length for various repair voltages

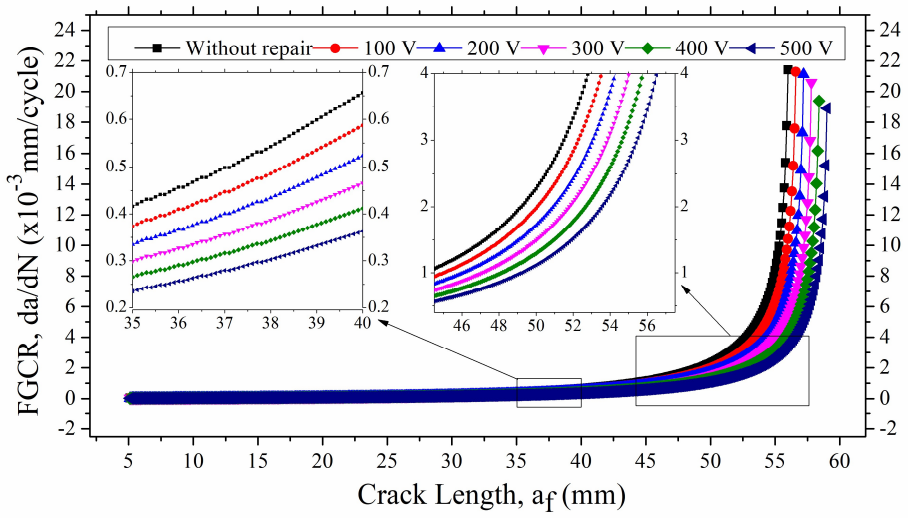

Figure 3.25: FCGR vs. number of loading cycles for various repair voltages

Figure 3.25 demonstrates the variation of FCGR for various loading cycles under different repair scenarios. As seen from the illustration, at the beginning of the loading cycles, no significant changes in FCGR are observed up to a particular limit of the loading cycles. Without repair configuration, this limit is approximately 150000 cycles. In contrast, 400000 cycles were found when repaired with 500 V. This may be because this region has a considerably lower SIF range. Another zone found in this case where a substantial increase has been seen in between 150000 cycles to 250000 cycles without repair conditions, whereas 350000 cycles to 450000 cycles for repairing with 500 V scenario. The sharp rise in FCGR is found after 275000, 300000, 335000, 375000, 420000, and 470000 cycles correspond to without repair, 100 V, 200 V, 300 V, 400 V, and 500 V, respectively. Figure 3.25 shows

almost vertical segments after the specific number of cycles mentioned above, and the gap between this vertical line continuously increases with the rise in applied voltage. Though the increase in applied voltage is 100 V for all the cases, the increase in cycles before the sharp rise is relatively higher at a higher applied voltage. This is due to enhanced actuation by the piezoelectric materials at higher voltages. For a detailed discussion, a fixed FCGR is taken, say 0.002 mm/cycle, and the corresponding number of loading cycles is determined, as shown in Figure 3.25. It has been found that after 219365, 250347, 284607, 324995, 371178, and 425560 loading cycles, FCGR reached 0.002 mm/cycle.

3.5 Summary

This chapter proposed an analytical model for repairing a bottom-edged cracked I-section beam using the reverse piezoelectric effect. The patch was attached to the upper surface of the top flange of the I-beam. The proposed repair approach was carried out by employing the actuation effect offered by the piezoelectric patch. The extension due to actuation provides the opposite moment compared to the moment caused by the external loading. A four-point bending scenario has been chosen to analyze static and cyclic tensile loading with SR=0.1. The effect of shifting the neutral axis due to the presence of the crack was also considered. The compressive stress produced by the actuation of the piezoelectric patch under external voltage significantly minimizes the stress at the crack tip due to the powerful bonding of the patch with the cracked beam. Afterward, numerical FE solutions were obtained on the ABAQUS platform to validate the accuracy of the suggested analytical model. The developed FE model was first validated with published literature, followed by verifying the present analytical approach. A significant reduction in SIF was found after repair. The best repair was achieved with 500 V, and the long crack exhibits comparatively higher repair performance at fixed repair voltage. A patch of thickness 0.1 mm offers significant SIF reduction at low applied voltages, but its limited mechanical robustness and lower repair capacity under increased loads are drawbacks. Thicker patches (1 mm) enable higher repair capacity and reduced SIF at higher voltages but require a stronger voltage application. An optimum thickness of 0.5 mm was proposed, which provides adequate repair performance without exceeding voltage limits, making it a practical choice. The maximum load-carrying capacity could be enhanced after repair. However, for a fixed repair voltage, a longer crack improved the fracture load more than a shorter crack length. The SIF range is significantly reduced under cyclic tensile load after repair. At the same time, the voltage was applied between zero and the maximum value with zero phase difference concerning the

mechanical loading. As a result, the FCGR was also considerably reduced after repair. Higher repair voltage results in a more significant actuation effect, resulting in delayed crack propagation, and, hence, extended fatigue life was achieved. The proposed approach highlighted the potential use of piezoelectric actuators to inhibit premature failure and expand the service life of the bottom-edge cracked I-beams. Furthermore, this approach could enhance the durability and reliability of damaged structures with similar configurations.

Appendix A

The area (A) of the un-cracked section is given by,

$$A = ht_w + 2t_f b_f \tag{A.3.1}$$

The moment of inertia (I) of the un-cracked cross-section is given by,

$$I = \left[\frac{1}{12}t_w h^3 + 2\left\{\frac{1}{12}b_f t_f^3 + t_f b_f \left(\frac{h}{2} + \frac{t_f}{2}\right)^2\right\}\right] \tag{A.3.2}$$

The parameters λ_1, λ_2, η_1 and η_2 related to the beam geometry and crack length for a $\geq t_f$ are given by,

$$\lambda_1 = \int_0^{\xi} \frac{1}{\left[t_f b_f + t_w\left(h + t_f - a\sqrt{1-\zeta^2}\right)\right]} d\zeta \tag{A.3.3}$$

$$\lambda_2 = \int_{\xi}^{1} \frac{1}{\left[ht_w + t_f b_f + b_f\left(t_f - a\sqrt{1-\zeta^2}\right)\right]} d\zeta \tag{A.3.4}$$

$$\eta_1 = \int_0^{\xi} \frac{1}{\left(\begin{array}{c}\frac{b_f}{12}t_f^3 + b_f t_f\left\{1.5t_f + h - NA_1(\zeta)\right\}^2 + \frac{t_w}{12}\left(h + t_f - a\sqrt{1-\zeta^2}\right)^3 \\ + \left[NA_1(\zeta) - \frac{1}{2}\left(h + t_f + a\sqrt{1-\zeta^2}\right)\right]^2 \left(h + t_f - a\sqrt{1-\zeta^2}\right)t_w\end{array}\right)} d\zeta \tag{A.3.5}$$

$$\eta_2 = \int_{\xi}^{1} \frac{1}{\left(\begin{array}{c}\frac{b_f}{12}t_f^3 + b_f t_f\left\{1.5t_f + h - NA_2(\zeta)\right\}^2 + \frac{t_w^3}{12} + t_w h\left[NA_2(\zeta) - \left(t_f + \frac{h}{2}\right)\right]^2 \\ + \frac{b_f}{12}\left(t_f - a\sqrt{1-\zeta^2}\right)^3 + \left[NA_2(\zeta) - \frac{1}{2}\left(t_f + a\sqrt{1-\zeta^2}\right)\right]^2 \left(t_f - a\sqrt{1-\zeta^2}\right)b_f\end{array}\right)} d\zeta \tag{A.3.6}$$

$$NA_1(\zeta) = \frac{\left(1.5t_f + h\right)b_f t_f + 0.5\left[\left(h + t_f\right)^2 - a^2\left(1-\zeta^2\right)\right]t_w}{t_f b_f + \left(h + t_f - a\sqrt{1-\zeta^2}\right)t_w} \tag{A.3.7}$$

$$NA_2(\zeta) = \frac{\left(1.5t_f + h\right)b_f t_f + ht_w\left(\frac{h}{2} + t_f\right) + 0.5\left[t_f^2 - a^2\left(1-\zeta^2\right)\right]b_f}{ht_w + t_f b_f + \left(t_f - a\sqrt{1-\zeta^2}\right)b_f} \tag{A.3.8}$$

Where $\xi = \sqrt{1 - \left(\frac{t_f}{a}\right)^2}$ and $\zeta = \frac{x}{b}$ (A.3.9)

$$Y_{nc} = NA_1(0) - \left(\frac{h_w}{2} + t_f\right) \tag{A.3.10}$$

Chapter 4

REPAIR OF CRACKS EMANATING FROM ELLIPTICAL HOLES USING PIEZOELECTRIC ACTUATORS

4.1 Introduction

Tension plates with holes are likely among the most common structural components in engineering applications, from aerospace to civil infrastructure. Holes are purposefully provided into these plates to facilitate connections, reduce weight, or accommodate specific design requirements. However, these holes act as stress concentrators, leading to a significant increase in localized stress. The hole's geometry is the main factor in determining the stress concentration factor (SCF) value, as elliptical shapes of holes exhibit a complex distribution of the stresses. Consequently, cracks can initiate and propagate from the boundary of these holes, particularly under cyclic fatigue loading, ultimately compromising the structural integrity and potentially leading to catastrophic failure. The repair of such cracks plays a vital role in restoring component integrity and durability.

As discussed in the literature survey, most of the repair works have been restricted to the simpler geometries of straight cracks or circular holes, with very little consideration paid to the more complicated stress fields associated with elliptical holes in tension plates. Furthermore, existing literature lacks comprehensive studies on utilizing piezoelectric patches for active crack repair in plates with elliptical holes. Considering the common existence of elliptical holes in real applications, there exists significant potential for studies on the efficacy of piezoelectric actuators in repairing cracks emanating from these geometries. More work is needed to solve this interaction between the piezoelectric actuator-generated stress fields and the elliptical hole-caused local stress concentration effects.

Therefore, this chapter intends to address these deficiencies by proposing an integrated approach to repairing cracks emanating from elliptical holes in tensile plates using piezoelectric actuators. This study integrates analytical modeling with numerical validation to understand the complex interactions of the stress fields and actuator-induced stress. This chapter aims to develop a closed-form analytical solution of stress intensity factor (SIF) for the crack emanating from an elliptical hole repaired by strategically located piezoelectric actuators. the proposed approach is validated with the finite element (FE) simulations

performed on the ABAQUS platform. The reduction of SIF for various geometric parameters of the elliptical hole, crack, and piezoelectric actuators is discussed. Finally, the fatigue crack growth (FCG) and fatigue life are estimated for different hole geometries.

4.2 Problem Formulation

This section derives the SIF of the crack emanating from an elliptical hole for an infinitely loaded tensile plate before and after repair using piezoelectric actuators. The ellipse with semi-major and semi-minor axes a_1 and b_1 are considered here. The plate is subjected to a tensile stress σ_0 at an infinite distance, as shown in Figure 4.1. To repair the cracked plate, it is proposed to strategically place eight patches above and below the crack on both sides, as shown in Figure 4.1.

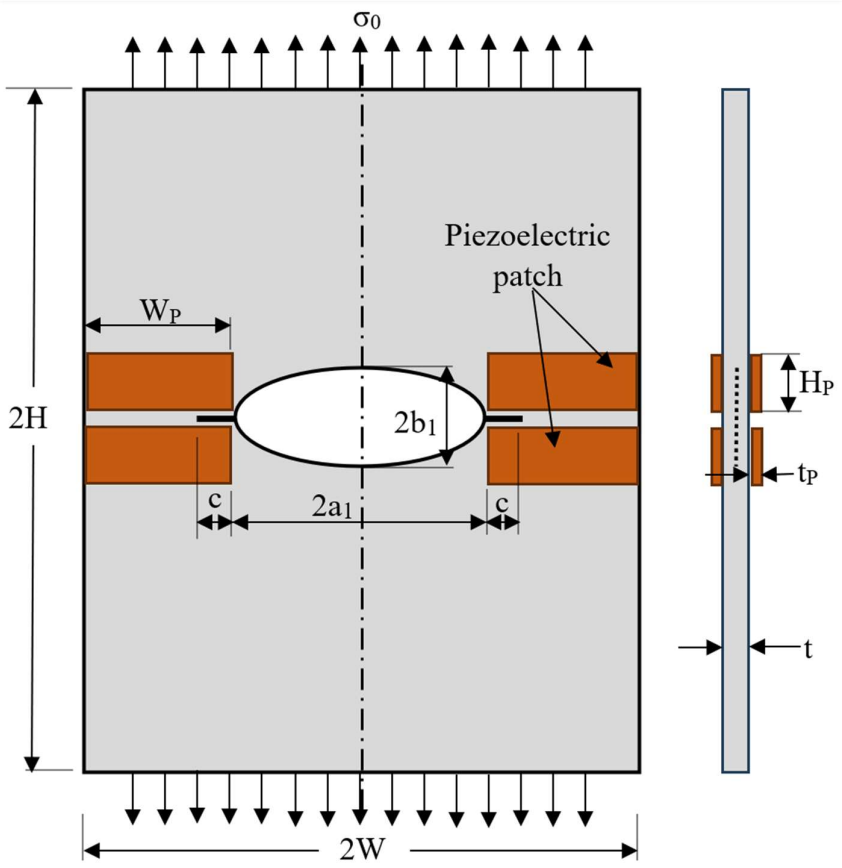

Figure 4.1: Schematic diagram of the plate with cracks emanating from an elliptical hole integrated with piezoelectric patches

4.2.1 Estimation for Cracks Emanating from an Elliptical Hole

The complex potential method helps to obtain the stress distribution along the loading direction and can be expressed as [Weißgraeber et al. (2016)],

$$\sigma_y = \sigma_0 \left[\frac{\left(\frac{a_1}{b_1}+1\right)+\frac{a_1}{b_1}\frac{x}{\sqrt{x^2-{a_1}^2+{b_1}^2}}\left\{\left(\frac{a_1}{b_1}\right)^2-\frac{a_1}{b_1}-3+\frac{x^2}{x^2-{a_1}^2+{b_1}^2}\right\}}{\left(\frac{a_1}{b_1}+1\right)\left(\frac{a_1}{b_1}-1\right)^2} \right], for\ x \geq a_1, y = 0 \quad (4.1)$$

The expression mentioned in Eq. (4.1) provides the stress concentration factor (SCF). To illustrate the SIF at the crack root, which emanates from the elliptical hole, the symmetric cracks of the length of 'c' are considered, as shown in Figure 4.1. Previous researchers proposed various approximate formulas for SIF [Kotousov and Jones (2002), Kujawski (1991), Lukáš (1987), Schijve (1980)]. The solution proposed by Lukáš (1987), given by Eq. (4.2), was used widely, and this approximate model was also verified with published numerical data [Newman (1971)].

$$K_I = \sigma_0 \frac{1.122\left(1+\frac{2a_1}{b_1}\right)}{\sqrt{1+4.5\frac{a_1 c}{b_1^2}}}\sqrt{\pi c} \quad (4.2)$$

But, the shortcoming of this model was that it limits for the short crack emanating from shallow notch only. Another lacuna of this model is that it does not reveal the limiting cases, such as center crack. ($b_1 \rightarrow 0$) and edge crack ($b_1 \rightarrow \infty$). Considering the above shortfalls, Weißgraeber et al. (2016) proposed an improved SIF approximation as that of Lukáš (1987) and given by Eq. (4.3). This SIF solution ideally considers the extensive range of cracks and the limit mentioned above in cases of the cracks. This improved model was well-verified with the FE solutions on the ABAQUS platform.

$$K_I = \sigma_0 \frac{1.122\left(1+\frac{2a_1}{b_1}\right)}{\sqrt{1+5.04\frac{a_1 c}{b_1^2}\left(\frac{a_1}{a_1+c}\right)^{1-tan\ (3b_1/2c)}}}\sqrt{\pi c} \quad (4.3)$$

4.2.2 SIF Reduction via Piezoelectric Actuators

The piezoelectric patches are polarized along the thickness, and the d_{31} mode is activated to produce the extension mode along the loading direction or the direction perpendicular to the cracked surface. The extensional strain in the patch leads to the development of compressive stress at the crack tip. The SIF, due to only the actuation provided by the piezoelectric patch, is a negative quantity, which is fictitious. However, the sum eventually gives a positive value when added to SIF for any mechanical load only via the superposition theorem of LEFM. So, the calculation of SIF under actuation is now essential.

The weight function method developed by Bueckner (1970) is an essential technique for determining SIF in the case of complex stress distributions. For a given stress distribution $\sigma(x)$ in the uncracked component, the SIF K_I, is determined as follows:

$$K_I = \int_0^c h(x,c) \cdot \sigma(x) dx \tag{4.4}$$

where $h(x,c)$ represents the weight function. As demonstrated by Rice (1972), this function can be determined using the crack opening displacements (CODs) of a reference load case (denoted by subscript r) and the corresponding reference SIF, K_r.

$$h(x,c) = \frac{É}{K_r} u_r(x,c) \tag{4.5}$$

The modulus É is equal to Young's modulus E in the case of plane stress, and for plane strain, it is given by $É = E/(1-\nu^2)$, where ν represents the Poisson ratio. Equation (4.5) is frequently employed as the foundation for deriving approximate weight functions. The crack-opening displacements can be described by Eq. (4.6) using a power series.

$$u_r(x,c) = \sum_{m=0}^{\infty} C_m \left(1 - \frac{x}{c}\right)^{m+\frac{1}{2}} \tag{4.6}$$

Where the coefficient C_m depends on the structure's geometry and is determined based on the following conditions as discussed by Petroski and Achenbach (1978),

- The crack-tip displacement is related to the stress intensity factor as follows:

$$u_r(x \to c) = \sqrt{\frac{8}{\pi}} \frac{K_{Ir}}{É} \sqrt{c-x} \tag{4.7}$$

- The energy balance condition requires [Petroski and Achenbach (1978)],

$$\int_0^c K_{Ir}^2 dc = É \int_0^c \sigma_r(x)\, u_r(x,c) dx \tag{4.8}$$

- The second and third derivatives of COD become equal to zero for an edge crack [Fett (1991), Fett et al. (1987)]

$$\frac{\partial^2 u}{\partial x^2} = 0, \text{ and } \frac{\partial^3 u}{\partial x^3} = 0, \text{ for } x = 0 \tag{4.9}$$

- ln order to fulfill the requirement of symmetry concerning the center of the hole $x = -a_1$, we can additionally introduce the following conditions:

$$\frac{\partial^2 u}{\partial x^2} = 0 \text{ for } x = -a_1 \tag{4.10}$$

ln order to determine the weight function for the crack/notch problem, the numerical results of Newman (1971) and Nisitani (1978) for $a_1/\rho \leq 1$ were chosen as the reference stress intensity factor and the stress distribution, Eq. (4.1), as the reference stress σ_r. In the case of a symmetrical crack configuration (cracks at both sides of the notch), which has been considered by Newman (1971) and Nisitani (1978), the well-known formula for the weight function of a symmetrically loaded crack can be rewritten as,

$$h = \frac{1}{\sqrt{\pi c}}\left(\sqrt{\frac{2a_1+c+x}{c-x}} + \sqrt{\frac{c-x}{2a_1+c+x}}\right) \tag{4.11}$$

Weight functions for cracks in front of elliptical internal notches were determined with Eqs. (4.6)-(4.11). The results are expressed in terms of the function $g\left({}^{x}/_{c}, {}^{a_1}/_{\rho}\right)$ and written according to the following expression,

$$h = \sqrt{\frac{2}{\pi c}} \cdot \frac{g\left({}^{x}/_{c}, {}^{a_1}/_{\rho}\right)}{\sqrt{1-{}^{x}/_{c}}} \tag{4.12}$$

In the above expression, the values of the function $g\left({}^{x}/_{c}, {}^{a_1}/_{\rho}\right)$ are reported by Fett (1993) for various a_1/ρ, c/ρ and x/c. As this study aims to find the SIF at crack root only ($x = c$), $x/c = 1.0$ is only considered here. And it is found that for $x/c = 1.0$, $g\left({}^{x}/_{c}, {}^{a_1}/_{\rho}\right) = 1.0$ for all a_1/ρ, c/ρ.

As the overall configuration mentioned in Figure 4.1 is symmetric about the y-axis, the half model is considered for further mathematical derivation. The stress intensity factor (SIF) under the effect of actuation, K_P, can be determined for a cracked body by utilizing the weight function, $h(x,c)$, and the piezoelectric stress (σ_{Piezo}), as described in the following expression [Abuzaid et al. (2018)].

$$K_{Piezo} = \int_0^c h(x,c) \cdot \sigma_{Piezo} dx \tag{4.13}$$

If piezoelectric actuators are bonded on the cracked plate completely, then $\sigma_{Piezo} = \{E \cdot t \cdot T \cdot d_{31} \cdot V/A \cdot t_P \cdot (\psi + \alpha)\}$ and this stress has equal distribution at right angles to the crack surface. Here, 'T' is the distributed electrode width, 'A' represents the plate's effective cross-sectional area, $\psi = EWt/E_P W_P t_P$, and $\alpha = 2$ for extensional loading [Crawley and Luis (1987)].

Now, SIF, after repair (K_A) can be expressed as,

$$K_A = K_I + K_{Piezo}$$

$$K_A = \left[\sigma_0 \frac{1.122\left(1+\frac{2a_1}{b_1}\right)}{\sqrt{1+5.04\frac{a_1 c}{b_1^2}\left(\frac{a_1}{a_1+c}\right)^{1-tan\ (3b_1/2c)}}} \sqrt{\pi c} + \int_0^c h(x,c) \cdot \sigma_{Piezo} \cdot dx \right] \tag{4.14}$$

4.2.3 FCGR and Fatigue Life Estimation

In this section, we aim to determine the fatigue crack growth (FCG) and the fatigue life of a cracked structure subjected to cyclic tension. To achieve this, we utilize the most commonly used version of NASA's FCG model, initially introduced by Forman and Mettu (1990), which describes all three sections of the well-known crack growth curve [Anderson (2017)].

$$\frac{dc}{dN} = C \cdot (\Delta K)^m \cdot \frac{\left(1-\frac{\Delta K_{th}}{\Delta K}\right)^p}{\left(1-\frac{K_{max}}{K_{Ic}}\right)^q} \tag{4.15}$$

The above expression describes the FCGR (measured in millimeters per cycle). C, m, p, and q are empirically determined material constants. Determining the SIF range ($\Delta K = K_{max} - K_{min}$) between maximum and minimum loading is vital for predicting the FCG and estimating the number of loading cycles needed to reach the fracture toughness of the material. This SIF range can be calculated by deriving from the preceding sections. It is primarily influenced by the variation in stress magnitude ($\Delta\sigma = \sigma_{max} - \sigma_{min}$) and the change in the applied repair voltage ($\Delta V = V_{max} - V_{min}$).

The crack growth concerning the number of loading cycles is determined by taking the incremental crack propagation (Δc_i) against incremental loading cycles (ΔN_i), where $\Delta c_i = c_{i+1} - c_i$ and $\Delta N_i = N_{i+1} - N_i$. In every iteration, Δc_i is calculated for a specific ΔN_i. Then, crack length (c_f), SIF range (ΔK), and maximum SIF (K_{max}) are updated. This iteration is repeated until either the maximum SIF (K_{max}) reaches the value of the fracture toughness (K_{IC}) or the crack length (c_f) reaches the critical crack length a_c. The fatigue life for all the situations can be directly obtained by integrating Eq. (4.14) from the initial crack length c_o to the final crack length c_f ($c_f = c_c$).

Fatigue life after repair is obtained from the numerical integration of Eq. (4.15),

$$N_f = \int_0^{N_f} dN = \int_{c_o}^{c_c} \left[\frac{1}{C \cdot (\Delta K)^m \cdot \frac{\left(1-\frac{\Delta K_{th}}{\Delta K}\right)^p}{\left(1-\frac{K_{max}}{K_{Ic}}\right)^q}} \right] dc \tag{4.16}$$

The critical crack length (c_c) depends upon the applied load, the structural configuration of the cracked beam, and the repair parameters. It is derived from the fracture toughness (K_{IC}) of the material and is expressed as:

$K_{IC} = (K_I)_{at\ c_c}$ for without repair condition

$K_{IC} = (K_A)_{at\ c_c}$ for active repair condition

The SIF range in the absence of piezoelectric actuators can be derived from Eq. (4.2), and expressed as,

$$\Delta K_I = \Delta\sigma_0 \frac{1.122\left(1+\frac{2a_1}{b_1}\right)}{\sqrt{1+5.04\frac{a_1 c}{b_1^2}\left(\frac{a_1}{a_1+c}\right)^{1-tan\ (3b_1/2c)}}} \sqrt{\pi c} \tag{4.17}$$

Substituting this value into Eq. (4.16), we obtain:

$$\frac{dc}{dN} = C \cdot \left[\Delta\sigma_0 \frac{1.122\left(1+\frac{2a_1}{b_1}\right)}{\sqrt{1+5.04\frac{a_1 c}{b_1^2}\left(\frac{a_1}{a_1+c}\right)^{1-tanh(3b_1/2c)}}} \sqrt{\pi c} \right]^m \cdot \frac{\left(1-\frac{\Delta K_{th}}{\Delta\sigma_0 \frac{1.122\left(1+\frac{2a_1}{b_1}\right)}{\sqrt{1+5.04\frac{a_1 c}{b_1^2}\left(\frac{a_1}{a_1+c}\right)^{1-tanh(3b_1/2c)}}} \sqrt{\pi c}}\right)^p}{\left(1-\frac{K_{max}}{K_{Ic}}\right)^q} \tag{4.18}$$

In the same way, the SIF range after repair with piezoelectric actuators can be derived from Eq. (4.14) and expressed as,

$$\Delta K_A = \left[\Delta\sigma_0 \frac{1.122\left(1+\frac{2a_1}{b_1}\right)}{\sqrt{1+5.04\frac{a_1 c}{b_1^2}\left(\frac{a_1}{a_1+c}\right)^{1-tan\ (3b_1/2c)}}} \sqrt{\pi c} + \int_0^c h(x,c) \cdot \Delta\sigma_{Piezo} \cdot dx \right] \tag{4.19}$$

Substituting this value into Eq. (4.15), we obtain,

$$\frac{dc}{dN} = C \cdot \left[\Delta\sigma_0 \frac{1.122\left(1+\frac{2a_1}{b_1}\right)}{\sqrt{1+5.04\frac{a_1 c}{b_1^2}\left(\frac{a_1}{a_1+c}\right)^{1-tan\ (3b_1/2c)}}} \sqrt{\pi c} + \int_0^c h(x,c) \cdot \Delta\sigma_{Piezo} \cdot dx \right]^m \cdot \frac{\left(1 - \frac{\Delta K_{th}}{\Delta\sigma_0 \frac{1.122\left(1+\frac{2a_1}{b_1}\right)}{\sqrt{1+5.04\frac{a_1 c}{b_1^2}\left(\frac{a_1}{a_1+c}\right)^{1-tanh(3b_1/2c)}}} \sqrt{\pi c} + \int_0^c h(x,c) \cdot \Delta\sigma_{Piezo} \cdot dx} \right)^p}{\left(1-\frac{K_{max}}{K_{Ic}}\right)^q} \tag{4.20}$$

By incorporating Eqs. (4.18) and (4.20) into (4.16), the fatigue life can be calculated for without repair and after repair, respectively.

4.3 Finite Element Analysis and Validation

In this section, numerical simulations were performed using the ABAQUS FE software to validate the results obtained from the current analysis. Firstly, a specimen with a crack emanating from an elliptical hole is modeled and compared with analytical results and the previously published FE solutions [Weißgraeber et al. (2016)] to validate the present FE modeling. Secondly, the repair of the crack using a piezoelectric patch has been carried out to validate the present analytical approach. A half model is considered for FE analysis.

4.3.1 FE Modelling of the Cracked Specimen with Piezoelectric Patch

Five deformable bodies are initially generated to represent one plate and four piezoelectric patches, with their dimensions and material properties detailed in Table 4.1 Table 4.2. An elliptical hole is positioned at the center of the plate, as illustrated in Figure 4.2a. The plate model is partitioned to account for the crack located at the vertex of the elliptical hole. A seam crack of the specified length is introduced along the major axis direction of the elliptical hole, as shown in Figure 4.2b. The piezoelectric patches are defined with a local material orientation by creating a datum where axis '3' aligns with the patches' depth. It is important to note that in ABAQUS, direction '3' corresponds to the polarization direction. The piezoelectric patches and the cracked plate are connected using a 'tie interaction' within the interaction module. The bottom of the plate is subjected to an 'ENCASTRE' boundary condition. At the same time, the right-side x-displacement is constrained to zero ($U_1 = 0$), as illustrated in Figure 4.2c. The cracked plate is modeled using a '3D stress' element, whereas the piezoelectric patches are modeled with a 'piezoelectric

element.' The model is discretized using hexahedral elements with an approximate global size of 0.005 m. The meshed model is shown in Figure 4.3. External voltage is applied to each piezoelectric patch by setting up two electrical boundary conditions on the opposing faces of the patch. The voltage on the face attached to the cracked plate is maintained at zero, while a finite voltage value is applied to the top face. Only the cracked plate is analyzed for validation, using dimensions consistent with the study presented in ref. [Weißgraeber et al. (2016)].

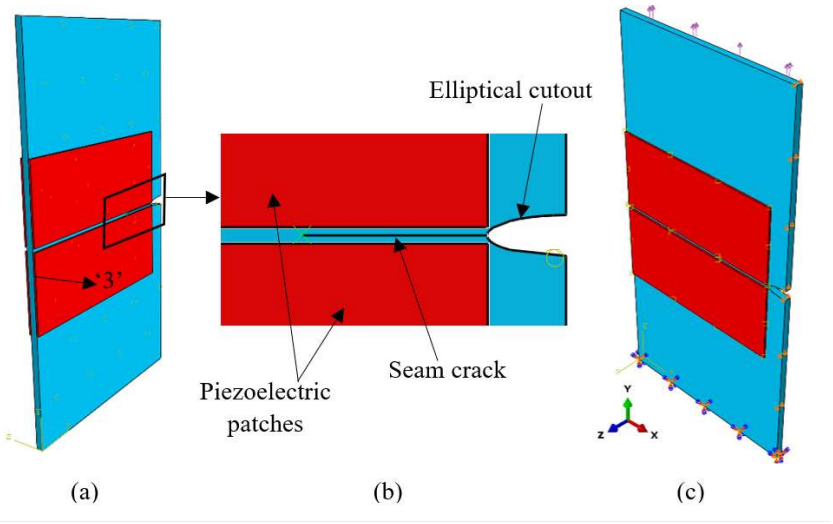

Figure 4.2: FE model on the ABAQUS platform, a_1 = 5 mm, b_1 = 1.25 mm, and c = 11.67 mm (a) Half of the cracked plate with piezoelectric patches assembled on both sides (b) Enlarged view near the crack (c) Boundary conditions applied to the model

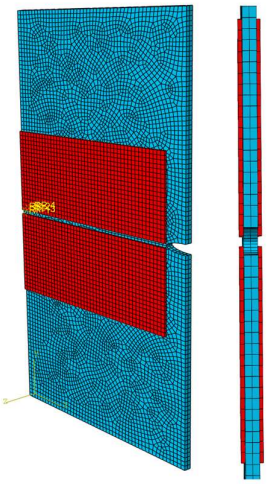

Figure 4.3: FE mesh model

4.3.2 Validation of FE Model Without Piezoelectric Patch

A total of 11 numerical simulations have been performed to validate the present FE model for cracked plates with elliptical holes only. For all the cases, the semi-major axis of the elliptical hole was taken 5 mm. Figure 4.4 depicts the deformed shape of the plate after simulation. Figure 4.5a represents the comparison of normalized SIF of present FE findings with published results [Weißgraeber et al. (2016)] for a fixed aspect ratio (AR) of the elliptical hole, $a_1/b_1=4$ ($a_1=5$ mm, $b_1=1.25$ mm) and different normalized crack lengths [$s=c/(a_1+c)$]. Figure 4.5b represents SIF values concerning the aspect ratios (1, 2, 2.5, and 4) for a fixed normalized crack length s=0.7. As can be interpreted from the comparison with the published findings of the normalized SIF, the present analysis matches the published literature well.

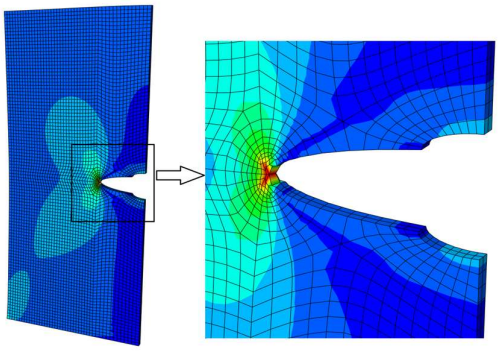

Figure 4.4: FE model of the cracked plate after simulation (without repair)

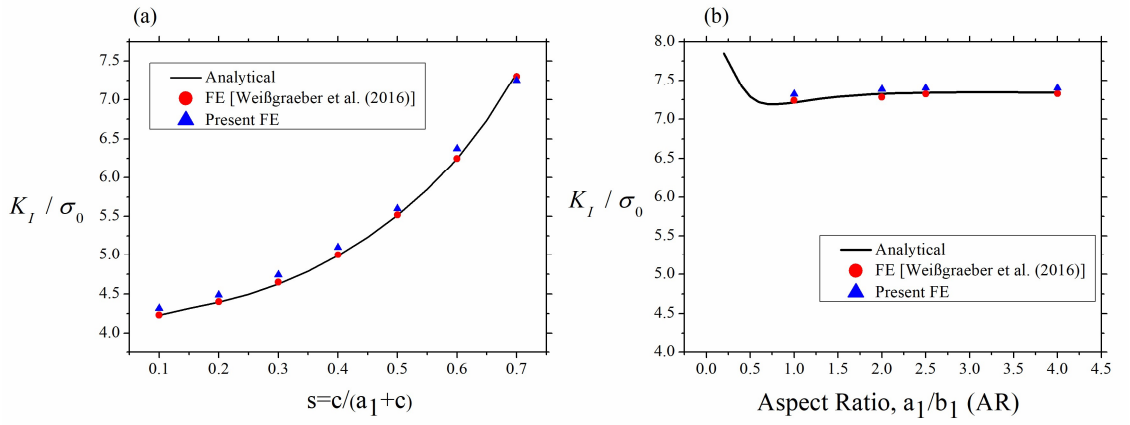

Figure 4.5: Comparison of the analytical and present FE findings with the published FE results [Weißgraeber et al. (2016)]

4.3.3 Validation of FE Model with Piezoelectric Patch

In the previous section, the FE model was well-verified for a plate with a crack emanating from an elliptical hole for static loading without a repair case. The present

analytical approach proposed to reduce SIF at the crack root by the actuation provided by the piezoelectric patches. The analytical model developed in this article regarding the repair by the piezoelectric patch (Figure 4.1) is now verified with the FE analysis. The plate is made of Al 6061-T6, whereas PZT-5H is utilized for actuation. It is important to note that the piezoelectric patch is supplied with a voltage of 500 V. The normalized crack lengths, [$s=c/(a_1+c)$], taken for this analysis range from 0.2 to 0.7; thus, crack lengths become 1.25 mm, 2.143 mm, 3.333 mm, 5 mm, 7.5 mm, and 11.67 mm, respectively. The elliptical hole's aspect ratios (AR) are taken as 2, 3, and 4 for a fixed semi-major axis length, a_1 = 5 mm. Subsequently, the results are compared for authentication, as depicted in Figure 4.6. The graphical comparison between the outcomes obtained using the FEA and the analytical method demonstrates a strong agreement. Figure 4.7 presents the deformed finite element models of the cracked plate after a 500 V application to the piezoelectric patch.

Table 4.1: Mechanical properties and crack growth parameters of Al 6061-T6 material [Fossati et al. (2021)]

Parameter	**Value**
Elastic Modulus (E_s)(GPa)	68.9
Poisson's ratio (ν)	0.33
Tensile yield strength (MPa)	276
Ultimate tensile strength (MPa)	310
Density (Kg/m^3)	2700
$\Delta K_{th}\left(MPa\sqrt{mm}\right)$ at SR=0.1	45.52
$K_{IC}\left(MPa\sqrt{mm}\right)$	938.2
C	5.079e-10
m	2.3
p	0.5
q	0.5

Table 4.2: Geometric parameters for plate and piezoelectric patch

Dimensions	**Al 6061-T6 (mm)**	**PZT-5H (mm)**
Height	H=100	H_P=25
Width	W=50	W_P=45
Thickness	t=1.6	t_P=0.5

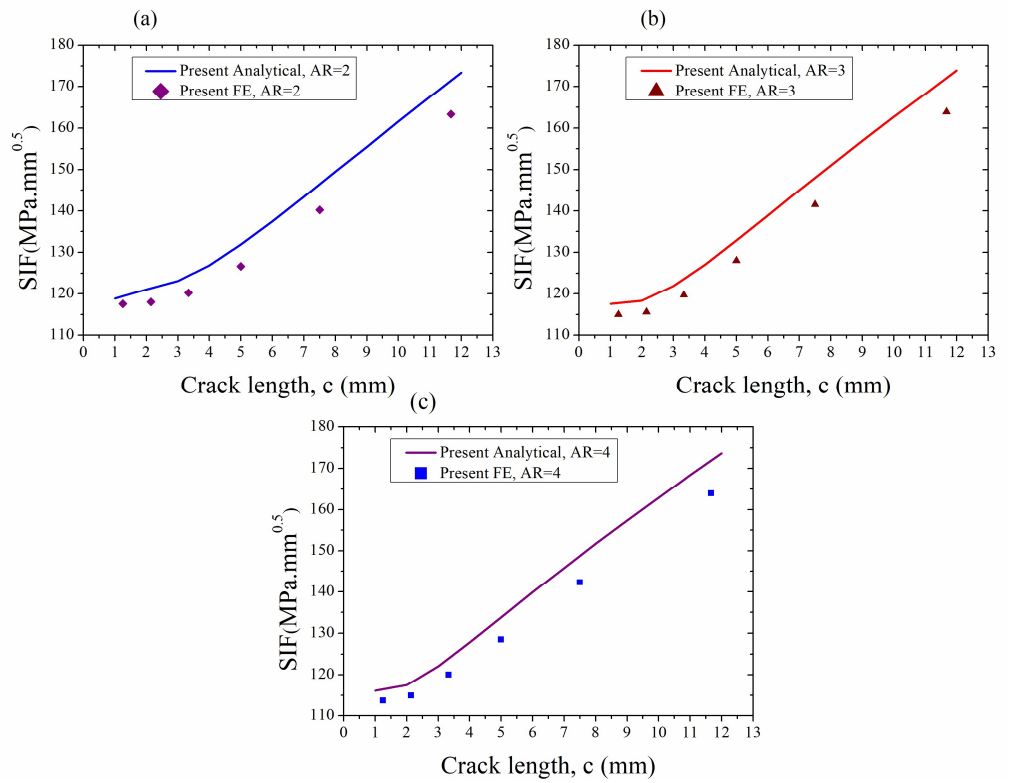

Figure 4.6: Comparison of the present analytical results with those obtained from FEA in ABAQUS

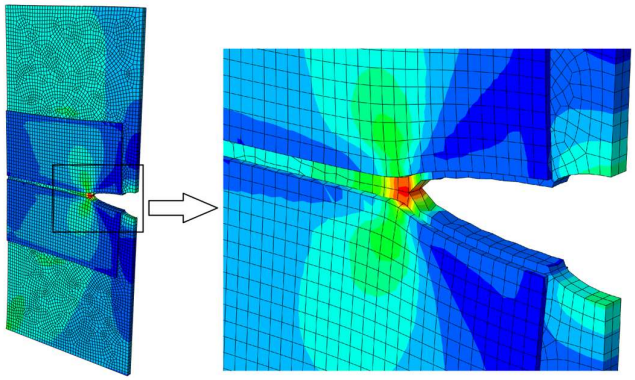

Figure 4.7: Deformed FE model of the repaired plate under the application of a 500 V

4.4 Results and Discussion

Once the findings of the proposed approach are validated with FE analysis in the presence of the piezoelectric patch, various analytical studies are conducted to estimate the SIF for different aspect ratios, semi-major axis lengths, and different crack lengths. Subsequently, the SIF range, FCGR, and fatigue life are calculated under cyclic tensile loading using the proposed analytical method, taking into account the aforementioned parameters.

4.4.1 Effect of Applied Voltage and Patch Thickness on Repair Efficiency

This section discusses how different applied voltages and patch thicknesses influence SIF to suggest the ideal patch thickness and voltage for repairing the cracked plate. The SIFs are estimated under a tensile stress of 30 MPa for various repair voltages ranging from 0, 100, 200, 300, 400, and 500 V. The geometries of the elliptical hole are taken as a_1=10 mm and a_1/b_1=4. The variation of SIF about various repair voltages at various patch thicknesses ranges from 0.1 mm to 0.5 mm, depicted in Figure 4.8 for the two different crack lengths, 5 mm and 10 mm, respectively. A significant decrease in SIF is observed as the repair voltage increases from zero for every patch thickness and the crack length. The amount of SIF reduction is higher as the repair voltage increases due to the piezoelectric material possessing more extensional strain, which provides more compressive stress at the crack tip, reducing effective stress at the crack tip.

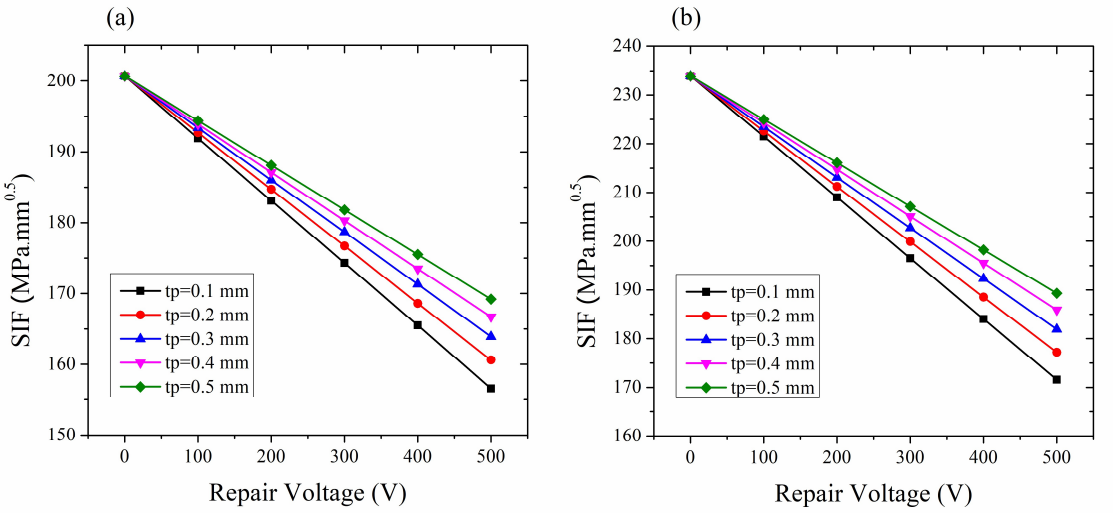

Figure 4.8: Comparison of repaired and without repair conditions for various thicknesses a_1=10 mm, AR=4 (a) c=5 mm (b) c=10 mm

Choosing the proper thickness of the piezoelectric patch is very important, as the actuation mainly produced depends on the stiffness ratio and the piezoelectric strain [Zhou et al. (2024)]. In the previous section, the thickness was taken as 0.5 mm for the conciseness of the validation study. Furthermore, Figure 4.8 also shows that patches of low thickness are most capable of repair. Besides that, it is to be noted that it is possible to apply a certain amount of this electric field to any piezoelectric material, usually from 1 kV/mm to 2 kV/mm. However, in the above analysis, it can be said that for a thickness of 0.1 mm when 500 volts is applied, the electric field is 5 kV per millimeter, which is practically impossible to apply on

the patch. Therefore, selecting the maximum voltage that can be used for a given thickness is considered based on the maximum permissible electric field, as the electric field is represented by kilovolts per unit thickness.

This analysis assumes that this maximum limit is 1 kV per millimeter, and another study is carried out for different thicknesses where the electric field is limited to 1 kV/mm. A 5 mm crack length, a semimajor axis of 10 mm length, and an aspect ratio of 4 are taken to conduct this study. Figure 4.9a shows the variation of SIF concerning electric fields ranging from 0 to 1 kV/mm for different patch thicknesses. In terms of absolute voltage, thin actuators perform better, as shown in Figure 4.8. Under the application of 100 V, a 0.1 mm patch gives a 4.38% reduction in SIF, whereas a 0.5 mm patch provides a 3.13% reduction in SIF compared to a 0 V application. Here, it is noted that, considering a permissible electric field of 1 kV/mm, 100 V is the maximum permissible absolute voltage for a 0.1 mm patch, whereas 500 V is for a 0.5 mm patch.

From the above discussion, it can be said that a thin patch can give good results when low actuation is required, i.e., when mechanical load is relatively low and if there is a restriction regarding the upper limit of absolute voltage. However, to obtain higher actuation as and when required with the increase in external mechanical load, the apparent repair capacity of the thin patch is much lower. To address this, another study is conducted at the maximum permissible limit of the electric field, and the maximum possible performance of patches of different thicknesses can be interpreted. Figure 4.9b shows the SIF after repair for different thicknesses ranging from 0.1 mm to 0.5 mm and the voltage applied for each thickness so that, in all cases, the electric field remains fixed at 1 kV/mm. The amount of applied voltage for a particular thickness is calculated from the maximum allowable electric field. Note that the absolute voltage for a 0.1 mm patch is 100 V; for a 0.5 mm patch, it is 500 V under 1 kV/mm application. For all the crack lengths considered here, the SIF is reduced significantly with the increase in patch thicknesses. The reduction of SIFs at 1 kV/mm as compared to 0 kV/mm is 4.38%, 7.97%, 10.96%, 13.55%, and 15.69 % for the 0.1 mm, 0.2 mm, 0.3 mm, 0.4 mm, and 0.5 mm the thicknesses of the patch, respectively. In these two scenarios, it can be seen that a 0.5 mm patch can repair much more, even at a fixed 1 kV/mm electric field. However, the amount of piezoelectric strain is the same in both cases, and the effect of stiffness ratio can bounce better results for comparatively thicker patches.

Therefore, it can be seen that SIF decreases more sharply for lower thickness when a lower range of repair voltage is chosen. Nevertheless, the lower thickness of the patch leads to

mechanical failure [Anton et al. (2012), Wang et al. (2019)]. However, if the external mechanical load increases for a given configuration, a patch of low thickness becomes less effective. Furthermore, the maximum repair capacity is lower for lower patch thicknesses. Considering these cases, a patch thickness of 0.5 mm is carefully chosen for the rest of the analysis.

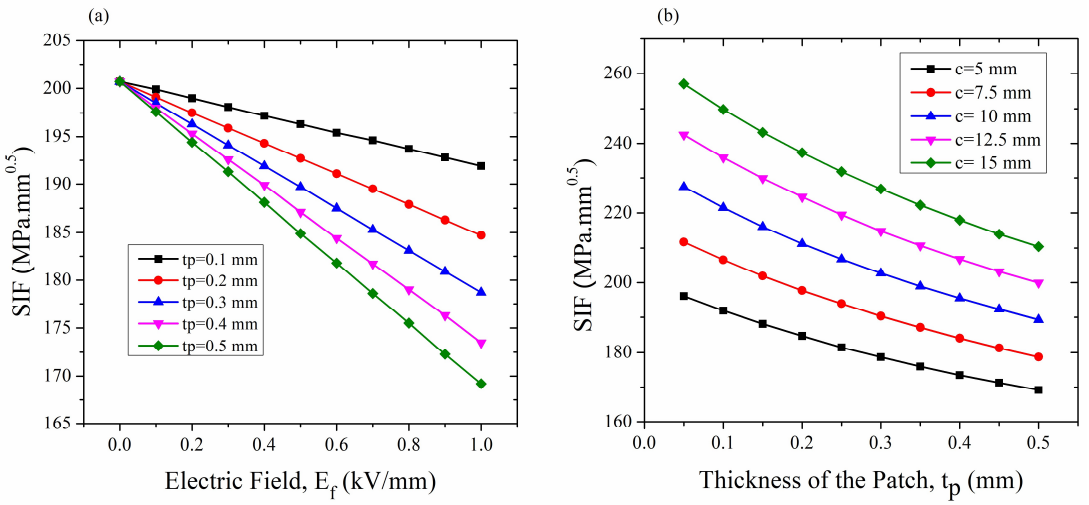

Figure 4.9: (a) SIF vs. Electric field for various thicknesses of the patch, c= 5 mm (b) SIF vs. thickness of the patch for various crack lengths at constant Electric Field (E_f=1kV/mm) a_1=10 mm, AR=4

4.4.2 SIF Variation with Crack Length, Semi-Major Axis, and Aspect Ratio

The previous section identified suitable thicknesses and corresponding voltages. Based on that, it is essential to analyze the stress intensity factors (SIFs) to understand crack propagation behavior under static tensile stress. This section focuses on SIF calculations for different crack lengths, semi-major axis lengths, and aspect ratios (AR) for a patch thickness of 0.5 mm and a repair voltage of 500 V. The analysis explores crack lengths ranging from 1 mm to 15 mm, semi-major axis lengths from 5 mm to 15 mm, and aspect ratios (AR) of 1, 2, 3, and 4. The goal is to examine how these parameters influence SIFs under a constant tensile load of 30 MPa. Figure 4.10 illustrates the variation of SIFs via a 3D plot with crack length on the x-axis, the semi-major axis of the elliptical hole on the y-axis, and SIF on the z-axis for both without repair and repaired conditions at an applied voltage of 500 V. This detailed examination of SIFs for various geometric parameters is crucial for determining failure risks and the effectiveness of repair techniques.

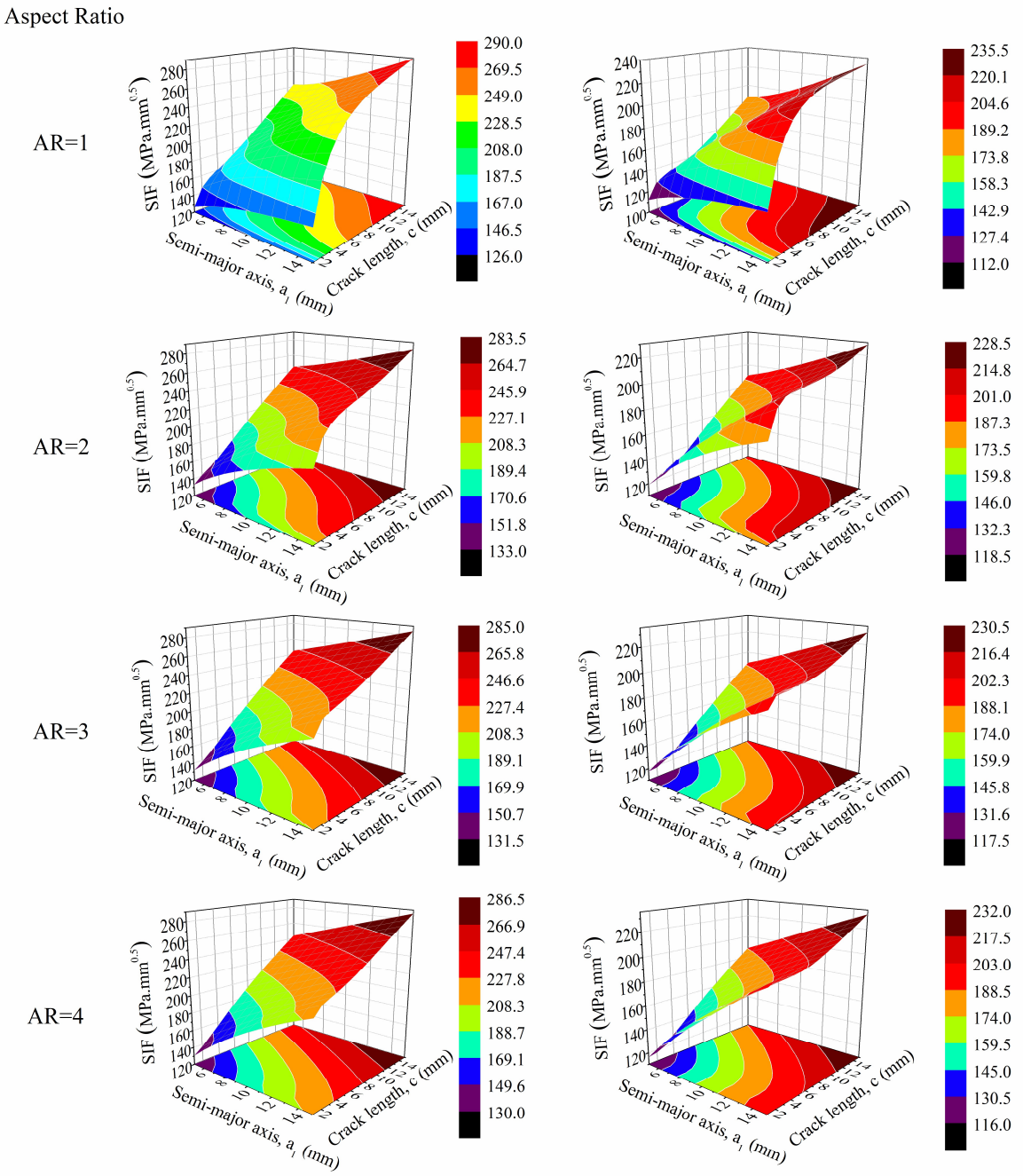

(a) Repair Voltage=0 V (b) Repair Voltage=500 V

Figure 4.10: SIFs for various hole and crack geometries

4.4.2.1 Effect of crack length (c)

The effect of crack length on stress intensity factor (SIF) is significant when emanating from an elliptical hole and repaired using piezoelectric patches. As the crack length increases, the SIF tends to rise due to the greater stress concentration at the crack tip, especially around discontinuities like an elliptical hole. Under an applied voltage of 500 V,

the piezoelectric patch can induce strain, which helps reduce the SIF by counteracting the mechanical stresses.

It is observed that for a fixed semi-major axis and aspect ratio, the SIF increases with crack length, as shown in Figure 4.10. The percentage reduction in the stress intensity factor (SIF) concerning the crack length is represented in Figure 4.11 for semi-major axis lengths 5 mm, 10 mm and 15 mm and aspect ratios (AR) ranging from 1 to 4. As can be seen in the illustration, this reduction is more significant for longer cracks when using a piezoelectric patch, as the increased stress concentration at the crack tip makes the crack more sensitive to the applied strain from the patch. While SIF naturally increases with crack length, the strain induced by the piezoelectric patch counteracts the mechanical stresses more effectively in longer cracks, resulting in a more significant reduction in SIF. Thus, with all other parameters constant, the decrease in SIF percentage compared to without repair condition is higher for longer cracks because the applied strain likely has a more significant impact on larger stress fields at the crack tip. At a_1=5 mm, AR=1, the reduction is 21.53% for crack length, c=10 mm, significantly higher than the 19.1% observed for c=5 mm.

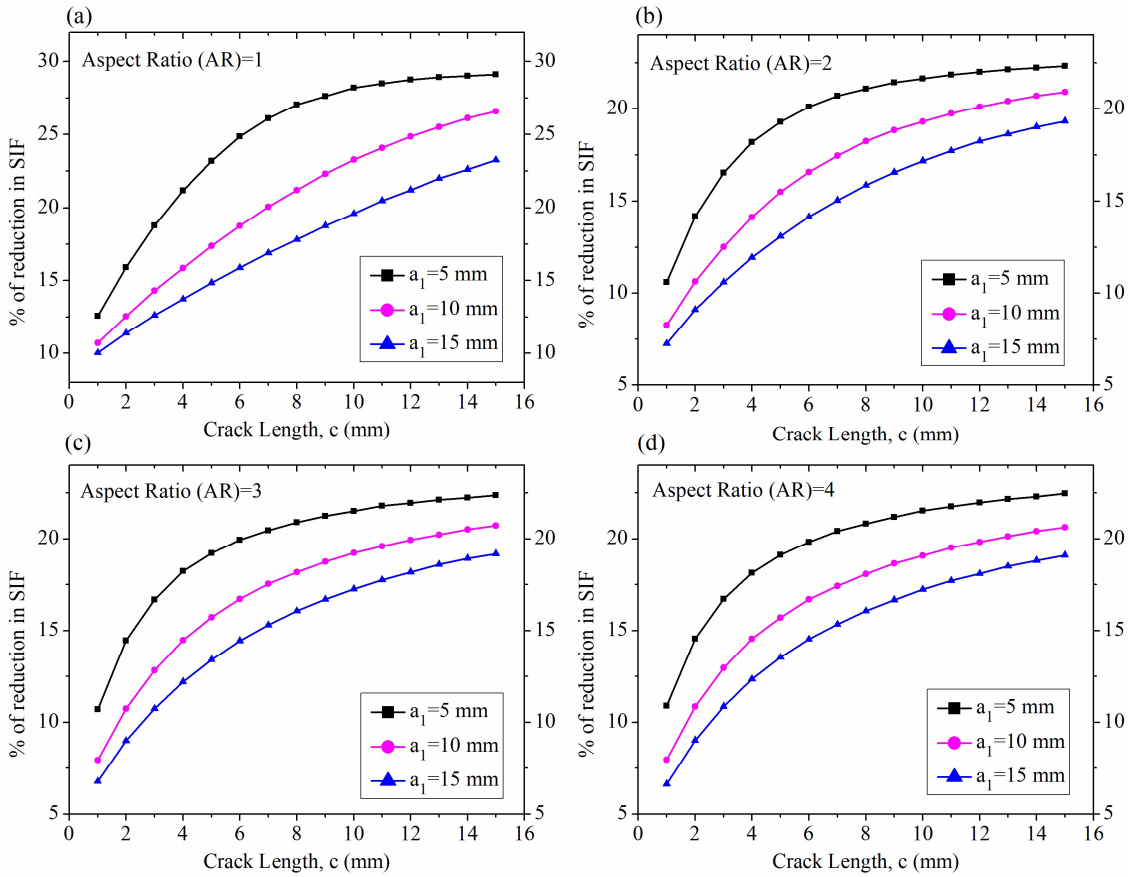

Figure 4.11: Percentage of reduction in SIF for various hole and crack geometries

4.4.2.2 Effect of Semi-Major Axis Length (a_1)

The semi-major axis of the hole also plays a vital role, with larger semi-major axes typically resulting in higher SIF values due to the increased stress concentration around larger holes for a given crack length, as shown in Figure 4.10. Figure 4.12 represents the percentage reduction in SIF, focusing on the effect of using piezoelectric patch for different values of the semi-major axis ranging from 5 mm to 15 mm and for four different aspect ratios (AR=1, 2, 3, and 4). The percentage reduction in SIF values is represented for two crack lengths, 5 mm and 10 mm (Figure 4.12). As the semi-major axis increases from 5 to 15, the percentage reduction in SIF consistently decreases across all aspect ratios (AR=1 to AR=4) and all crack lengths, indicating that the piezoelectric patch has a more noticeable effect on reducing SIF for shorter semi-major axes. This suggests that the actuation by the piezoelectric patch is insufficient for larger elliptical holes as extensive stress distribution exists around the crack tip, resulting in less SIF reduction. The highest reduction is observed at a_1=5 mm and AR=1; hence, the patch is more effective in smaller hole and longer crack length configurations. This implies that the piezoelectric patch is more effective in reducing SIF for longer cracks, especially at smaller semi-major axes. This explains the overall decrease in the percentage reduction in SIF as the semi-major axis increases, particularly noticeable in AR=1.

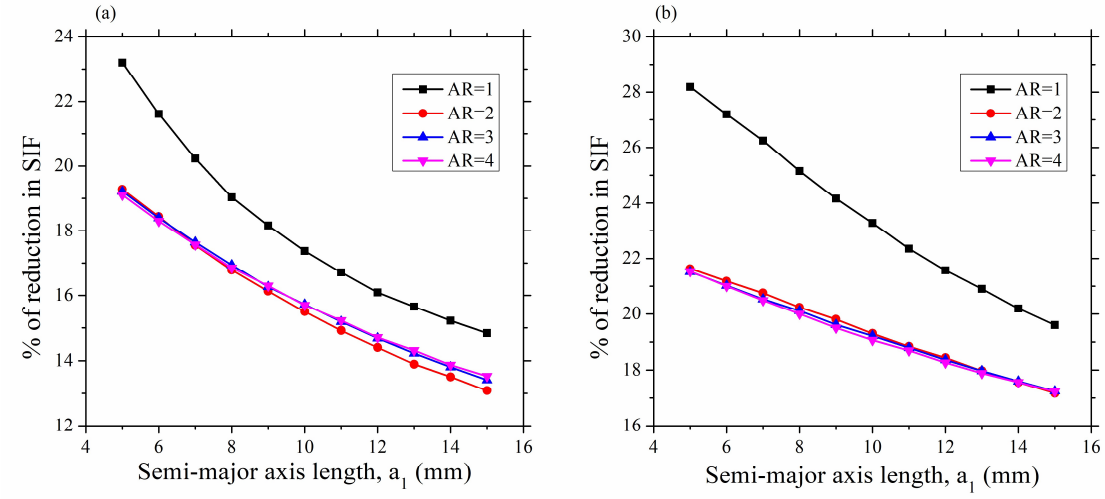

Figure 4.12: Percentage of reduction in SIF for various hole geometry for crack length (a) c=5 mm (b) c=10 mm

4.4.2.3 Effect of Aspect Ratio (AR)

The aspect ratio (AR) also plays a vital role, with higher aspect ratios (AR=2, 3, and 4) showing less reduction in SIF across all values of 'a_1' and 'c,' indicating that the geometry of the elliptical hole influences how effectively the patch can reduce stress. The reduction in

SIF is found less for aspect ratios AR=2, 3, and 4 than AR=1 because the stress distribution around the elliptical hole becomes less concentrated as the aspect ratio increases. When AR=1, the elliptical hole is closer to a circular shape, and stress concentrations at the crack tip exhibit greater exposure to variations induced by external control mechanisms such as piezoelectric actuation. This allows the piezoelectric patch to more effectively counteract mechanical stresses by inducing strain in a relatively confined area.

As the aspect ratio increases (AR=2, 3, 4), the shape of the elliptical hole elongates for a fixed semi-major axis. However, for elongated geometries (high AR), the crack's stress field becomes less influenced by local changes introduced by these actuators. This means that further increases in AR result in minimal changes to the stress distribution around the crack. The reduction in SIFs for AR=2, 3, and 4 remains almost the same because, at these aspect ratios, the stress concentration near the crack tip reaches a steady state. After all, the influence of geometry stabilizes. While the hole becomes more elongated, the change in stress concentration between AR=2 and AR=4 is relatively minor compared to the shift from AR=1 to AR=2. For instance, at a_1=5 mm, the reduction in SIF was found to be 23.19%, 19.28%, 19.2%, and 19.1% for AR=1, 2, 3, and 4, respectively, for a crack length of 5 mm as shown in Figure 4.12a. Thus, the piezoelectric patch effectiveness levels out across AR=2, 3, and 4, leading to similar percentage reductions in SIF across all values of 'a_1' and 'c'. This suggests that the hole's shape, except AR=1, doesn't significantly alter the patch's performance, as the overall stress field behaves similarly for higher AR values.

4.4.3 SIF Range, Fatigue Crack Growth (FCG), and Fatigue Life (N_f) Analysis

The SIF range, which quantifies the effect of stress distribution near a crack tip, highly depends on the geometries of the crack and elliptical hole. This section analyses the SIF range between the stress range of 80 MPa and 8 MPa (SR=0.1) about crack length, semi-major axis length (a_1), and aspect ratio (AR) under conditions with and without piezoelectric repair (V = 0 and V = 500). As crack length (c) increases, the SIF range steadily increases across all AR values and all repair conditions since longer cracks intensify the stress concentration near the crack tip, raising the SIF range values, as depicted in Figure 4.13. This higher SIF range in long cracks enhances the possibility of rapid crack propagation under cyclic loading, reducing the structure's overall durability.

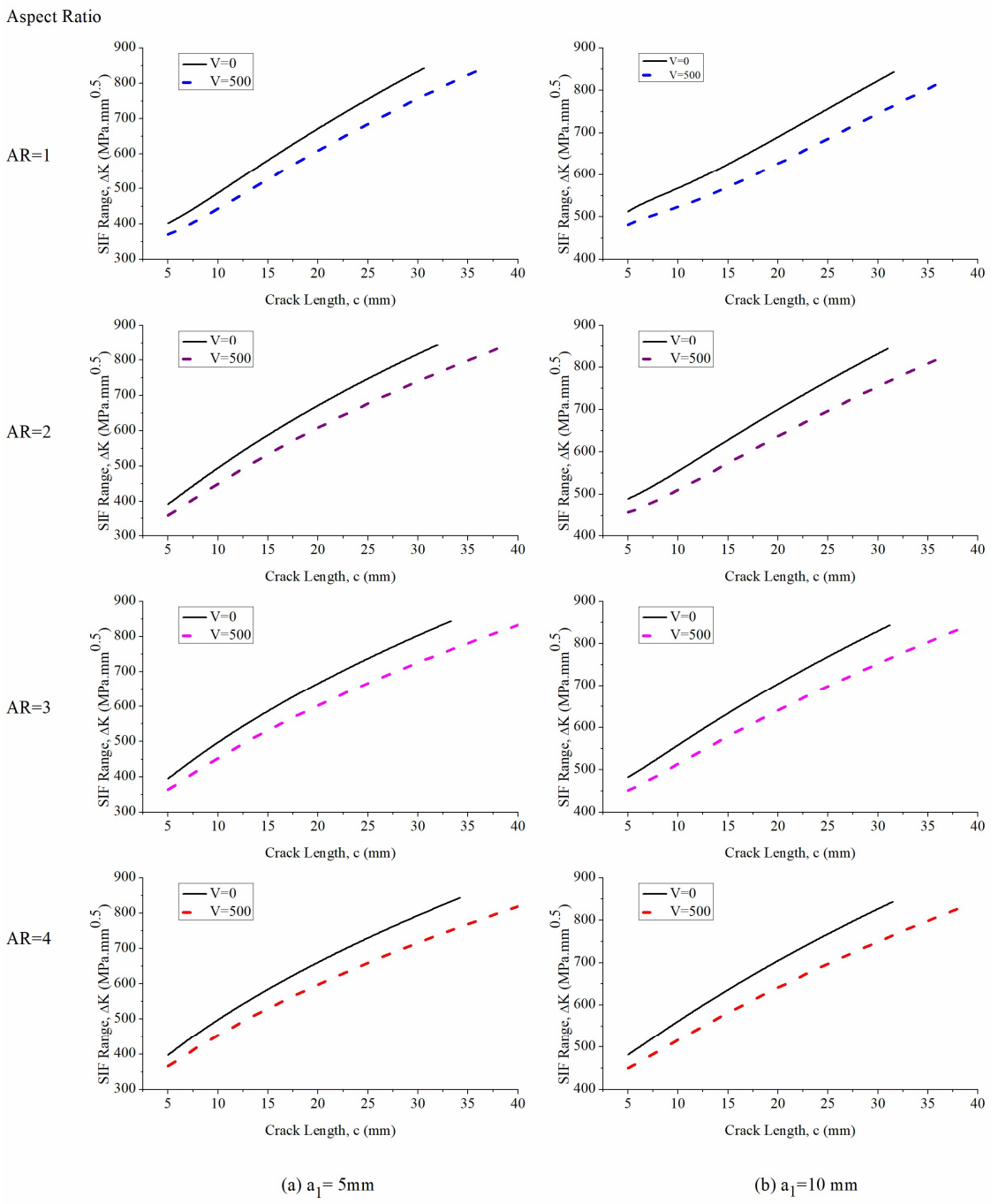

Figure 4.13: SIF Range vs. crack length (c) for various geometries of the elliptical hole

It is to be noted that, under fatigue loading, the SIF range remains constant before and after repair when a fixed voltage ($V_{max} = V_{min}, \Delta V = 0$) is applied throughout the loading cycles as the zero-voltage ratio (VR) offers the best repair performance as stated in Chapter 2. To minimize ΔK, ΔV must be kept at a higher value. To increase fatigue life, the maximum SIF (K_{max}) would be lowered by applying a higher maximum voltage (V_{max}). Therefore, to

achieve top repair performance, V_{min} is equal to zero (VR = 0), resulting in maximum ΔV for a fixed V_{max}. Hence, the piezoelectric patches are applied an external voltage of V_{max}=500, reducing the SIF range across all crack lengths and aspect ratios compared to without repair conditions. For instance, at a=5mm and AR = 4, the SIF range after repair (V= 500) decreases from 397 MPa.mm$^{0.5}$ to 365.4 MPa.mm$^{0.5}$ for c = 5 mm, whereas it decreases from 661.1 MPa.mm$^{0.5}$ to 598 MPa.mm$^{0.5}$ for c = 20 mm. The externally applied voltage causes the piezoelectric material to generate a compressive stress that opposes the existing maximum tensile stresses, resulting in a reduction in maximum SIF (K_{max}) thereby decreasing the overall SIF range. Consequently, the reduction in the SIF range can delay crack propagation, enhancing the fatigue life of the material.

Figure 4.14 illustrates the percentage reduction in the SIF range as a function of crack length for various semi-major axes (a_1) and aspect ratios (AR) after repair using a piezoelectric patch. The reduction of SIF reductions is more significant with longer cracks for all aspect ratios, as shown in Figure 4.14, reflecting an adequate control over the SIF range even as crack severity grows. This repair is essential in delaying crack growth at this stage, acting as an effective repair strategy under fatigue loading. For smaller semi-major axes (a_1=5 mm), the reduction of the SIF range shows a consistent increase with crack length, particularly for higher aspect ratios, where AR = 3 and AR = 4 surpass AR = 1 and AR = 2. For a_1=10 mm, a similar pattern is observed; however, the percentage reductions are generally lower than those obtained with the smaller semi-major axis. This finding emphasizes the significance of designing repair methods according to crack geometry, as higher aspect ratios and smaller semi-major axes provide the most significant reductions in the SIF range.

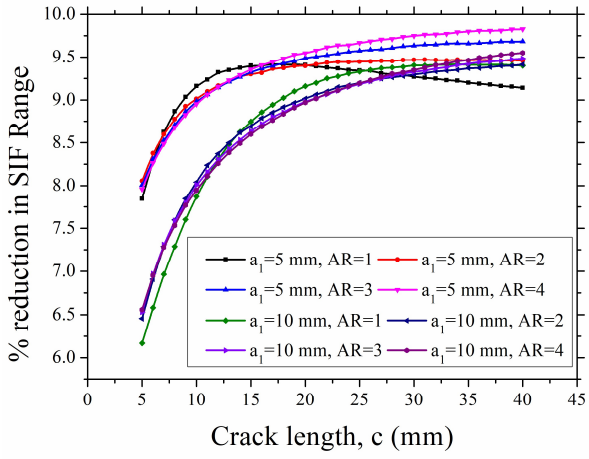

Figure 4.14: Percentage of reduction in SIF range concerning crack length for various geometries of elliptical hole

Figure 4.15 presents a log-log plot of the Fatigue Crack Growth Rate (FCGR) against the SIF range (ΔK) for different crack lengths (5 mm and 10 mm) and aspect ratios (AR=1, 2, 3, and 4), comparing without repair conditions with repairs conducted at 500 V. The plot follows a standard FCGR model approach [Anderson (2017)]. It reflects data for loading conditions that ensure the SIF range remains above the material's threshold limit ($\Delta K > \Delta K_{th}$) at the beginning of the cycle. This choice allows the focus to stay on Regions II and III, where significant crack propagation occurs. In Region II, a straight line on the log-log plot is observed; crack growth is stable and adheres to the Paris crack growth model [Paris and Erdogan (1963)]. In contrast, Region III exhibits exponential crack growth, where ΔK reaches elevated values. This rapid crack propagation drives the maximum SIF (K_{max}) towards the material's fracture toughness (K_{IC}), quickly leading to catastrophic failure. For this instance, when the crack grows to 10 mm, the FCGR is found to be 0.00121 mm/cycle and 0.000918 mm/cycle for 0 V and 500 V applications, respectively, for semi-major axis 5 mm and aspect ratio (AR) of 4. The difference between repair and without-repair scenarios highlights the influence of repair conditions on crack propagation rates, showing how repair can reduce the crack propagations and lifespan of the material under cyclic stress conditions.

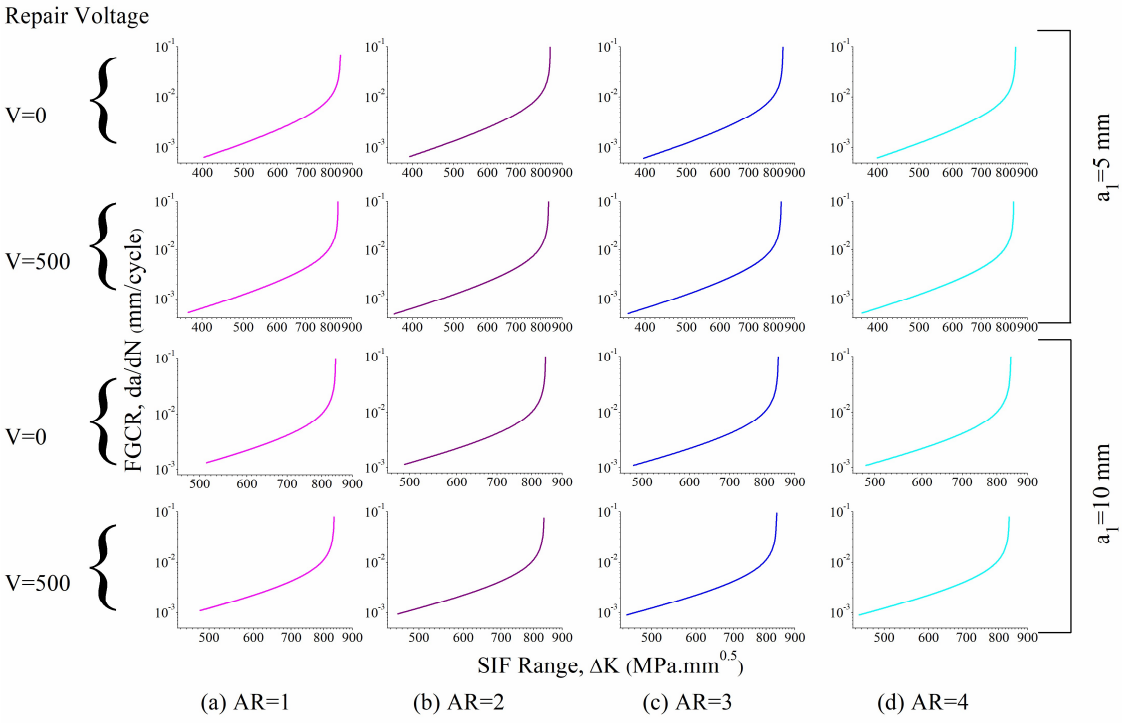

Figure 4.15: FCGR for various geometries of the elliptical hole

The fatigue crack growth (FCG) after several loading cycles is calculated until the critical crack length (c_c) is attained for the given configuration. Figure 4.16 depicts FCG with and without repair configurations, assuming an initial crack length of 5 mm. The semi-major axis lengths were 5 mm and 10 mm, with aspect ratios (AR) ranging from 1 to 4.

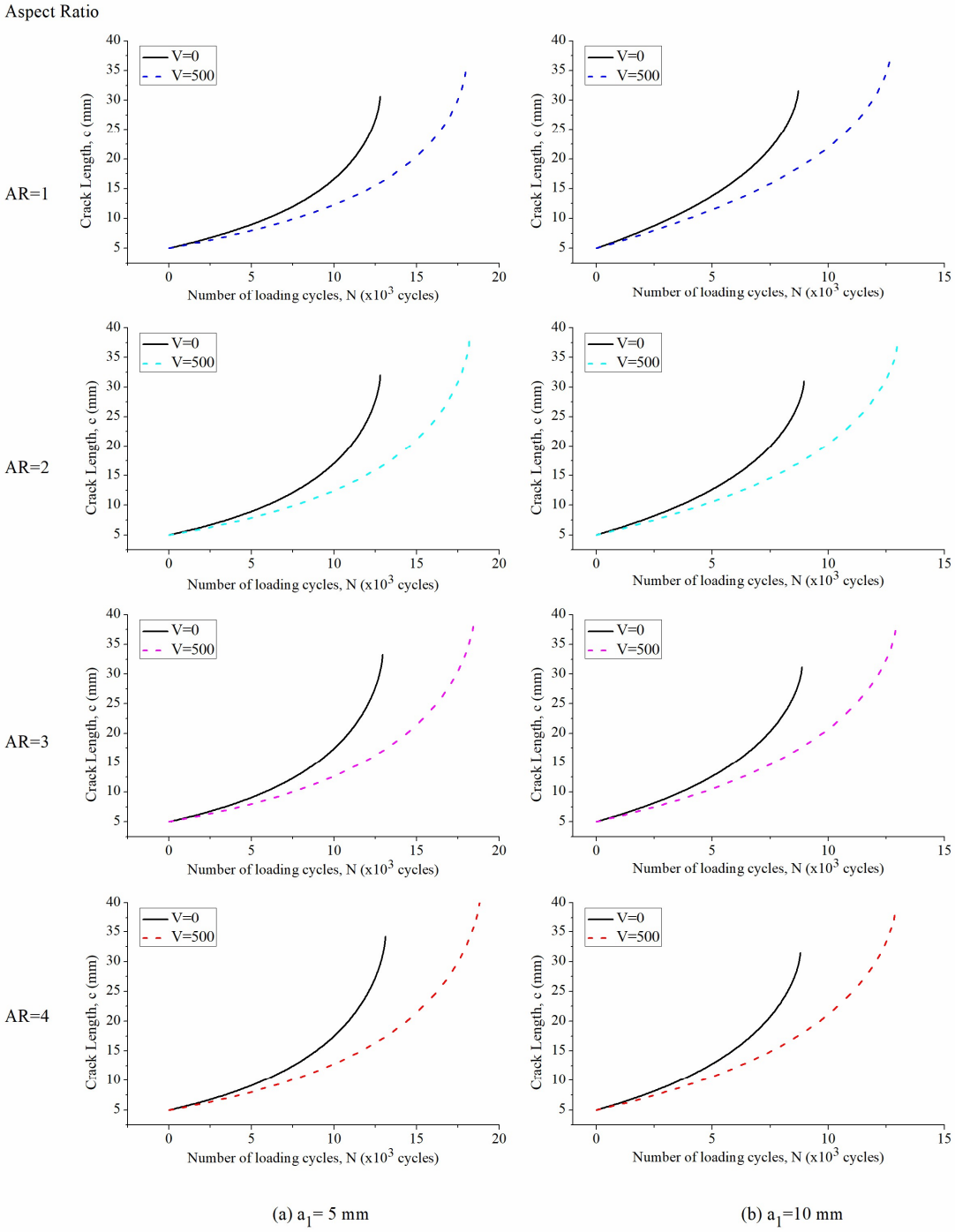

Figure 4.16: Final crack length (c) concerning the number of loading cycles (N) for various geometries of elliptical hole

The studies revealed that the repair causes the crack to grow more slowly than the one without a repair case. Since the SIF range drives crack growth, the actuation of the piezoelectric patch reduces the SIF range, enabling delayed crack growth. In particular, reaching a 30 mm crack length requires 12781, 12716, 12755, and 12841 cycles for aspect ratios 1, 2, 3, and 4, respectively. In contrast, when repaired with a 500 V, the cycles increase to 17493, 17366, 17402, and 17513, assuming semi-major axis lengths of 5 mm, as illustrated in Figure 4.16.

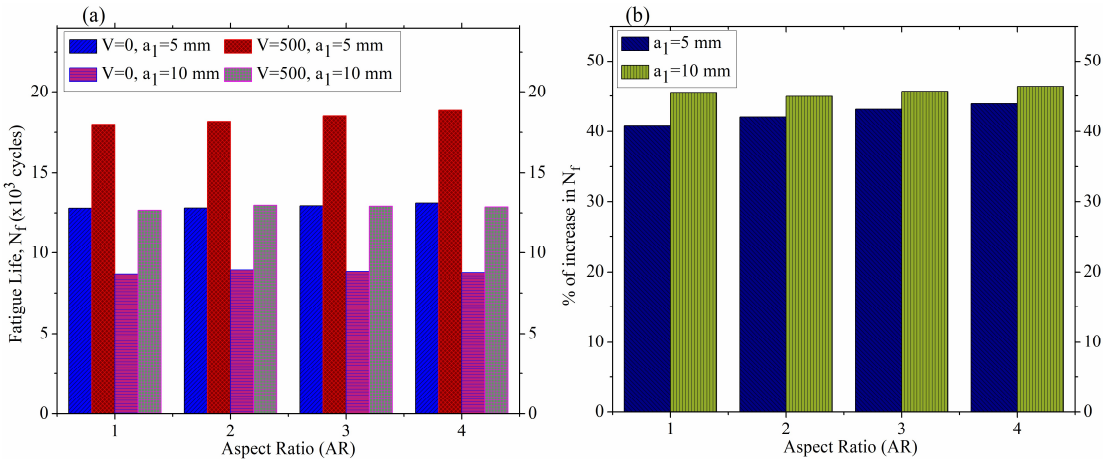

Figure 4.17: (a) Fatigue life for with and without repair condition (b) Percentage of increase in fatigue life for various geometries of elliptical hole

Following several rapid growth cycles at each repair voltage, the crack length attains the critical threshold, with the associated number of loading cycles dictating its fatigue lifetime. Figure 4.17a demonstrates the post-repair fatigue life, showcasing fatigue life across different geometric configurations, including semi-major axis lengths of 5 and 10 mm, with aspect ratios varying from 1 to 4, both with and without repair situations. Additionally, given the aforementioned geometric configurations, Figure 4.17b shows the percentage improvement in fatigue life when repaired with a 500 V compared to without-repair situations; for a semi-major axis length of 5 mm, 40.78%, 42.08%, 43.17%, and 43.91%, enhanced fatigue life is achieved for aspect ratios 1, 2, 3, and 4, respectively. The corresponding values for a semi-major axis length of 10 mm are 45.51%, 44.94%, 45.67%, and 46.36%. The repaired structure reveals a longer fatigue life, attributed to two primary factors. First, the piezoelectric patch's actuation reduces the SIF range by lowering the maximum SIF, while the minimum SIF remains unchanged due to zero voltage application at minimum external loading. This reduction in the SIF range slows crack growth, increasing the cycles required to reach the fracture toughness. Second, since fracture toughness influences

fatigue life, the reduced maximum SIF requires more loading cycles to get the critical crack length. Thus, the piezoelectric patch enhances the beam's fatigue resistance by delaying critical crack progression. Beyond critical length, uncontrolled crack propagation would lead to catastrophic failure.

4.5 Summary

This study aimed to enhance the structural integrity of cracked plates containing elliptical holes by utilizing piezoelectric actuators for active repair. This research employed linear elastic fracture mechanics (LEFM) principles to compute SIF using the Weight Function Method (WFM). A superposition approach integrated the effects of piezoelectric actuation on the SIF. Fatigue crack growth rate (FCGR) was estimated through established models, and parametric studies were conducted to assess the influence of geometric and actuation parameters. Numerical validation via ABAQUS further authenticate the reliability of the analytical framework. Applying piezoelectric patches under external voltage substantially reduces the SIF range across varying crack lengths and aspect ratios. This repair method effectively mitigates the intensifying effects of stress concentration due to crack propagation, particularly for longer cracks and higher ARs, presenting a promising approach for enhancing the fatigue resistance and longevity of structural materials under cyclic loading. However, the following essential findings have been drawn from this study:

- Piezoelectric actuators show a crucial role in mitigating crack propagation when emanating from an elliptical hole by actively reducing the stress intensity factor (SIF) enhances the structural integrity of damaged components.
- The effectiveness of piezoelectric patches in reducing stress intensity factors (SIF) changes with crack length, hole size, and aspect ratio. Longer cracks benefit more from the actuation; nevertheless, this effect diminishes as the hole size and aspect ratio increase.
- The aspect ratio (AR) of elliptical holes influences the repair efficiency, especially a more significant SIF reduction as the hole shape approaches a circular shape. Although changes in aspect ratio (AR) have minimal impact on repair efficiency for a fixed crack length and semi-major axis length. Additionally, the percentage reduction decreases as the aspect ratio (AR) increases, likely due to the increased stress concentration, implying that the patch becomes less effective for higher aspect ratios.

- A more significant decrease in SIF is observed for smaller semi-major axes, even though the total length of the opening, which is the sum of the semi-major axis and crack length, remaining constant.
- The thickness of piezoelectric actuators affects their performance. Thinner actuators are more suitable for lower loads, while thicker ones show superior mechanical performance under higher loads. This highlights the importance of selecting the right actuator based on the load conditions.
- The integration of piezoelectric patches leads to a notable extension of fatigue life, confirming their potential as an effective solution for prolonging the service life of structural components, especially when the cracks emanate from elliptical holes.

Chapter 5

REPAIR OF AN EDGE-CRACKED ARC-SHAPED SPECIMEN USING PIEZOELECTRIC ACTUATORS

5.1. Introduction

The utilization of piezoelectric materials for structural health monitoring and active repair has gained significant traction in recent decades. The ability of these materials to convert electrical energy into mechanical strain and vice versa allows for precise control of structural deformation, making them ideal for applications involving crack repair. Specifically, applying adhesively bonded piezoelectric patches to induce localized stress fields that counteract the stress concentration at crack tips has demonstrated promising results in mitigating crack propagation. This approach offers a potential solution to extend the lifespan of critical structural components, reducing maintenance costs and enhancing safety.

While extensive research has focused on repairing plate and beam specimens of regular sections using piezoelectric actuators, a critical gap exists in understanding and implementing this technique for arc-shaped specimens. The practical necessity for repairing arc-shaped components arises from extensive use in various engineering applications, including pipelines, curved structural members in aerospace and automotive industries, and pressure vessels. These components are often subjected to complex loading conditions, including cyclic stresses and environmental factors, which can lead to the formation and propagation of cracks. Effective and reliable repair techniques for such structures are paramount to ensure their continued functionality and prevent catastrophic failures. Thus, the lack of studies addressing the specific challenges associated with repairing arc-shaped specimens represents a significant limitation in the current state of knowledge.

This chapter aims to address this critical gap by investigating the feasibility and effectiveness of piezoelectric actuators for repairing edge-cracked arc-shaped specimens, encompassing both static and fatigue repair analyses. Firstly, the chapter details the methodology employed to develop an analytical model based on Linear Elastic Fracture Mechanics (LEFM) and the Weight Function Method (WFM) to determine the mode-I stress intensity factor (SIF) under both static loading conditions. This model incorporates the effects

of piezoelectric actuation, allowing for analysis of the static repair of the arc-shaped specimen under constant uniaxial tensile loading. The effectiveness of the piezoelectric patch in reducing the Mode-I SIF is evaluated, providing insights into the static repair performance. Parametric studies are conducted to examine the influence of various factors, including the dimensions of the specimen, the crack length, and the dimensions of the piezoelectric patch, on the repair efficiency. Specifically, the effects of patch thickness and width are thoroughly investigated to determine optimal configurations for maximizing stress reduction. Secondly, the chapter delves into the fatigue repair of the arc-shaped specimen under cyclic tensile loading. By applying the Paris model, the fatigue crack growth rate (FCGR) is predicted before and after the application of piezoelectric actuation. This analysis assesses the ability of the piezoelectric patch to reduce FCGR and extend the fatigue life of the specimen. The influence of various parameters, such as the applied voltage and the number of loading cycles, is also highlighted to govern the effectiveness of the active repair strategy.

5.2. Problem Formulation

Estimating SIF under static loading for scenarios such as without and active repair becomes essential since the SIF range (ΔK) impacts both FCGR and fatigue life. This analysis is carried out for an arc-shaped specimen with an edge crack of length 'a', which is exposed to a load of P, as shown in Figure 5.1. The crack length is along the x-direction. At the same time, the y-direction denotes the loading direction, and it is perpendicular to the crack length or x-direction, whereas the thickness is along the z-direction.

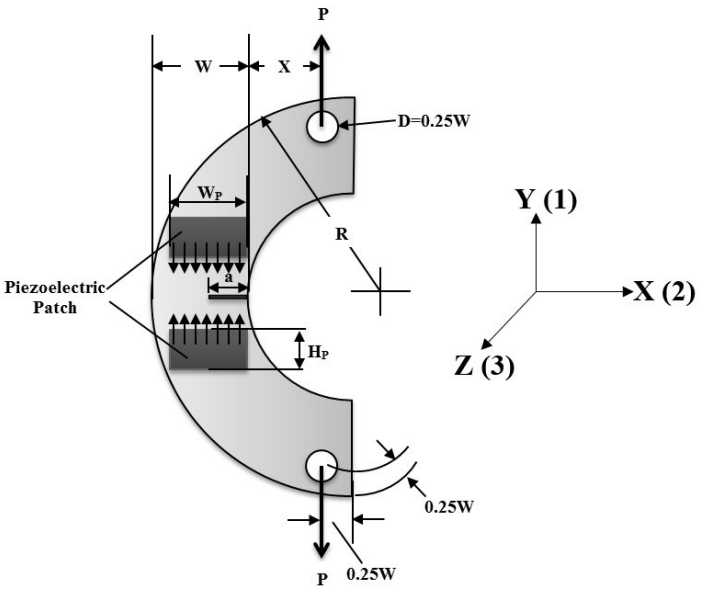

Figure 5.1: Edge cracked arc-shaped specimen was repaired with a piezoelectric patch

5.2.1 SIF Estimation for the Cracked Specimen

In this configuration, Mode-I is the only effectual mode considered, and the Mode-I SIF for an arc-shaped edge cracked specimen is calculated using LEFM and given by Eq. (5.1) as proposed by Tada et al. (2000).

$$K_I = \sigma_0\sqrt{\pi a} \tag{5.1}$$

where,

$$\sigma_0 = \frac{P}{t_{s.}W_s} \tag{5.2}$$

where t_s and W_s are the thickness and width of the specimen.

As the geometry of the cracked specimen affects the fracture parameters, a shape correction factor is introduced [Tada et al. (2000)], and the modified mode-I SIF can be written as,

$$K_I = \sigma_0\sqrt{\pi a}\ \cdot F_1\left(\frac{a}{W}\right)\cdot F_2\left(\frac{a}{W},\frac{X}{W},\frac{W}{R}\right) \tag{5.3}$$

Where shape correction factors can be expressed as,

$$F_1\left(\frac{a}{W}\right) = \frac{3.74-6.30\frac{a}{W}+6.32\left(\frac{a}{W}\right)^2-2.43\left(\frac{a}{W}\right)^3}{\sqrt{\pi}\left(1-\frac{a}{W}\right)^{1.5}} \tag{5.4}$$

$$F_2\left(\frac{a}{W},\frac{X}{W},\frac{W}{R}\right) = \left(3\frac{X}{W}+1.9+1.1\frac{a}{W}\right)\cdot\left[1+0.25\cdot(1-\frac{a}{W})^2\cdot\frac{W}{R}\right] \tag{5.5}$$

Where X is the distance between the crack mouth and the line of action of the load, and R is the radius of the specimen's outer surface, as shown in Figure 5.1.

5.2.2 SIF Reduction via Active Repair

The SIF of the piezoelectric patch integrated cracked specimen is estimated by using the superposition method of LEFM, where two different scenarios are considered to calculate their total SIF (K_A) after repair and can be written as,

$$K_A = K_I + K_{Piezo} \tag{5.6}$$

where K_{Piezo} is SIF only exists under the piezoelectric actuation effect, which is evaluated by the weight function method (WFM) [Bueckner (1970)] and can be written as,

$$K_{Piezo} = \int_0^a h(x, y, a) \cdot \sigma_{Piezo} \cdot dx \tag{5.7}$$

Where $h(x, y, a)$ is the weight function, É represents Young's modulus in plane strain or plane stress conditions. The weight function is derived from in-plane crack opening displacement, which belongs to the Westergaard stress function [Anderson (2017)] as computed in Chapter 2 and 4. σ_{Piezo} is the stress created by the piezoelectric materials. The piezoelectric patch is polarized along the thickness or 3-direction, and d_{31} is the only effective mode considered here, which indicates the patch is strained along the perpendicular direction of the crack or in the 1-direction when the voltage is applied along the 3-direction. For perfect bonding between the piezoelectric patch and the cracked specimen, piezoelectric stress is given by Eq. (5.8). Moreover, this stress has equal distribution at right angles to the cracked surface.

$$\sigma_{Piezo} = \frac{E_s t_s T}{A(\psi + \alpha)} \cdot \frac{d_{31} V}{t_p} \tag{5.8}$$

Where, E_s is Young's modulus of the specimen, E_p, W_p, t_p Young's modulus, width and thickness of the piezoelectric patch, respectively, T is the width of distributed electrodes on the piezoelectric patch, A is the effective cross-sectional area of the specimen, d_{31} is the piezoelectric strain coefficient, V is the applied voltage, $\alpha = 2$ for extensional loading and $\psi = E_s W_s t_s / E_P W_P t_P$, [Crawley and Luis (1987)]. So, the total SIF can be written as,

$$K_A = \sigma_0 \sqrt{\pi a} + \int_0^a h(x, y, a) \cdot \sigma_{Piezo} \cdot dx \tag{5.9}$$

Given that the solution derived from Eq. (5.9), depending on the application of LEFM principles, it is necessary to account for the shape correction factor [Tada et al. (2000)], resulting in a potential modification of Eq. (5.9), as follows:

$$K_A = \left[\sigma_0 \sqrt{\pi a} + \int_0^a h(x, y, a) \cdot \sigma_{Piezo} \cdot dx \right] \cdot F_1\left(\frac{a}{W}\right) \cdot F_2\left(\frac{a}{W}, \frac{X}{W}, \frac{W}{R}\right) \tag{5.10}$$

5.2.3 FCGR and Fatigue Life Estimation

The specimen is subjected to cyclic tensile loads having maximum stress and minimum stress σ_{max} and σ_{min}, respectively, and the corresponding SIFs are K_{max} and K_{min}. The Paris

crack growth model is used here to predict FCGR under cyclic tensile stress and is expressed as [Paris and Erdogan (1963)].

$$\frac{da}{dN} = C \cdot (\Delta K)^m \tag{5.11}$$

5.2.3.1 Without repair

The SIF range ($\Delta K = K_{max} - K_{min}$) for the cracked specimen under σ_{max} and σ_{min} can be calculated from the Eq. (5.3) and written as,

$$\Delta K_I = (\sigma_{max} - \sigma_{min}) \cdot \sqrt{\pi a} \cdot F_1\left(\frac{a}{W}\right) \cdot F_2\left(\frac{a}{W}, \frac{X}{W}, \frac{W}{R}\right) \tag{5.12}$$

FCGR is now calculated by putting the expression of Eq. (5.12) into Paris crack growth model and expressed as,

$$\frac{da}{dN} = C \cdot \left[(\sigma_{max} - \sigma_{min}) \cdot \sqrt{\pi a} \cdot F_1\left(\frac{a}{W}\right) \cdot F_2\left(\frac{a}{W}, \frac{X}{W}, \frac{W}{R}\right)\right]^m \tag{5.13}$$

The fatigue life is calculated from the material property fracture toughness (K_{IC}) such a way that K_{max} reaches the value of K_{IC}. The fatigue life is calculated by integrating the Eq. (5.13) within the limit of initial crack length (a_o) and critical crack length (a_c). The fatigue life can be written as,

$$\left(N_f\right)_{without\ repair} = \int_{a_o}^{a_c} \frac{da}{C \cdot \left[(\sigma_{max} - \sigma_{min}) \cdot \sqrt{\pi a} \cdot F_1\left(\frac{a}{W}\right) \cdot F_2\left(\frac{a}{W}, \frac{X}{W}, \frac{W}{R}\right)\right]^m} \tag{5.14}$$

5.2.3.2 Active repair

The voltage is applied to the patch as V_{max} and V_{min} with no phase difference with the mechanical load. The SIF range ($\Delta K = K_{max} - K_{min}$) for the cracked specimen after repair can be calculated from the Eq. (5.10) and written as,

$$\Delta K_A = \left[(\sigma_{max} - \sigma_{min}) \cdot \sqrt{\pi a} + \int_0^a h(x, y, a) \cdot \Delta\sigma_{Piezo} \cdot dx\right] \cdot F_1\left(\frac{a}{W}\right) \cdot F_2\left(\frac{a}{W}, \frac{X}{W}, \frac{W}{R}\right) \tag{5.15}$$

FCGR can be expressed as,

$$\frac{da}{dN} = C \cdot \left[\left\{ (\sigma_{max} - \sigma_{min}) \cdot \sqrt{\pi a} + \int_0^a h(x, y, a) \cdot \Delta\sigma_{Piezo} \cdot dx \right\} \cdot F_1\left(\frac{a}{W}\right) \cdot F_2\left(\frac{a}{W}, \frac{X}{W}, \frac{W}{R}\right) \right]^m \tag{5.16}$$

The fatigue life can be written as,

$$\left(N_f\right)_{after\ repair} = \int_{a_o}^{a_c} \frac{da}{C \cdot \left[\left\{ \begin{matrix} (\sigma_{max} - \sigma_{min}) \cdot \sqrt{\pi a} \\ + \int_0^a h(x, y, a) \cdot \Delta\sigma_{Piezo} \cdot dx \end{matrix} \right\} \cdot F_1\left(\frac{a}{W}\right) \cdot F_2\left(\frac{a}{W}, \frac{X}{W}, \frac{W}{R}\right) \right]^m} \tag{5.17}$$

5.3. Results and Discussion

In this section, various studies were conducted to observe the efficacy of the repair method. For this study, the piezoelectric materials are PZT-5H, and the cracked specimen is Al 2024-T3. The effect of adhesive was not considered for this analysis. The actuator width is so kept that it covers the entire crack length. The voltage is applied to the piezoelectric actuators so that extensional strain occurs, causing compressive stress at the crack tip. When an external voltage is applied, the piezoelectric patch is kept closer to the crack plane to provide the highest possible compressive stress. It is exposed to a maximum stress of 10 MPa while maintaining a stress ratio (SR) of 0.1. This amount of load is chosen in such a way that the SIF range remains more significant than the threshold limit ($\Delta K > \Delta K_{th}$). The voltage is set to maximum for the highest stress and zero for the minimum stress, as discussed in Chapter 2. Piezoelectric materials have a maximum electric field limit for proper function, and the absolute voltage is determined by its thickness. For PZT-5H, it is about 1-2 kV/mm [Udayakumar et al. (1995)]. For safe operation by the piezoelectric materials, a maximum of 1 kV/mm is chosen, and subsequently, the maximum possible voltage becomes 500 V as the thickness chosen is 0.5 mm.

The parameters of the geometry of the specimen and piezoelectric patch are as follows: $\mathrm{W_s} = 40$ mm, $a_i = 8$ mm, $\mathrm{R} = 80$ mm, $\mathrm{X} = 0, 20$ mm, $\mathrm{t_s} = 1.6$ mm, $\mathrm{W_p} = 20, 25, 30$ mm, $\mathrm{H_p} = 25$ mm and $\mathrm{t_p} = 0.5, 0.75, 1.0$ mm. The material properties of the specimen are given in Table 5.1 and the material properties of PZT-5H are presented in Table 5.2.

Table 5.1: Mechanical properties and crack growth parameters of Al 2024-T3 plate material

Parameter	Value
Elastic Modulus (E_s)(GPa)	74
Poisson's ratio (ν)	0.33
Tensile yield strength (MPa)	345
Ultimate tensile strength (MPa)	483
Density (Kg/m^3)	2780
$\Delta K_{th}\left(MPa\sqrt{m}\right)$ at SR=0.1	3.61
$K_{IC}\left(MPa\sqrt{m}\right)$	33.16
C	7.172×10^{-8}
m	3.0089

Table 5.2: Properties of piezoelectric material PZT-5H

Piezoelectric coefficient (10^{-12} C/N)	Flexibility coefficient (10^{-12} m^2/N)	Density (Kg/m^3)
d_{31}=-274 d_{33}=593 d_{15}=741	s_{11}=16.5, s_{12}=-4.78, s_{14}=-8.45, s_{33}=20.7, s_{44}=43.5, s_{66}=2(s_{11}-s_{12})	7500

5.3.1 Comparison of Repaired and Without Repaired Specimens

To evaluate the effectiveness of the piezoelectric actuator-based repair technique, a comparative study has been conducted examining cracked and repaired specimens subjected to varying external voltages. The piezoelectric patches, with dimensions of $t_p = 0.5$ mm, $H_p = 25$ mm, and $W_p = 30$ mm, were applied to specimens containing crack lengths ranging from 1 mm to 10 mm. Specimens were subjected to a constant tensile stress of 10 MPa in all cases.

The analytical Stress Intensity Factor (SIF) results, presented in Figure 5.2, demonstrate the impact of different geometric configurations ($X/W = 0.5$ and 0) and repair conditions on crack behavior. Notably, a significant reduction in SIF was observed upon applying external voltage to the piezoelectric patches. Specifically, a 21.1% reduction in SIF was achieved with an applied voltage of 500 V, while a 4.2% reduction was observed at 100 V, both compared to the without repair condition.

This reduction can be attributed to the positive strain induced by the piezoelectric material, which effectively modifies the stress distribution near the crack tip. The compressive stress generated by the actuator, directly proportional to the applied electric field, counteracts the tensile stress concentration at the crack tip, thereby reducing the overall SIF. The linear relationship between applied voltage and SIF reduction suggests that maximizing the applied voltage is crucial for achieving optimal repair performance. As expected, the total SIF increased with increasing crack length. However, the repair efficacy, as measured by the percentage reduction in SIF, remained consistent across all crack lengths for a given applied voltage. This indicates that the piezoelectric repair technique is effective regardless of the initial crack size, suggesting a robust solution.

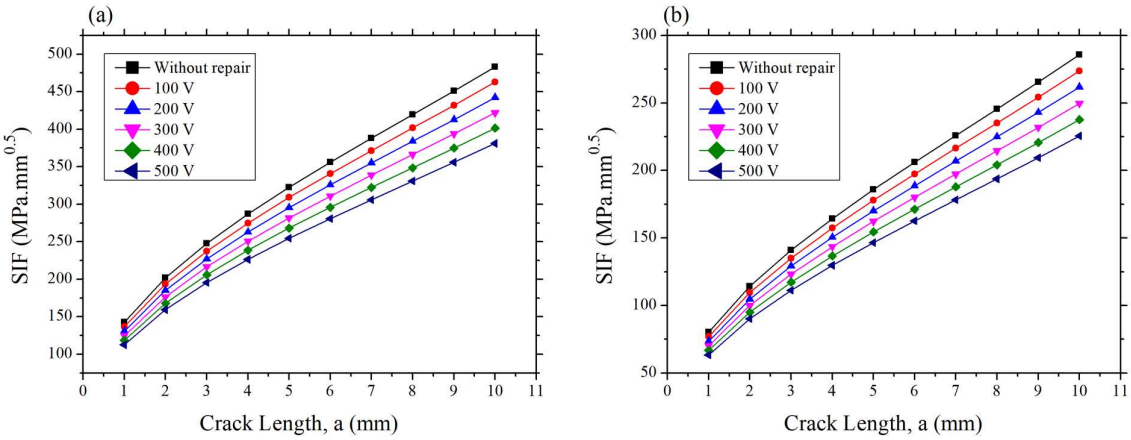

Figure 5.2: SIF variations concerning various crack lengths and repair voltages (a) $X/W = 0.5$ (b) $X/W = 0$

5.3.2 Influence of Piezoelectric Patch Thickness and Size

Figure 5.3 illustrates the variation of Stress Intensity Factors (SIFs) as a function of piezoelectric patch thickness (t_p) and applied repair voltage. This analysis was conducted for a fixed crack length ($a = 8\ mm$) and piezoelectric actuator dimensions of $W_p = 30$ mm and $H_p = 25$ mm, with patch thicknesses of 0.5 mm, 0.75 mm, and 1 mm. While the adhesive bonding of the piezoelectric patch enhances the overall stiffness of the structure, the passive stiffness contribution of the patch itself was not considered in this study. As expected, when no voltage is applied (0 V), the SIFs remain unaffected by the presence of the piezoelectric patch, indicating the absence of induced compressive stress. However, a significant influence is observed with the application of repair voltages. At a consistently applied voltage of 500 V, an increase in patch thickness from 0.5 mm to 1 mm resulted in a 5.8% increase in the total SIFs.

Conversely, the SIFs exhibited a linear decrease with increasing repair voltage across all patch thicknesses. Notably, at 500 V, the SIF reduction was 21.1% for a 0.5 mm patch, 18.5% for a 0.75 mm patch, and 16.5% for a 1 mm patch, observed across different geometric configurations ($X/W = 0.5$ and 0). This demonstrates the effectiveness of piezoelectric actuation in mitigating crack propagation, with thinner patches yielding a more pronounced reduction in SIFs under the same voltage.

These findings suggest that to minimize SIFs and enhance crack repair, employing thinner piezoelectric actuators with higher applied voltages is advantageous, even though thicker patches contribute to structural reinforcement. This can be attributed to the inverse relationship between the strain generated by the piezoelectric actuator and its thickness. Thinner patches produce excellent strain under the same applied voltage, resulting in a more significant compressive stress field at the crack tip and a more substantial reduction in SIFs.

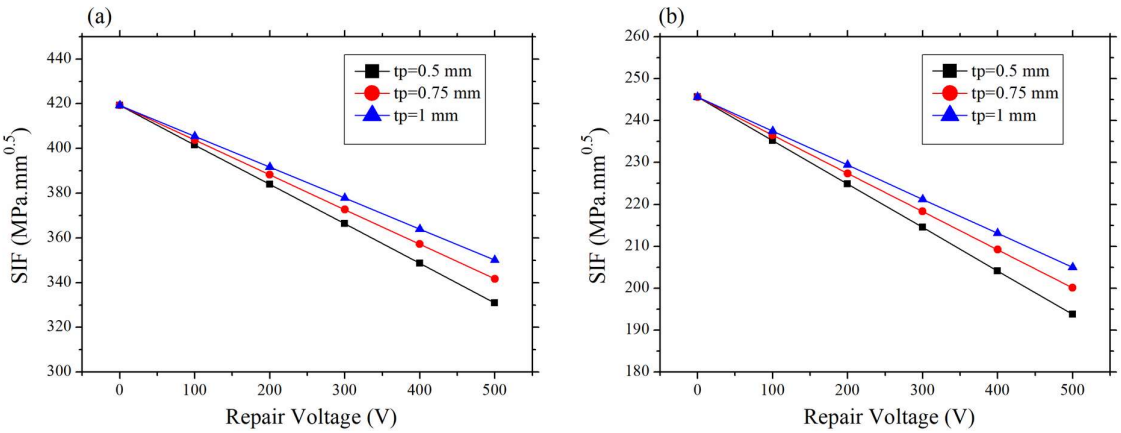

Figure 5.3: SIF variations for different piezoelectric actuator thicknesses under different repair voltages with crack length (a) of 8 mm (a) $X/W = 0.5$ (b) $X/W = 0$

The size of the piezoelectric patch, particularly its width, proved to be a critical factor in reducing SIFs, as patch geometry directly influences the compressive stress field near the crack tip. Figure 5.4 illustrates the SIF variations for patch widths (W_p) of 20, 25, and 30 mm, with constant height ($H_p = 25$ mm), crack length ($a = 8\ mm$), and thickness ($t_p = 0.5$ mm). Under a 500V application, SIF reductions were 21.1%, 15.35%, and 10.33% for widths 20, 25, and 30 mm, respectively, demonstrating an inverse relationship between patch width and SIF reduction. This highlights the efficacy of wider patches in mitigating stress concentration. This trend can be attributed to the expanded area over which compressive stress acts, facilitated by a larger patch. A wider compressive stress distribution effectively counteracts tensile stress, significantly reducing SIF. Additionally, the maximum possible electrode width, fundamentally

limited by patch width, allows for more uniform electric field application and resulting compressive stress. The investigation established that increased patch width significantly reduces SIFs, highlighting the importance of patch geometry for optimal repair performance. Careful consideration of patch width is essential for maximizing piezoelectric patch effectiveness in crack mitigation.

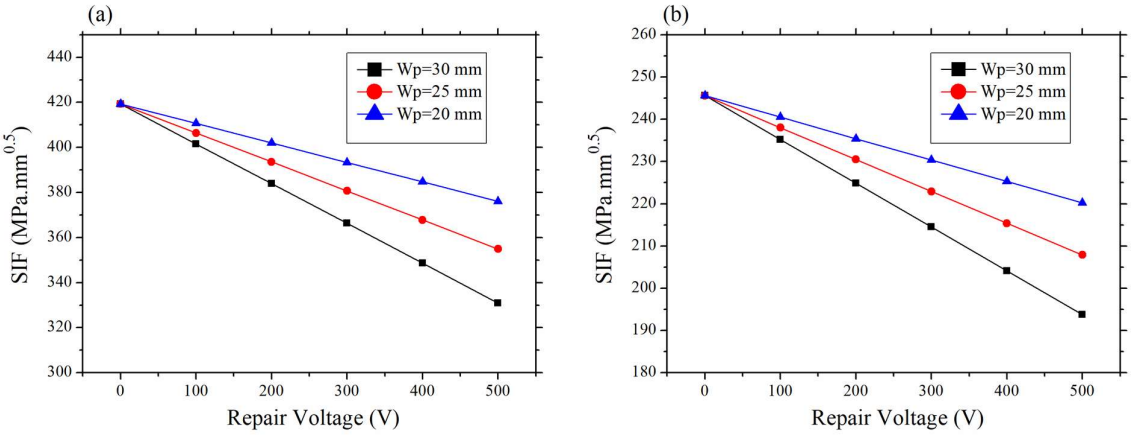

Figure 5.4: SIF variations for different piezoelectric actuators widths under different repair voltages with crack length, a=8 mm (a) $X/W = 0.5$ (b) $X/W = 0$

5.3.3 SIF Range, Fatigue Crack Growth, and Fatigue Life Analysis

The crack length continuously increases under cyclic tensile loading. The results were taken approximately within the Paris region. The final crack length (a_f) concerning the number of loading cycles (N) is represented in Figure 5.5 for the cracked specimen's different geometry, $(X/W = 0 \text{ and } 0.5)$ under various repair voltages. This illustration shows that the growth of cracks is slowed down as the repair voltage increases. This can be characterized by the patch's compressive stress, which lowers the effect of tensile stress at the fracture tip.

The above result was taken up to the critical crack length. (a_c), which is calculated when the $K_{max} = K_{IC}$ of the material, under plane stress conditions. The fatigue life under different repair voltages is shown in Figure 5.6a for the different geometry of the specimen. As the patch provides compressive stress at the crack's tip, more loading cycles are required to reach the critical crack length, achieving enhanced service life. The percentage of enhanced fatigue life is shown in Figure 5.6b for different geometries of the specimen. It is observed that a 124% higher fatigue life is obtained for $X/W = 0$, whereas a 130% enhanced fatigue life is obtained for $X/W = 0.5$ under the application of 500 V as compared to without repair conditions.

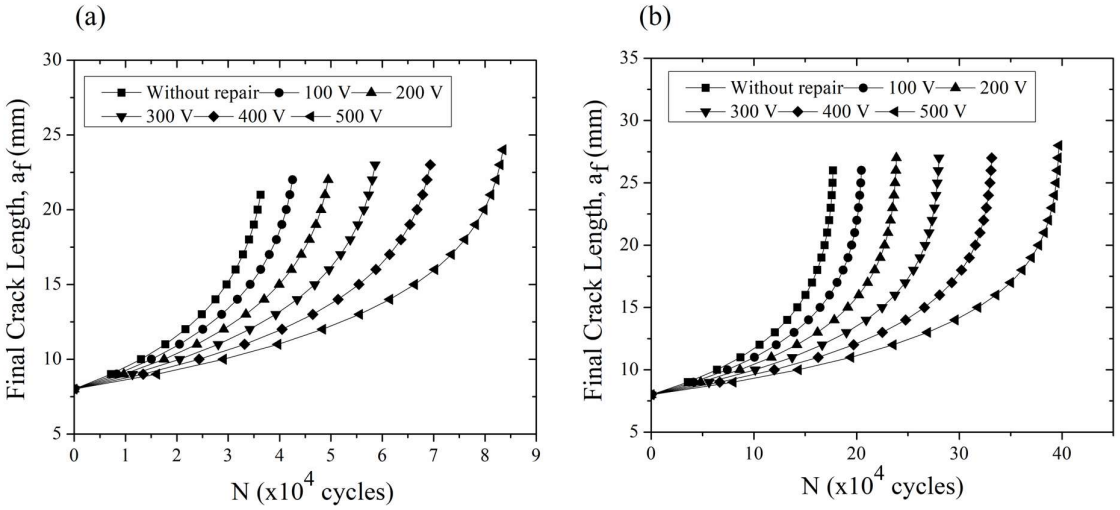

Figure 5.5: Final crack length (a_f) vs. number of loading cycles (N) for various repair voltage (a) $X/W = 0.5$ (b) $X/W = 0$

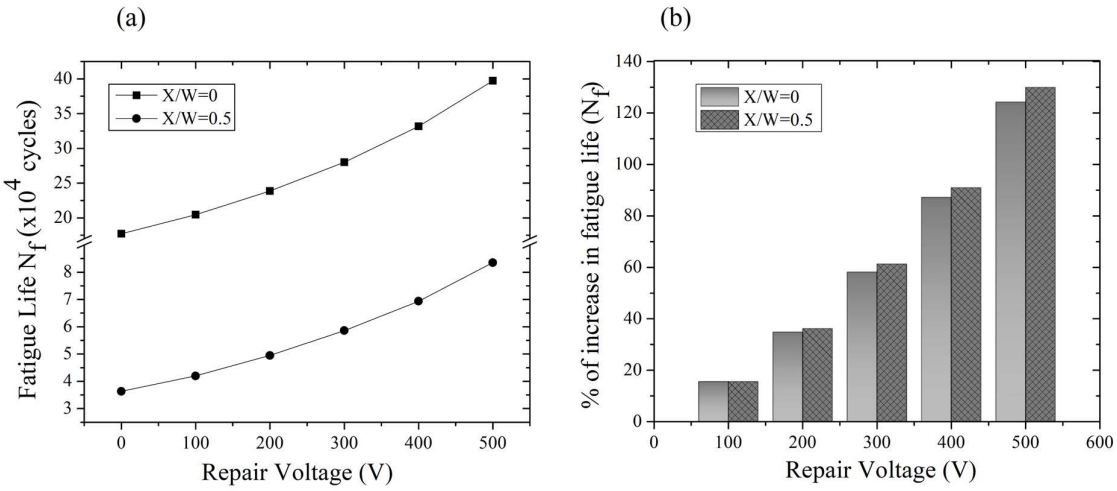

Figure 5.6: (a) Fatigue life variation (b) Percentage of fatigue life increase for different repair voltages.

Figure 5.7 illustrates how the SIF range (ΔK) varies for various repair voltages based on the number of cycles for different geometries. At 20,000 loading cycles, a 24.72% reduced SIF range is obtained under a repair voltage of 500 V compared to when no repair conditions were applied for $X/W = 0.5$. In contrast, a 35.49% reduced SIF range is found for $X/W = 0$ after 1,00,000 cycles under the same repair configuration. This is seen because the patch's actuation effect reduces the maximum SIF due to the maximum voltage application at maximum loading. In contrast, the zero-voltage application at minimum loading does not affect

the minimum SIF. As a result, the difference between the maximum and minimum SIFs is reduced.

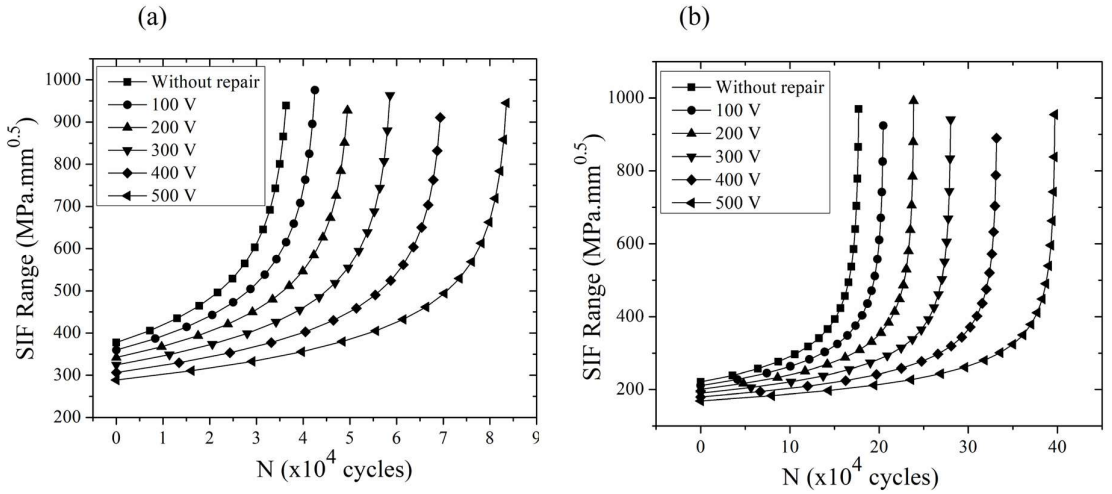

Figure 5.7: SIF range (ΔK) vs. number of loading cycles (N) under different repair voltages (a) X/W=0.5 (b) X/W=0

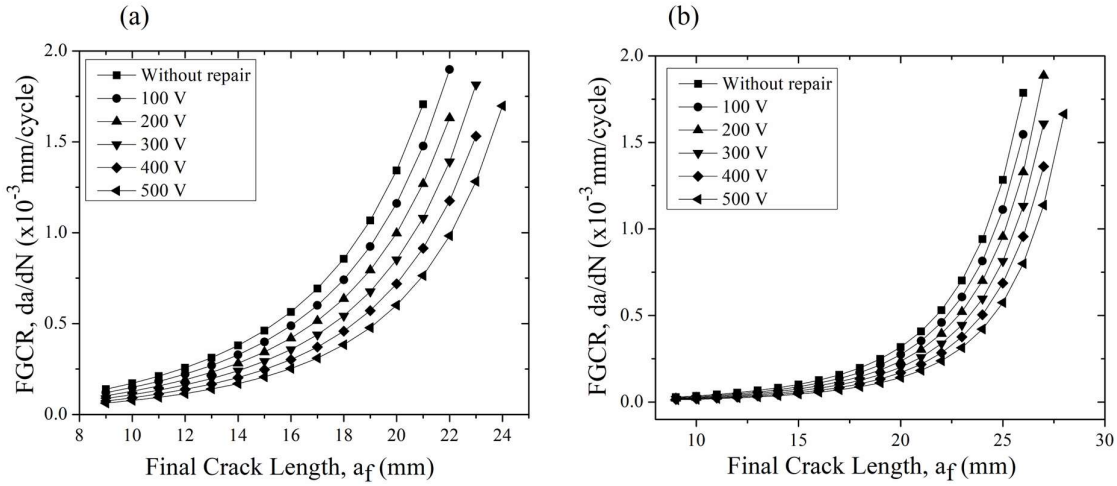

Figure 5.8: FCGR vs. Final crack length (a_f) (a) X/W=0.5 (b) X/W=0

The FCGR is prominently influenced by the SIF range, which drives the crack growth, which can be minimized by applying suitable voltages to the patch, as demonstrated in the previous discussion. Now, to comprehend the variation of FCGR concerning the final crack length (a_f), a study is conducted under different voltages for $X/W = 0.5$ and 0, as illustrated in Figure 5.8. It has been noted that crack growth rates are delayed at higher repair voltages for both configurations. In the scenario where $X/W = 0.5$, a similar rate of increase in FCGR is observed starting from the initial crack length. However, a significant rise in FCGR occurs after

the crack length reaches 20 mm, especially when *X/W = 0* is chosen. It is worth noting that when a higher repair voltage is utilized, a delayed crack growth rate is observed.

In addition, Figure 5.9a illustrates the FCGR about different repair voltages once the crack length reaches 15 mm. The FCGR values are 1.02×10^{-4} and 4.56×10^{-5} mm/cycle for $X/W = 0.5$, while for $X/W = 0$, the values are 4.62×10^{-4} and 2.07×10^{-4} mm/cycle under without repair and with a voltage application of 500 V, respectively. Figure 5.9b illustrates the reduction in FCGR percentage when various repair voltages are applied once the crack length reaches 15 mm for both geometries. The application of repair voltages of 100, 200, 300, 400, and 500 V results in a decrease in FCGR by approximately 13%, 25%, 36%, 46%, and 55%, respectively, at any final crack length $(a_f \leq a_c)$ as compared to the case without any repair.

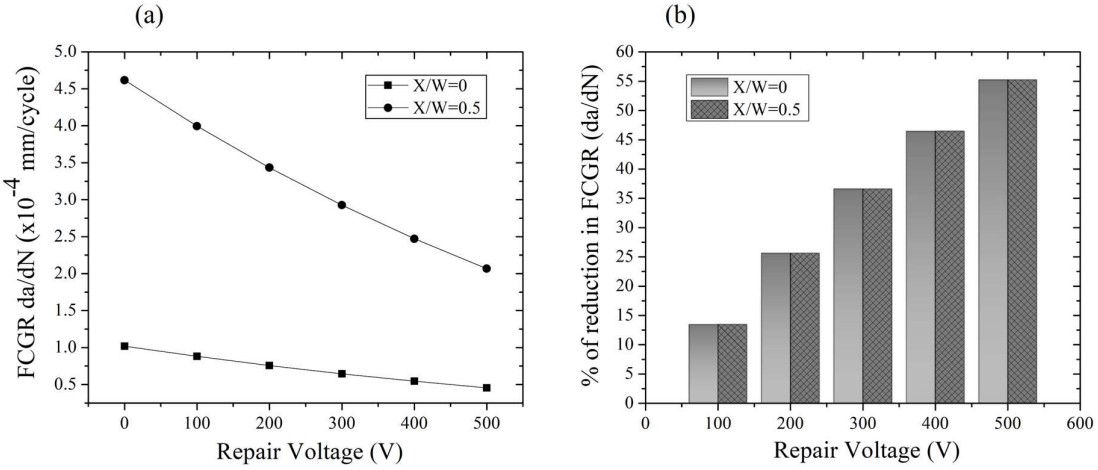

Figure 5.9: (a) FCGR (b) Percentage of FCGR reduction for different repair voltages for crack length 15 mm

Furthermore, the FCGR is depicted in the number of loading cycles at different repair voltages, as illustrated in Figure 5.10. Initially, the growth is relatively consistent across all repair scenarios. However, a noticeable increase is observed after a specific range for all configurations. In the case of $X/W = 0.5$, substantial growth occurs after 20,000 cycles without external voltages. Conversely, this severe growth is observed after 70,000 cycles under 500 V, as depicted in Figure 5.10a. For $X/W = 0$, significant growth is observed after 1,50,000 cycles in the case of a 0 V application. On the other hand, this severe growth is seen after 3,50,000 cycles under 500 V, as shown in Figure 5.10b.

Figure 5.11 illustrates the FCGR concerning the SIF range for different repair voltages and the without repair case for both the specimen geometry, i.e., $X/W = 0.5$ and 0. As the

SIF range drives the propagation of the crack and the Paris model is adopted to predict the FCGR, it is evident that for the exact value of the SIF range, Eq. (5.15) would provide the same results and an almost undistinguishable curve for all the repair cases. In the case of $X/W = 0.5$, the SIF range was initially relatively high compared to when $X/W = 0$. Due to this fact, lower FCGR is found at the beginning of the loading cycles in the case of $X/W = 0$, as represented in Figure 5.11b, whereas the crack grows at a higher rate at the start of the loading cycles, as shown in Figure 5.11a.

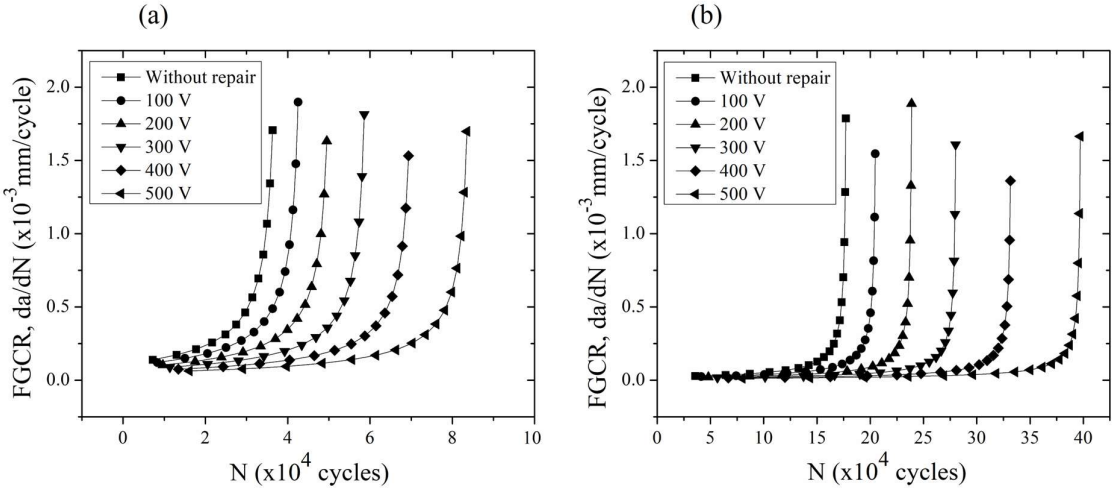

Figure 5.10: FCGR vs. number of loading cycles (N) (a) $X/W = 0.5$ (b) $X/W = 0$

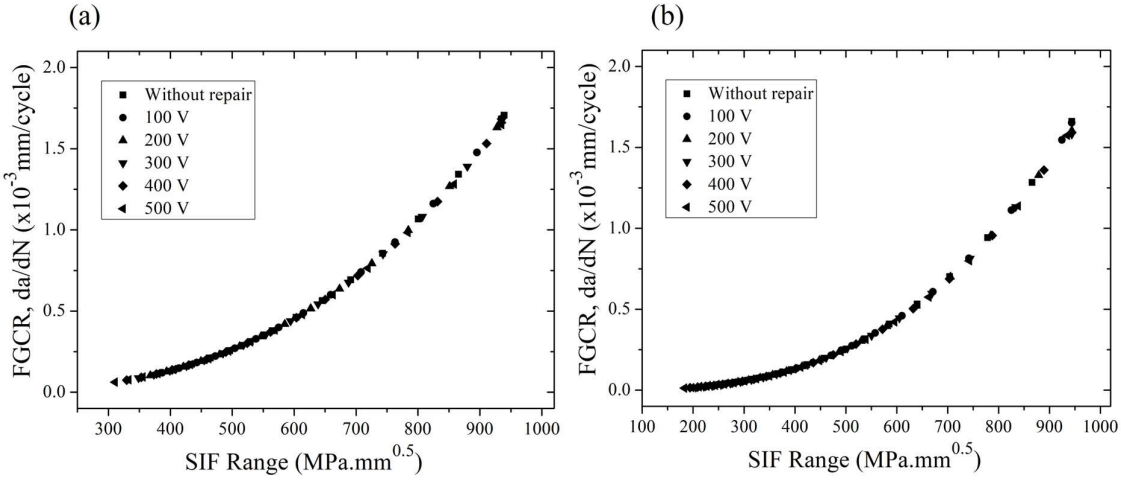

Figure 5.11: FCGR vs. SIF range (ΔK) (a) $X/W = 0.5$ (b) $X/W = 0$

Moreover, an investigation has been carried out to more thoroughly understand the FCGR at the end of the half fatigue life cycle $(N/N_f = 0.5)$, when interpreting fatigue life within the context of that specific repair configuration. Figure 5.12 illustrates the fluctuation of

FCGR concerning repair voltages for $N/N_f = 0.5$. It is evident that when the structural component reaches half of its service life, a significantly reduced FCGR is found under 500 V, compared to the conditions without any repair. Hence, the above findings indicate that the application of voltage to the piezoelectric patch effectively retards crack growth and proves highly successful in repairing damaged structures, thereby extending their service life.

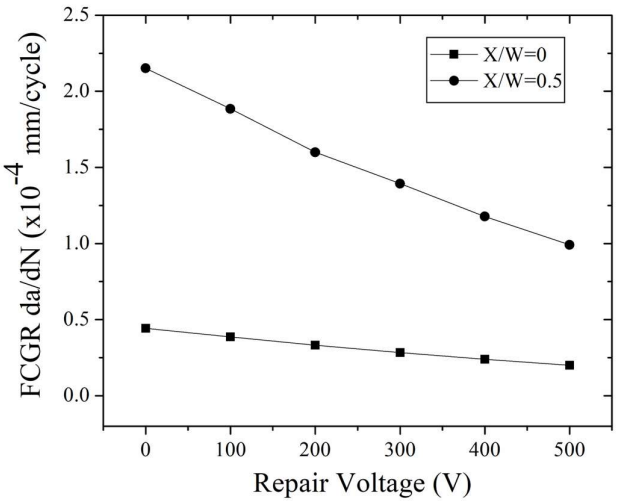

Figure 5.12: FCGR for various repair voltages at half of its fatigue life cycle $(N/N_f = 0.5)$

5.4. Summary

This chapter investigated the feasibility and effectiveness of adhesively bonded piezoelectric actuators to repair edge-cracked arc-shaped specimens under static and fatigue loading conditions. The primary objectives were to determine the Mode-I stress intensity factor (SIF) analytically and fatigue crack growth rate (FCGR), and to demonstrate the reduction of these parameters through the application of external voltage to the piezoelectric patches, thereby extending the specimen's service life. The methodology employed linear elastic fracture mechanics (LEFM), including the superposition principle and the weight function method (WFM), to model the crack behavior and the actuator's effect. The Paris model was used to predict FCGR under cyclic loading. The findings from the static repair revealed a significant reduction in the Mode-I SIF upon applying voltage to the piezoelectric actuators. This reduction was attributed to the compressive stress generated by the actuators near the crack tip, effectively counteracting the tensile stress induced by the external load. The Parametric analysis underscores optimizing actuator dimensions and applied voltage for maximum repair performance. Firstly, increasing the applied voltage directly correlated with a more significant reduction in SIF. Thinner piezoelectric patches with higher applied voltages yielded the most

substantial SIF reductions. This is due to the strain produced inversely with patch thickness. Thirdly, a larger width of the piezoelectric patch significantly enhanced repair performance. Moreover, it was observed that the SIF increased with crack length, requiring higher voltages for effective repair at longer crack lengths. The findings from the fatigue repair demonstrated a notable decrease in FCGR and a substantial increase in fatigue life with the application of external voltage. The piezoelectric actuators delayed crack growth by compressing stress at the crack tip, requiring more loading cycles to reach the critical crack length. Notably, a significant enhancement in fatigue life was observed, with 1.3 times rise achieved under a 500V repair voltage compared to the without repair condition. The SIF range (ΔK) was also reduced, indicating a decrease in the driving force for crack propagation. Furthermore, higher repair voltages consistently resulted in delayed crack growth rates and a substantial reduction in FCGR at various stages of the fatigue life. This study provided a comprehensive understanding of the potential of piezoelectric actuators in the active repair of edge-cracked arc-shaped specimens, contributing to the development of more reliable and durable engineering structures.

Chapter 6

STRENGTHENING OF AN EDGE-CRACKED PLATE UNDER BENDING USING PIEZOELECTRIC ACTUATORS

6.1 Introduction

Plates are fundamental structural elements extensively used in aerospace, automotive, and civil engineering applications due to their high strength-to-weight ratio and ability to withstand various loading conditions. In many practical scenarios, plates are subjected to bending loads, making them susceptible to stress concentrations and potential failure. In practical applications, these plates are susceptible to crack initiation under bending-induced stress due to factors like fatigue, manufacturing defects, or impact loads, which can significantly reduce their load-carrying capacity. If left unaddressed, these cracks can reduce load-bearing capacity, cause excessive vibrations, and, in extreme cases, catastrophic failure. Consequently, repairing cracks in structural plates is crucial to maintaining their integrity and extending their service life. Several crack repair techniques have been developed, including composite and metallic patching, stop-hole drilling, and hybrid approaches that combine fiber-reinforced polymer (FRP) patches with other methods. While these methods effectively delay crack propagation, their efficiency in cases involving bending loads remains limited due to the complex stress distributions involved.

The literature survey in Chapter 1 indicates various studies on repairing cracked plates using piezoelectric patches under different loading conditions, such as tensile, shear, and dynamic loads. Researchers have successfully applied piezoelectric actuators to mitigate crack propagation and reduce stress intensity factors (SIF) in center-cracked, edge-cracked, and delaminated plates. These studies highlight the advantages of piezoelectric patches in actively controlling stress fields through applied voltage, thereby enhancing structural integrity. Experimental and numerical investigations have demonstrated the effectiveness of piezoelectric patches in extending fatigue life and improving the mechanical response of cracked components. However, despite these advancements, research on repairing cracks in plates subjected to bending loads has received relatively less attention. The unique stress distribution in bending scenarios requires a specific approach, which remains an unexplored domain in current literature. Addressing this gap can overlay the method for novel active repair techniques

tailored for bending-dominated structural applications.

This chapter aims to mitigate the severity of cracks in bending plates by using the actuation capabilities of piezoelectric patches. To achieve this, the research employs a novel approach where two piezoelectric patches with identical polarities are strategically positioned above the shifted neutral axis of the plate. This configuration induces an extensional strain within the plate above the neutral axis, generating a counteracting negative bending moment that balances the externally applied bending load. Stress Intensity Factors (SIFs) are determined using Tada's formula [Tada et al. (2000)], which is based on Linear Elastic Fracture Mechanics (LEFM). The superposition principle is then used to find the net SIF. This is done by adding the SIFs of the cracked plate under the initial bending load to the SIFs that come only from the piezoelectric actuation. This methodology predicts a reduction in the overall SIF, indicating a decrease in crack severity. To validate the efficacy of this proposed approach, the findings are rigorously compared with Finite Element (FE) simulations conducted using the ABAQUS software package. This comparative analysis serves to enhance the reliability of the developed model.

6.2 Problem Formulation

This investigation focuses on the critical estimation of the Stress Intensity Factor (SIF) within a static loading regime, explicitly focusing on active repair scenarios. This emphasis arises from the pivotal role of SIF reduction in determining the efficacy of any potential repair strategies. A three-point bending plate featuring an edge crack of length 'a' is analyzed. The plate is subjected to a load 'P' applied along the direction of the crack, as illustrated in Figure 6.1. The crack propagation occurs in the y-direction, while the applied load 'P' acts in the same direction. This loading configuration induces a bending stress perpendicular to the crack length, or in the x-direction, with the plate thickness oriented in the z-direction.

6.2.1 SIF Estimation for the Cracked Specimen

Only Mode-I Stress Intensity Factors (SIFs) were deemed significant for the present analysis. The Mode-I SIF for an edge-cracked plate with unit thickness under bending loading was determined through Linear Elastic Fracture Mechanics (LEFM) principles. Based on the established formulation by Tada et al. (2000), this calculation is presented in Eq. (6.1).

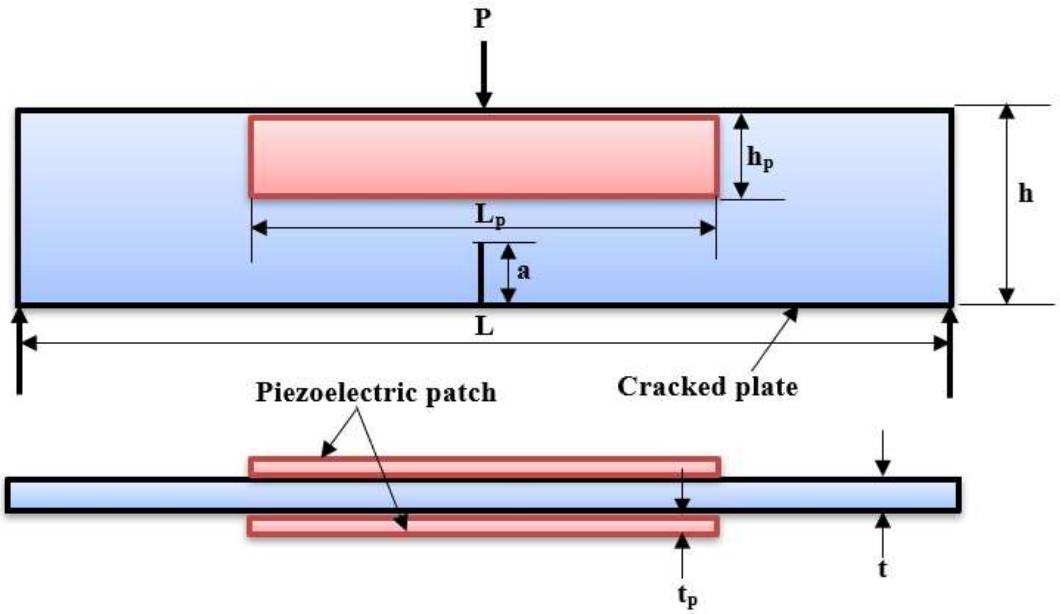

Figure 6.1: Schematic diagram of the cracked plate repaired with piezoelectric actuators

$$K_I = \sigma\sqrt{\pi a}\, F\left(\frac{a}{h}\right) \tag{6.1}$$

where,

$$\sigma = \frac{6M}{h^2},\ M = \frac{PL}{4} \tag{6.2}$$

Where L, h, and t are the specimen's length, height, and thickness, respectively.

Here, to address the influence of the cracked specimen's geometry on the fracture parameters, a shape correction factor, denoted as $F\left(\frac{a}{h}\right)$, is incorporated into the analysis. This factor, crucial for accurate fracture parameter determination, is formulated following the approach proposed by Tada et al. (2000).

For $\frac{L}{h} = 4$,

$$F\left(\frac{a}{h}\right) = \frac{1.99 - \frac{a}{h}\left(1-\frac{a}{h}\right)\left[2.15 - 3.93\frac{a}{h} + 2.7\left(\frac{a}{h}\right)^2\right]}{\sqrt{\pi}\left(1+2\frac{a}{h}\right)\left(1-\frac{a}{h}\right)^{1.5}} \tag{6.3}$$

For $\frac{L}{h} = 8$,

$$F\left(\frac{a}{h}\right) = 1.106 - 1.552\frac{a}{h} + 7.71\left(\frac{a}{h}\right)^2 - 13.53\left(\frac{a}{h}\right)^3 + 14.23\left(\frac{a}{h}\right)^4 \tag{6.4}$$

6.2.2 SIF Reduction via Active Repair

To effectively repair a cracked plate, it is imperative to mitigate the net stress concentration at the crack tip. This study investigates a novel approach utilizing piezoelectric patches to counteract the detrimental moment induced by external loading. As illustrated in Figure 6.1, two piezoelectric patches are strategically positioned symmetrically on the opposing surfaces of the plate, precisely above the neutral axis. Assuming a consistent polarity across the longitudinal axis of both patches and a polarization direction perpendicular to this axis, applying an electrical voltage to these patches generates a resultant axial force [Maleki and Mohammadi (2017)].

The piezoelectric patch employed in this investigation exhibits polarization along its thickness (axis 3). Consequently, the dominant piezoelectric effect considered is d_{31}. This signifies that when a voltage is applied along the thickness direction (axis 3), the patch experiences strain perpendicular to its thickness, specifically along axis 1, which aligns with the direction perpendicular to the crack within the specimen. Assuming a state of perfect adhesion between the piezoelectric patch and the cracked component, the mathematical expression describing the tensile force generated can be formulated as follows [Crawley and Luis (1987)],

$$F_P = \frac{E_s t_s T}{(\psi+\alpha)} \cdot \frac{d_{31} V}{t_p} \tag{6.5}$$

where,

$$\psi = E_s W_s t_s / E_p W_p t_p \tag{6.6}$$

In the above expression, E_s represents Young's modulus of the cracked plate while E_p, W_p, and t_p denotes Young's modulus, width, and thickness of the integrated piezoelectric patch. The parameter T characterizes the width of the distributed electrodes on the piezoelectric patch. The effective cross-sectional area of the specimen is denoted by A and d_{31} signifies the piezoelectric strain coefficient. The applied voltage is represented by V, with the coefficient α As established in previous research, assuming a value of $\alpha = 6$ for extensional loading conditions [Crawley and Luis (1987)].

This specific configuration would result in the induction of a localized bending moment within the plate, which can be mathematically expressed as follows:

$$M_a = -2 \cdot F_P \cdot \left(\frac{h-h_p}{2}\right) \tag{6.7}$$

When the patch length is less than the plate dimensions, the applied electrical stimulus induces a localized stress field within the plate. This localized stress manifests as either a tensile or compressive axial load depending on the polarity (positive or negative) or the direction of the applied voltage [Maleki and Mohammadi (2017)]. The SIF existing under the piezoelectric actuation effect, K_{Piezo}, can be written as,

$$K_{Piezo} = \sigma_p \sqrt{\pi a}\, F\left(\frac{a}{h}\right) \tag{6.8}$$

where,

$$\sigma_p = \frac{6M_a}{h^2} \tag{6.9}$$

The superposition principle of LEFM was employed to determine the piezoelectric patch-integrated, cracked specimen's stress intensity factor (SIF). This involved analyzing two distinct scenarios to subsequently calculate the overall SIF (K_A) after repair. The mathematical expression for K_A can be formulated as follows,

$$K_A = K_I + K_{Piezo} \tag{6.10}$$

The SIF denoted by K_{Piezo}, is uniquely attributable to the induced stresses generated by the piezoelectric actuation mechanism. This particular SIF term emerges solely due to the internal stresses developed within the material due to the applied electric field across the piezoelectric layers, with no influence from other sources of mechanical loading or external forces.

6.3 Finite Element (FE) Modelling and Validation

A finite element (FE) model was developed using ABAQUS to validate the analytical results of piezoelectric-actuator-based crack repair of a bottom edge cracked plate under bending. The model comprised a plate and two piezoelectric patches, represented as deformable bodies, with their dimensions and material properties specified in Tables 6.1 and 6.2. The plate was partitioned to include a seam crack along its bottom edge at the mid-plane, reflecting the crack geometry. The piezoelectric patches were assigned local material orientations by creating a datum, with axis '3' aligned with the patch thickness, representing the polarization direction. This orientation is crucial for accurately representing how electricity affects the patch material in the ABAQUS software. The plate was modeled using '3D stress' elements, while the piezoelectric patches were represented by 'piezoelectric elements'. The piezoelectric patches were bonded to the cracked plate using tie constraints defined in the interaction module,

ensuring a seamless transfer of forces and moments. Figure 6.2 visually depicts the assembled 3D model, showcasing the integrated piezoelectric patches. A three-point bending load was applied to the top edge of the plate along the cracked surface. The actuation of the piezoelectric patches was modeled by applying electrical boundary conditions: one face of each patch, bonded to the plate, was provided with zero voltage, while the opposite face was assigned a finite voltage to induce extensional strain. This configuration created a counteracting moment at the crack tip, reducing the stress intensity factor (SIF). The SIF is determined by evaluating the J-integral [Weißgraeber et al. (2016)]. This integral is computed along a closed path encircling the crack tip, measuring the energy release rate associated with crack growth.

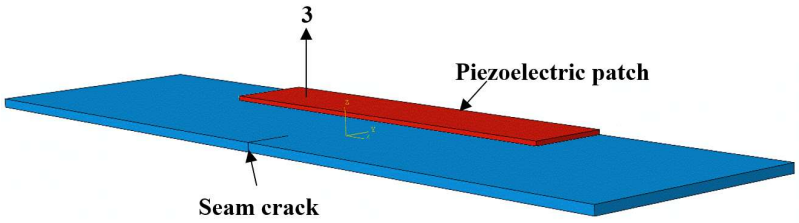

Figure 6.2: Piezoelectric patch assembly on a cracked plate modeled in ABAQUS

Table 6.1: Geometric parameters of repaired configurations (Figure 6.1)

Dimensions	Al 2024-T3	PZT-5H
Height (mm)	h=25	h_p=10
Length (mm)	L=100	L_p=50
Thickness (mm)	t=1	t_p=0.25, 0.5, 0.75 and 1

Table 6.2: Mechanical properties of Al 2024-T3 plate material

Elastic Modulus (E) (GPa)	Poisson's ratio (v)	Tensile yield strength (MPa)	Ultimate tensile strength (MPa)	Density Kg/m^3
74	0.33	345	483	2780

6.3.1 Validation of the Cracked Plate Model

To validate the finite element (FE) model, the study focused exclusively on cracked plates subjected to bending loads. Stress Intensity Factors (SIFs) were determined for crack lengths of 3 mm, 4 mm, and 5 mm, applying a 100 N load in each case. The SIF values obtained from the FE analysis were rigorously compared with those predicted by well-established analytical solutions presented in Tada et al. (2000). Figure 6.3 depicts the deformed configuration of the

plate with a 5 mm crack. A comparative summary of the SIF values obtained from both analytical and FE methods is presented in Table 6.3, demonstrating excellent agreement and validating the accuracy of the present FE model.

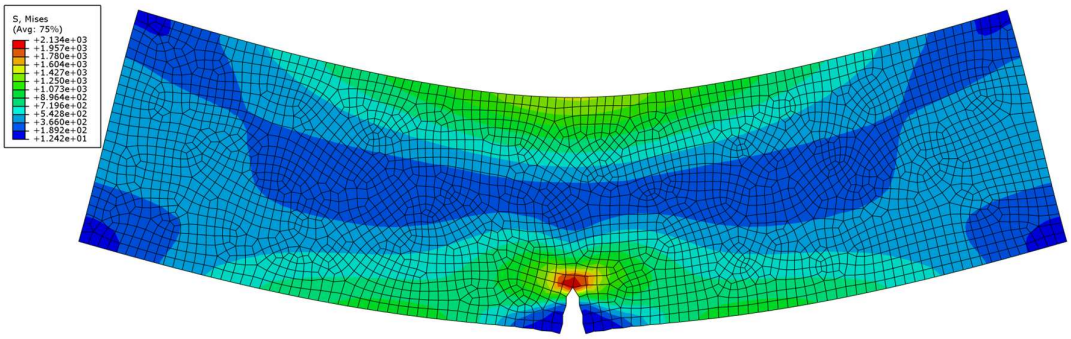

Figure 6.3: Deformed cracked plate model (crack length: 5 mm)

Table 6.3: Comparison of FE and Analytical results for a cracked plate

Crack length	**SIF (MPa.mm$^{0.5}$)**	
(mm)	**Present FE**	**Analytical** [Tada et al. (2000)]
3	71.25	73.45
4	82.22	83.9
5	91.64	93.99

6.3.2 Validation of the Repaired Plate Model

This study investigates a method to reduce the severity of cracks in structures. Piezoelectric patches are attached to the structure and activated with an external electrical voltage. To assess the effectiveness of this method, the results from the present analytical model are compared with those obtained from finite element (FE) simulations. An external voltage of 200 volts is applied to the piezoelectric patches. The plate is then subjected to a load of 100 N, and the analysis is performed for different crack lengths. The Stress Intensity Factor (SIF), a measure of the stress concentration at the crack tip, is calculated. Figure 6.4a illustrates the overall deformation of the structure while Figure 6.4b provides a magnified view of the region around the crack tip. The results show a significant reduction in stress at the crack tip compared to the case without the piezoelectric patches, as evident in Figure 6.3. Table 6.4 presents the SIF values obtained from the analytical model and the FE simulations. The FE simulation results closely match the predictions of the analytical model, demonstrating the accuracy of the present analytical model and the effectiveness of piezoelectric-based crack repair. These

findings emphasize the value of combining FE analysis with analytical methods for validating structural repair techniques.

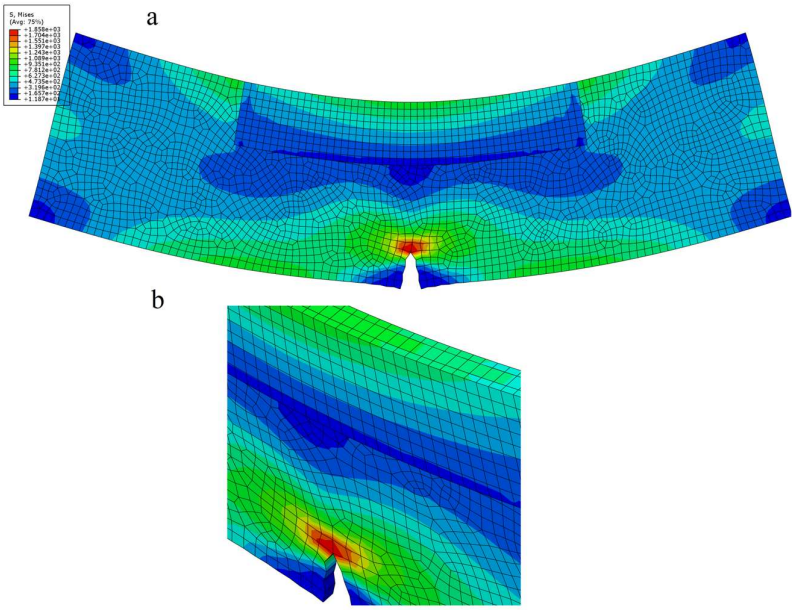

Figure 6.4: Deformed model of cracked plate repaired with piezoelectric actuators with 200 V (a) front view (b) enlarged view of the cracked region

Table 6.4: Comparison of FE and Analytical results for a repaired plate under a repair voltage of 200 V

Crack length (mm)	SIF (MPa.mm$^{0.5}$)	
	Analytical	**Present FE**
3	52.65	48.44
4	83.9	77.86
5	77.79	71.41

6.4 Results and Discussion

The finite element (FE) analysis results presented in the previous section demonstrated strong agreement with the predictions of the analytical model. Building upon this validation, this section investigates the impact of various key parameters on the stress intensity factors (SIFs) at the crack tip. These parameters include the applied repair voltage, crack length, and patch thickness. A three-point bending test was conducted on a specimen subjected to a 100 N load, as illustrated in Figure 6.1. The material and geometric properties of the specimen are detailed in Tables 6.1 and 6.2. The SIFs were computed for a fixed crack length of 5 mm and

patch thickness of 0.5 mm, while systematically varying the repair voltage. A reference case was also included in the analysis. This case did not have any repair voltage applied. The purpose of this reference case was to evaluate the effectiveness of the repair techniques. The study considered piezoelectric patches with 0.25 mm, 0.5 mm, 0.75 mm, and 1 mm thicknesses. To ensure optimal performance, the maximum electric field applied to the patches was limited to 1 kV/mm. For the 0.25 mm thick patch, the maximum applicable voltage was calculated to be 250 V. To maintain a safe operating margin, a maximum voltage of 200 V was selected for the present analysis.

6.4.1 Comparison of Repaired and Unrepaired Specimens

Figure 6.5 demonstrates a significant decrease in stress intensity factors (SIFs) following repair. This decrease becomes more pronounced as the repair voltage increases. This improvement is attributed to the enhanced actuation of the patch, which becomes more effective with higher voltages. This actuation generates a counteracting moment at the crack plane. This counteracting moment opposes the applied bending moment, reducing the crack tip's effective stress. Specifically, 5.37%, 10.74%, 16.11%, and 21.48% SIF reductions were observed for repair voltages of 50 V, 100 V, 150 V, and 200 V, respectively. These results indicate that higher repair voltages lead to more effective crack closure due to stronger patch actuation. This finding emphasizes the importance of voltage-controlled actuation in mitigating the net stress at the crack tip. This behavior highlights the critical role of selecting appropriate repair voltages in optimizing mechanical performance and extending the service life of damaged components.

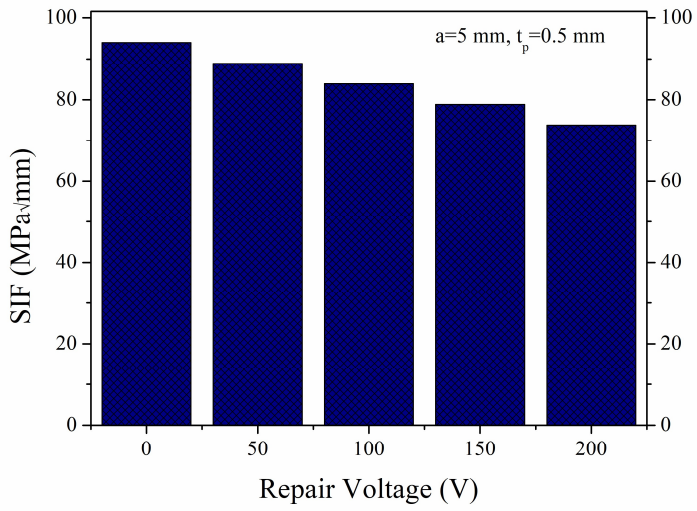

Figure 6.5: Comparison of SIFs with and without repair configurations

6.4.2 Influence of Patch Thickness

The selection of piezoelectric patch thickness significantly influences repair efficacy. This is attributed to the interplay between the patch's stiffness and its piezoelectric strain. Figure 6.6 illustrates the impact of varying repair voltages (0-200 V) on the stress intensity factor (SIF) for different crack lengths. The results demonstrate that thinner actuators generally exhibit superior SIF reduction. For instance, a 200 V application resulted in SIF reductions of 30.01%, 21.48%, 8.36%, and 6.84% for a 5 mm crack, respectively. It is crucial to note that each patch's maximum allowable electric field limits its performance. This field is defined as the applied voltage per unit patch thickness. For example, at an electric field of 0.2 kV/mm, SIF reductions were 10.74% for a 0.5 mm patch and 7.97% for a 1 mm patch. Conversely, at 0.4 kV/mm, the reductions were 15.01% for a 0.25 mm patch and 21.48% for a 0.5 mm patch. While thinner patches generally provide better SIF reduction under fixed voltage conditions (e.g., 15.01% for a 0.25 mm patch at 100 V compared to 6.84% for a 1 mm patch at 100 V), thicker patches can achieve significantly higher repair effectiveness due to their ability to withstand greater maximum voltages.

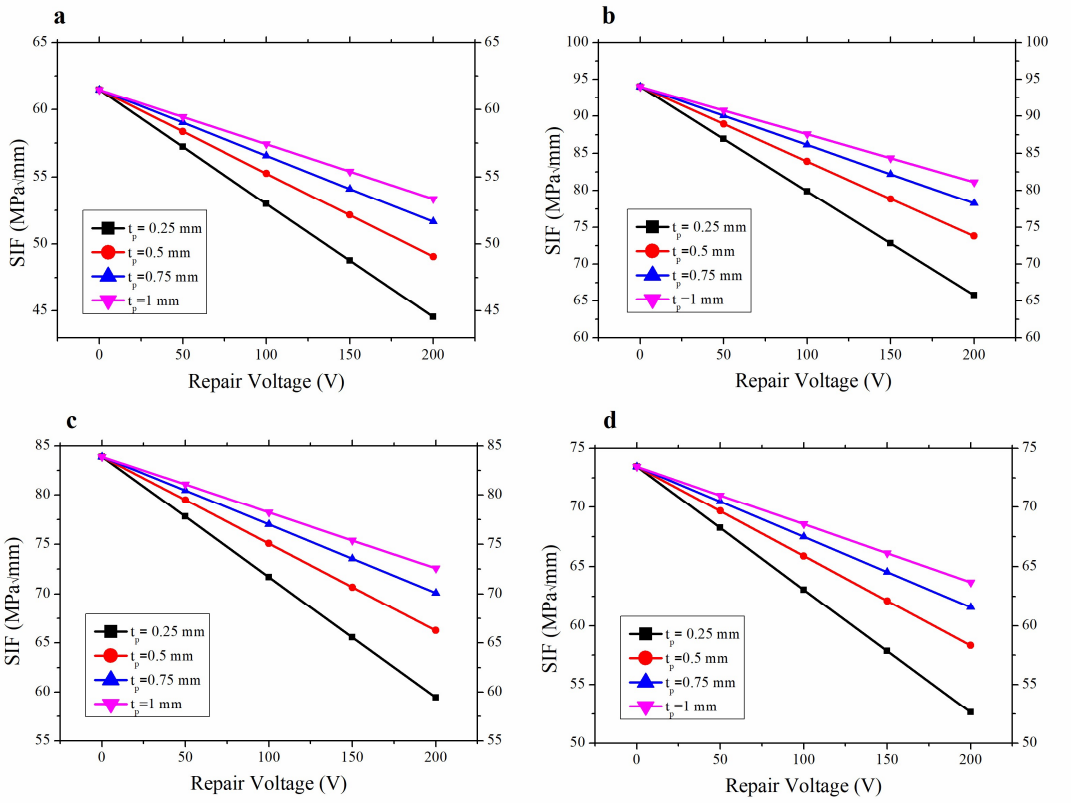

Figure 6.6: SIF vs. repair voltages concerning various patch thicknesses for crack lengths (a) a=2 mm (b) a=3 mm (c) a=4 mm (d) a=5 mm

Thinner piezoelectric patches (e.g., 0.25 mm), such as those with a thickness of 0.25 mm, exhibit effective actuation under limited voltage and low mechanical loading conditions. However, their ability to repair damage diminishes significantly when subjected to higher external mechanical loads. In contrast, thicker patches, for example, those with a thickness of 1 mm, demonstrate superior damage repair capabilities. This is evident in their ability to significantly reduce stress intensity factors (SIFs), which is crucial for preventing crack propagation. Thinner patches face practical limitations. Their reduced thickness can lead to mechanical failure under increased loading. Furthermore, they are more susceptible to dielectric breakdown due to higher electric field intensities at the same applied voltage. These factors limit their effectiveness under demanding mechanical conditions. Thicker patches, such as the 1 mm variant, offer improved repair performance due to their higher stiffness ratio, which enhances their ability to counteract applied loads. They also exhibit greater robustness against mechanical failure. The selection of an optimal patch thickness involved carefully considering several critical factors. These factors included the device's performance, durability under operational conditions, and the maximum allowable voltage across the patch. After thoroughly analyzing these factors, a patch thickness of 0.5 mm was identified as the most suitable for subsequent investigations. This choice represents a balanced compromise that ensures acceptable levels of performance and durability while remaining within the constraints imposed by voltage limitations.

6.4.3 Influence of Crack Length

The influence of crack length on repair effectiveness was investigated by analyzing cracks ranging from 2 mm to 6 mm long, utilizing a 0.5 mm thick patch. Figure 6.7a demonstrates the variation of the stress intensity factor (SIF) concerning the crack length, considering various repair voltages. As anticipated, the SIF increased with increasing crack length. This is attributed to the amplified stress concentration at the crack tip for longer cracks. However, this analysis primarily evaluates the repair performance of the patch within the specified configuration. Figure 6.7b illustrates the significant reduction in SIF achieved through the repair process across all crack lengths. The percentage reduction in SIF is presented for repair voltages of 50 V, 100 V, 150 V, and 200 V. A noteworthy observation is that the SIF reduction is more substantial for longer cracks at a constant repair voltage. For instance, at a repair voltage of 200 V, the SIF reduction was 23.33% for a 2 mm crack, while a 6 mm crack exhibited a more pronounced decrease of 26.67% compared to the without repair condition. This enhanced stress mitigation at the crack tip for longer cracks can be attributed to two factors.

Firstly, the increased force concentration at the crack tip for longer cracks leads to a more significant stress reduction. Secondly, the smaller cross-sectional area at the cracked section for longer cracks amplifies the patch's ability to reduce stress, thereby improving overall repair performance effectively.

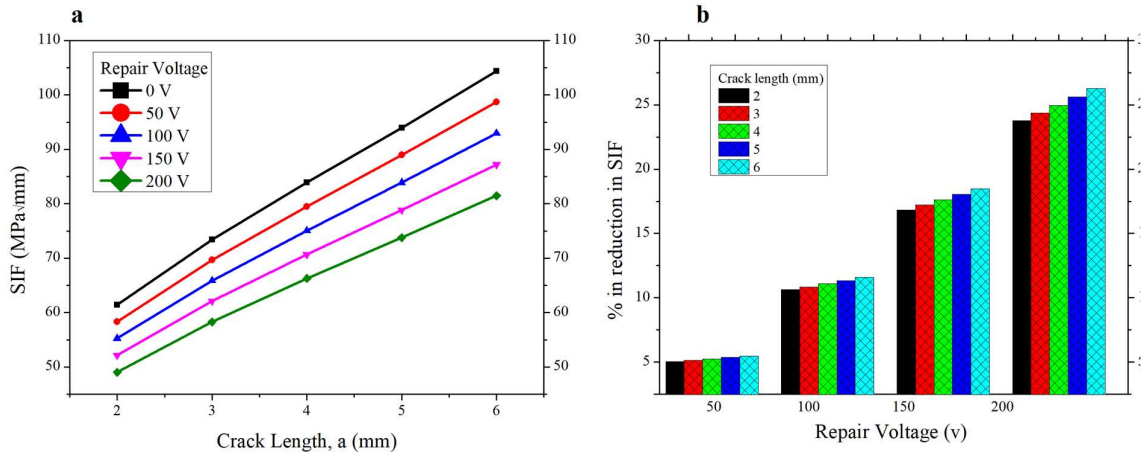

Figure 6.7: (a) SIF vs. crack length for various repair voltages (b) percentage of reduction in SIF for various crack lengths and repair voltages

6.5 Summary

This chapter explored an innovative repair methodology that leverages the electromechanical coupling properties of piezoelectric actuators to actively mitigate crack severity in bending-loaded plates. By strategically placing piezoelectric patches on the cracked plate and applying a controlled external voltage, the proposed approach generates a counteracting moment to reduce the stress intensity at the crack tip, thereby enhancing structural durability and delaying failure. The methodology employed in this study is grounded in Linear Elastic Fracture Mechanics (LEFM) principles, particularly the evaluation of Stress Intensity Factors (SIFs) to quantify crack severity. The repair mechanism is designed to place two piezoelectric patches with identical polarities above the cracked plate's shifted neutral axis, inducing extensional strain and generating a negative bending moment that counterbalances the applied load. The analytical model incorporates Tada's formula to compute SIFs and applies the superposition principle to determine the net SIF after repair. Finite Element (FE) simulations were conducted using ABAQUS to validate the analytical findings, allowing for a comparative analysis of theoretical and numerical results. The study investigated the effects of key parameters, such as crack length, patch thickness, and applied voltage, to assess the efficacy of piezoelectric repair. Notably, a significant reduction in SIF was observed. These findings

indicate that thinner patches perform efficiently under lower voltage applications, whereas thicker patches are better suited for higher load scenarios. The results confirm that piezoelectric patches can be effectively utilized to repair cracked plates under bending loads, extending the lifespan of structural components and reducing maintenance costs. Despite its promising outcomes, the study acknowledges certain limitations. The research primarily focuses on idealized conditions, including uniform material properties and simplified boundary constraints, which may differ from real-world applications. Additionally, the long-term durability of piezoelectric patches under fluctuating environmental and mechanical conditions remains to be explored. Future studies could investigate integrating this technique with other passive repair methods, optimize actuator placement for enhanced efficiency, and assess the feasibility of multi-layered piezoelectric configurations for improved performance. Furthermore, experimental validation is necessary to support the numerical and analytical findings. In conclusion, this research provides a novel, cost-effective solution for strengthening bending-loaded cracked plates using piezoelectric actuators. By reducing crack severity and enhancing load-bearing capacity, this method offers significant implications for aerospace, automotive, and civil engineering applications. The findings advance active structural repair technologies and intelligent material-based repair systems innovations.

This page is intentionally left blank

CONCLUSION AND FUTURE SCOPE OF WORK

7.1 Conclusion

This thesis investigates the use of piezoelectric actuators to mitigate the severity of cracks in structural components through the reverse piezoelectric effect. It demonstrates how active crack suppression enhances structural durability by leveraging electromechanical actuation. Furthermore, the effectiveness of piezoelectric patches in repairing cracks and extending fatigue life is evaluated for various structural geometries. The analysis integrates Linear Elastic Fracture Mechanics (LEFM) with analytical modeling to quantify the effectiveness of piezoelectric actuation. Calculations of Stress Intensity Factor (SIF) are performed using the Weight Function Method (WFM) and Tada's formula, with the superposition principle employed to estimate the net reduction in SIF due to induced piezoelectric stresses. The study extends its findings to fatigue crack growth rate (FCGR) estimation using the standard FCGR model, explaining the enhancement in fatigue life after repair. The analytical models formulated in this research are thoroughly validated via numerical finite element simulations, demonstrating their accuracy and reliability. The analytical and numerical methods demonstrate significant agreement, confirming the validity of the established methodology. The analytical findings are verified through finite element (FE) simulations in ABAQUS, ensuring the reliability of the proposed approach.

The study conducted in this thesis follows an organized approach to investigating the application of piezoelectric actuators for repairing cracks in structural components. An analytical model is initially developed for a double-edge cracked infinite plate, integrating both active and passive effects of piezoelectric patches. The Stress Intensity Factor (SIF) is determined using the Weight Function Method (WFM), while Rose's equation incorporates the passive effect. A hybrid repair approach is also explored, integrating active and passive mechanisms. The influence of patch thickness, voltage ratio, and externally applied voltage on fatigue life enhancement is examined for passive, active, and hybrid repair scenarios.

Moreover, an investigation is conducted into repairing cracks emanating from elliptical holes in a plate. The Weight Function Method (WFM) and a superposition technique are employed to estimate the total SIF. Furthermore, the influence of geometric parameters such as

the semi-major axis, aspect ratio, and patch thickness on SIF reduction and fatigue life enhancement is investigated. Additionally, the effectiveness of piezoelectric actuators in mitigating fatigue crack growth in an edge-cracked arc-shaped specimen is examined. The WFM is employed to determine the SIF, and the study evaluates the effects of geometric parameters of the specimen, patch thickness, and externally applied voltage on the overall repair efficiency of the arc-shaped cracked specimen.

Furthermore, the study extends to a bottom-edged cracked I-beam under four-point bending, considering the influence of the shifted neutral axis caused by the crack. The crack surface widening energy release rate is utilized to determine the SIFs. The effects of crack length, patch thickness, and externally applied voltage on SIFs, fracture load, and fatigue life are systematically investigated. Finally, a novel repair methodology is developed for edge-cracked plate-like structures subjected to bending loads. The study primarily focuses on static repair. The impact of crack length, patch thickness, and applied voltage on repair efficiency is thoroughly discussed.

To emphasize the significance of this thesis in the field, key findings from the analysis are outlined below:

- Piezoelectric actuators reduce stress intensity factors (SIF), reduce crack propagation, and enhance structural integrity across various configurations. The application of piezoelectric patches significantly enhances fatigue life under cyclic loading conditions.
- Integrating the piezoelectric patch's active and passive effects provides better results in enhancing fatigue life compared to depending on either method alone, especially in the context of cracked plates, where it is possible to fix the patch onto the cracked surface.
- The selection and application of repair voltage are crucial for optimizing SIF reduction and extending fatigue life, as they improve load-bearing capacity, delay in crack initiation, and significantly enhance service life. A cyclic voltage and mechanical loading applied with a zero-phase difference significantly improve fatigue life compared to a constant voltage. The zero-voltage ratio (VR) consistently exhibits the best fatigue life enhancement.
- Patch thickness is found to be a vital design parameter. Piezoelectric strain remains consistent across all patch thicknesses within a uniform electric field. Thinner

patches perform better at lower voltages under low load conditions, while thicker patches are more effective in handling higher mechanical stresses, highlighting the existence of application-specific optimal patch thicknesses.

- It is found that patch width plays a crucial role in reducing SIFs, with wider patches facilitating a more effective compressive stress distribution, thereby enhancing crack mitigation. Optimizing patch geometry is essential for maximizing the efficacy of piezoelectric repair.
- The structural integrity of transverse load-bearing members is significantly improved by the counteracting moments produced by piezoelectric actuation, resulting in effective crack growth suppression and enhanced load-bearing capacity.
- Longer cracks consistently exhibit a more noticeable response to piezoelectric repair, demonstrating more significant percentage reductions in SIF and more substantial extensions of fatigue life. The percentage of improved fracture load is significantly higher in I-beam structures, particularly for larger crack sizes, showcasing its effectiveness in various structural applications.
- The shape and size of cracks and holes significantly affect the performance of piezoelectric-based repairs for cracks emanating from elliptical holes. When the total opening length of the plate (the sum of the semi-major axis and the crack length) is kept constant, a greater reduction in SIF is observed for smaller semi-major axes. The aspect ratio (AR) of elliptical holes marginally influences repair performance at a fixed semimajor axis length and crack length, except when the hole approximates a circular shape.

Another critical factor influencing the overall effectiveness of piezoelectric crack repair is the material properties of the actuator. The current work employs Lead Zirconate Titanate (PZT) due to its superior electromechanical coupling coefficient, high dielectric permittivity, and strong mechanical endurance, making it highly efficient for stress modulation and fatigue life improvement. The actuation capability is further governed by properties such as elastic modulus, which enhances load transfer and crack surface closure, and piezoelectric coefficients, which dictate the induced strain and actuation force. Together, these properties determine the magnitude of stress intensity factor reduction achievable during repair. Optimizing such material characteristics is therefore essential for ensuring reliable and effective piezoelectric-based crack mitigation.

7.2 Practical Application of the Findings

The outcomes of this thesis hold considerable practical implications for many engineering disciplines. By leveraging piezoelectric actuators for active repair, engineers can strengthen structural robustness and prolong the operational lifespan of critical components across sectors like aerospace, civil infrastructure, and mechanical engineering. In the aerospace domain, for instance, strategically positioned piezoelectric patches can effectively remediate fatigue cracks in aircraft wings and fuselages, thereby reducing maintenance costs and enhancing safety margins. Similarly, these patches can be deployed in bridges and buildings for continuous crack monitoring and timely repair, preventing catastrophic structural failures. Marine engineering applications, such as ships and offshore platforms, can use piezoelectric actuation to enhance the operational reliability of structural components subjected to severe environmental conditions. Additionally, railway systems can integrate piezoelectric repair techniques to mitigate fatigue damage in tracks and supporting infrastructure, ensuring safer and more efficient transport networks. The renewable energy sector, particularly wind turbine blades and solar panel support structures, can benefit from these findings by increasing resilience against cyclic loading conditions. Moreover, defense and military applications can gain from autonomous repair capabilities in military aircraft, naval vessels, and armored vehicles, improving mission readiness and reducing operational maintenance. Modifying the repair strategy through precise voltage and patch thickness optimization enables highly efficient and targeted maintenance interventions, creating more durable and reliable structures.

7.3 Advantages, Limitations and Challenges

Piezoelectric actuators offer significant advantages over conventional crack repair techniques, such as mechanical fastening, adhesive bonding, and welding. Traditional repair approaches often lead to added weight, stress concentration, and reduced fatigue strength. In contrast, piezoelectric actuators provide a non-invasive, lightweight, and reversible means of applying controlled stresses to suppress crack propagation. Their ability to generate in-plane compressive stresses dynamically allows them to actively reduce stress intensity factors (SIFs) in real time, enhancing fatigue life and delaying crack propagation. Furthermore, piezoelectric repair systems also minimize structural downtime and enable non-destructive repair without the need for disassembly or physical alteration of the component, making them highly suitable for critical engineering applications requiring rapid and adaptive intervention. The actuation voltage can

be precisely adjusted to achieve desired stress redistribution, allowing adaptive control and long-term maintenance with minimal manual intervention.

While the study establishes the viability of piezoelectric actuators for crack repair, several limitations exist. The analytical and numerical investigations assume ideal bonding conditions between the actuator and the substrate, which may differ in real-world applications due to imperfect adhesion or interfacial delamination. Environmental influences such as temperature, humidity, and long-term material degradation are not incorporated but can significantly affect actuator performance. Moreover, the current thesis primarily focuses on linear elastic conditions and does not address nonlinear behavior, plastic deformation, or large deflection effects. The implementation of piezoelectric systems in large-scale structures poses challenges in terms of energy supply, control electrical system, and integration with complex geometries. The brittleness of ceramic-based materials like PZT and their potential depolarization under extreme conditions also limit their applicability in highly dynamic environments. Future work should also focus on developing robust bonding interfaces and proposal of methods to overcome these real-world limitations.

7.4 Future Scope

The research presented in this thesis puts a strong foundation for applying piezoelectric actuators in structural repair. However, several paths remain unexplored, offering productive ground for future investigations. A comprehensive understanding of the influence of environmental factors, such as temperature and humidity, on the long-term performance of piezoelectric repairs is crucial. Furthermore, exploring the behavior of these repairs under dynamic and complex loading conditions, including impact and fatigue under variable amplitude loading, would provide valuable understanding. Developing advanced actuator materials with enhanced durability and efficiency, alongside optimization algorithms for patch placement and design, presents another significant area of focus. Integrating real-time monitoring systems with the repair strategy would enable adaptive control and enhance the reliability of the repair. Finally, developing scalable and cost-effective manufacturing techniques for piezoelectric actuators is essential for extensive industrial adoption.

Considering the collective findings of this thesis, future research should focus on:

- Conducting detailed studies to evaluate the performance of piezoelectric repairs under diverse environmental conditions, including temperature variations, humidity, and corrosive environments, to ensure long-term reliability.

- Investigating the response of piezoelectric repaired structures under various dynamic loading scenarios, such as impact loading and variable amplitude fatigue, to assess their robustness in real-world applications.
- Exploring and developing novel piezoelectric materials with improved electromechanical properties, enhanced durability, and excellent resistance to environmental degradation, facilitating their extensive adoption in industrial applications and reducing overall repair costs.
- Developing sophisticated optimization algorithms and methodologies to determine the optimal size, shape, and placement of piezoelectric patches for specific structural configurations and loading conditions, maximizing repair effectiveness.
- Integrating advanced Structural Health Monitoring (SHM) frameworks with piezoelectric repair systems through embedded sensor–actuator networks for continuous condition tracking and autonomous crack detection.
- Developing adaptive control mechanisms that utilize real-time SHM data to activate piezoelectric actuation on demand, enabling intelligent, self-regulating repair strategies.
- Implementing wireless, scalable SHM–actuation networks that support predictive maintenance and self-healing functionalities to enhance structural reliability and service life.

BIBLIOGRAPHY

A

Aabid, A., Hrairi, M., Ali, J. S. M. and Sebaey, T. A. (2022). A Review on Reductions in the Stress-Intensity Factor of Cracked Plates Using Bonded Composite Patches. Materials, 15(9), 3086. https://doi.org/10.3390/ma15093086

Aabid, A., Hrairi, M., Mohamed Ali, S. J. and Ibrahim, Y. E. (2023). Review of Piezoelectric Actuator Applications in Damaged Structures: Challenges and Opportunities. ACS Omega, 8(3), 2844–2860. https://doi.org/10.1021/acsomega.2c06573

Aabid, A., Raheman, M. A., Ibrahim, Y. E., Anjum, A., Hrairi, M., Parveez, B., Parveen, N. and Mohammed Zayan, J. (2021). A Systematic Review of Piezoelectric Materials and Energy Harvesters for Industrial Applications. Sensors, 21(12), 4145. https://doi.org/10.3390/s21124145

Abuzaid, A., Dawood, M. S. and Hrairi, M. (2015). Effects of Adhesive Bond on Active Repair of Aluminium Plate Using Piezoelectric Patch. Applied Mechanics and Materials, 799–800, 788–793. https://doi.org/10.4028/www.scientific.net/AMM.799-800.788

Abuzaid, A., Hrairi, M. and Dawood, M. (2018a). Evaluating the Reduction of Stress Intensity Factor in Center-Cracked Plates Using Piezoelectric Actuators. Actuators, 7(2), 25. https://doi.org/10.3390/act7020025

Abuzaid, A., Hrairi, M. and Dawood, M. S. (2015a). Mode I Stress Intensity Factor for a Cracked Plate with an Integrated Piezoelectric Actuator. Advanced Materials Research, 1115, 517–522. https://doi.org/10.4028/www.scientific.net/AMR.1115.517

Abuzaid, A., Hrairi, M. and Dawood, M. S. (2017). Modeling approach to evaluating reduction in stress intensity factor in center-cracked plate with piezoelectric actuator patches. Journal of Intelligent Material Systems and Structures, 28(10), 1334–1345. https://doi.org/10.1177/1045389X16672562

Abuzaid, A., Hrairi, M. and Dawood, M. S. (2018b). Experimental and numerical analysis of piezoelectric active repair of edge-cracked plate. Journal of Intelligent Material Systems and Structures, 29(18), 3656–3666. https://doi.org/10.1177/1045389X18798949

Abuzaid, A., Hrairi, M. and Dawood, M. S. I. (2015b). Survey of Active Structural Control and Repair Using Piezoelectric Patches. Actuators, 4(2), 77–98. https://doi.org/10.3390/act4020077

Abuzaid, A., Hrairi, M. and Kabrein, H. (2020). Stress analysis of plate with opposite semicircular notches and adhesively bonded piezoelectric actuators. Vibroengineering Procedia, 31, 134–139. https://doi.org/10.21595/vp.2020.21311

Ahmad, A. and Bond, L. J. (Eds.). (2018). Nondestructive Evaluation of Materials. ASM International. https://doi.org/10.31399/asm.hb.v17.9781627081900

Alaimo, A., Milazzo, A. and Orlando, C. (2009). Boundary elements analysis of adhesively bonded piezoelectric active repair. Engineering Fracture Mechanics, 76(4), 500–511. https://doi.org/10.1016/j.engfracmech.2008.10.008

Alaimo, A., Milazzo, A. and Orlando, C. (2011). On the dynamic behavior of piezoelectric active repair by the boundary element method. Journal of Intelligent Material Systems and Structures, 22(18), 2137–2146. https://doi.org/10.1177/1045389X11425281

Alaimo, A., Milazzo, A. and Orlando, C. (2016). A smart composite-piezoelectric one-dimensional finite element model for vibration damping analysis. Journal of Intelligent Material Systems and Structures, 27(10), 1362–1375. https://doi.org/10.1177/1045389X15591380

Al-Ashtari, W. (2016). A Novel Analytical Model to Design Piezoelectric Patches Used to Repair Cracked Beams. Journal of Engineering, 22(6), 117–136. https://doi.org/10.31026/j.eng.2016.06.09

Aliabadi M. H. (2003). The boundary element method. Volume 2: Applications in solids and structures. In Bautechnik (Issue 2). https://doi.org/10.1002/bate.200301300

Al-Karawi, H., von Bock und Polach, R. U. F. and Al-Emrani, M. (2020). Fatigue crack repair in welded structures via tungsten inert gas remelting and high frequency mechanical impact. Journal of Constructional Steel Research, 172, 106200. https://doi.org/10.1016/j.jcsr.2020.106200

Allahyari, S. M. R. and Golabi, S. (2020). Reducing Stress Concentration Around a Hole in a Thin-Wall Cylinder Subjected to Internal Pressure Using Piezoelectric Patches. Iranian Journal of Science and Technology, Transactions of Mechanical Engineering, 44(4), 933–948. https://doi.org/10.1007/s40997-019-00319-7

Anderson, T. L. (2017). Fracture Mechanics. CRC Press. https://doi.org/10.1201/9781315370293

Anton, S. R., Erturk, A. and Inman, D. J. (2012). Bending Strength of Piezoelectric Ceramics and Single Crystals for Multifunctional Load-Bearing Applications. IEEE Transactions on Ultrasonics, Ferroelectrics and Frequency Control 59(6), 1085–92. https://doi.org/10.1109/TUFFC.2012.2299

Ariaei, A., Ziaei-Rad, S. and Ghayour, M. (2010). Repair of a cracked Timoshenko beam subjected to a moving mass using piezoelectric patches. International Journal of Mechanical Sciences, 52(8), 1074–1091. https://doi.org/10.1016/j.ijmecsci.2010.04.001

Arnau, A. and Soares, D. (2008). Fundamentals of Piezoelectricity. In Piezoelectric Transducers and Applications (pp. 1–38). Springer Berlin Heidelberg. https://doi.org/10.1007/978-3-540-77508-9_1

Ayatollahi, M. R., Razavi, N. and Chamani, H. R. (2014). A numerical study on the effect of symmetric crack flank holes on fatigue life extension of a SENT specimen. Fatigue & Fracture of Engineering Materials & Structures, 37(10), 1153–1164. https://doi.org/10.1111/ffe.12199

B

Badr, B. M. and Ali, W. G. (2011). Applications of Piezoelectric Materials. Advanced Materials Research, 189–193, 3612–3620. https://doi.org/10.4028/www.scientific.net/AMR.189-193.3612

Bafandeh, M. R., Gharahkhani, R. and Lee, J. S. (2015). Dielectric and piezoelectric properties of sodium potassium niobate-based ceramics sintered in microwave furnace. Materials Chemistry and Physics, 156, 254–260. https://doi.org/10.1016/j.matchemphys.2015.03.018

Belytschko, T. and Black, T. (1999). Elastic Crack Growth in Finite Elements with Minimal Remeshing. International Journal for Numerical Methods in Engineering, 45(5), 601–620. https://doi.org/10.1002/(SICI)1097-0207(19990620)45:5<601::AID-NME598>3.0.CO;2-S

Broek, D. (1982). Elementary engineering fracture mechanics. Springer Netherlands. https://doi.org/10.1007/978-94-009-4333-9

Bueckner, H. F. (1970). A Novel Principle of the Computation of Stress Intensity Factors. Zeitschrift Fuer Angewandte Mathematik & Mechanik, 50(9), 529–546. https://trid.trb.org/view/3976

C

Caimmi, F. and Pavan, A. (2013). A numerical study of crack–fibre interaction at varying fibre orientation. Engineering Fracture Mechanics, 101, 129–139. https://doi.org/10.1016/j.engfracmech.2012.07.026

Chan, S. K., Tuba, I. S. and Wilson, W. K. (1970). On the finite element method in linear fracture mechanics. Engineering Fracture Mechanics, 2(1), 1–17. https://doi.org/10.1016/0013-7944(70)90026-3

Chan, W. S. and Vedhagiri, S. (2001). Analysis of Composite Bonded/Bolted Joints Used in Repairing. Journal of Composite Materials, 35(12), 1045–1061. https://doi.org/10.1177/002199801772662325

Chee, C. Y. K., Tong, L. and Steven, G. P. (1998). A Review on the Modelling of Piezoelectric Sensors and Actuators Incorporated in Intelligent Structures. Journal of Intelligent Material Systems and Structures, 9(1), 3–19. https://doi.org/10.1177/1045389X9800900101

Chen, T., Wang, X. and Qi, M. (2018). Fatigue improvements of cracked rectangular hollow section steel beams strengthened with CFRP plates. Thin-Walled Structures, 122, 371–377. https://doi.org/10.1016/j.tws.2017.10.019

Cheng, J. and Li, G. (2008). Stress analyses of a smart composite pipe joint integrated with piezoelectric composite layers under torsion loading. International Journal of Solids and Structures, 45(5), 1153–1178. https://doi.org/10.1016/j.ijsolstr.2007.07.027

Cheng, J. and Taheri, F. (2005). A novel smart adhesively bonded joint system. Smart Materials and Structures, 14(5), 971–981. https://doi.org/10.1088/0964-1726/14/5/035

Cheng, J., Qian, C., Zhao, M., Lee, S. R., Tong, P. and Zhang, T. Y. (2000). Effects of electric fields on the bending behavior of PZT-5Hpiezoelectric laminates. Smart materials and structures, 9(6), 824. https://doi.org/10.1088/0964-1726/9/6/312

Cheng, J., Taheri, F. and Han, H. (2006). Strength improvement of a smart adhesive bonded joint system by partially integrated piezoelectric patches. Journal of Adhesion Science and Technology, 20(6), 503–518. https://doi.org/10.1163/156856106777213285

Cheng, J., Wu, X., Li, G., Pang, S.-S. and Taheri, F. (2007). Design and analysis of a smart composite pipe joint system integrated with piezoelectric layers under bending. International Journal of Solids and Structures, 44(1), 298–319. https://doi.org/10.1016/j.ijsolstr.2006.04.021

Colombi, P. and Fava, G. (2015). Experimental study on the fatigue behaviour of cracked steel beams repaired with CFRP plates. Engineering Fracture Mechanics, 145, 128–142. https://doi.org/10.1016/j.engfracmech.2015.04.009

Crawley, E. F. and de Luis, J. (1987). Use of piezoelectric actuators as elements of intelligent structures. AIAA Journal, 25(10), 1373–1385. https://doi.org/10.2514/3.9792

D

Dai, J., Zhao, P., Su, H. and Wang, Y. (2020). Mechanical Behavior of Single Patch Composite Repaired Al Alloy Plates: Experimental and Numerical Analysis. Materials, 13(12), 2740. https://doi.org/10.3390/ma13122740

Davis, M. and Bond, D. (1999). Principles and practices of adhesive bonded structural joints and repairs. International Journal of Adhesion and Adhesives, 19(2–3), 91–105. https://doi.org/10.1016/S0143-7496(98)00026-8

Deng, J., Fei, Z., Wu, Z., Li, J. and Huang, W. (2023). Integrating SMA and CFRP for fatigue strengthening of edge-cracked steel plates. Journal of Constructional Steel Research, 206, 107931. https://doi.org/10.1016/j.jcsr.2023.107931

Dowling Norman E., Kampe Stephen L. and Kral Milo V. (Eds.). (2021). Mechanical behavior of materials: engineering methods for deformation, fracture, and fatigue (5th ed.). Pearson Education.

Duan, W. H., Quek, S. T. and Wang, Q. (2008). Finite element analysis of the piezoelectric-based repair of a delaminated beam. Smart Materials and Structures, 17(1), 015017. https://doi.org/10.1088/0964-1726/17/01/015017

Duan, W. H., Wang, Q. and Quek, S. T. (2010). Applications of Piezoelectric Materials in Structural Health Monitoring and Repair: Selected Research Examples. Materials, 3(12), 5169–5194. https://doi.org/10.3390/ma3125169

Duong, C. N. and Wang, C. H. (2004). On the Characterization of Fatigue Crack Growth in a Plate With a Single-Sided Repair. Journal of Engineering Materials and Technology, 126(2), 192–198. https://doi.org/10.1115/1.1647129

Duong, C. N., Verhoeven, S. and Guijt, C. B. (2006). Analytical and experimental study of load attractions and fatigue crack growths in two-sided bonded repairs. Composite Structures, 73(4), 394–402. https://doi.org/10.1016/j.compstruct.2005.02.011

E

Elahi, H. (2021). The investigation on structural health monitoring of aerospace structures via piezoelectric aeroelastic energy harvesting. Microsystem Technologies, 27(7), 2605–2613. https://doi.org/10.1007/s00542-020-05017-y

Errouane, H., Sereir, Z. and Chateauneuf, A. (2014). Numerical model for optimal design of composite patch repair of cracked aluminum plates under tension. International Journal of Adhesion and Adhesives, 49, 64–72. https://doi.org/10.1016/j.ijadhadh.2013.12.004

F

Fesharaki, J. J. and Golabi, S. (2017). Effect of stiffness ratio of piezoelectric patches and plate on stress concentration reduction in a plate with a hole. Mechanics of Advanced Materials and Structures, 24(3), 253–259. https://doi.org/10.1080/15376494.2016.1139214

Fesharaki, J. J., Madani, S. G. and Golabi, S. (2016). Effect of stiffness and thickness ratio of host plate and piezoelectric patches on reduction of the stress concentration factor. International Journal of Advanced Structural Engineering, 8(3), 229–242. https://doi.org/10.1007/s40091-016-0125-x

Fett, T. (1991). Conditions for the determination of approximate COD fields. Engineering Fracture Mechanics, 39(5), 905–914. https://doi.org/10.1016/0013-7944(91)90196-8

Fett, T. (1993). Stress intensity factors and weight functions for cracks in front of notches. Kernforschungszentrum Karlsruhe.

Fett, T., Mattheck, C. and Munz, D. (1987). On the calculation of crack opening displacement from the stress intensity factor. Engineering Fracture Mechanics, 27(6), 697–715. https://doi.org/10.1016/0013-7944(87)90159-7

Forman, R. G. and Mettu, S. R. (1990). Behavior of surface and corner cracks subjected to tensile and bending loads in Ti-6Al-4V alloy (No. S-611).

Fossati, M., Pagani, M., Giglio, M. and Manes, A. (2021). Fatigue crack propagation in a helicopter component subjected to impact damage. Defence Technology, 17(2), 416–428. https://doi.org/10.1016/j.dt.2020.02.005

G

Ghafoori, E. and Motavalli, M. (2011). Analytical calculation of stress intensity factor of cracked steel I-beams with experimental analysis and 3D digital image correlation measurements. Engineering Fracture Mechanics, 78(18), 3226-3242. https://doi.org/10.1016/j.engfracmech.2011.09.012

Ghafoori, E., Motavalli, M., Botsis, J., Herwig, A. and Galli, M. (2012). Fatigue strengthening of damaged metallic beams using prestressed unbonded and bonded CFRP plates. International Journal of Fatigue, 44, 303–315. https://doi.org/10.1016/j.ijfatigue.2012.03.006

Ghafoori, E., Schumacher, A. and Motavalli, M. (2012). Fatigue behavior of notched steel beams reinforced with bonded CFRP plates: Determination of prestressing level for crack arrest. Engineering Structures, 45, 270–283. https://doi.org/10.1016/j.engstruct.2012.06.047

Gonzáles, G. L. G., Diaz, J. G., González, J. A. O., Castro, J. T. P. and Freire, J. D. F. (2017). Determining SIFs using DIC considering crack closure and blunting. In Experimental and Applied Mechanics, Volume 4: Proceedings of the 2016 Annual Conference on Experimental and Applied Mechanics (pp. 25-36). Springer International Publishing. https://doi.org/10.1007/978-3-319-42028-8_4

Guo, Y. and Li, P. (2024). Effect of Residual Stress and Microstructure on the Fatigue Crack Growth Behavior of Aluminum Friction Stir Welded Joints. Materials, 17(2), 385. https://doi.org/10.3390/ma17020385

Gurney, T. R. (1979). Fatigue of welded structures. CUP Archive.

H

Hafiz, T. A. and Abdel Wahab, M. M. (2015). Predicting the fatigue life of adhesively-bonded composite joints under mode I fracture conditions. In Fatigue and Fracture of Adhesively-Bonded Composite Joints (pp. 401–417). Elsevier. https://doi.org/10.1016/B978-0-85709-806-1.00014-8

Hall, D. A. (2001). Review Nonlinearity in piezoelectric ceramics. Journal of Materials Science, 36(19), 4575–4601. https://doi.org/10.1023/A:1017959111402

Hamam, R., Hild, F. and Roux, S. (2007). Stress Intensity Factor Gauging by Digital Image Correlation: Application in Cyclic Fatigue. Strain, 43(3), 181–192. https://doi.org/10.1111/j.1475-1305.2007.00345.x

Harilal, R., Vyasarayani, C. P. and Ramji, M. (2015). A linear least squares approach for evaluation of crack tip stress field parameters using DIC. Optics and Lasers in Engineering, 75, 95–102. https://doi.org/10.1016/j.optlaseng.2015.07.004

Hasegawa, K., Crocombe, A. D., Coppuck, F., Jewel, D. and Maher, S. (2015). Characterising bonded joints with a thick and flexible adhesive layer–Part 1: Fracture testing and behaviour. International Journal of Adhesion and Adhesives, 63, 124–131. https://doi.org/10.1016/j.ijadhadh.2015.09.003

Huang, C., Chen, T., Xia, Z. and Jiang, L. (2022). Numerical study of surface fatigue crack growth in steel plates repaired with CFRP. Engineering Structures, 268, 114743. https://doi.org/10.1016/j.engstruct.2022.114743

Huynh, T. C., Lee, S. Y., Dang, N. L. and Kim, J. T. (2019). Sensing region characteristics of smart piezoelectric interface for damage monitoring in plate-like structures. Sensors, 19(6), 1377. https://doi.org/10.3390/s19061377

I

Inoue, J. I., Kanda, K., Fujita, T. and Maenaka, K. (2015). Thin-film piezoelectric bimorph actuators with increased thickness using double Pb [Zr, Ti] O3 layers. Journal of Micromechanics and Microengineering, 25(5), 055001. https://doi.org/10.1088/0960-1317/25/5/055001

Irwin, G. R. (1957). Analysis of Stresses and Strains Near the End of a Crack Traversing a Plate. Journal of Applied Mechanics, 24(3), 361–364. https://doi.org/10.1115/1.4011547

J

Jafari Fesharaki, J. and Golabi, S. I. (2015). Optimum pattern of piezoelectric actuator placement for stress concentration reduction in a plate with a hole using particle swarm optimization algorithm. Proceedings of the Institution of Mechanical Engineers, Part C: Journal of Mechanical Engineering Science, 229(4), 614-628. https://doi.org/10.1177/0954406214538617

Jafari Fesharaki, J., Madani, S. G. and Golabi, S. I. (2020). Best pattern for placement of piezoelectric actuators in classical plate to reduce stress concentration using PSO algorithm. Mechanics of Advanced Materials and Structures, 27(2), 141-151. https://doi.org/10.1080/15376494.2018.1472332

Jin, C. and Wang, X. (2011). Analytical modelling of the electromechanical behaviour of surface-bonded piezoelectric actuators including the adhesive layer. Engineering Fracture Mechanics, 78(13), 2547–2562. https://doi.org/10.1016/j.engfracmech.2011.06.014

Jin, C., Wang, X. D. and Zuo, M. J. (2010). The dynamic behaviour of surface-bonded piezoelectric actuators with debonded adhesive layers. Acta Mechanica, 211(3–4), 215–235. https://doi.org/10.1007/s00707-009-0231-y

K

Khalili, S. M. R., Farsani, R. E. and Khoeini, A. (2010). Effect of piezoelectric patches on the behavior of adhesively bonded single lap joints. The Journal of Adhesion, 86(5-6), 601-629. https://doi.org/10.1080/00218464.2010.484315

Khiem, N. T., Hai, T. T. and Huong, L. Q. (2023). Modal analysis of cracked FGM beam with piezoelectric layer. Mechanics Based Design of Structures and Machines, 51(9), 5120–5140. https://doi.org/10.1080/15397734.2021.1992775

Kondratiev, A., Píštěk, V., Smovziuk, L., Shevtsova, M., Fomina, A., Kučera, P. and Prokop, A. (2021). Effects of the Temperature–Time Regime of Curing of Composite Patch on Repair Process Efficiency. Polymers, 13(24), 4342. https://doi.org/10.3390/polym13244342

Kong, D., Zhou, P., Li, C., Hong, B. and Xian, G. (2023). Stress intensity factor of through-wall-cracked steel pipe wrapped with prestressed CFRP composites. Engineering Fracture Mechanics, 283, 109218. https://doi.org/10.1016/j.engfracmech.2023.109218

Kotousov, A. and Jones, R. (2002). Method for Calculating the Stress Intensity Factor for Small-to-Medium Edge Cracks. International Journal of Fracture, 115(3), 43–48. https://doi.org/10.1023/A:1022644023867

Kradinov, V., Hanauska, J., Barut, A., Madenci, E. and Ambur, D. R. (2002). Bolted patch repair of composite panels with a cutout. Composite Structures, 56(4), 423–444. https://doi.org/10.1016/S0263-8223(02)00027-2

Kujawski, D. (1991). Estimations of stress intensity factors for small cracks at notches. Fatigue & Fracture of Engineering Materials & Structures, 14(10), 953-965. https://doi.org/10.1111/j.1460-2695.1991.tb00005.x

Kumar Mishra, R. (2018). A Review on Fracture Mechanics in Piezoelectric Structures. Materials Today: Proceedings, 5(2), 5407–5413. https://doi.org/10.1016/j.matpr.2017.12.127

Kumar, D., Budarapu, P. R. and Pradhan, A. K. (2023). Numerical analysis of lap shear joints made of functionally graded materials. Journal of the Brazilian Society of Mechanical Sciences and Engineering, 45(2), 94. https://doi.org/10.1007/s40430-022-03874-4

Kumar, R., Pathak, H., Singh, A. and Tiwari, M. (2021). Modeling of crack repair using piezoelectric material: XFEM approach. Engineering Computations, 38(2), 586–617. https://doi.org/10.1108/EC-01-2020-0001

Kumar, R., Singh, A. and Tiwari, M. (2020a). Investigation of Crack Repair in Orthotropic Composite by Piezoelectric Patching. Materials Today: Proceedings, 21, 1303–1312. https://doi.org/10.1016/j.matpr.2020.01.167

Kumar, R., Singh, A. and Tiwari, M. (2020b). Investigation of crack repair using piezoelectric material under thermo-mechanical loading. Journal of Intelligent Material Systems and Structures, 31(19), 2243–2260. https://doi.org/10.1177/1045389X20943946

L

Li, X., Xie, Z., Zhao, W., Zhang, Y., Gong, Y. and Hu, N. (2021). Failure prediction of irregular arranged multi-bolt composite repair based on finite fracture mechanics model. Engineering Fracture Mechanics, 242, 107456. https://doi.org/10.1016/j.engfracmech.2020.107456

Li, Z., Jiang, X., Hopman, H., Zhu, L. and Liu, Z. (2020). External surface cracked offshore steel pipes reinforced with composite repair system subjected to cyclic bending: An experimental investigation. Theoretical and Applied Fracture Mechanics, 109, 102703. https://doi.org/10.1016/j.tafmec.2020.102703

Li, Z., Jiang, X., Hopman, H., Zhu, L., Liu, Z. and Tang, W. (2021). Experimental investigation on FRP-reinforced surface cracked steel plates subjected to cyclic tension. Mechanics of Advanced Materials and Structures, 28(24), 2551–2565. https://doi.org/10.1080/15376494.2020.1746448

Lin, X. J., Zhou, K. C., Zhang, X. Y. and Zhang, D. (2013). Development, modeling and application of piezoelectric fiber composites. Transactions of nonferrous metals society of china, 23(1), 98-107. https://doi.org/10.1016/S1003-6326(13)62435-8

Liu, H., Al-Mahaidi, R. and Zhao, X. L. (2009). Experimental study of fatigue crack growth behaviour in adhesively reinforced steel structures. Composite Structures, 90(1), 12-20. https://doi.org/10.1016/j.compstruct.2009.02.016

Liu, T. J. C. (2007). Fracture mechanics and crack contact analyses of the active repair of multi-layered piezoelectric patches bonded on cracked structures. Theoretical and Applied Fracture Mechanics, 47(2), 120–132. https://doi.org/10.1016/j.tafmec.2006.11.004

Liu, T. J.-C. (2008). Crack repair performance of piezoelectric actuator estimated by slope continuity and fracture mechanics. Engineering Fracture Mechanics, 75(8), 2566–2574. https://doi.org/10.1016/j.engfracmech.2007.11.004

Liu, Z., Li, Z., Huang, C. and Jiang, X. (2022). An investigation on the fatigue performance of cracked steel plates reinforced with FRP and stop hole. Mechanics of Advanced Materials and Structures, 29(25), 3646–3657. https://doi.org/10.1080/15376494.2021.1907005

Lukáš, P. (1987). Stress intensity factor for small notch-emanated cracks. Engineering Fracture Mechanics, 26(3), 471–473. https://doi.org/10.1016/0013-7944(87)90027-0

M

Maleki, V. A. and Mohammadi, N. (2017). Buckling analysis of cracked functionally graded material column with piezoelectric patches. Smart Materials and Structures, 26(3). https://doi.org/10.1088/1361-665X/aa5324

Manthiramoorthy, K. and Krishnaveni, A. (2017). A, K. Fracture Parameter Evaluation Using Digital Image Correlation Technique. Int. J. Eng. Technol. Sci. Res, 4(11), 306-311.

Mathieu, F., Hild, F. and Roux, S. (2012). Identification of a crack propagation law by digital image correlation. International Journal of Fatigue, 36(1), 146–154. https://doi.org/10.1016/j.ijfatigue.2011.08.004

Mogadpalli, G. P. and Parameswaran, V. (2008). Determination of Stress Intensity Factor for Cracks in Orthotropic Composite Materials using Digital Image Correlation. Strain, 44(6), 446–452. https://doi.org/10.1111/j.1475-1305.2007.00391.x

Mohammadi, S., Yousefi, M. and Khazaei, M. (2021). A review on composite patch repairs and the most important parameters affecting its efficiency and durability. Journal of Reinforced Plastics and Composites, 40(1–2), 3–15. https://doi.org/10.1177/0731684420941602

Mokhtarishirazabad, M., Lopez-Crespo, P. and Zanganeh, M. (2018). Stress intensity factor monitoring under cyclic loading by digital image correlation. Fatigue & Fracture of Engineering Materials & Structures, 41(10), 2162–2171. https://doi.org/10.1111/ffe.12825

N

Narayanan, S. and Balamurugan, V. (2003). Finite element modelling of piezolaminated smart structures for active vibration control with distributed sensors and actuators. Journal of Sound and Vibration, 262(3), 529–562. https://doi.org/10.1016/S0022-460X(03)00110-X

Newman, J. C. (1971). An improved method of collocation for the stress analysis of cracked plates with various shaped boundaries. National Aeronautics and Space Administration.

Nijmeijer, A., Kruidhof, H. and Hennings, D. (1997). Synthesis and Properties of Lead Magnesium Niobate Zirconate Relaxor Materials. Journal of the American Ceramic Society, 80(10), 2717–2721. https://doi.org/10.1111/j.1151-2916.1997.tb03182.x

Nisitani, H. (1978). Solutions of notch problems by body force method. In G.C. Sih (Ed.), Stress analysis of notch problems (Vol. 5, pp. 1–68). Springer Netherlands. https://doi.org/10.1007/978-94-009-9923-7_1

Nogas-Ćwikiel, E. (2011). Fabrication of Mn Doped PZT for Ceramic-Polymer Composites. Archives of Metallurgy and Materials, 56(4). https://doi.org/10.2478/v10172-011-0118-5

O

Orifici, A. C. and Krueger, R. (2012). Benchmark assessment of automated delamination propagation capabilities in finite element codes for static loading. Finite Elements in Analysis and Design, 54, 28–36. https://doi.org/10.1016/j.finel.2012.01.006

Ouinas, D., Bouiadjra, B. B., Serier, B. and SaidBekkouche, M. (2007). Comparison of the effectiveness of boron/epoxy and graphite/epoxy patches for repaired cracks emanating from a semicircular notch edge. Composite Structures, 80(4), 514–522. https://doi.org/10.1016/j.compstruct.2006.07.005

P

Paris, P. and Erdogan, F. (1963). A Critical Analysis of Crack Propagation Laws. Journal of Basic Engineering, 85(4), 528–533. https://doi.org/10.1115/1.3656900

Park, G., Sohn, H., Farrar, C. R. and Inman, D. J. (2003). Overview of Piezoelectric Impedance-Based Health Monitoring and Path Forward. The Shock and Vibration Digest, 35(6), 451–463. https://doi.org/10.1177/05831024030356001

Park, J. H., Ogiso, T. and Atluri, S. N. (1992). Analysis of cracks in aging aircraft structures, with and without composite-patch repairs. Computational Mechanics, 10–10(3–4), 169–201. https://doi.org/10.1007/BF00370088

Petroski, H. J. and Achenbach, J. D. (1978). Computation of the weight function from a stress intensity factor. Engineering Fracture Mechanics, 10(2), 257–266. https://doi.org/10.1016/0013-7944(78)90009-7

Platz, R., Stapp, C. and Hanselka, H. (2011). Statistical approach to evaluating active reduction of crack propagation in aluminumpanels with piezoelectric actuator patches. Smart Materials and Structures, 20(8), 085009. https://doi.org/10.1088/0964-1726/20/8/085009

Providakis, C. P. (2007). Repair of Cracked Structures under Dynamic Load Using Electromechanical Admittance Approach. Key Engineering Materials, 348–349, 49–52. https://doi.org/10.4028/www.scientific.net/KEM.348-349.49

R

Rabinovitch, O. (2007). Piezoelectric Control of Edge Debonding in Beams Strengthened with Composite Materials: Part I – Analytical Modeling. Journal of Composite Materials, 41(5), 525–546. https://doi.org/10.1177/0021998306063790

Raju, I. S. and Newman, J. C. (1979). Stress-intensity factors for a wide range of semi-elliptical surface cracks in finite-thickness plates. Engineering Fracture Mechanics, 11(4), 817–829. https://doi.org/10.1016/0013-7944(79)90139-5

Ratwani, M. M. (1979). Analysis of Cracked, Adhesively Bonded Laminated Structures. AIAA Journal, 17(9), 988–994. https://doi.org/10.2514/3.61263

Rice, J. R. (1968). A Path Independent Integral and the Approximate Analysis of Strain Concentration by Notches and Cracks. Journal of Applied Mechanics, 35(2), 379–386. https://doi.org/10.1115/1.3601206

Rice, J. R. (1972). Some remarks on elastic crack-tip stress fields. International Journal of Solids and Structures, 8(6), 751–758. https://doi.org/10.1016/0020-7683(72)90040-6

Richter-Trummer, V., Moreira, P. M. G. P., Pastrama, S. D., Vaz, M. A. P. and de Castro, P. M. S. T. (2010). Methodology for in situ stress intensity factor determination on cracked structures by digital image correlation. International Journal of Structural Integrity, 1(4), 344–357. https://doi.org/10.1108/17579861011099178

Rodriguez-Sanchez, J. E., Rodriguez-Castellanos, A., Perez-Guerrero, F., Carbajal-Romero, M. F. and Liu, S. (2011). Offshore fatigue crack repair by grinding and wet welding, Fatigue Fract. Eng. M., 34, 487–497. https://doi.org/10.1111/j.1460-2695.2010.01541.x

Rose, L. R. F. and Wang, C. H. (2002). Analytical methods for designing composite repairs. In Advances in the bonded composite repair of metallic aircraft structure (pp. 137-175). Elsevier Science Ltd. https://doi.org/10.1016/B978-008042699-0/50009-7

Rose, L.R.F. (1988). Theoretical analysis of crack patching. In: Baker, A.A., Jones, R. (eds) Bonded Repair of Aircraft Structures. Engineering Application of Fracture Mechanics, vol 7. Springer, Dordrecht. https://doi.org/10.1007/978-94-009-2752-0_5

Roux-Langlois, C., Gravouil, A., Baietto, M. C., Réthoré, J., Mathieu, F., Hild, F. and Roux, S. (2015). DIC identification and X-FEM simulation of fatigue crack growth based on the

Williams' series. International Journal of Solids and Structures, 53, 38-47. https://doi.org/10.1016/j.ijsolstr.2014.10.026

Roy, G., Panigrahi, B. K. and Pohit, G. (2021a). Evaluation and Repair of Cracks on Statically Loaded Beams Using Piezoelectric Actuation. International Journal of Manufacturing, Materials, and Mechanical Engineering, 11(1), 34–49. https://doi.org/10.4018/IJMMME.2021010103

Roy, G., Panigrahi, B. and Pohit, G. (2021b). Crack identification in beam-type structural elements using a piezoelectric sensor. Nondestructive Testing and Evaluation, 36(6), 597–615. https://doi.org/10.1080/10589759.2020.1843652

Roy, G., Panigrahi, B. and Pohit, G. (2023). Identification of crack by vibration analysis and restoration of dynamic response in beams using PZT sensor/actuator. Nondestructive Testing and Evaluation, 38(2), 211–232. https://doi.org/10.1080/10589759.2022.2094378

Royston, T. J. and Houston, B. H. (1998). Modeling and measurement of nonlinear dynamic behavior in piezoelectric ceramics with application to 1-3 composites. The Journal of the Acoustical Society of America, 104(5), 2814-2827. https://doi.org/10.1121/1.423866

Rybicki, E. F. and Kanninen, M. F. (1977). A finite element calculation of stress intensity factors by a modified crack closure integral. Engineering Fracture Mechanics, 9(4), 931–938. https://doi.org/10.1016/0013-7944(77)90013-3

S

Sarangi, H., Murthy, K. S. R. K. and Chakraborty, D. (2010a). Optimum strain gage location for evaluating stress intensity factors in single and double ended cracked configurations. Engineering Fracture Mechanics, 77(16), 3190–3203. https://doi.org/10.1016/j.engfracmech.2010.08.003

Sarangi, H., Murthy, K. S. R. K. and Chakraborty, D. (2010b). Radial locations of strain gages for accurate measurement of mode I stress intensity factor. Materials & Design, 31(6), 2840–2850. https://doi.org/10.1016/j.matdes.2009.12.043

Sarangi, H., Murthy, K. S. R. K. and Chakraborty, D. (2013). Experimental verification of optimal strain gage locations for the accurate determination of mode I stress intensity factors. Engineering Fracture Mechanics, 110, 189–200. https://doi.org/10.1016/j.engfracmech.2013.07.014

Schijve, J. (1980). Stress gradients around notches. Fatigue & Fracture of Engineering Materials & Structures, 3(4), 325-338. https://doi.org/10.1111/j.1460-2695.1980.tb01382.x

Shah, D. K., Joshi, S. P. and Chan, W. S. (1994). Stress concentration reduction in a plate with a hole using piezoceramic layers. Smart Materials and Structures, 3(3), 302–308. https://doi.org/10.1088/0964-1726/3/3/006

Shindo, Y., Miura, M., Takeda, T., Narita, F. and Watanabe, S. (2013). Piezoelectric control of delamination response in woven fabric composites under mode I loading. Acta Mechanica, 224(6), 1315–1322. https://doi.org/10.1007/s00707-013-0862-x

Shindo, Y., Watanabe, S., Takeda, T., Miura, M. and Narita, F. (2013). Controllability of cryogenic Mode I delamination behavior in woven fabric composites using piezoelectric actuators. Engineering Fracture Mechanics, 102, 171–179. https://doi.org/10.1016/j.engfracmech.2013.01.013

Shivakumar, K. N. and Raju, I. S. (1992). An equivalent domain integral method for three-dimensional mixed-mode fracture problems. Engineering Fracture Mechanics, 42(6), 935–959. https://doi.org/10.1016/0013-7944(92)90134-Z

Suresh, S. (1998). Fatigue of Materials. Cambridge University Press. https://doi.org/10.1017/CBO9780511806575

T

Tada, H., Paris, P. C. and Irwin, G. R. (2000). The Stress Analysis of Cracks Handbook, Third Edition. ASME Press. https://doi.org/10.1115/1.801535

Taeyong Lee and Lakes, R. S. (2001). Damping properties of lead metaniobate. IEEE Transactions on Ultrasonics, Ferroelectrics and Frequency Control, 48(1), 48–52. https://doi.org/10.1109/58.895906

Tan, W., Na, J. and Zhou, Z. (2021). Effect of Service Temperature on Mechanical Properties of Adhesive Joints after Hygrothermal Aging. Polymers, 13(21), 3741. https://doi.org/10.3390/polym13213741

Taşdemir, B. (2013). Determination of stress intensity factor using digital image correlation method. Matter, 2(1), 20-24.

Tavares, P. J., Gomes, F. S. and Moreira, P. M. G. P. (2014). A Hybrid Experimental-numerical Sif Determination Technique. Procedia Materials Science, 3, 190–197. https://doi.org/10.1016/j.mspro.2014.06.034

Tsamasphyros, G. J., Kanderakis, G. N., Karalekas, D., Rapti, D., Gdoutos, E. E., Zacharopoulos, D. and Marioli-Riga, Z. P. (2001). Study of composite patch repair by analytical and numerical methods. Fatigue & Fracture of Engineering Materials & Structures, 24(10), 631–636. https://doi.org/10.1046/j.1460-2695.2001.00414.x

U

Udayakumar, K. R., Schuele, P. J., Chen, J., Krupanidhi, S. B. and Cross, L. E. (1995). Thickness-dependent electrical characteristics of lead zirconate titanate thin films. Journal of Applied Physics, 77(8), 3981–3986. https://doi.org/10.1063/1.359508

V

Valadi, Z., Bayesteh, H. and Mohammadi, S. (2020). XFEM fracture analysis of cracked pipeline with and without FRP composite repairs. Mechanics of Advanced Materials and Structures, 27(22), 1888–1899. https://doi.org/10.1080/15376494.2018.1529844

W

Wang, H. T., Wu, G. and Pang, Y. Y. (2018). Theoretical and Numerical Study on Stress Intensity Factors for FRP-Strengthened Steel Plates with Double-Edged Cracks. Sensors, 18(7), 2356. https://doi.org/10.3390/s18072356

Wang, H. T., Wu, G. and Pang, Y. Y. (2018). Theoretical and Numerical Study on Stress Intensity Factors for FRP-Strengthened Steel Plates with Double-Edged Cracks. Sensors, 18(7), 2356. https://doi.org/10.3390/s18072356

Wang, L., Bai, R. and Chen, H. (2013). Analytical modeling of the interface crack between a piezoelectric actuator and an elastic substrate considering shear effects. International Journal of Mechanical Sciences, 66, 141–148. https://doi.org/10.1016/j.ijmecsci.2012.11.002

Wang, Q. (2002). On buckling of column structures with a pair of piezoelectric layers. Engineering Structures, 24(2), 199–205. https://doi.org/10.1016/S0141-0296(01)00088-8

Wang, Q. S. (2010). Active buckling control of beams using piezoelectric actuators and strain gauge sensors. Smart Materials and Structures, 19(6), 065022. https://doi.org/10.1088/0964-1726/19/6/065022

Wang, Q. and Chase, J. G. (2003). Buckling analysis of cracked column structures and piezoelectric-based repair and enhancement of axial load capacity. International Journal of Structural Stability and Dynamics, 3(01), 17-33. https://doi.org/10.1142/S0219455403000793

Wang, Q. and Quek, S. T. (2004). Repair of delaminated beams via piezoelectric patches. Smart Materials and Structures, 13(5), 1222–1229. https://doi.org/10.1088/0964-1726/13/5/026

Wang, Q. and Quek, S. T. (2005). Repair of cracked column under axially compressive load via piezoelectric patch. Computers and Structures, 83(15–16), 1355–1363. https://doi.org/10.1016/j.compstruc.2004.09.018

Wang, Q. and Wu, N. (2012). A review on structural enhancement and repair using piezoelectric materials and shape memory alloys. Smart Materials and Structures, 21(1), 013001. https://doi.org/10.1088/0964-1726/21/1/013001

Wang, Q., Quek, S. T. and Liew, K. M. (2002). On the repair of a cracked beam with a piezoelectric patch. Smart Materials and Structures, 11(3), 311. https://doi.org/10.1088/0964-1726/11/3/311

Wang, Q., Zhou, G. Y. and Quek, S. T. (2005). Repair of Delaminated Beams Subjected to Compressive Force via Piezoelectric Layers. Advances in Structural Engineering, 8(4), 411–425. https://doi.org/10.1260/136943305774353142

Wang, R., Tang, E. and Yang, G. (2019). Dynamic Piezoelectric Properties of PZT-5H Under Shock Compression. Physica Status Solidi (a), 216(6). https://doi.org/10.1002/pssa.201800859

Wang, R., Tang, E. and Yang, G. (2019). Dynamic piezoelectric properties of PZT-5H under shock compression. physica status solidi (a), 216(6), 1800859. https://doi.org/10.1002/pssa.201800859

Weißgraeber, P., Felger, J., Geipel, D. and Becker, W. (2016). Cracks at elliptical holes: Stress intensity factor and Finite Fracture Mechanics solution. European Journal of Mechanics - A/Solids, 55, 192–198. https://doi.org/10.1016/j.euromechsol.2015.09.002

Wu, N. and Wang, Q. (2010). Repair of vibrating delaminated beam structures using piezoelectric patches. Smart Materials and Structures, 19(3), 035027. https://doi.org/10.1088/0964-1726/19/3/035027

Wu, N. and Wang, Q. (2011). An experimental study on the repair of a notched beam subjected to dynamic loading with piezoelectric patches. Smart Materials and Structures, 20(11), 115023. https://doi.org/10.1088/0964-1726/20/11/115023

X

Xie, Y. J., Wang, X. H. and Lin, Y. C. (2004). Stress intensity factors for cracked rectangular cross-section thin-walled tubes. Engineering Fracture Mechanics, 71(11), 1501-1513. https://doi.org/10.1016/S0013-7944(03)00217-0

Y

Yoneyama, S., Morimoto, Y. and Takashi, M. (2006). Automatic Evaluation of Mixed-mode Stress Intensity Factors Utilizing Digital Image Correlation. Strain, 42(1), 21–29. https://doi.org/10.1111/j.1475-1305.2006.00246.x

Younis, N. T. and Kang, B. (2011). Averaging effects of a strain gage. Journal of Mechanical Science and Technology, 25(1), 163–169. https://doi.org/10.1007/s12206-010-1020-1

Yu, Q. Q. and Wu, Y. F. (2017). Fatigue Strengthening of Cracked Steel Beams with Different Configurations and Materials. Journal of Composites for Construction, 21(2). https://doi.org/10.1061/(ASCE)CC.1943-5614.0000750

Yu, Q. Q. and Wu, Y. F. (2018). Fatigue retrofitting of cracked steel beams with CFRP laminates. Composite Structures, 192, 232–244. https://doi.org/10.1016/j.compstruct.2018.02.090

Z

Zaccardi, C., Mazette, A. and Chamoin, L. (2022). Numerical Studies of Smart Structure With Piezoelectric Actuators to Enhance Surface Integrity. Procedia CIRP, 108, 147–151. https://doi.org/10.1016/j.procir.2022.03.027

Zheng, Y. (2007). Experimental and theoretical research on fatigue behavior of steel structures strengthened with CFRP. Tsinghua University, Beijing, China.

Zhou, X., Wu, S., Wang, X., Wang, Z., Zhu, Q., Sun, J., ... & Lu, Q. (2024). Review on piezoelectric actuators: materials, classifications, applications, and recent trends. Frontiers of Mechanical Engineering, 19(1), 6. https://doi.org/10.1007/s11465-023-0772-0

Zhou, X., Wu, S., Wang, X., Wang, Z., Zhu, Q., Sun, J., Huang, P., Wang, X., Huang, W. and Lu, Q. (2024). Review on piezoelectric actuators: materials, classifications, applications, and recent trends. Frontiers of Mechanical Engineering, 19(1), 6. https://doi.org/10.1007/s11465-023-0772-0

Zhu, S. and Liu, H. (2021). Finite element analysis of the three-dimensional crack and defects in piezoelectric materials under the electro-mechanical coupling field. Journal of Intelligent Material Systems and Structures, 32(15), 1662–1677. https://doi.org/10.1177/1045389X20983884

Arabian Journal for Science and Engineering (2024) 49:11479–11499
https://doi.org/10.1007/s13369-023-08703-x

RESEARCH ARTICLE-MECHANICAL ENGINEERING

Piezoelectric Actuator/Patch-Based Hybrid Repair and Fatigue Life Expansion of a Double-Edged Damaged Plate: An Analytical Approach and Numerical Validation

Sourav Pattanayak[1,2] · **Goutam Roy**[3] · **G. Pohit**[2]

Received: 6 September 2023 / Accepted: 28 December 2023 / Published online: 4 February 2024
© King Fahd University of Petroleum & Minerals 2024

Abstract
This study examines the use of piezoelectric materials/patches for passive, active, and hybrid repairs of a double-edged cracked plate. The study considers the stiffness effect of the piezoelectric patch for passive repair, the actuation effect of piezoelectric materials for active repair, and their combination as hybrid repair. The analytical model for cracked structures is developed using linear elastic fracture mechanics, which calculates the stress intensity factor (SIF) for various repair techniques under constant tensile load. The passive effect of the piezoelectric patch is determined using Rose's equations, while the stress produced by the piezoelectric material is computed using the weight function method. The fatigue life cycle for various repair configurations is determined under cyclic tensile loading using the Paris law with a stress ratio (R) of 0.1 and different voltage ratios (VR). The model is verified with experimental results and analytical fatigue life with FE solutions using ABAQUS software. It is to be noted that an analytical model is developed for the first time to account for both passive and active repairs, i.e., hybrid repair, and to verify the efficacy of the model using published experimental and FE solutions using ABAQUS. A parametric study is conducted to choose the best-sized piezoelectric actuator/patch, voltage, and voltage ratio. The results show a significant reduction in Mode-I SIF for all repair cases, with hybrid repair achieving the greatest reduction and extending fatigue life by 174.88, 116.23, and 37.92% as compared to without repair, active, and passive repairs, respectively, under 500 V with zero VR application.

Keywords Stress intensity factor (SIF) · Linear elastic fracture mechanics (LEFM) · Fatigue crack growth rate (FCGR) · Cracked plate · Piezoelectric actuator · Active repair · Stress ratio (R)

List of symbols

K_I	SIF of the cracked plate without repair
σ_0	Uniaxial tensile load
a	Crack length
W	Half-width of the plate
$F\left(\frac{a}{W}\right)$	Non-dimensional geometry correction factor
σ_P	Reduced stress at the crack plane after fixing the patch
σ_R	Stress developed in the patch
A	Cross-sectional area of the plate
A_R	Cross-sectional area of the patch
S	Stiffness ratio
E_P	Young's modulus of the patch
t_P	Thickness of the patch
W_P	Half-width of the patch
E	Young's modulus of the plate
t	Thickness of the plate
c	Physical parameter related to passive repair
k	Spring constant
υ	Poisson's ratio of the plate
β	Shear stress transfer length
G_A	Shear modulus of the adhesive material
t_A	Adhesive thickness
y_{max}	The distance of the extreme fibers of the cracked plate from the neutral axis
I_{Plate}	Moment of inertia of the plate

✉ G. Pohit
gpohit@gmail.com

[1] Department of Mechanical Engineering, Haldia Institute of Technology, Haldia 721657, India

[2] Department of Mechanical Engineering, Jadavpur University, Kolkata 700032, India

[3] Department of Mechanical Engineering, Narula Institute of Technology, Kolkata 700109, India

MECHANICS OF ADVANCED MATERIALS AND STRUCTURES
https://doi.org/10.1080/15376494.2024.2423062

Taylor & Francis
Taylor & Francis Group

ORIGINAL ARTICLE

Check for updates

A novel approach to enhance the structural integrity of a bottom-edge cracked I-beam with piezoelectric actuators

Sourav Pattanayak[a,b], Goutam Roy[c], and G. Pohit[b]

[a]Department of Mechanical Engineering, Haldia Institute of Technology, Haldia, India; [b]Department of Mechanical Engineering, Jadavpur University, Kolkata, India; [c]Department of Mechanical Engineering, Narula Institute of Technology, Kolkata, India

ABSTRACT

Structural health monitoring and repair have become increasingly crucial in confirming the safety and longevity of damaged structures. This study presents a novel approach to enhancing the structural integrity and extending the fatigue life of a bottom-edge cracked I-beam by applying piezoelectric actuators strategically placed along the crack location by actively suppressing crack propagation. An innovative actuation system induces controlled deformations in the I-beam, effectively reducing the Stress Intensity Factor (SIF) and preventing crack propagation. The efficacy of the proposed approach is validated through a series of numerical results on the ABAQUS platform, including static loading, fatigue loading, and crack growth monitoring. Various parameters, like maximum loading capacity under static loading, interpretation of crack growth rate, and service life, are monitored and analyzed throughout the cyclic loading process. The results demonstrate that the application of 500 V to the piezoelectric actuators significantly reduces the SIF by 16.62% under a 2 kN total load, a 2.86% enhanced maximum load-carrying capacity is obtained, delayed crack propagation is found after repair, and a 72.67% extended service life is achieved under a load range of 0.2 kN to 2 kN. Overall, the outcomes of this research lead to the development of innovative and efficient techniques for delaying the propagation of cracks, thereby preventing the premature onset of catastrophic failure of cracked I-beams.

ARTICLE HISTORY
Received 29 June 2024
Accepted 25 October 2024

KEYWORDS
Stress intensity factor (SIF); cracked I-Beam; piezoelectric actuators; active repair; fracture load; fatigue crack growth rate (FCGR); fatigue life

1. Introduction

Structural integrity is crucial in engineering, as the failure of structural components can have devastating consequences. Structural Health Monitoring (SHM) is a continuous process that assesses the condition, detects damage, and determines its ability to perform well over time while ensuring the safety and longevity of structures by gathering real-time data, enabling timely interventions and maintenance activities. Early crack detection and repair become essential, as unaddressed cracks can propagate and cause catastrophic failures.

Beams are especially susceptible to fatigue and damage over time, being a principal load-bearing component. Cracks in beams, whether brought on by cyclic loading or material flaws, can seriously affect their structural performance [1–4]. Traditional crack repair techniques, such as welding [5,6], bolting [7,8], and adhesive bonding [8–15], have been used in engineering for decades. However, conventional repair techniques have limitations and challenges. Welding can create residual stresses and heat-affected zones, potentially weakening the surrounding material and threatening its structural integrity [16–18]. Extensive drilling and machining may be required for bolting, resulting in additional material removal and structural weakness [19]. Adhesive bonding may only be appropriate for some materials or loading conditions, and achieving adequate bond strength can be difficult. The adhesive-bonded repair technique uses specialized adhesives to bond Carbon-fiber-reinforced polymer (CFRP) to cracked surfaces and provide structural reinforcement [11,20–22]. Furthermore, traditional repair methods can be expensive, time-consuming, and disruptive to existing operations or services, highlighting the need for innovative and efficient repair methods to address these limitations and ensure long-term structural performance and safety. In recent years, cutting-edge materials and technologies like piezoelectric patch repair [23–32], prestressed CFRP [33–35], and shape memory alloy (SMA) have created new opportunities for repairing and improving the performance of damaged structures.

Piezoelectric materials can produce mechanical motion from electrical energy and vice versa, enabling them to cause precisely controlled deformations in structures by applying a voltage. This capability allows real-time monitoring and repair facilities, improving the safety and reliability of the cracked component. Piezoelectric actuators can reduce stress, redistribute loads, and enhance beam structural integrity by interacting with damaged structures. Overall, the lightweight design, low power consumption, and compatibility with SHM systems make piezoelectric actuators versatile and efficient for various engineering applications. Crawley

CONTACT G. Pohit gpohit@gmail.com Department of Mechanical Engineering, Jadavpur University, Kolkata, India.
© 2024 Taylor & Francis Group, LLC

Applied Research

RESEARCH ARTICLE

Strengthening of an Edge-Cracked Plate Under Bending Using Piezoelectric Actuators

Sourav Pattanayak[1,2] | Supriyo Roy[1] | Prasanta Sahoo[2] | Goutam Pohit[2]

[1]Department of Mechanical Engineering, Haldia Institute of Technology, Haldia, India | [2]Department of Mechanical Engineering, Jadavpur University, Kolkata, India

Correspondence: Sourav Pattanayak (souravpattanayak18@gmail.com)

Received: 25 February 2025 | **Revised:** 12 April 2025 | **Accepted:** 17 April 2025

Keywords: active repair | cracked plate | fracture mechanics | piezoelectric actuators | stress intensity factors (SIF)

ABSTRACT

Monitoring structural stability and repairing damaged components has grown in importance to ensure the safety and longevity of various engineering structures. This paper presents an innovative method for improving the performance and delaying the failure of edge-cracked plate-like structures by incorporating piezoelectric actuators during bending. The proposed method uses two piezoelectric actuators strategically placed along the plate's surface to create a counter-moment that reduces the severity of the crack. The analytical model was based on well-known stress intensity factor (SIF) solutions for the cracked plate, while the SIF after actuation was calculated with the counter moment produced by the piezoelectric patch. The superposition principle was then used to determine the total SIF after repair. The proposed technique was validated against the ABAQUS-based finite element solutions. SIFs are calculated for various parameters like crack length, patch thickness, and repair voltage. The results demonstrate that the integration of piezoelectric actuators significantly enhances the beam's structural integrity by reducing the SIF. A 21.48% reduced SIF was obtained under 200 V repair voltage for a 5 mm crack length and 0.5 mm patch thickness. Overall, this novel approach offers a promising method for increasing the integrity of cracked structural components, particularly under bending, reducing maintenance costs, and enhancing overall safety.

1 | Introduction

Structural components often experience damage that harms functionality, typically due to continuous fatigue stress. Damage to these components increases their exposure to vibrations, reduces load-carrying capacity, and, in severe cases, may result in complete structural failure. Repairing such damage offers a cost-effective solution for extending the functional life of these structures. Among the established repair techniques, composite and metallic patch repairs have been widely adopted for mitigating structural failures [1–4]. An alternative repair technique is the stop-hole method [5], or a combination of stop-hole and FRP patches [6], along with the actuation effects of piezoelectric materials, depending on the loading conditions. Although composite patch repair has been widely investigated and proven highly effective, its ability to mitigate crack severity is limited when there is a change in the loading conditions. Recent advancements, however, have explored innovative methods such as piezoelectric actuators, which, when attached to damaged structures, enable repair through controlled external voltage applications [7]. As a result, piezoelectric materials offer a unique advantage in active structural repair due to their electromechanical coupling properties, since repair can be regulated by an externally provided voltage as needed. The benefits of this active repair include addressing a wide range of potential issues by simply applying one patch to the cracked surface. Adopting piezoelectric patches as a repair method provides technical benefits in restoring structural integrity and offers possible economic advantages, including reduced maintenance costs and extended service life, which are essential for industrial applications.

© 2025 Wiley-VCH GmbH.

Reduction in Mode-I SIF of an Edge Cracked C-Shaped Specimen Using Piezoelectric Actuator

Sourav Pattanayak[1,2]*, *Goutam Pohit*[2]

[1] Department of Mechanical Engineering, Haldia Institute of Technology, Haldia, West Bengal, 721628, India
[2] Department of Mechanical Engineering, Jadavpur University, Kolkata, 700032, India

Abstract. The focus of the current research is on the feasibility of an adhesively bound piezoelectric actuator in the active repair of an edge-cracked C-shaped specimen. First, only constant uniaxial tensile loading is used to determine the Mode-I stress intensity factor. The Mode-I stress intensity factor is then examined while taking into account the actuation effect provided by the piezoelectric patch when an external voltage is applied. For an edge-cracked C-shaped specimen, the total stress intensity factor is determined analytically using the concept of the superposition principle of the linear-elastic crack problem. The outcome demonstrates a considerable decrease in the Mode-I stress intensity factor following active repair using the piezoelectric actuator. Parametric analysis has been carried out to comprehend repair performance and choose the best-sized actuators for active repair.

Keywords: Stress Intensity Factor; Active Repair; Piezoelectric Actuator; Fracture Mechanics

1. Introduction

Active repair of a damaged structure utilizing piezoelectric (PZT) actuators has significantly reduced crack damage progression in structures due to its electro-mechanical impact during the past few decades. Similarly, there are many other forms of passive restoration of damaged structures employing composite materials, which has been quite popular in recent years. Transducers made of piezoelectric materials can function as a sensor or an actuator. Typically, the sensor will be used to determine the health state, while the actuator will be utilized to repair the structure. Piezoelectric actuators have demonstrated the ability to reduce and regulate the shear stress concentration and joint edge peel in adhesively bonded joint systems during the past 20 years. As a result, the research of piezoelectric actuator applications in damaged structures and adhesively bonded combination systems is based on three distinct repair inquiry methodologies: analytical, numerical, and experimental. A piezoelectric actuator can also be used for other investigations, such as the control of delamination in composite material beams.

*Corresponding author: souravpattanayak18@gmail.com

© The Authors, published by EDP Sciences. This is an open access article distributed under the terms of the Creative Commons Attribution License 4.0 (https://creativecommons.org/licenses/by/4.0/).

Study on Fatigue Crack Propagation Reduction and Extended Service Life in an Arc-Shaped Cracked Specimen Using Piezoelectric Patch

Sourav Pattanayak and Goutam Pohit

Abstract This study examines the role of an adhesively joined piezoelectric actuator in reducing crack propagation rate in an arc-shaped edge-cracked specimen while exposed to fatigue loading. This study employs the linear elastic fracture mechanics (LEFM) concept to determine the mode-I stress intensity factor (SIF) for maximum and minimum tensile stresses applied on the cracked specimen. The weight function method (WFM) determines the Mode-I SIF under actuation alone. On the other hand, the total SIF is obtained by applying the superposition principle of LEFM. The cracked structure's fatigue crack growth rate (FCGR) before and after repair is determined using the Paris model, considering a stress ratio (SR) of 0.1. The investigation of various cracked structure geometries demonstrates a substantial reduction in FCGR when external voltages are applied, significantly improving fatigue life. A 55.22% reduced FCGR and a 130% enhanced fatigue life are achieved under a repair voltage of 500 V compared to without a repair condition. Notably, since the geometric characteristics of both components are crucial in preventing crack propagation, careful selection of the specimen's geometry and the piezoelectric actuator can significantly extend service life.

Keywords Stress intensity factor (SIF) · Linear elastic fracture mechanics (LEFM) · Piezoelectric materials · Paris law · Fatigue crack growth rate (FCGR)

Nomenclatures

A	Cross-sectional area of the specimen (m^2)
a	Crack length (m)

S. Pattanayak (✉)
Department of Mechanical Engineering, Haldia Institute of Technology, Haldia 721657, India
e-mail: souravpattanayak18@gmail.com

S. Pattanayak · G. Pohit
Department of Mechanical Engineering, Jadavpur University, Kolkata 700032, India

© The Author(s), under exclusive license to Springer Nature Singapore Pte Ltd. 2025

P. Sahoo and T. K. Barman (eds.), *Advances in Materials, Manufacturing and Design*,
Lecture Notes in Mechanical Engineering,
https://doi.org/10.1007/978-981-97-6667-3_22

Sourav Pattanayak